IMPROVED PHASE BEHAVIOR PREDICTIONS OF PETROLEUM RESERVOIR FLUIDS FROM A CUBIC EQUATION OF STATE

Ingolf Søreide

A Dissertation for the Fulfillment
of Requirements for the Degree
of Doktor Ingeniør

The Norwegian Institute of Technology
Department of Petroleum Technology
and Applied Geophysics

April 1989

NTH-TRYKK

Preface to
Second Printing

Ingolf Søreide's thesis has found wide circulation since being first presented in 1989 as fulfillment of the requirements for his dr.ing. degree at the Department of Petroleum Engineering and Applied Geophysics, U. of Trondheim, Norwegian Institute of Technology.

The continued requests for copies of Ingolf's thesis is a tribute in itself. I also would like to compliment the lasting value of methods and discussions given in Ingolf's original thesis. With permission from Ingolf I am making a second printing of his thesis which will hopefully be appreciated by many in the years to come.

The contents of this thesis are, in their entirety, the same as in the original thesis published April 1989. A two-page errata sheet is included prior to the Acknowledgement section. Any additional errors that are found can be reported to Ingolf directly (Norsk Hydro a/s, P.O. Box 200, N-1321 Stabekk, Norway) or to me (Deptartment of Petroleum Engineering, UNIT-NTH, 7034 Trondheim, Norway).

January 5, 1994

Curtis H. Whitson
professor

ERRATA

Page	Eq./Line/ Location	Correction
5	Eq. 1.8a	$\Omega_a = [9(2^{1/3}-1)]^{-1} = 0.42748023..$
11	Eq. 1.24	$m = 0.480 + 1.574\omega - 0.176\omega^2$
11	Eq. 1.26	$m = 0.48508 + 1.55171\omega + 0.1561\omega^2$
20	Eq. 1.52a	$-3Z_c = -3\Omega_b + (\Omega_c+\Omega_d-1)$
20	Eq. 1.52b	$3Z_c^2 = 3\Omega_b^2 - 2\Omega_b(\Omega_c+\Omega_d-1) + \Omega_a + \Omega_c\Omega_d - \Omega_c - \Omega_d$
20	Eq. 1.52c	$-Z_c^3 = -\Omega_b^3 + \Omega_b^2(\Omega_c+\Omega_d-1) - \Omega_b(\Omega_a+\Omega_c\Omega_d-\Omega_c-\Omega_d) - \Omega_c\Omega_d$
23	Eq. 1.63b	$A_{mj} = \sum_{j=1}^{N} x_j A_{ij}$
24	Eq. 1.65c	$\theta = \sum_{i=1}^{N} \sum_{j=1}^{N} x_i x_j \theta_{ij}$, θ=B,C,D
48	Eq. 2.29a	$V_{min} = 1/(1-K_{max})$
48	Eq. 2.29b	$V_{max} = 1/(1-K_{min})$
54	l. 5 from bottom	from ...decent... to ...descent...
56	Eq. 2.55	$\mu_1 = \dfrac{(b_{02}b_{12}-b_{01}b_{22})}{(b_{11}b_{22}-b_{12}b_{12})}$
56	Eq. 2.56	$\mu_2 = \dfrac{(b_{01}b_{12}-b_{02}b_{11})}{(b_{11}b_{22}-b_{12}b_{12})}$
57	l. 9 from bottom	from ...shown Fig.... to ...shown in Fig.
59	heading	from <u>...Mixture</u> to <u>...Mixtures</u>
89	Eq. 3.59	$T_b = T_b^{\infty} - a \exp[bM + c\gamma + dM\gamma]\, M^e\, \gamma^f$
89	l. 7 from bottom	from ...MAXD=4.05... to ...MAXD=5.04...
100	Tab 3.12, Note 5	from [γ_o=0.7037] to [γ_o=0.8066]
107	l. 16 from top	from ...bed used... to ...be used...
107	l. 19 from top	from . An disadvantage... to . A disadvantage....
162	Fig. 5.18,legend	from 3 164.5 to 3 163.5
169	Fig.5.22,title	from ...at 250°F [121.1°C] to ...at 200°F [93.3°C]

ERRATA (CONT'D)

Page	Eq./Line/ Location	Correction

45 Fig. 2.3

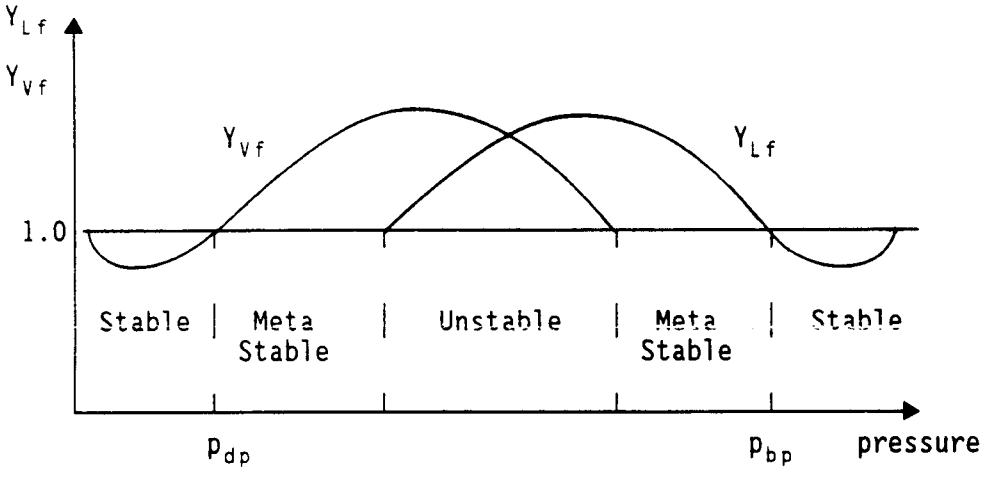

Fig. 2.3 Behavior of molenumbers Y_{Lf} and Y_{Vf} at constant temperature, $T<T_c$, for a reservoir oil.

ACKNOWLEDGEMENT

I will express my sincere gratitude to Professor Curtis H. Whitson and Professor Jon Kleppe for supervision and encouragement throughout this thesis work. I will also thank other colleagues at the Division of Petroleum Engineering and Applied Geophysics, Norwegian Institute of Technology for help and useful discussions.

During the four-month visit to The Laboratory of Energetics, Technical University of Denmark it was a pleasure to work with Jan Reffstrup and his colleagues.

The opportunity to undertake this study has been possible with financial support provided by:

- The Mobil Fund at the Norwegian Institute of Technology.
- The Nordic Council, Program for Energy Research.
- The Nordic Foundation for Industrial Development.
- Society of Petroleum Engineers - Stavanger Section.
- Norges Tekniske Høgskoles Fond.

Last, but not least, I am indebted to Heidi Marie for her understanding and support during the course of this work. Support from my parents is also gratefully acknowledged.

SUMMARY

Cubic equations of state

Cubic equations of state (EOS) have gained wide acceptance for thermodynamic equilibrium calculations, especially for systems containing non-polar substances such as hydrocarbons and light non-hydrocarbons. In petroleum engineering, equations of state have found applications for phase and volumetric behavior predictions at high pressures, including:

(1) Reservoir modeling with a compositional simulator where an EOS is used to describe volumetric and phase behavior. Reservoir processes requiring compositional modeling include enhanced oil recovery by gas injection, and depletion of volatile oil and gas condensate reservoirs. In both cases there are large changes in reservoir and produced fluid compositions that effect the recovery process.

(2) Generating pressure-volume-temperature (PVT) parameters for reservoir simulators using black-oil (BO) or modified black-oil (MBO) PVT formulations, and also to develop equilibrium K-value tables for limited compositional simulators describing phase equilibrium with tabulated K-values.

(3) Production and process engineering to describe fluid flow through production tubing, surface separator and process equipment, and transportation pipelines.

A cubic equation of state is a thermodynamical model relating volume of a pure component to pressure and temperature. Using the principle of corresponding states, component critical properties and acentric factor are used to characterize a given component. The EOS is extended for fluid mixtures using mixing rules. Thus, an EOS fluid characterization generally requires mixture composition and component properties: molecular weight, acentric factor, critical pressure and critical temperature.

The reason why petroleum engineers have relied on equations of state is that they have a wide range of applicability, they are relative simple, and they are internally consistent at the critical point. The latter is particularly important for compositional simulators modeling miscible processes where near-critical mixtures dominate the recovery process. Some disadvantages of the EOS are that:

(1) it requires an accurate description of all the components found in the mixture;

(2) it can be computationally expensive as the number of mixture components increases; and

(3) it fails to predict, a'priori, accurate phase behavior and liquid volumes in certain p-T-x regions.

This thesis reviews some of the most common equations of state used for petroleum engineering applications. Particular emphasis is given to the four-parameter Martin EOS which has been used for phase calculations in this work.

The so-called volume translation approach has improved EOS volumetric predictions by introducing a linear translation of the volume coordinate without affecting vapor-liquid equilibrium (VLE). In this work this approach has been extended for the Peng-Robinson and the Soave-Redlich-Kwong EOSs. It is shown that the pure component volume correction variable can be determined as a function of reduced temperature.

VLE Calculations

The vapor-liquid equilibrium calculations of special importance in petroleum engineering are stability analysis, isothermal flash, and saturation pressure calculations. Stability analysis determines if a composition is thermodynamically stable, or tends to split into two (or more) phases at a specified pressure and temperature; it is used in conjunction with flash and saturation pressure calculations to ensure that two phases exist and to provide reliable K-value estimates. Pressure, temperature and overall composition are specified in flash calculations, and relative amounts and compositions of each phase are determined. The flash algorithm described here is based on the so-called "negative flash" approach which conveniently permits relative vapor fraction to go outside the interval 0 to 1. For a given temperature and mixture composition the saturation pressure calculation yields the pressure at which an incipient phase is formed, and its composition. The non-linear system of equations introduced in VLE calculations are solved by the General Dominant Eigenvalue Method (GDEM) which is an accelerated successive substitution method.

Heptanes-Plus Characterization

Naturally occurring petroleum fluids are complex mixtures including light and intermediate hydrocarbons, a few non-hydrocarbons and a large number of heptanes and heavier components (C_{7+}). Laboratory analyses of such reservoir fluids usually give a limited description of the heavy components. Hydrocarbons heavier than hexane, which is the heaviest "pure" component reported, are normally lumped into a C_{7+} fraction with measured molecular weight and specific gravity. Unless a C_{7+} fractional distillation analysis exists, the C_{7+} fraction is split into pseudocomponents which are defined by estimated inspection properties; molecular weight, specific gravity and normal boiling point. The recommended split method which combines the gamma distribution function with Gaussian quadrature theory, yields mole fractions and molecular weights for an arbitrary number of pseudocomponents. Specific gravities and normal boiling points are estimated from developed correlations.

Pseudocomponent critical properties must be calculated from generalized correlations as functions of the inspection properties. C_{7+} acentric factors are determined from a proposed procedure resulting in normal boiling points correctly predicted by the EOS. Similarly, a volume translation method for pseudocomponents is proposed which results in correctly predicted liquid density at standard conditions.

Phase behavior prediction can be improved with binary interaction parameters (BIPs) used in EOS mixing rules to model intermolecular forces of dissimilar components. Interaction parameters for non-hydrocarbon--hydrocarbon binaries and for methane--C_{7+} binaries are either tabulated or can be estimated from generalized correlations.

Regression

A sample of reservoir fluid is usually brought to a laboratory for PVT measurements, yielding experimental phase and volumetric data. Since the predictive capabilities of equations of state may be poor, prediction of such experimental PVT data may be inadequate. Thus, it is usually necessary to adjust the predicted EOS characterization using non-linear regression to obtain an acceptable match. This tuning procedure is not straightforward. Selecting appropriate parameters to adjust is based mainly on experience. Several non-linear least-squares regression methods have been implemented and tested, of which the rotational discrimination method is recommended. This method deals effectively with null-effect and linearly dependent parameters and yields qualitative information concerning parameter identifiability and confidence.

Conclusions

The main objective of this study has been to develop an EOS characterization procedure for improved prediction of phase and volumetric behavior of reservoir fluids. With the proposed C_{7+} characterization procedure, this objective has to certain extent been achieved. Further improvements are achieved by multiparameter regression.

TABLE OF CONTENTS

TABLE OF CONTENTS (cont'd)

CHAPTER 1
CUBIC EQUATIONS OF STATE

1.1 Introduction

An equation of state (EOS) may be looked upon as a mathematical relationship between the molar volume, v, of a fluid and the pressure and temperature of the actual system. These equations are based on the theorem of corresponding states proposed by van der Waals (1873) where reduced molar volume, v_r, or compressibility factor, Z, can be expressed for all ideal fluids in terms of their reduced pressure, p_r, and temperature, T_r:

$$Z = Z(p_r,T_r) \tag{1.1a}$$

or

$$v_r = v_r(p_r,T_r) \tag{1.1b}$$

with $v_r=v/v_c$, $p_r=p/p_c$, and $T_r=T/T_c$, where v_c, p_c and T_c are critical properties. The above relations hold only for simple fluids with spherical molecules. For more complex fluids, an additional third fluid parameter may be introduced to compensate for the molecule's deviation from spherical symmetry. Such a parameter is the Pitzer acentric factor, ω, defined as (Pitzer et al., 1955)

$$\omega = -1-\log_{10} p_r^s \Big|_{T_r=0.7} \tag{1.2}$$

where p_r^s is the reduced, vapor pressure a at reduced temperature of 0.7.

The ideal gas law, pv=RT, usually applied to low-pressure gases only, represents a simple equation of state based on the theorem of corresponding states.

Several types of equations of state can be used for both phases of hydrocarbons and non-polar non-hydrocarbons such as N_2, CO_2, and H_2S. Perhaps the most common equation is the cubic equation of state, first proposed by van der Waals (1873). Other types are expanded virial equations, such as Benedict-Webb-Rubin EOSs (1940) as modified by Starling (1971) and Starling and Han (1972). Cubic and BWR equations are basically empirical. A more

complex theoretical approach based on perturbed hard chain theory is presented by Beret and Prausnitz (1975) and by Donahue and Prausnitz (1978). The cubic equation of state has proven to be valuable for high-pressure phase behavior predictions, and this thesis deals exclusively with such equations. According to Abbott (1973) there are several features that any EOS should try to honor:

1. The steep portion of the subcritical isotherm for small volumes, line A-B on Fig. 1.1.

2. Multiple volume roots at a saturated vapor pressure, B and D on Fig. 1.1.

3. Ideal gas law behavior as volume tends to infinity, line D-F on Fig. 1.1.

4. Adjoining roots at the critical point C on Fig. 1.1., resulting in vapor and liquid phase physical properties to converge as the critical point is approached.

Several techniques exist for developing cubic equations of state. Some are based on mathematical or numerical constraints, and the EOS parameters are determined by solving the resulting system of equations. These EOSs are generally less accurate for physical property prediction in a specific region or for specific systems, but have a wide range of applicability (Abbott, 1979). The other alternative is to determine EOS parameters using non-linear regression yielding an equation which matches a specific set of experimental data. Such a data set may include vapor pressure and saturated volume data for hydrocarbons from methane to dodecane (nC_{12}) and some light non-hydrocarbons. Equations developed following this method, called "brute-force", are usually accurate for the PVT regions represented by the experimental data, but may give erroneous results outside these regions.

Originally, the cubic EOS was only applied to the vapor phase with surprising accuracy. Later developments have concentrated on improved prediction of liquid phase properties. Additional adjustable parameters have been included and the temperature and substance dependencies have become more and more

complex. Mixing rules for calculating mixture EOS parameters from pure component parameters have also been improved by including the so-called binary interaction parameters (BIPs).

Several excellent reviews on cubic EOSs, their applicability and limitations are found in the literature including Martin (1967, 1979), Abbott (1973, 1979), Gray (1979), Yarborough (1979), Tsonopolous and Heidman (1985), and Firoozabadi (1988). This section reviews the most commonly used cubic EOSs in petroleum engineering.

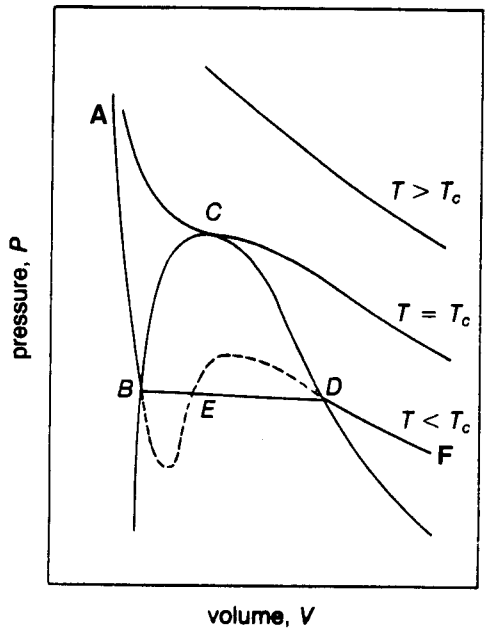

Fig. 1.1 Pressure versus volume plot for a pure component (from Lee and Erbar, 1983).

1.2 Cubic EOS Review

Two-Parameter EOS

The era of cubic EOS started with the work of van der Waals (vdW) in 1873. He developed a pressure explicit, two- parameter equation consisting of two terms:

$$p = p_{rep} + p_{att} \tag{1.3}$$

The term p_{rep} represents the hard sphere repulsive forces and should be capable of modeling ideal gas law departures such as caused by intermolecular repulsions dominating at high temperatures. This term also considers that molecules take up a certain volume. However, the repulsive forces are known to be only approximately represented by most cubic EOSs (Abbott, 1979) which is typically reflected by erroneous liquid volume predictions. The term p_{att} represents the attractive forces, and may be looked upon as a pressure change due to intermolecular forces.

van der Waals expressed these two terms in a simple way, resulting in the following relation

$$p = \frac{RT}{v-b} - \frac{a}{v^2} \tag{1.4}$$

where a and b are EOS parameters.

The critical point is defined by the three conditions: p_c, T_c, and v_c. Equations of the van der Waals form have two adjustable parameters, and it is only possible to satisfy two of the three conditions: (p_c,T_c), (p_c,v_c) or (T_c,v_c). van der Waals observed that the critical isotherm of the p-v curve (Fig 1.1) has a horizontal slope and an inflection point at the critical point. By honoring the conditions p_c and T_c, he mathematically expressed this as

$$\left.\frac{\partial p}{\partial v}\right|_{T_c,p_c} = 0 \tag{1.5a}$$

$$\left.\frac{\partial^2 p}{\partial v^2}\right|_{T_c,p_c} = 0 \tag{1.5b}$$

These relations have later been referred to as the van der Waals critical criteria.

The next step was taken by Redlich and Kwong (RK) in 1949 with a slight modification of the attractive-term

$$p = \frac{RT}{v-b} - \frac{a(T)}{v(v-b)} \tag{1.6}$$

As indicated, the a parameter now includes a temperature dependency. Using the vdW critical criteria, Redlich and Kwong expressed parameters a and b as

$$a = \Omega_a \frac{(RT_c)^2}{p_c} T^{-0.5} \tag{1.7a}$$

$$b = \Omega_b \frac{RT_c}{p_c} \tag{1.7b}$$

with numerical constants Ω_a and Ω_b given by

$$\Omega_a = [9(2^{1/3}-1)^{-1}] = 0.42748023.. \tag{1.8a}$$

$$\Omega_b = (1/3)(2^{1/3}-1) = 0.08664035.. \tag{1.8b}$$

The a parameter is often given in terms of a_c and α

$$a = a_c\alpha(T) \tag{1.9}$$

where a_c represents the value of a at the critical point, and α represents a temperature-dependent correction to a_c. For RK EOS, $\alpha=T_r^{-0.5}$, with $\alpha=1$ at $T_r=1$.

Redlich and Kwong proposed the following mixing rules for calculating mixture EOS parameters, denoted a_m and b_m:

$$a_m = (\Sigma_i z_i \sqrt{a_i})^2 \tag{1.10a}$$

$$b_m = \Sigma_i z_i b_i \tag{1.10b}$$

where z_i is mole fraction of component i.

Applying the van der Waals criteria to a two-parameter EOS yields a universal critical compressibility factor, Z_c=1/3. Experimental Z_c values are substance dependent, e.g. Z_c=0.288 for methane and Z_c=0.237 for dodecane. Thus, the universal Z_c=1/3 may result in poor RK EOS prediction of vapor-liquid equilibrium (VLE) data in the critical region. Also, it yields overestimated liquid volumes of intermediate and heavy components.

Another deficiency with the RK EOS is the temperature dependency of α, resulting in inaccurate vapor pressures at low reduced temperatures, especially for heavy components. Later developments have shown that vapor pressure predictions are improved if the α function also includes a substance dependent term.

The original RK is practically no longer used, but it deserves credit as the starting point for many later EOS developments. The RK EOS was clearly superior to other more complicated equations available in the 1940's.

Chueh and Prausnitz (1967a) proposed an important new direction in the development of cubic EOSs by relaxing the vdW critical criteria (Eqs. 1.5a,b) when determining the EOS parameters. The RK constants Ω_a and Ω_b were originally determined to give a good representation of VLE data in the critical region for light substances. Chueh and Prausnitz's objective was to achieve a reasonable accuracy over a wider temperature range. Ω_a and Ω_b were treated as empirical constants and were determined separately for each substance by matching volumetric data of the saturated vapor from the normal boiling point to the critical temperature. The α function originally included in the RK EOS is retained by Chueh and Prausnitz. Also, a relatively complex modification of the mixing rule for a_m is proposed.

In 1970 Zudkevitch and Joffe presented a modification to the RK EOS based on the work of Chueh and Prausnitz. The idea of treating Ω_a and Ω_b as empirical constants was adopted. At first one set of EOS constants were determined for each phase by forcing the EOS to simultaneously match pure component saturated density and fugacity data. "Experimental" fugacity values were obtained from

a general correlation given by Lyckman et al. (1965). Finally Zudkevitch and Joffe determined to utilize liquid constants Ω_a and Ω_b also for the vapor phase. This approach does not necessarily lead to prediction of a correctly EOS-vapor pressure.

In the supercritical region ($T_r>1$) Ω_a and Ω_b are assigned values determined at the critical point.

$$\Omega_a = \Omega_a(T_r), \quad T_r<1 \tag{1.11a}$$

$$\Omega_a = \Omega_a(T_r=1), \quad T_r\geq 1 \tag{1.11b}$$

$$\Omega_b = \Omega_b(T_r), \quad T_r<1 \tag{1.12a}$$

$$\Omega_b = \Omega_b(T_r=1), \quad T_r\geq 1 \tag{1.12b}$$

Zudkevitch and Joffe used a modified RK mixing rule for a_m, following the proposals from Chueh and Prausnitz (1967a)

$$a_m = \Sigma_i\Sigma_j \; z_i z_j a_{ij} \tag{1.13}$$

but proposed themselves a somewhat simpler expression for a_{ij}

$$a_{ii} = a_i, \quad i=j \tag{1.14a}$$

$$a_{ij} = (a_i a_j)^{0.5}(1-k_{ij}), \quad i\neq j \tag{1.14b}$$

where k_{ij} is an empirically determined parameter modeling the interaction between binaries (i,j) with different molecular structure. The binary interaction parameters (BIPs) are assumed to be independent of pressure, temperature and composition.

Four months later Joffe, Schroeder and Zudkevitch (1970) slightly modified the Ω_a and Ω_b calculation procedure. They no longer fit EOS predicted vapor and liquid phase fugacities to values estimated from a general fugacity correlation, but instead force the EOS to match saturated vapor pressure data. Joffe et al. note that their method can only be used in the subcritical temperature region ($T_r<1$) and therefore use the earlier procedure presented by Zudkevitch and Joffe for supercritical temperatures. The Joffe et al. procedure has become the "norm", though the modification is typically referred to as the ZJRK EOS after the first method.

Whitson (1983b) applied the ZJRK EOS in a study performed to reveal the predictive capability of various EOS applied to petroleum reservoir fluids. He found that the ZJRK do not predict accurate phase behavior without adjustments and that it normally overpredicts liquid densities, while vapor densities are always underpredicted. Coats and Smart (1986) also applied the ZJRK EOS to simulate PVT data for twelve different reservoir fluids, and confirms the above conclusions given by Whitson (1983b). It should be noted that these studies to some extent are influenced by the heptanes-plus (C_{7+}) characterization procedure, especially for gas condensates, and do not reflect the performance of the EOS alone. This is discussed later in Chapter 5.

Harmens (1975) also modified the RK EOS, and treated the problem of obtaining accurate Ω_a and Ω_b parameters in the critical region as follows: (1.) at $T_r=1$, use the original RK EOS constants, Ω_a and Ω_b, (2.) at $T_r \leq 0.96$, use the Joffe et al. approach to determine Ω_a and Ω_b, (3.) for $0.96<T_r<1.0$, use linear interpolation to determine Ω_a and Ω_b at T_r between the values at $T_r=0.96$ and $T_r=1$.

Hamam et al. (1977) used p_c and v_c to represent vapor pressure and saturated liquid volume, respectively, at the critical point. This results in substance dependent Ω_a and Ω_b constants.

Yarborough (1979) used, with some modifications, the Joffe et al. (1970) approach to determine Ω_a and Ω_b constants of heavy petroleum fractions. He applied generalized correlations for saturated liquid density and vapor pressure instead of pure component data. The resulting EOS constants are expressed as cubic spline equations of temperature ($T_r=0.15$-1.0) and acentric factor ($\omega=0.0$-1.5). For components above their critical temperature, Yarborough applied the values obtained at $T_r=1.0$

$$\Omega_a = \Omega_a(T_r,\omega), \quad T_r<1 \tag{1.15a}$$

$$\Omega_a = \Omega_a(1,\omega), \quad T_r\geq 1 \tag{1.15b}$$

$$\Omega_b = \Omega_b(T_r,\omega), \quad T_r<1 \tag{1.16a}$$

$$\Omega_b = \Omega_b(1,\omega), \quad T_r\geq 1 \tag{1.16b}$$

The general correlations for saturated physical and thermodynamic properties used to determine Ω_a and Ω_b, are valid up to n-decane, only. Thus, the accuracy of these constants for heavier petroleum fractions may be questionable. Yarborough also studied the effects of non-zero BIPs in the RK EOS. He concluded that interaction parameters for hydrocarbon-hydrocarbon (HC) binaries have small effects on VLE prediction, but that BIPs should be used for non-hydrocarbons. Yarborough found that prediction of phase and volumetric behavior of synthetic hydrocarbon mixtures with well-defined components are generally good. However, for a high-shrinkage, volatile oil he observed that predicted densities were 10-15 percent high.

Turek at al. (1980) further developed the work of Yarborough, especially for application to CO_2 reservoir systems. Ω_a and Ω_b for CO_2 are described as functions of temperature, also above T_r=1. Further, a modification to the mixing rule for b_m, including a second set of binary interaction parameters. These BIPs, denoted ℓ_{ij}, are used in a linear mixing rule

$$b_m = 1/2\ \Sigma_i\Sigma_j z_i z_j (1+\ell_{ij})(b_i+b_j) \qquad (1.17)$$

Ω_a and Ω_b constants for CO_2 as well as a and b parameter BIPs were determined from binary CO_2--n-alkane VLE data. These modifications represent a significant improvement over the phase behavior results obtained by Yarborough on CO_2-rich petroleum mixtures, but predicted densities may still be improved (Firoozabadi, 1988).

Chaback and Turek (1986) studied the temperature dependency of Ω_a and Ω_b for several light hydrocarbons and the non-hydrocarbons: N_2, CO_2 and H_2S. A characterization procedure for the C_{7+} fraction is also presented. In addition, non-zero a_m and b_m parameter interaction coefficients for CO_2-C_{N+} and C_1-C_{N+} binaries are used. Results are shown to be promising for modeling phase and volumetric behavior of CO_2-rich petroleum mixtures.

Wilson (1969) retains the original Ω_a and Ω_b constants of the RK EOS, but modifies the temperature dependency of the α function and introduces a substance dependency by including acentric factor, ω

$$\alpha = T_r\ g(T_r,\omega) \qquad (1.18)$$

The function $g=\alpha/T_r$ is given by

$$g = 1 + m(1/T_r-1) \tag{1.19}$$

The component dependency is included in the slope m of the g function which Wilson relates to acentric factor

$$m = 1.57 + 1.62\omega \tag{1.20}$$

This expression was developed to force the EOS to match the slope of the vapor pressure curve at the critical point. This slope is directly related to the definition of Pitzer's acentric factor (Eq. 1.2).

The Wilson EOS was developed by fitting only light component vapor pressure data, thus resulting in poor prediction of vapor pressures for heavier components. Also, the α function results in poor extrapolation into the supercritical region. These shortcomings might explain the limited use of this EOS.

Cubic EOSs used in VLE calculations for hydrocarbon mixtures gained wider acceptance with the Soave (1972) modification of the RK EOS (SRK). Earlier, it was claimed that RK EOSs poor prediction of VLE for multicomponent mixtures was connected to the mixing rules. Soave did not agree with this, and attempted to improve the temperature dependence of α. His intention was to correct the RK EOS from the following point of view: an equation accurately predicting VLE for pure components should be able to predict VLE data of mixtures with the same accuracy. Soave felt that pure component vapor-pressure information somehow had to be built into the EOS. His intention was never to improve the volumetric behavior of the RK EOS, but only to obtain a good match to vapor pressure data.

The attractive term of the cubic EOS has greatest influence on vapor pressure predictions. Consequently, Soave modified the temperature and substance dependency of the α function almost in the same manner as previously done by Wilson. Soave used the following approach:

- α is calculated at series of temperatures between T_r=0.4 and T_r=1.0 to match the saturated vapor pressure (equal phase fugacities) for several light components.
- The calculated α-values correlated well with T_r. By forcing α=1 at

T_r=1, the α function was expressed as

$$\alpha^{0.5} = 1 + m(1-T_r^{0.5}) \tag{1.21}$$

where m includes a substance dependency using acentric factor.

- It is assumed that reduced saturated vapor pressure, p_r^s, at T_r=0.7 can be estimated from the definition of the Pitzer acentric factor, ω, given by Eq. 1.2,

$$p_r^s\Big|_{T_r=0.7} = 10^{-1-\omega} \tag{1.22}$$

- The slope m of Eq. 1.21 is determined for $0.0 \le \omega \le 0.5$ using the $\alpha(\omega)$ values at T_r=0.7 and that α=1.0 at T_r=1.0

$$m = \frac{1.0-\alpha(\omega)^{0.5}}{1.0-0.7} \tag{1.23}$$

- Finally, m is expressed as a quadratic function of ω

$$m = 0.480 + 1.574\omega + 0.176\omega^2 \tag{1.24}$$

- Eq. 1.21 combined with Eq. 1.24 may be expressed

$$\alpha^{0.5} = 1 + [0.480 + 1.574\omega + 0.176\omega^2](1-T_r^{0.5}) \tag{1.25}$$

Eq. 1.25 is strictly valid only for $0.0 \le \omega \le 0.55$, but it behaves reasonably also for higher ω values. However, at some high ω value (ω>3.0), the m function goes through a maximum. The functional form drawn by Soave has no physical explanation. Later, Soave proposed a modified $m(\omega)$ relation that does not give a maximum

$$m = 0.48508 + 1.55171\omega - 0.1561\omega^2 \tag{1.26}$$

In 1978, Graboski and Daubert presented a $m(\omega)$ relation determined by matching vapor pressures of hydrocarbons from an American Petroleum Institute (API) database

$$m = 0.47979 + 1.576\omega - 0.1925\omega^2 + 0.025\omega^3 \tag{1.27}$$

Tsonopolous and Heidman (1985) show there is little to gain in improving pure component vapor pressures using either Eq. 1.26 or 1.27.

The SRK EOS uses the original RK EOS Ω_a and Ω_b constants and thus Z_c=1/3. Soave in his original work also generalized the mixing rule for a_m making non-zero k_{ij}-values possible

$$a_m = \Sigma_i\Sigma_j z_i z_j (a_i a_j)^{0.5}(1-k_{ij}) \tag{1.28}$$

SRK is superior to the original RK for VLE and vapor density prediction for systems including HC and light non-HC. The main drawback with the Soave modification is underprediction of liquid densities, especially for mixtures with heavy components.

Reid et al. (1987) do not recommend using the SRK EOS at large reduced temperatures. They claim that the RK EOS gives a more accurate volume behavior in the supercritical region (p_r>1, T_r>1) because the slope of the vapor pressure curve at the critical point matches experimental data better than the SRK EOS does.

Among others, Pedersen et al. (1984a,b, 1985a,b, 1988), Whitson (1983b) and Firoozabadi (1988) have been using the SRK in phase behavior prediction of petroleum reservoir fluids. Due to the poor prediction of liquid densities, Pedersen at al. (1984a) suggested that this property be estimated from the Standing-Katz (1942) or the Alani-Kennedy (1960) methods.

Peng and Robinson (PR) in 1976 proposed a two-parameter EOS

$$p = \frac{RT}{v-b} - \frac{a(T)}{v(v+b)+b(v-b)} \tag{1.29}$$

This equation is developed closely following Soave's approach, except that Z_c=0.307401 instead of 1/3. This results in another set of EOS constants that fulfill the vdW's critical criteria: Ω_a=0.457235 and Ω_b=0.077796.

The α function has the same form as in the SRK EOS, with m related to ω as

$$m = 0.37464 + 1.5422\omega - 0.26992\omega^2 \tag{1.30}$$

Peng and Robinson applied the Soave procedure to determine the α function except at one point: for each substance the slope m of α are based on matched saturated vapor pressures in the temperature interval from normal boiling

point to the critical point. Soave based m only on two points: $p_r^s(\omega)$ at T_r=0.7 and p_c at T_r=1.0.

Robinson and Peng (1978) presented a modification to their original equation by replacing Eq. 1.30 with a cubic equation in ω valid in the range from 0.2 to 2.0.

$$m = 0.379642 + 1.48503\omega - 0.164423\omega^2 + 0.016666\omega^3 \qquad (1.31)$$

For ω<0.45, Eq. 1.31 performs almost identical to the original m-relation, but VLE prediction for the modified PR EOS is improved for components with ω>0.45.

The PR EOS underpredicts liquid molar volume of components lighter than n-heptane, and overpredicts liquid molar volume of heavier components. Vapor volumes are generally slightly overpredicted. PR and SRK predicted saturated volumes at T_r=0.7 are shown in Fig. 1.2 for various hydrocarbons. The improved volumetric prediction of the PR EOS compared to the SRK EOS, is mainly due to the slightly lower Z_c-factor chosen which is closer to the measured Z_c-factor for most hydrocarbons. Whitson (1983b) and Firoozabadi (1988) show that density prediction of reservoir fluids with the PR EOS is more accurate than with the SRK EOS. Coats and Smart (1986) shows that the predictive capabilities of ZJRK EOS is somewhat better than for PR EOS. Volumetric behavior of cubic EOSs is discussed further in Sections 1.4 and 5.

Enick et al. (1987) apply the PR EOS to describe the aqueous and hydrocarbon phases of reservoir fluid systems typically containing HC, H_2O and CO_2. To model the solubilities of both CO_2 in H_2O and H_2O in CO_2, the a_m mixing rule has been modified by relaxing the k_{ij}=k_{ji} assumption. The mixing rule is expressed

$$a_{ij} = [1-k_{ij}+(k_{ij}-k_{ji})x_i](a_i a_j)^{0.5} \qquad (1.32)$$

where x_i may refer to mole fraction in the liquid or the vapor phase. Eq. 1.32 reduces to the conventional quadratic mixing rule for k_{ij}=k_{ji}. Enick et al. also propose Ω_a and Ω_b constants for H_2O which results in correct saturated vapor pressures over the range of reservoir temperature.

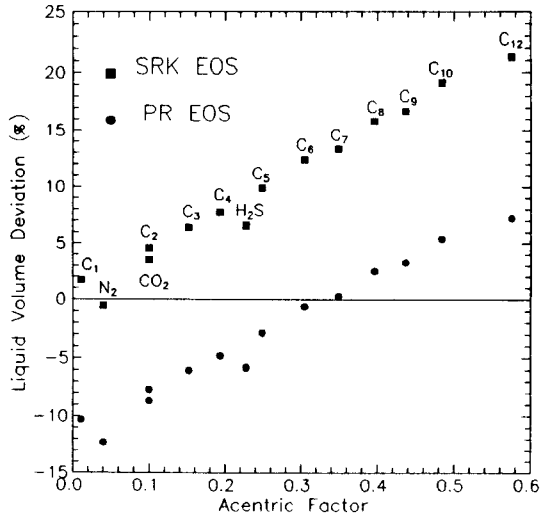

Fig. 1.2 Liquid molar volume deviation (%) at T_r=0.7 as a function of acentric factor (from Schmidt and Wenzel, 1980).

Three-Parameter EOS

Usdin and McAuliffe (UM, 1976) propose a three-parameter cubic EOS of the form

$$p = \frac{RT}{v-b} - \frac{a}{v(v+d)} \tag{1.33}$$

where the EOS parameters are denoted a, b, and d. Corresponding EOS constants Ω_a, Ω_b, and Ω_d, are defined using the vdW's critical criteria, though Z_c is calculated for each component by matching EOS predicted liquid density to experimental data at standard conditions instead of using the experimental value. Saturated density at atmospheric pressure is used for components that do not appear as a liquid at standard conditions.

The most significant difference between the UM EOS and the earlier RK modifications is the substance dependency for Z_c. The determined Z_c values, denoted Z_c^*, are listed for several alkanes from methane to tetradecane, and for some non-hydrocarbons. It is observed that these Z_c^* are slightly higher than the experimental values for all components. This is in agreement with the discussion given by Abbott (1979) who concludes that a horizontal translation of the critical point, such that $Z_c^*>Z_c$, (or $v_c^*>v_c$) allows the EOS to fit the steep portion of the critical isotherm better, loosing accuracy

only very close to the critical point.

Four different substance dependent properties are required to use the UM EOS: T_c, p_c, ω and Z_c^*. Since, Usdin and MCAuliffe do not propose a relation for Z_c^* in terms of any other property (e.g. ω), one additional parameter must be determined for undefined C_{7+} fractions.

The α function presented by Soave is used in the UM EOS, except that the slope m of α, is more complex and expressed in terms of T_r, ω and Z_c^*. Usdin and McAuliffe apply the mixing rules presented by Soave (1972). Liquid density prediction is improved with the UM EOS, but VLE accuracy is comparable with the earlier RK modifications. Thus, the increased complexity of α may not be fully repaid in improved VLE accuracy.

Fuller (1976) also used the Usdin and McAuliffe's cubic equation form with three adjustable EOS parameters. His objective was to improve liquid density prediction, while retaining the SRK's ability to calculate vapor pressures. In the subcritical temperature region saturated liquid volumes and vapor pressures are matched to experimental data at equilibrium conditions, i.e. equating fugacities in each phase. The procedure for determining Ω_a and Ω_b is similar to the procedure used in the ZJRK EOS (Joffe et al., 1970) resulting in temperature-dependent and substance-dependent EOS constants.

Fuller generalized the procedure for obtaining Ω_a, Ω_b and Z_c^* and expressed the constants as rather complex functions of parachor, P

$$Z_c^* = p_c v_c / RT_c = Z_c^*(P) \tag{1.34}$$

$$\Omega_a = \Omega_a(T_r, P) \tag{1.35a}$$

$$\Omega_b = \Omega_b(T_r, P) \tag{1.35b}$$

Fuller claims that the parachor is easily determined from a group contribution method. However, this makes the EOS more difficult to apply for mixtures containing heavy, undefined components. Trebble and Bishnoi (1986) found that the Fuller EOS, because of the temperature dependency of Ω_b, predicts negative heat capacity in the single phase region.

Whitson (1983b) also generalized the UM EOS along the lines previously drawn by Fuller, but proposed simpler functions for Ω_a and Ω_b. In addition Z_c^* was related to ω through the Pitzer correlation

$$Z_c^* = 0.291 - 0.080\omega \tag{1.36}$$

In 1980 Schmidt and Wenzel (SW) proposed a three-parameter EOS

$$p = \frac{RT}{v-b} - \frac{a_c\alpha(T)}{v^2+(1+3\omega)bv-3\omega b^2} \tag{1.37}$$

where acentric factor represents the third EOS parameter. Z_c^* is related through an intermediate parameter β_c to acentric factor

$$Z_c^* = \frac{1}{3(1+\beta_c\omega)} \tag{1.38}$$

where

$$\beta_c = 0.25989 - 0.0217\omega + 0.00375\omega^2 \tag{1.39}$$

Schmidt and Wenzel found that optimum volumetric and phase behavior predictions in the critical region are achieved with Z_c^* slightly higher than the experimental value.

The SW equation emulates, through the Z_c^*-ω relationship, the SRK and PR EOS for acentric factors equal to 0.0 and 0.35, respectively. Concerning liquid density prediction, these ω values represent the point at which each EOS give optimal performance, that is for SRK at ω=0.0, for PR at ω=0.35.

Schmidt and Wenzel express EOS constants Ω_a and Ω_b as functions of acentric factor

$$\Omega_a = \Omega_a(\omega) \tag{1.40a}$$

$$\Omega_b = \Omega_b(\omega) \tag{1.40b}$$

These coefficients are determined by applying the vdW critical criteria. The α function proposed by Soave was implemented in the SW EOS, but in a more complex form.

The main contribution of the SW equation as compared to earlier RK modifications is improved prediction of liquid densities and also vapor

pressures at low pressures.

Originally, a linear mixing rule was used to calculate the mixture acentric factor, ω_m. Later, this mixing rule has been modified by Nutakki et al. (1985) to

$$\omega_m = \frac{\Sigma_i \omega_i z_i b_i^{0.7}}{\Sigma_i z_i b_i^{0.7}} \tag{1.41}$$

Mixing rules for a_m and b_m are identical to those proposed by Soave (1972).

Firoozabadi (1988) shows that SW liquid densities in general are more accurate than for SRK or PR EOSs. He also concludes, based on a comparison of predicted K-values and saturation pressures for various gas condensates and crude oils, that the VLE performance of PR and SW is similar.

Harmens and Knapp (1980) proposed an EOS similar to the SW equation

$$p = \frac{RT}{v-b} - \frac{a(T)}{v^2-bcv-(c-1)b^2} \tag{1.42}$$

where the adjustable constants a, b, and c are determined as function of acentric factor. The temperature dependency in the α function is determined using the Soave approach. The resulting expression is given in terms of reduced temperature and acentric factor. Also, a separate expression is given for α in the supercritical region. However, in spite of this increased complexity, only marginal improvements are achieved (Edmister and Lee, 1983). Similar three-parameter EOS are also proposed by Patel and Teja (1982) and Heyen (1983).

For further description of three-parameter EOSs we refer to Adachi et al. (1983) who give a comprehensive review of sixteen cubic equations of state. They also propose a new three-parameter EOS.

Four-Parameter EOS

Martin proposed a volume cubic equation of state with four adjustable parameters. Two of these parameters are fixed by the vdW's critical criteria, and the two other can be determined from other algebraic criteria, or adjusted

to fit pure component experimental data. The Martin EOS is further discussed in the next section.

Adachi et al. (1984) also propose a four-parameter equation of state in the following form

$$p = \frac{RT}{v-b_1} - \frac{a(T)}{(v-b_2)(v+b_3)} \tag{1.43}$$

where the a parameter temperature dependency is determined following the Soave approach (1972). Parameters b_1, b_2, b_3 (and thus Z_c^*) are expressed in terms of acentric factor. A classical quadratic mixing rule is used to determine a_m, whereas linear mixing rules are applied to determine the other EOS parameters. Another four-parameter cubic EOS is proposed by Trebble and Bishnoi (1987).

The pressure-explicit cubic equation of state presented by Abbott (1979) is given on the most general form with five adjustable parameters. This equation can be written as

$$P = \frac{RT(v^2+\alpha v+\beta)}{v^3+\lambda v^2+\mu+\nu} \tag{1.44}$$

where α, β, λ, μ, and ν are the five EOS parameters.

EOS Comparisons

Trebble and Bishnoi (1986) compare accuracy and consistency of ten cubic EOS for polar and non-polar pure compounds. They concluded that "the Adachi-Lu-Sugie (1983) and the Patel-Teja EOSs appear to be more accurate than previous equations while maintaining thermodynamic consistency". Ahmed (1986) review the capabilities of eight different EOSs to the prediction of volumetric and phase behavior of gas condensate systems. He concludes that the SW EOS is superior to the other EOSs compared when considering prediction of volumetric properties of gas condensate systems. The PR is found to predict VLE most accurately. Firoozabadi (1988) recently compared phase behavior and volumetric prediction of reservoir fluids with the SRK, PR and SW EOSs. His work confirms the conclusions given by Ahmed.

1.3. Martin Four-Parameter EOS

The general two-term, four-parameter equation of state proposed by Martin (1979) expressed in terms of pressure is

$$p = \frac{RT}{v-b} - \frac{a}{(v-b+c)(v-b+d)} \tag{1.45}$$

where a, b, c, and d are the four EOS parameters to be determined.

The Martin EOS can be written in terms of the compressibility factor Z using the definition

$$pv=ZRT \tag{1.46}$$

Manipulating Eq. 1.45, results in

$$Z^3 + Z^2[-3B+(C+D-1)] + Z[3B^2-2B(C+D-1)+(A+CD-C-D)]$$
$$+ [-B^3+B^2(C+D-1)-B(A+CD-C-D)-CD] = 0 \tag{1.47}$$

Eq. 1.47 may be solved for Z by a direct solution or an iterative numerical method. Determination of the roots of cubic equations is discussed by Gundersen (1982) and Edmister and Lee (1983).

The EOS constants A, B, C, and D can be expressed in terms of the critical constants: Ω_a, Ω_b, Ω_c, and Ω_d

$$A = ap/(RT)^2 = \alpha\Omega_a p_r/T_r^2 \tag{1.48a}$$

$$B = bp/RT = \beta\Omega_b p_r/T_r \tag{1.48b}$$

$$C = cp/RT = \xi\Omega_c p_r/T_r \tag{1.48c}$$

$$D = dp/RT = \delta\Omega_d p_r/T_r \tag{1.48d}$$

Correction terms to the EOS constants: α, β, ξ, and δ, may all be temperature and substance dependent. From Eqs. 1.48 we see that

$$a = \alpha\Omega_a RT_c^2/p_c \tag{1.49a}$$

$$b = \beta\Omega_b RT_c/p_c \tag{1.49b}$$

$$c = \xi\Omega_c RT_c/p_c \tag{1.49c}$$

$$d = \delta\Omega_d RT_c/p_c \tag{1.49d}$$

Four criteria or equations may be specified to determine the four critical constants Ω_a, Ω_b, Ω_c, and Ω_d. Two of these may be determined using the vdW critical criteria and a third criterion is

$$Z = Z_c \tag{1.50}$$

Martin and Hou (1955) show that these three constraints can be fulfilled by requiring

$$(Z-Z_c)^3 = Z^3 - 3Z_cZ^2 + 3Z_c^2Z - Z_c^3 = 0 \tag{1.51}$$

at the critical point. Equating the Z terms in Eqs. 1.47 and 1.51 results in

$$3Z_c = -\Omega_b + (\Omega_c+\Omega_d+1) \tag{1.52a}$$

$$3Z_c^2 = 3\Omega_b^2 - 2\Omega_b(\Omega_c+\Omega_d+1) + \Omega_a + \Omega_c\Omega_d + \Omega_c + \Omega_d \tag{1.52b}$$

$$-Z_c^3 = -\Omega_b^3 + \Omega_b^2(\Omega_c+\Omega_d+1) - \Omega_b(\Omega_a+\Omega_c\Omega_d-\Omega_c-\Omega_d) - \Omega_c\Omega_d \tag{1.52c}$$

Martin suggests that a universal sum-chart value, denoted σ, be defined as

$$\sigma = Z_c - dz/dp_r \quad \text{at } p_r=0,\ T_r=0 \tag{1.53}$$

With this parameter it can be shown that a fourth criterion becomes

$$Z_c = \Omega_b - \Omega_a + \sigma \tag{1.54}$$

Substituting Eq. 1.54 into Eqs. 1.52a-c, results in the following expressions from which the EOS constants are determined

$$\Omega_b^3 + \Omega_b^2(3-3Z_c) + \Omega_b(3Z_c^2-6Z_c+2) + (-Z_c^3+3Z_c^2-2Z_c+1-\sigma) = 0 \tag{1.55a}$$

$$\Omega_a = \Omega_b + \sigma - Z_c \tag{1.55b}$$

$$\Omega_c^2 + \Omega_c(-u-1) + w = 0 \tag{1.55c}$$

$$\Omega_d = w/\Omega_c \tag{1.55d}$$

where

$$u = 3\Omega_b - 3Z_c \tag{1.56a}$$

$$w = Z_c^3 + 2\Omega_b^3 - 3Z_c\Omega_b^2 - 3\Omega_b(Z_c-\Omega_b)^2 \qquad (1.56b)$$

Ω_b is determined as the largest root of Eq. 1.55a. Either root of Eq. 1.55c can be chosen for Ω_c because of symmetry, and the second root will be equal to Ω_d. As proposed by Whitson (1983b), the fourth criterion can be expressed

$$\lambda = \Omega_c/\Omega_d \qquad (1.57)$$

He also discusses some limitations of the Martin EOS that arise from using the sum-chart value as a criterion for defining EOS constants; for example, that the last term of Eq. 1.55a should be less than zero. Table 1.1 specifies values for Z_c and σ, or alternatively Z_c and λ, which reduce the four-parameter Martin EOS to the PR, SRK/RK, or SW EOS.

TABLE 1.1 -- Critical Constants of Some Common EOS Defined in Terms of the Martin EOS Constants.

	Equation of State		
Martin EOS Constants	SRK/RK	PR	SW
Ω_a	0.42748	0.45723	$\Omega_a(\omega)$
Ω_b	0.08664	0.07780	$\Omega_b(\omega)$
Ω_c	Ω_b	$(2+\sqrt{2})\Omega_b$	$\Omega_c(\omega)$
Ω_d	$2\Omega_b$	$(2-\sqrt{2})\Omega_b$	$\Omega_d(\omega)$
λ	1	$2+\sqrt{2}$	$\lambda(\omega)$
Z_c	1/3	0.307401	$Z_c(\omega)$
σ	0.67417	0.68684	$\sigma(\omega)$

Coexistence of multiple phases in equilibrium requires that the chemical potential of each component in each phase be equal. For phase behavior calculations of petroleum reservoir fluids it is normally assumed that at most two phases exist. This may not be true for some mixtures at relative low temperatures where two immiscible liquid phases can be formed. In this study, however, it is assumed that only two phases are in coexistence, one liquid phase and one vapor phase. Also, it is assumed that fugacity can be applied to express the chemical potential in both phases.

The pure component fugacity coefficient, Φ, may be expressed in terms of the

fugacity, f, and pressure as

$$\ln\Phi = \ln(f/p) = \int_0^p (v/RT - 1/p)dp \tag{1.58}$$

Combining Eq. 1.58 with Eq. 1.45, results in

$$\ln\Phi = Z-1 - \ln(Z-B) + \frac{A}{C-D}\ln\left[\frac{Z-B+D}{Z-B+C}\right] \tag{1.59}$$

for pure components.

The fugacity coefficient of component i, Φ_i, in a multi-component mixture is defined as

$$\ln\Phi_i = \ln\left[\frac{f_i}{x_i p}\right] = \frac{-1}{RT}\int_\infty^v \left[\frac{\partial p}{\partial n_i} - \frac{RT}{v}\right]dv - \ln Z \tag{1.60}$$

where $\partial p/\partial n_i$ represents the derivative of pressure with respect to the mole number n_i.

Conventional mixing rules are used to determine the mixture EOS parameters a_m, b_m, c_m, and d_m

$$a_m = \sum_{i=1}^{N}\sum_{j=1}^{N} x_i x_j (a_i a_j)^{0.5}(1-k_{ij}) \tag{1.61a}$$

$$b_m = \sum_{i=1}^{N} x_i b_i \tag{1.61b}$$

$$c_m = \sum_{i=1}^{N} x_i c_i \tag{1.61c}$$

$$d_m = \sum_{i=1}^{N} x_i d_i \tag{1.61d}$$

which result in

$$\ln\Phi_i = -\ln(Z-B) + \frac{B_i}{Z-B} + \left[\frac{2A_{mj}}{C-D} + \frac{A(D_i-C_i)}{(C-D)^2}\right]\ln\left[\frac{Z-B+D}{Z-B+C}\right] + \frac{A}{D-C}\left[\frac{C_i-B_i}{Z-B+C} + \frac{B_i-D_i}{Z-B+D}\right] \quad (1.62)$$

where

$$A_{ij} = (A_iA_j)^{0.5}(1-k_{ij}) \quad (1.63a)$$

and

$$A_{mj} = \sum_{j=1}^{N} A_{ij} \quad (1.63b)$$

A_i, B_i, C_i, and D_i are given by Eqs. 1.48a-d for component i. A, B, C, and D are determined by combining Eqs. 1.48a-d with the corresponding Eqs. 1.61a-d.

A modification to the mixing rule for b_m was proposed by Turek et al. (1980), as given by Eq. 1.17. Similar mixing rules may be used for c_m and d_m. By combining Eq. 1.60 with Eq. 1.45, and using mixing rules as expressed by Eq. 1.17 for b_m, c_m, and d_m, Φ_i can be written as

$$\ln\Phi_i = -\ln(Z-B) + \frac{B_{mj}}{Z-B} + \left[\frac{2A_{mj}}{C-D} + \frac{A(D_{mj}-C_{mj})}{(C-D)^2}\right]\ln\left[\frac{Z-B+D}{Z-B+C}\right] + \frac{A}{D-C}\left[\frac{C_{mj}-B_{mj}}{Z-B+C} + \frac{B_{mj}-D_{mj}}{Z-B+D}\right] \quad (1.64)$$

where

$$\theta_{ij} = 0.5(\theta_i+\theta_j)(1-\ell_{ij}), \quad \theta=B,C,D \quad (1.65a)$$

$$\theta_{mj} = \sum_{j=1}^{N}(x_j-x_jx_i)\theta_{ij}, \quad \theta=B,C,D \quad (1.65b)$$

$$\theta = \sum_{i=1}^{N} \sum_{j=1}^{N} \theta_{ij}, \quad \theta=B,C,D \tag{1.65c}$$

These b_m, c_m, and d_m mixing rules reduces to the conventional linear mixing rule for $\ell_{ij}=0$.

1.4. Volume Translation

Introduction

Liquid volume predictions have never been accurate with two-parameter cubic EOSs such as the PR and SRK. This is illustrated in Fig. 1.2 where saturated liquid volume deviations determined at $T_r=0.7$ for the hydrocarbons C_1-C_{10} and N_2 are plotted versus acentric factor. This figure clearly reveals that the volume deviation is component dependent. Figs. 1.3 and 1.4 show deviation in saturated liquid volume for methane and n-hexane versus reduced temperature.

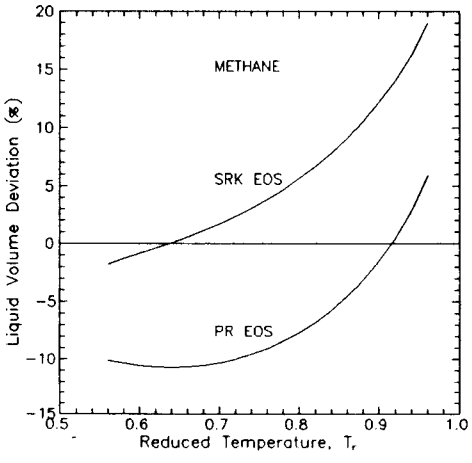

Fig. 1.3 Liquid molar volume deviation for methane as a function of reduced temperature, T_r (from Schmidt and Wenzel, 1980).

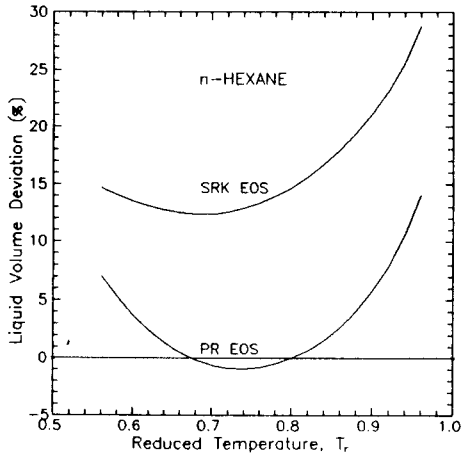

Fig. 1.4 Liquid molar volume deviation for n-hexane as a function of reduced temperature, T_r (from Schmidt and Wenzel, 1980).

It can be seen from these figures that the PR EOS underestimates saturated liquid volumes of light hydrocarbons (C_1-C_6), except very close to T_r=1.0, and overestimates liquid volumes of components heavier than n-heptane. Optimal volume prediction with the PR EOS is obtained for a component with ω=0.35. SRK EOS predicts saturated liquid volumes which are consistently too high, except for very light components ($\omega \approx 0.0$). The difference between these two EOSs is mainly due to the choice of universal Z_c-factors; Z_c=0.307401 for PR and Z_c=1/3 for SRK. Figs. 1.2-4 also show that liquid volume deviations resulting from the SW EOS are relatively small. This is due to a component dependent Z_c-factor. Pure component vapor molar volumes predicted from the PR, SRK and the SW EOSs are comparable, and are in general quite accurate except in the critical region (Firoozabadi, 1988).

Liquid volumes of petroleum mixtures will usually reflect the density errors on a component basis. For the PR EOS there is a tendency for component errors to cancel, yielding relatively accurate mixture liquid volumes. Even so, the PR EOS may predict liquid densities for reservoir fluids with more than 10% error. PR predicted vapor phase Z-factors for reservoir fluids may be 5% in error and even greater with the SRK EOS.

In an attempt to fit the EOS predicted critical isotherm to measured data, Martin (1967) introduced a concept he called volume translation which can be described as follows. Consider the coexistence curve for a pure component in a p-v diagram and its critical isotherm as shown in Fig. 1.5. A linear

translation of the volume coordinate will result in a horizontal shift in the critical isotherm along the volume axis, and the critical volume may be matched more precisely. Also subcritical isotherms and the coexistence curve will be horizontally shifted. This shift in volume is relative large (in percentage) at small volumes and thus has a significant effect on liquid molar volume prediction. At large volumes the shift in volume is small on a percentage basis, and may not influence vapor molar volume prediction very much. Martin propose that a volume translation parameter should be determined such that the critical isotherm match measured data where it is desired best to fit these data.

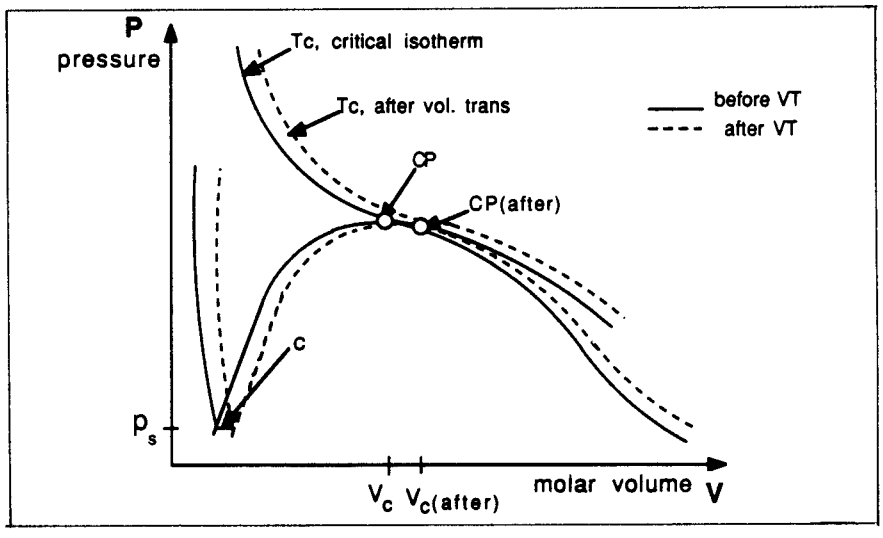

Fig. 1.5 p-v diagram for a pure component illustrating the effect of volume translation.

Peneloux et al. (1982) further developed the volume translation concept along the lines first drawn up by Martin, even though Martin is not referenced in their work. They defined a "correct" molar volume, $\underline{v}$, in terms of a volume translation constant, c, and SRK EOS predicted molar volume v_{EOS}

$$\underline{v} = v_{EOS} - c \tag{1.66}$$

For the SRK EOS, inserting the correction term yields

$$p = \frac{RT}{(\underline{v}-\underline{b})} - \frac{a}{(\underline{v}+c)(\underline{v}+\underline{b}+2c)} \tag{1.67}$$

with $\underline{b}=b_{EOS}-c$. Peneloux et al. show that Eq. 1.67 yields the same vapor-liquid equilibrium (VLE) predictions as the original SRK EOS. This is because

constant c vanishes in the VLE equations, i.e. fugacity ratios. This was a significant contribution to the volume translation technique, and as a consequence the method became very easy to implement in existing two-parameter EOS models.

Pure Components

Peneloux et al. chose to define the volume correction constant c for a component as the difference between experimental v_e and EOS-predicted saturated liquid volume v_{EOS} at T_r=0.7

$$c = v_{EOS} - v_e \Big|_{T_r=0.7} \tag{1.68}$$

They also present a relation for c in terms of T_c, p_c and Rackett compressibility factor, Z_{RA}, for pure hydrocarbons in the range C_1-C_{10}

$$c = 0.40768 \frac{RT_c}{p_c} (0.29441 - Z_{RA}) \tag{1.69}$$

Jhaveri and Youngren (1984) applied the volume translation concept to the PR EOS. These authors define the volume correction constant c in terms of the EOS b parameter as a dimensionless shift parameter, s

$$s = c/b \tag{1.70}$$

Shift parameters are presented for some light and intermediate hydrocarbons (C_1-C_6). These parameters are also determined such that Eq. 1.70 combined with e.g. 1.68 will fit experimental saturated liquid molar volumes at T_r=0.7. A simple relation expressing the shift parameter in terms of molecular weight is also proposed by Jhaveri and Youngren

$$s = 1 - dM^{-e} \tag{1.71}$$

Reasonable shift parameters can be determined for light and intermediate hydrocarbons (C_1-C_6) with d=1.4 and e=0.0685.

Chou and Prausnitz (1988) refined the procedure presented by Peneloux et al. (1982) for improving SRK volume prediction. The volume correction c determined at T_r=0.7 for a saturated component, was adjusted to match the true volume deviation at higher reduced temperatures, i.e. $0.7 \leq T_r < 1.0$. Chou and Prausnitz applied their method to several pure components and a few binary mixtures, and

concluded that volume prediction is improved with their method.

Mixtures

For a mixture with N components the total liquid volume correction, c_L, is determined using a linear mixing rule

$$c_L = \sum_{i=1}^{N} x_i c_i \tag{1.72}$$

where x_i is the liquid mole fraction. The corrected mixture liquid volume, v_L, then becomes

$$v_L = v_{L,EOS} - c_L \tag{1.73}$$

where $v_{L,EOS}$ denotes EOS predicted liquid volume. For consistency, volume translation is also applied to correct the vapor phase molar volume. Then vapor volume correction, c_V, is determined from

$$c_V = \sum_{i=1}^{N} y_i c_i \tag{1.74}$$

where y_i is the vapor mole fraction, and the vapor phase volume, v_V, becomes

$$v_V = v_{V,EOS} - c_V \tag{1.75}$$

where $v_{V,EOS}$ denotes EOS predicted vapor volume. Peneloux et al. show that volume translation applied to mixtures do not affect VLE results because the effect of c cancels when ratios of fugacities are used.

Petroleum Fractions

Peneloux et al. (1982) apply Eq. 1.69 to estimate volume translation constant c for heavy petroleum fractions. Z_{RA} are expressed by polynomials of fifth degree for paraffins, napthenes and aromatics. Polynomial coefficients were determined by matching experimental data (T_c,p_c,ω,ρ_L) of heavy hydrocarbons and petroleum fractions (Robinson and Peng, 1978). However, these polynomials show some peculiar behavior when extrapolated to heavy fractions. Fig. 1.6 shows that estimated Z_{RA} values increase exponentially for fractions with carbon number higher than 50 (M>700). Thus, estimating the volume correction parameter from these correlations can not be recommended for heavy petroleum fractions.

Jhaveri and Youngren (1984) suggest that the shift parameter s for petroleum fractions can be determined from Eq. 1.71. They propose adjusting d and e such that pseudocomponent liquid density match the experimental specific gravity at standard conditions. Jhaveri and Youngren report d and e values to determine s for heavy components with various molecular structure (PNA), and for several C_{7+} fractions of reservoir fluids. We have found that good initial estimates for d and e are d=2.46 and e=0.18, respectively.

Chien and Monroy (1986) present a method for predicting the shift parameter s for petroleum fractions with the PR EOS. The resulting correlation is rather complex, and relates shift parameter to molecular weight, boiling point, and specific gravity. Also, this method is based on a specific characterization procedure; for example critical properties are estimated from the original Riazi-Daubert correlations (Riazi and Daubert, 1980), and acentric factor and binary interaction coefficients are estimated from correlations proposed by Chien and Monroy (in the same work).

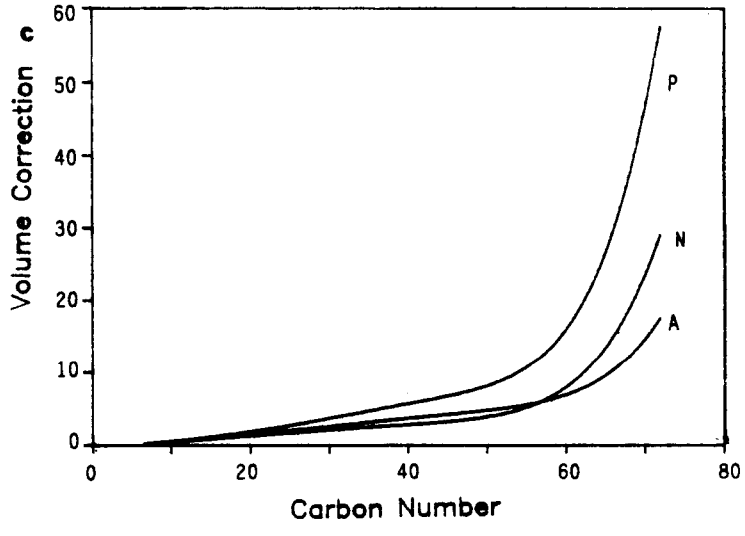

Fig. 1.6 Volume correction constant c versus carbon number. c is calculated from the Peneloux et al. c-correlations for P-, N-, and A- fractions.

Proposed Methods

Deviation between true and EOS predicted saturated molar volumes for pure components is a function of reduced temperature. Thus, a temperature dependent shift parameter correlation for light and intermediate components has been developed using the following procedure:

1. Specify $T_r=T/T_c$ within the interval from T_b/T_c to 1.0.

2. Estimate saturated vapor pressure, p_s, from the Lee-Kesler vapor pressure correlation, (API Technical Data Book, 1976).

3. Adjust p_s to equalize component fugacities in the liquid and the vapor phase.

4. At p_s and T, calculate the "true" saturated liquid molar volume, v_{sL}, from the modified Rackett correlation given in terms of critical properties; T_c, p_c, and the Rackett compressibility factor, Z_{RA}, (API Technical Data Book, 1976)

$$v_{sL} = [RT_c/p_c]\, Z_{RA}^{[1+(1-T_r)^{2/7}]} \tag{1.76}$$

5. Calculate EOS saturated liquid molar volume, v_{sL} ,

$$v_{sL,EOS} = Z_{sL}RT/p_s \tag{1.77}$$

where Z_{sL} represents the EOS predicted liquid compressibility factor.

6. Determine the shift parameter; $s=(v_{sL,EOS}-v_{sL})/b$, where $b=\Omega_b RT_c/p_c$.

7. For each component, repeat the procedure at various reduced temperatures within the interval $[T_b/T_c,0.98]$.

SRK and PR EOS shift parameters were generated for several light and intermediate hydrocarbons. A correlation given in terms of reduced temperature and acentric factor are proposed to fit these shift parameters

$$s = |T_r-a_1|^{a_2} + a_3 + a_4\omega + a_5\exp[a_6(T_r-1)] \tag{1.78}$$

One set of constants a_1-a_6 was determined from non-linear regression to fit the volume deviation data for the PR EOS. Another set of constants was determined to fit the volume deviation data for the SRK EOS. These two sets are presented in Table 1.2. Eq. 1.78 fits the generated PR and the SRK EOS shift parameters with absolute average deviations of 0.95 and 0.78 percent,

respectively. Components lighter than propane is not included since usually $T>T_c$ in petroleum engineering applications.

TABLE 1.2 -- Best-Fit Correlation Constants of Eq. 1.78 for PR and SRK EOSs.

Constant	PR EOS	SRK EOS
a_1	0.74145	0.90385
a_2	1.35489	3.71304
a_3	-0.16410	0.0
a_4	0.47894	0.58662
a_5	0.42829	0.36907
a_6	25.3301	10.3691
AAD,%	0.95	0.78

Note:
1. Components for which Eq. 1.78 is valid: C_3, iC_4, nC_4, iC_5 nC_5, nC_6-C_{10}, benzene, cyclohexane, 2,3-dimetylbutane, 2,2-dimethylpentane.

In Figs. 1.7a,b,c, PR EOS shift parameters are plotted versus reduced temperature; Fig 1.7a for N_2, H_2S and CO_2, Fig. 1.7b for C_1-nC_6, and Fig. 1.7c for C_7-C_{10}. Figs. 1.8a,b,c show similar plots for SRK EOS shift parameters.

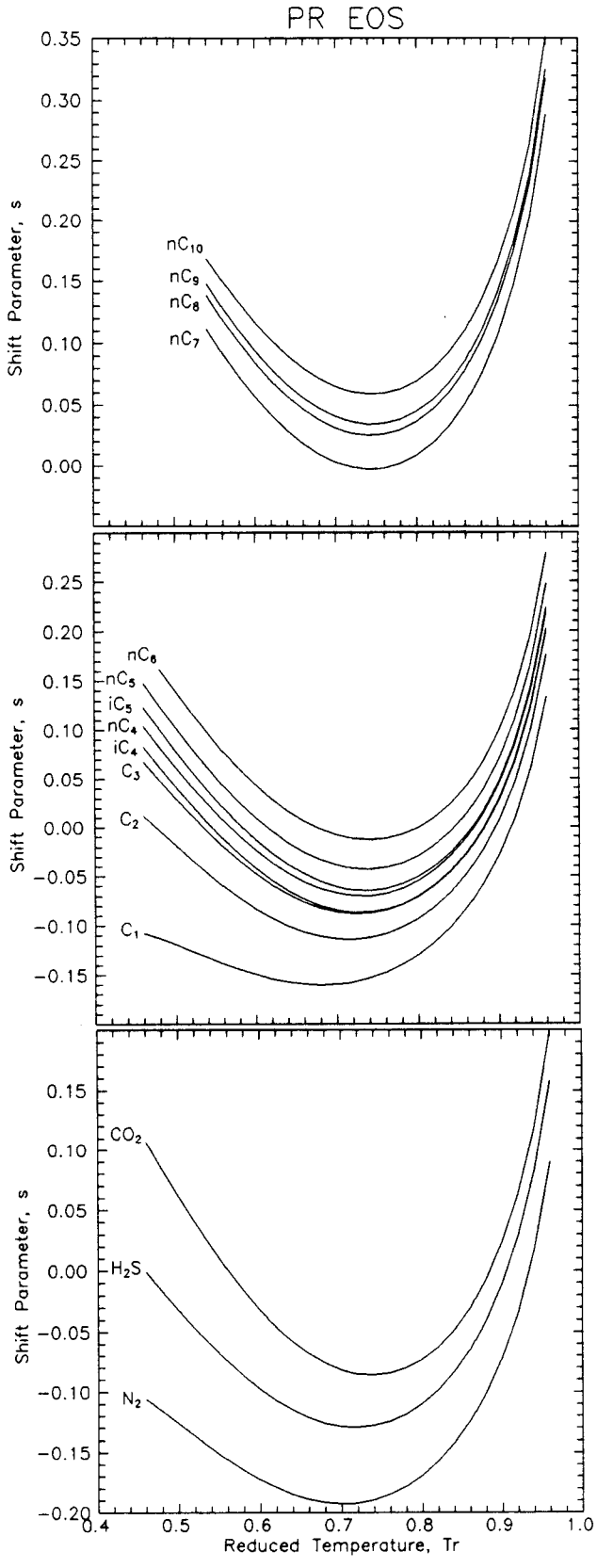

Fig. 1.7 PR EOS shift parameters for various components at subcritical temperatures in the range $0.4 \leq T_r \leq 1.0$.

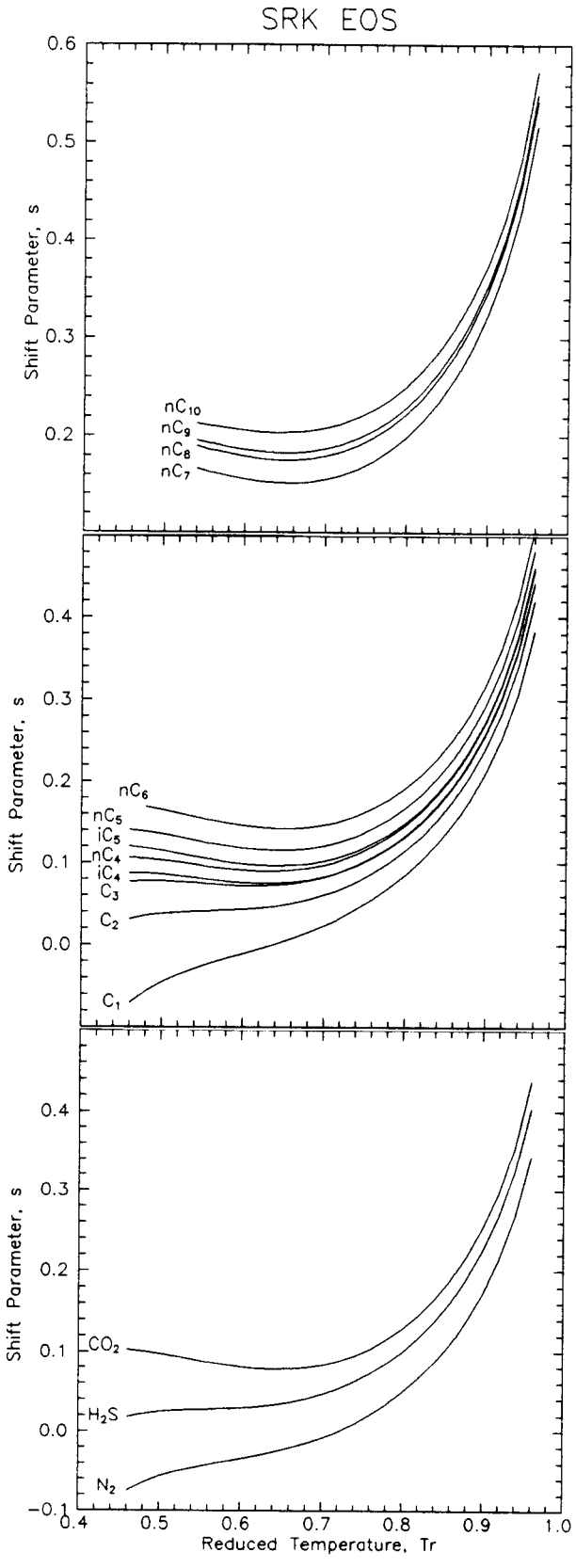

Fig. 1.8 SRK EOS shift parameters for various components at subcritical temperatures in the range $0.4 \leq T_r \leq 1.0$.

Table 1.3 presents PR and SRK EOS shift parameters for some pure hydrocarbons (C_1-C_{10}) and light non-hydrocarbons (N_2, CO_2, and H_2S). These are determined to match saturated liquid volumes obtained from Eq. 1.77 at T_r=0.7.

TABLE 1.3 -- Shift Parameters For Various Saturated Components at Reduced Temperature of 0.7.

Component	PR EOS	SRK EOS
Nitrogen	-0.1927	-0.0079
Carbon Dioxide	-0.0817	0.0833
Hydrogen Sulfide	-0.1288	0.0466
Methane	-0.1595	0.0234
Ethane	-0.1134	0.0605
Propane	-0.0863	0.0825
iso-Butane	-0.0844	0.0830
n-Butane	-0.0675	0.0975
iso-Pentane	-0.0608	0.1022
n-Pentane	-0.0390	0.1209
Benzene	-0.0400	0.1215
Cyclo-Hexane	-0.0688	0.0954
2,3-Dimetylbutane	-0.0463	0.1144
n-Hexane	-0.0080	0.1467
2,2-Dimethylpentane	-0.0370	0.1212
n-Heptane	0.0033	0.1554
n-Octane	0.0314	0.1794
n-Nonane	0.0408	0.1868
n-Decane	0.0655	0.2080
n-Dodecane	0.0850	0.2245

Simulation of hydrocarbon phase behavior with an EOS are performed at various (p,T) conditions. These may vary from standard conditions to high pressures and temperatures encountered in petroleum reservoirs; e.g., p≈6000 psia [400 bar] and T≈300°F [150°C]. For light components such as CO_2, N_2, C_1, C_2, and to some extent C_3, these temperatures are higher than the respective critical temperatures, $T>T_c$. In this work shift parameters have been determined also for such components. The following procedure resulted in shift parameters expressed as a function of reduced temperature for some components which usually have $T_r>1$:

1. Specify $T_r=T/T_c$ where T is within the range from 60° to 300°F [15.5°,149°C] and such that $T_r>1$.

2. Specify pressure p within the interval from 15 to 6000 psia [1.0, 413.8 bar].

3. Calculate "true" molar volume, v_{LK}, at conditions (p,T) from the Lee-Kesler compressibility factor correlation (API Technical Data Book, 1976)

$$v_{LK} = Z_{LK}RT/p \tag{1.79}$$

4. Calculate EOS molar volume, v_{EOS}, at conditions (p,T).

5. Determine the shift parameter at (p,T);

$$s(p,T)=(v_{LK}-v_{EOS})/b \text{ where } b=\Omega_b RT_c/p_c.$$

6. At reduced temperature $T_r=T/T_c$, calculate a weight averaged shift parameter, $s(T_r)$, based on $s(p_j,T)$ estimated at j=1,...,N various pressure levels, according to

$$s(T_r) = \frac{\sum_{j=1}^{N} w_j s(p_j,T_r)}{\sum_{j=1}^{N} w_j} \tag{1.80}$$

where the weighting factor, w_j, is expressed

$$w_j = \left| \frac{s(p_j,T_r)b}{v_{LK}} \right| \tag{1.81}$$

For each component this resulted in a weighted shift parameter at various reduced temperatures, and these data are described for the PR EOS using a linear relationship between s and T_r

$$s = a_1 + a_2T_r \tag{1.82}$$

The coefficients a_1 and a_2 of Eq. 1.82 are shown in Table 1.4 for the actual components. The same procedure was applied to determine SRK EOS supercritical shift parameters. The resulting correlation is given by

$$s = a_1 + a_2T_r + a_3T_r^2 \tag{1.83}$$

The coefficients a_1, a_2, and a_3 of Eq. 1.83 are shown in Table 1.5. PR and SRK shift parameters are plotted versus reduced temperatures in Figs. 1.9 and 1.10, respectively.

TABLE 1.4 -- Correlation Coefficients in Eq. 1.82 for the PR EOS for Various Components.

	PR EOS	
Component	a_1	a_2
Carbon Dioxide	0.42109	-0.31366
Nitrogen	-0.09984	-0.02984
Methane	-0.09427	-0.03728
Ethane	-0.12318	0.00189
Propane	-0.02243	-0.06774

TABLE 1.5 -- Correlation Coefficients in Eq. 1.83 for the SRK EOS for Various Components.

	SRK EOS		
Component	a_1	a_2	a_3
Carbon Dioxide	-0.17715	0.76596	-0.32755
Nitrogen	0.08745	-0.00124	0.0
Methane	0.26240	-0.16439	0.03705
Ethane	0.22896	-0.05771	0.0
Propane	0.22363	-0.03603	0.0

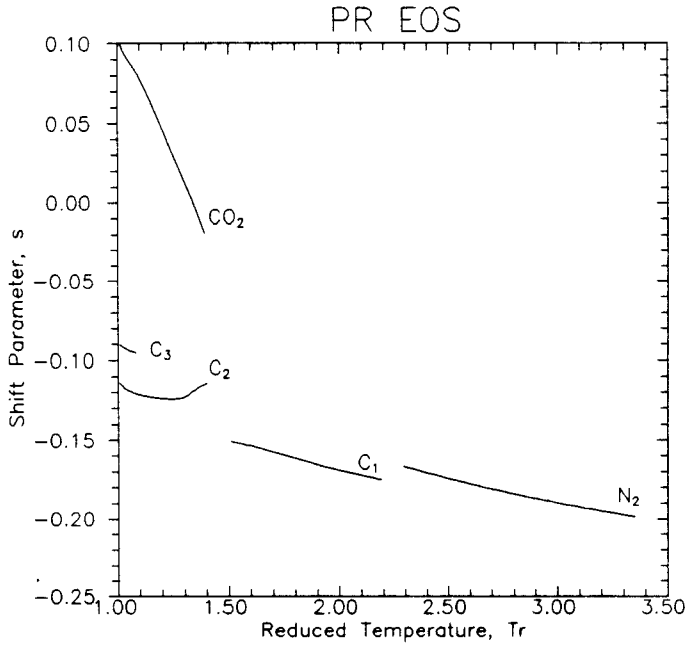

Fig. 1.9 PR EOS shift parameters for various light components at supercritical temperatures, T_r>1.0.

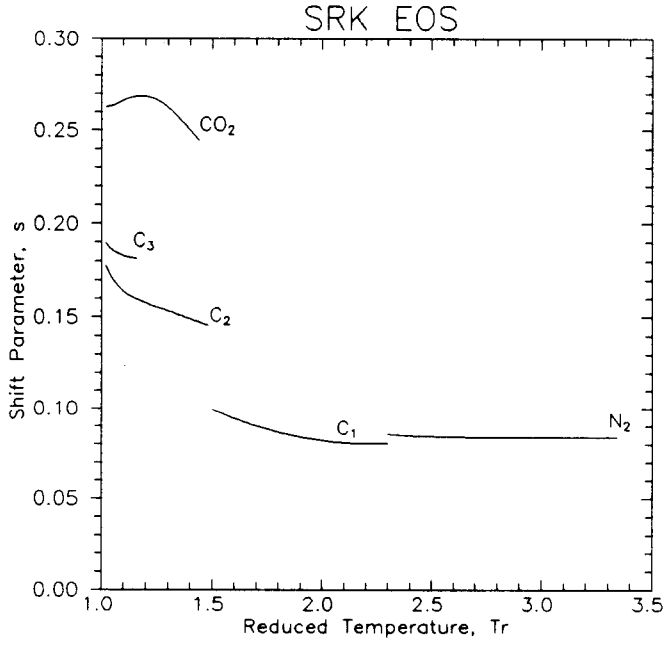

Fig. 1.10 SRK EOS shift parameters for various light components at supercritical temperatures, T_r>1.0.

CHAPTER 2
VAPOR-LIQUID EQUILIBRIUM CALCULATIONS

2.1 Introduction

An EOS based phase behavior model for prediction of phase and volumetric behavior of petroleum reservoir fluids includes routines for performing stability analysis, isothermal flash and saturation pressure calculations. These routines are all used in conjunction with simulating pressure-volume-temperature (PVT) experiments such as constant composition expansion (CCE), differential liberation expansion (DLE), and constant volume depletion, (CVD). Also, multi-contact vaporization (MCV) experiments can be simulated. Several descriptions of such PVT experiments are found in the literature including Pedersen et al. (1984b), Jhaveri and Youngren (1986) and Zick (1987).

A successive substitution (SS) related method, called the General Dominant Eigenvalue Method, is used to promote convergence of the non-linear system of equations introduced in VLE calculations. Some example calculations show that the method usually results in rapid convergence even in the critical region.

2.2 Stability Analysis

Stability analysis determines the minimum number of stable phases present for a given system at specified pressure and temperature. As such it may be used as a preliminary step in flash calculations to ensure that two phases exist and to provide reliable K-value estimates for the flash calculation. Stability analysis is also incorporated in saturation pressure calculations.

Baker et al. (1982) have shown that equating component fugacities in the vapor and liquid phase is not a sufficient criterion for equilibrium. In addition the Gibbs free energy of the system must be minimized, which Baker at al. show is equivalent to the condition that Gibbs tangent plane do not intersect the Gibbs energy surface. Baker et al. presents a mathematical proof for this

Gibbs tangent plane criterion and Michelsen (1982a) gives a numerical algorithm for performing stability analysis based on it.

Stability of an N-component mixture for which normalized mole fractions are given by $\underline{z}=[z_1,\ldots,z_N]^T$, requires that its Gibbs free energy, G_o, is at a global minimum

$$G_o = \sum_{i=1}^{N} z_i \mu_i(\underline{z}) \tag{2.1}$$

at the specified pressure and temperature. $\mu_i(\underline{z})$ are the chemical potentials of components i in the mixture. Suppose that one mole of the mixture is split in two phases. ϵ moles ($\epsilon<<1$) are transferred to the new phase (II) with composition $\underline{y}=[y_1,\ldots,y_N]^T$ with chemical potentials $\underline{\mu}(\underline{y})$ and $1-\epsilon$ moles are left in phase I. An energy balance is set up to determine if this phase split results in a positive or negative change in the mixture Gibbs free energy:

$$\Delta G = G_I + G_{II} - G_o \tag{2.2}$$

where

$$G_I = G_o - \epsilon[\sum_{i=1}^{N} y_i \mu_i(\underline{z})] \tag{2.3a}$$

and

$$G_{II} = \epsilon[\sum_{i=1}^{N} y_i \mu_i(\underline{y})] \tag{2.3b}$$

If the phase split represents a lower energy level such that $G_I+G_{II}<G_o$ ($\Delta G<0$) for all possible compositions $\underline{y}$, the mixture is unstable and will split into at least two phases. However, if $\Delta G\geq 0$, the mixture with composition $\underline{z}$ is stable and no phase split will occur.

The tangent plane distance (TPD) is illustrated in Fig. 2.1 for a binary mixture with feed composition $\underline{z}$ (z_1,z_2). $G(\underline{y})$ represents the Gibbs energy surface (here: a curve) for all trial compositions $\underline{y}$ (y_1,y_2). Thus

$$G(\underline{y}) = \sum_{i=1}^{N} y_i \mu_i(\underline{y}) \tag{2.4}$$

A straight line, denoted T in Fig. 2.1, is tangent to the energy curve at

composition $\underline{z}$. The energy level of this tangent at composition $\underline{y}$ is expressed as (Baker et al. 1982)

$$T(\underline{y}) = G(\underline{z}) + \sum_{i=1}^{N} \left[\frac{\partial G(\underline{z})}{\partial y_i} \right] (y_i - z_i) = \sum_{i=1}^{N} y_i \mu_i(\underline{z}) \qquad (2.5)$$

The tangent plane distance, TPD, at composition $\underline{y}$ can be defined as the distance between the tangent $T(\underline{y})$ and the Gibbs energy surface $G(\underline{y})$

$$TPD(\underline{y}) = G(\underline{y}) - T(\underline{y}) \qquad (2.6)$$

The condition for stability of a mixture for all possible compositions $\underline{y}$, is that $TPD(\underline{y}) \geq 0.0$. This can be expressed in terms of chemical potential by combining Eqs. 2.4 and 2.5 into Eq. 2.6

$$TPD = \sum_{i=1}^{N} y_i [\mu_i(\underline{y}) - \mu_i(\underline{z})] \geq 0 \qquad (2.7)$$

or, when referring to Fig. 2.1, the energy curve G must be above the tangent T at any composition $\underline{y}$. This is not the case for the $\underline{z}$ chosen in Fig.2.1, so the feed will split into two phases.

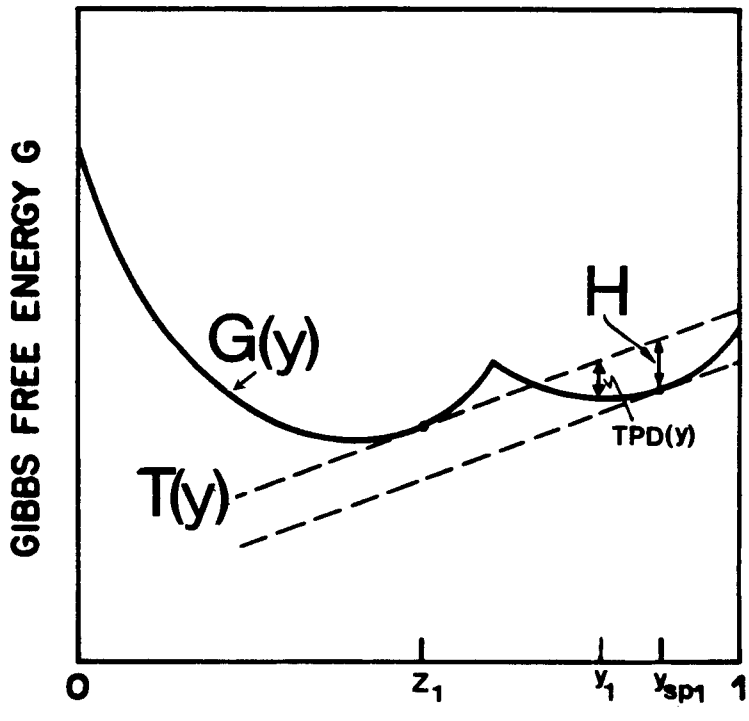

Fig. 2.1 Molar Gibbs free energy of mixing for a binary mixture with composition $\underline{z}$. Also shown is the tangent plane and tangent plane distance (from Nghiem and Li, 1988).

At composition $\underline{y}_{sp}$ the tangent $T(\underline{y}_{sp})$ is parallel to the tangent $T(\underline{z})$. This point is called a stationary point, and represents a local minimum in the Gibbs energy surface where the derivatives with respect to all independent variables equal zero. N-1 such local minima exist for an N-component mixture. This can mathematically be expressed as

$$\frac{\partial[TPD(\underline{y}_{sp})]}{\partial y_i} = 0, \quad i=1,\ldots,N-1 \tag{2.8}$$

Combining Eqs. 2.8 and 2.7 results in

$$\mu_i(\underline{y}_{sp})-\mu_i(\underline{z}) = H, \quad i=1,\ldots,N \tag{2.9}$$

where H is a constant. The corresponding TPD-value is written

$$TPD(\underline{y}_{sp}) = \sum_{i=1}^{N} y_i H = H \tag{2.10}$$

since $\Sigma_i y_i=1$, $i=1,\ldots,N$.

For the binary mixture illustrated in Fig. 2.1, H can be interpreted as the vertical distance between the two parallel tangents to the energy curve at compositions $\underline{y}$ and $\underline{z}$, respectively. It is also seen that H must be equal to TPD because at $\underline{y}=\underline{z}$ ($\underline{z}$ is also a stationary point) the value of H is zero. Stability of a mixture requires that $H \geq 0$ at all stationary points.

In terms of the fugacity coefficient Φ and mole fractions the stability criterion can be formulated as (Michelsen, 1982a)

$$g(\underline{y}) = \frac{TPD(\underline{y})}{RT} = \sum_{i=1}^{N} y_i[\ln y_i+\ln\Phi_i(\underline{y})-\ln z_i-\ln\Phi_i(\underline{z})] \geq 0 \tag{2.11}$$

and the stationarity criterion becomes

$$\ln y_i + \ln\Phi_i(\underline{y}) - \ln z_i - \ln\Phi_i(\underline{z}) = h \tag{2.12}$$

where h is a constant. If a variable Y_i, which may be interpreted as a mole number, is defined as

$$Y_i = y_i e^{-h} \tag{2.13}$$

Eq. 2.12 becomes

$$\ln Y_i - \ln\Phi_i(\underline{y}) - \ln z_i - \ln\Phi_i(\underline{z}) = 0 \tag{2.14}$$

Stability at all stationary points requires that $h \geq 0$, which is equivalent to requiring that $\Sigma_i Y_i \leq 1$, $i=1,\ldots,N$. If $\Sigma_i Y_i > 1$, $i=1,\ldots,N$, a new phase is formed with estimated composition given by

$$y_i = Y_i / \left(\sum_{j=1}^{N} Y_j \right) \tag{2.15}$$

Component fugacities are composition dependent, especially at high pressures and in the critical region. Thus, Eq. 2.14 becomes a non-linear function of composition and an iterative method with K-values as iteration-variables can be used to determine the compositions Y_i. Here, an accelerated successive substitution (SS) method is used, as can be expressed by

$$X_i^{(n+1)} = X_i^{(n)} + \Delta X_i^{(n)} \tag{2.16}$$

where $X_i = \ln Y_i$. For three or four subsequent SS iterations, ΔX_i is given by direct substitution

$$\Delta X_i^{(n)} = \ln\left[\frac{1}{\sum_{j=1}^{N} Y_j} \frac{f_i(\underline{z})}{f_i(\underline{y})} \right]^{(n)} \tag{2.17}$$

Each fourth or fifth iteration, a promotion step is performed to accelerate convergence with the General Dominant Eigenvalue Method (GDEM) of Crowe and Nishio (1975). The GDEM method is described in Section 2.5, and ΔX_i for the promotion step is determined by Eq. 2.61.

A convergence criterion for the stability analysis calculation may be defined as follows (Zick, 1985)

$$\sum_{i=1}^{N} \left[1 - \frac{f_i(\underline{z})}{\sum_{j=1}^{N} Y_j \, f_i(\underline{y})} \right]^2 < \epsilon \tag{2.18}$$

where typically $\epsilon = 10^{-12}$. A trivial solution check is given by

$$\sum_{i=1}^{N} (1-K_i^2) \leq 10^{-4} \tag{2.19}$$

Initially, the new phase composition may be estimated from empirical K-value relations. Such relations are proposed by Wilson (1969)

$$K_i = p_{ri}^{-1} e^{5.3727(1+\omega_i)(1-T_{ri}^{-1})} \tag{2.20}$$

and Whitson and Torp (1981)

$$K_i = \left[\frac{p_{ci}}{p_k} \right]^{A-1} p_{ri}^{-1} e^{5.3727(1+\omega_i)(1-T_{ri}^{-1})} \tag{2.21a}$$

where

$$A = 1-\left[\frac{p-p_{sc}}{p_k-p_{sc}} \right]^{0.6} \tag{2.21b}$$

p_k is an estimate for convergence pressure and p_{sc} is the atmospheric pressure. The Wilson relation can be shown to be identical to the graphical $K_i$vs.F_i-plot given by Hoffmann et al. (1952) at atmospheric pressure. Eqs. 2.21a and 2.21b generalizes the Wilson relation by making use of the fact that the ($K_i$vs.F_i)-plot varies as a function of pressure. Thus, the Whitson-Torp K-value relation intuitively should be better than the Wilson relation at $p>p_{sc}$, provided p_k is reasonable. However, it is recommended that initial K-values for the stability analysis be obtained from the Wilson relation, because "poor" initial K-values give less chance of arriving at a trivial solution when a non-trivial solution exists.

The stability test should be performed twice for the same feed at specified conditions (p,T), once with the feed defined as a liquid-like phase, resulting in Y_{Lf}, and once with the feed defined as a vapor-like phase, resulting in Y_{Vf}. Initially, composition of the second phase is obtained from K-value estimates (Eq. 2.20) as $Y_{i,Lf}=K_i z_i$ and $Y_{i,Vf}=K_i/z_i$, respectively. Instability may be indicated by none, one or both of these two tests, depending on the calculated Y_{Lf} and Y_{Vf}. Fig. 2.2 shows the phase envelope with unstable and metastable regions for a reservoir oil. The unstable region is characterized by $Y_{Lf}>1.0$, $Y_{Vf}>1.0$. In the upper metastable region, $Y_{Lf}>1.0$ and $Y_{Vf}<1.0$, and vice versa for the lower metastable region. The stability limit defines the p-T conditions at which $Y_{Lf}=1.0$ or $Y_{Vf}=1.0$. In Fig. 2.3. the interpretation of

these regions is graphically given in terms of Y_{Lf} and Y_{Vf} behavior along the line A-A in Fig. 2.2.

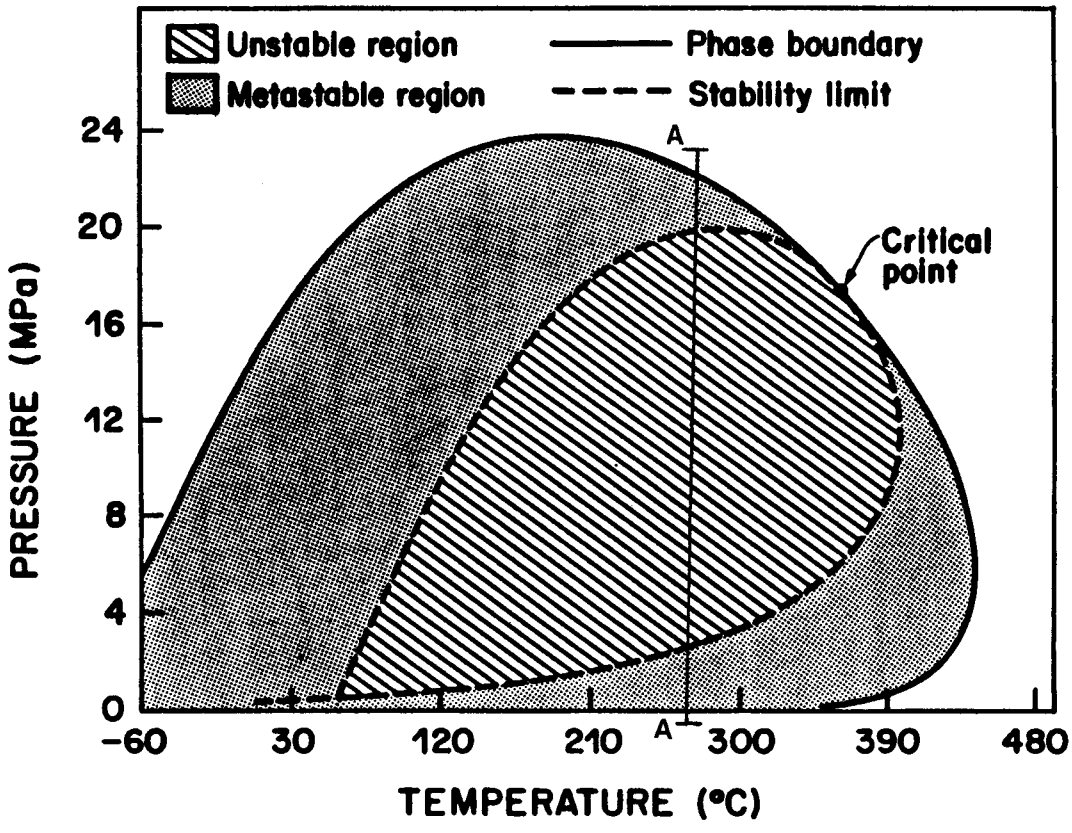

Fig. 2.2 Phase envelope of a reservoir oil with unstable and metastable regions indicated (from Nghiem and Li, 1988).

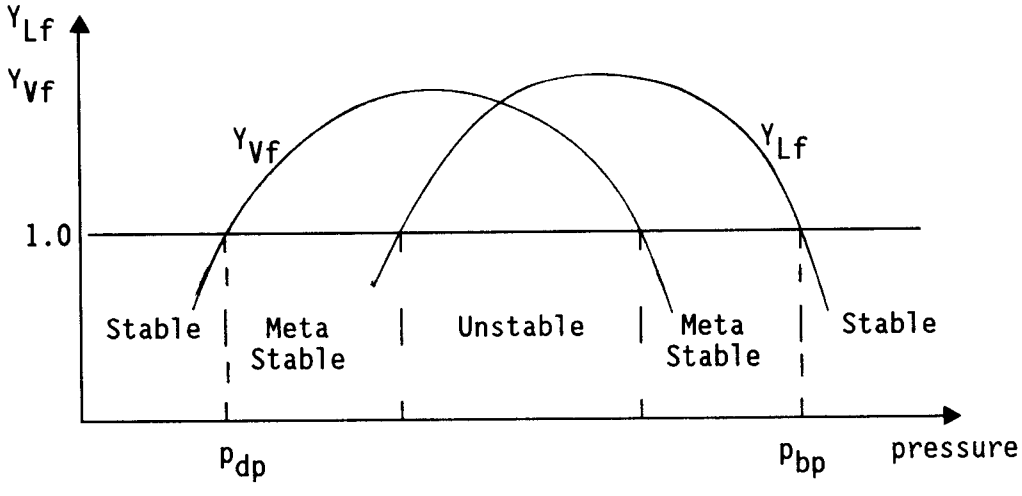

Fig. 2.3 Behavior of molenumbers Y_{Lf} and Y_{Vf} at constant temperature, $T<T_c$, for a reservoir oil.

2.3 Two-Phase Flash

For a given pressure, temperature, and feed composition, the flash or phase-split calculation results in the relative amount of each phase, and the respective phase equilibrium compositions. The flash equilibrium problem is illustrated in Fig. 2.4 for a binary mixture in terms of Gibbs free energy and the tangent plane. The mixture with feed composition $\underline{z}$ is here split into two phases with equilibrium compositions $\underline{x}$ and $\underline{y}$.

The solution to the phase-split problem is restricted by three constraints:

1. No net driving force, chemical or gravity forces, can exist in an equilibrium mixture, causing the components to move from one phase to another, i.e. at equilibrium the change in Gibbs free energy associated with the phase-split must be at a minimum.

2. Chemical potential for each component in each phase must be equal.

3. The component material balance must be preserved.

When one mole of an N-component system with feed composition $\underline{z}$ is flashed, the component material balance can be written

$$(1-V)x_i + Vy_i = z_i, \quad i=1,\ldots,N \tag{2.22}$$

where V is vapor mole fraction. The term (1-V) represents liquid mole fraction, L, since L+V=1. x_i and y_i represent liquid and vapor phase mole fractions of component i, respectively, and should like z_i sum to unity

$$\sum_{i=1}^{N} x_i = \sum_{i=1}^{N} y_i = \sum_{i=1}^{N} z_i = 1 \tag{2.23}$$

The equilibrium constant, K_i, for component i is given by

$$y_i = K_i x_i, \quad i=1,\ldots,N \tag{2.24}$$

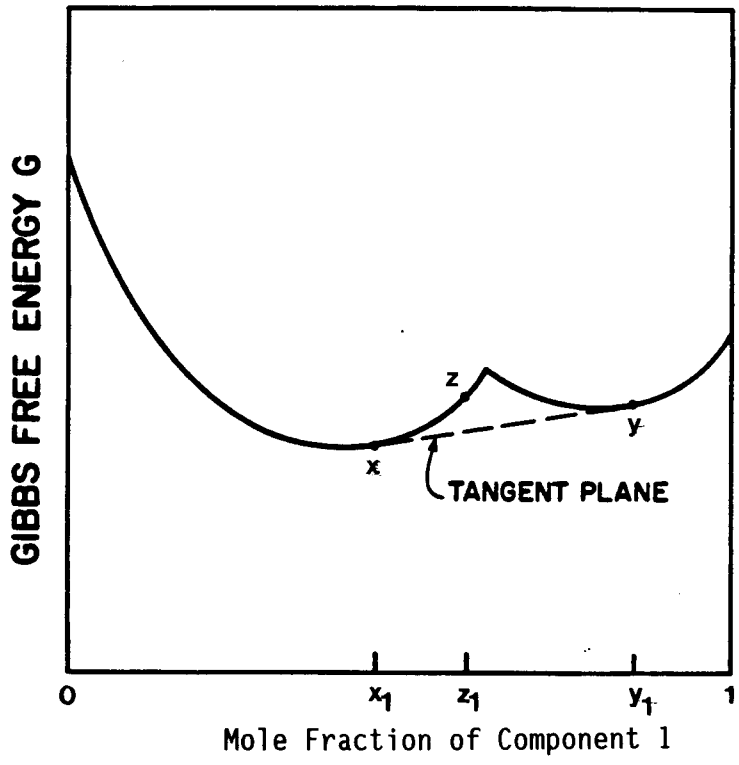

Fig. 2.4 Molar Gibbs free energy and tangent plane for a binary mixture at equilibrium conditions (from Nghiem and Li, 1988).

Combining Eqs. 2.22 and 2.24, yields an expression for x_i in terms of z_i, K_i and V

$$x_i = \frac{z_i}{1+V(K_i-1)} \quad , \quad i=1,\ldots,N \tag{2.25}$$

and likewise for y_i,

$$y_i = \frac{z_i K_i}{1+V(K_i-1)}, \quad i=1,\ldots,N \tag{2.26}$$

Rachford and Rice (1952) defined a function F(V)

$$F(V) = \sum_{i=1}^{N} (y_i-x_i) = 0 \tag{2.27}$$

which may be combined with Eqs. 2.25 and 2.26 to yield

$$F(V) = \sum_{i=1}^{N} \frac{z_i(K_i-1)}{1+V(K_i-1)} = 0 \qquad (2.28)$$

A Newton-Raphson iterative method may be used to determine V such that F(V)=0 (e.g. $F(V)<10^{-12}$). F(V) is a monotonic, decreasing function with one root in the interval $[V_{min},V_{max}]$. The physical bounds V_{min} and V_{max} ensuring non-negative $\underline{x}$ and $\underline{y}$ are determined from

$$V_{min} = 1/(1+K_{max}) \qquad (2.29a)$$

$$V_{max} = 1/(1+K_{min}) \qquad (2.29b)$$

where K_{max} and K_{min} represent the maximum and minimum equilibrium K-value, respectively. Fig. 2.5 illustrates two possible F(V) functions within the interval $[V_{min},V_{max}]$, with a root V in the interval [0,1] and $[1,V_{max}]$, respectively. Additional solutions to Eq. 2.28 exist outside these bounds, but will result in negative phase mole fractions. A physical interpretation of V is only possible within the interval [0,1], but from a mathematical point of view it is convenient to allow V to go outside this interval. The flash algorithm may converge to a single-phase solution with $V_{min}<V<0.0$ or $1.0<V<V_{max}$, and still satisfy the material balance and the equal-fugacity constraints. This approach, named negative flash, was first mentioned by Li and Nghiem (1982), and later extended by Zick (1985). Theoretical aspects and applications of the negative flash are discussed in detail by Whitson and Michelsen (1989).

The second criterion for equilibrium stated that component chemical potential, or here fugacity, must be equal in each phase

$$f_{Li}(\underline{x}) = f_{Vi}(\underline{y}), \quad i=1,\ldots,N \qquad (2.30)$$

Subscripts L and V denotes liquid and vapor phases, respectively. $\underline{x}=[x_1,\ldots,x_N]^T$ represents the liquid composition and $\underline{y}=[y_1,\ldots,y_N]^T$ the vapor composition. Eq. 2.30 may be written in terms of mole fractions and fugacity coefficients, Φ_i

$$x_i\Phi_{Li}(\underline{x}) = y_i\Phi_{Vi}(\underline{y}), \quad i=1,\ldots,N \qquad (2.31)$$

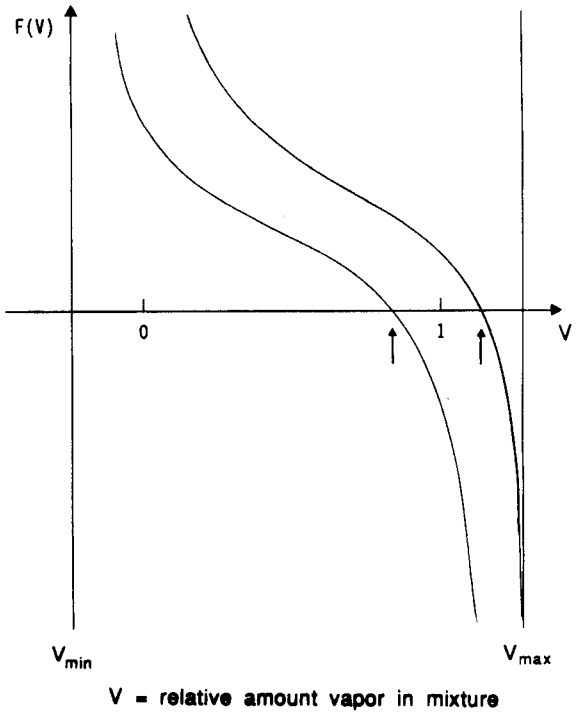

Fig. 2.5 Plot of F(V) versus V.

Combining Eq. 2.24 with Eq. 2.31 results in K-values defined in terms of the fugacity coefficients

$$K_i = \frac{\Phi_{Li}(\underline{x})}{\Phi_{Vi}(\underline{y})} \tag{2.32}$$

Because $f_{Li}=f_{Li}(p,T,\underline{x})$ and $f_{Vi}=f_{Vi}(p,T,\underline{y})$, Eq. 2.28 becomes a non-linear function of composition and must be solved using an iterative method with K-values as iteration-variables; for example an accelerated SS method. With $X_i=\ln K_i$, direct substitution gives ΔX_i as

$$\Delta X_i^{(n)} = \ln\left[\frac{f_{Li}(\underline{x})}{f_{Vi}(\underline{y})}\right]^{(n)} \tag{2.33}$$

Michelsen (1982b) uses GDEM to accelerate convergence after each five SS iterations. The iteration equation for the GDEM promotion step is given by Eq. 2.54. Flash calculation solution methods and their performance are reviewed by Mehra et al. (1983), Enick et al. (1987), and Gupta et al. (1988). Such methods are also briefly discussed in Section 2.5.

Reduction of Gibbs free energy is ensured for SS iterations, but not for the

promotion iteration. Reduced molar Gibbs free energy, g=G/RT, which may be expressed as

$$g = \sum_{i=1}^{N} Vy_i \ln f_{Vi} + (1-V)x_i \ln f_{Li} \qquad (2.34)$$

should then be calculated before and after each promotion step to check that g is reduced. In case g increases, the promotion should be truncated, or in worst case replaced by an additional SS iteration. A promotion step which results in V going outside the [0,1] interval should also be replaced by a SS iteration because Gibbs free energy no longer can be used to check the promotion in the single phase region. When already in the single phase region (V<0.0 or V>1.0), GDEM may be used to promote the SS iteration with the risk of arriving at a trivial solution, but the desired solution is usually found. However, unconstrained minimization methods, e.g. such as proposed by Trangenstein (1985) should be applied with care since the solution to the negative flash in this region is a saddle point (Whitson and Michelsen, 1989).

Equilibrium convergence is achieved when the equal-fugacity constraint is fulfilled. This may be expressed as

$$\sum_{i=1}^{N} (f_{Li}/f_{Vi}-1)^2 < 10^{-12} \qquad (2.35)$$

The equilibrium criterion is also fulfilled if composition of the two phases becomes identical, i.e. a trivial solution is obtained. Thus, the flash calculation should be terminated when all K-values approaches unity as expressed by Eq. 2.19. Arrival at a trivial solution can usually be explained by poor K-value estimates. The flash calculation seldom arrives at the trivial solution with K-value estimates from stability analysis.

Gupta et al. propose using liquid and vapor compositions as iteration variables instead of K-values. However, this method results in a lower convergence rate compared to the conventional K-value method.

2.4 Saturation Pressure

Saturation pressure is an important parameter for description of phase and volumetric behavior of hydrocarbon mixtures. Also, it is important to determine the type of saturation pressure, i.e. if it is a bubble point or a dew point. In Fig. 2.2 it is seen that two dew points may exist at a specified temperature above the mixture critical temperature. At temperatures above the cricondentherm, no saturation pressures exist.

The saturation pressure problem can be defined as follows: For an N-component mixture with given feed composition $\underline{z}$ and specified temperature T, determine the pressure p and incipient phase composition $\underline{y}$.

Since the system consists of non-linear, coupled equations the problem must be solved by an iterative method. Typically, a Newton-Raphson (NR) or a direct substitution method is used. The formulation used in this work, given by Michelsen (1985), is a combination of these two methods, a Newton-Raphson method is used to update the pressure and a SS method accelerated with GDEM is used to update the incipient phase composition. For an N-component mixture, we have N+1 equations with N+1 unknowns ($\underline{y}$,p). The N equations describing the equilibrium conditions can be written

$$f_i(\underline{z},p) - f_i(\underline{y},p) = 0, \quad i=1,\ldots,N \tag{2.36}$$

and the additional N+1'st equation is expressed

$$1 - \sum_{i=1}^{N} Y_i = 0 \tag{2.37}$$

Y_i which can be interpreted as a molenumber, is defined as

$$Y_i \equiv z_i \frac{\Phi_i(\underline{z},p)}{\Phi_i(\underline{y},p)} \tag{2.38}$$

where Φ_i is the fugacity coefficient. Incipient phase mole fractions are determined from

$$y_i = Y_i / \sum_{j=1}^{N} Y_j \tag{2.39}$$

In terms of tangent plane and Gibbs free energy, the solution to the saturation pressure problem can be described as follows: A mixture with composition $\underline{z}$ is stable at a saturation point defined by the conditions p_s and T. Thus TPD must be non-negative at all compositions $\underline{y}$. Eq. 2.36 requires that equilibrium exists between the feed and the incipient phase at a saturation point. This implies that $\underline{y}$ is a stationary point, and that the tangents to the Gibbs free energy surface at compositions $\underline{z}$ and $\underline{y}$ must be parallel in all dimensions. Eq. 2.37 requires that the distance between the corresponding parallel tangents is zero, that is the stationary distance is zero, $TPD(\underline{y}_{sp})=0$. This can be illustrated in Fig. 2.5 for a binary mixture with feed composition $\underline{z}=\underline{x}$.

By combining Eq. 2.37 with 2.36 the solution to the problem becomes finding $F_s(\underline{y},p)=0$ where $F_s(\underline{y},p)$ is defined as

$$F_s(\underline{y},p) \equiv \left[\sum_{i=1}^{N} z_i \frac{\Phi_i(\underline{z},p)}{\Phi_i(\underline{y},p)} \right] - 1 \tag{2.40}$$

We further define the following terms $S_y = \Sigma_i Y_i$, $f_{yi}=f_i(\underline{y},p)$ and $f_{zi}=f_i(\underline{z},p)$. Pressure updating using a Newton method can be formulated as

$$p^{(n+1)} = p^{(n)} + \left[\frac{F_s(\underline{y},p)}{\frac{\partial F_s}{\partial p}(\underline{y},p)} \right]^{(n)} \tag{2.41}$$

where

$$F_s(\underline{y},p) = \left[\sum_{i=1}^{N} y_i \frac{f_{zi}}{f_{yi}} \right] - 1 \tag{2.42}$$

and

$$\frac{\partial F_s}{\partial p}(\underline{y},p) = \sum_{i=1}^{N} y_i \frac{f_{zi}}{f_{yi}} \left[\frac{\partial f_{zi}}{\partial p} \frac{1}{f_{zi}} - \frac{\partial f_{yi}}{\partial p} \frac{1}{f_{yi}} \right] \tag{2.43}$$

The incipient phase composition is updated using the SS method accelerated with GDEM. The iteration equation is given by Eq. 2.16 with $X_i=\ln Y_i$ and ΔX_i expressed by Eq. 2.17 for three or four subsequent SS iterations. Each fourth or fifth iteration a promotion step is performed to accelerate convergence with GDEM, and ΔX_i is determined from Eq. 2.61 given in Section 2.5.

Convergence of the saturation pressure problem is achieved upon fulfillment of the two following criteria (Zick, 1985)

$$\left|\left(\sum_{i=1}^{N} Y_i\right)-1\right| < \epsilon_1 \tag{2.44a}$$

$$\sum_{i=1}^{N} \left[\frac{\ln(f_{z\,i}/f_{y\,i})}{\ln K_i}\right]^2 < \epsilon_2 \tag{2.44b}$$

where e.g. $\epsilon_1=10^{-13}$ and $\epsilon_2=10^{-8}$. These criteria are in most cases tight enough to ensure K-values with 3-4 significant digits, but may be further reduced close to the critical point.

In case the trivial solution, as defined by Eq. 2.19, is obtained, continue with the other type of saturation point (e.g. change from dew point to bubble point).

2.5 General Dominant Eigenvalue Method

Most VLE calculations involve coupled non-linear equations that typically are solved using a direct substitution method. In the critical region fugacities are strong functions of composition and the convergence rate may be slow. An example of this is shown below.

The norm of the error vector, e, of $\underline{X}$ for VLE calculations can be defined as

$$e = \sum_{i=1}^{N} \left|\Delta X_i^{(n)}\right| \tag{2.45}$$

Reduction of e depends on the absolute value of the largest eigenvalue λ_{max} of the convergence matrix, (Michelsen, 1982a)

$$e^{(n+1)} = |\lambda|_{max} e^{(n)} \tag{2.46}$$

The SS convergence matrix **S** may be expressed as

$$S_{ij} = \lim_{n\to\infty} \left[\frac{\partial X_i^{(n+1)}}{\partial X_j^{(n)}} \right] \tag{2.47}$$

The necessary and sufficient condition for convergence of an iterative method is that $|\lambda|_{max}$ is less than unity. With two-parameter EOSs, Michelsen (1982b) shows for the flash problem that two eigenvalues of **S** approach unity at the critical point. He also shows for the stability analysis (and thus for the saturation pressure problem) that one eigenvalue of **S** approaches unity at the critical point (Michelsen, 1982a).

The number of SS iterations, n, needed to reduce the amplitude of e a factor of 10^{-m} can be estimated from (Lapidus and Pinder, 1982)

$$n \geq \frac{m}{-\log|\lambda|_{max}} \tag{2.48}$$

For m=6 and $|\lambda|_{max}$=0.5, 20 iterations are required, while 48 and 270 iterations are required as $|\lambda|_{max}$=0.75 and 0.95, respectively. Thus, VLE calculations in the critical region using the SS method may need hundreds of iterations to converge, if convergence is achieved at all.

An acceleration method will speed up the convergence rate of SS significantly. In this work the General Dominant Eigenvalue Method (GDEM) proposed by Crowe and Nishio (1975) has been used. Other accelerated SS methods are proposed by Risnes et al. (1981) and Mehra et al. (1983). Newton type methods are given by Fussel and Yanosik (1978) and Asselineau et al. (1979). Nghiem and Aziz (1979) presented an algorithm using the Powell's method which is a combination of a Newton and a steepest decent method.

Newton methods require good initial K-value estimates to ensure convergence, while the SS+GDEM method is more robust and not that sensitive to the initial K-value estimates. The rate of convergence may be faster with a Newton method compared to a SS+GDEM method provided that the initial K-value estimates are

very good. This is usually the case in a fully compositional simulator. Some iteration schemes start with an accelerated SS method, and then switches to a Newton type method, e.g. Michelsen (1982b) proposes to switch to a Newton-Raphson method if convergence for the flash problem is not achieved within 12 iterations (2 GDEM promotions).

Formulation

When accelerating the SS method with GDEM, the iteration equation for the promotion step can generally be written as

$$X_i^{(n+1)} = X_i^{(n)} + \sum_{k=1}^{\nu} \theta_k \Delta X_i^{(n+1-k)} \tag{2.49}$$

where the iteration variable, X_i, is updated with ΔX_i for a conventional SS iteration. ν is the number of dominant eigenvalues of the convergence matrix **S** and θ_k is defined as

$$\theta_k = \left(\sum_{j=k}^{\nu} \mu_j\right)/\left(1 - \sum_{j=1}^{\nu} \mu_j\right) \tag{2.50}$$

The eigencoefficient, μ_j, is the j'th coefficient of the characteristic polynomial

$$\sum_{j=0}^{\nu} \mu_j \lambda^{\nu-1} = 0 \tag{2.51}$$

with eigenvalue λ_j. μ_j, j=1,...,ν are satisfying the set of linear equations

$$\sum_{j=1}^{\nu} b_{kj}\mu_j = b_{k0}, \quad k=1,\ldots,\nu \tag{2.52}$$

where b_{kj} can be expressed in terms of the correction term ΔX_i

$$b_{kj} = \sum_{i=1}^{N} \Delta X_i^{(n-k)} \Delta X_i^{(n-j)} \tag{2.53}$$

The flash problem has two dominant eigenvalues and thus the promotion step can be expressed as

$$X_i^{(n+1)} = X_i^{(n)} + \frac{\Delta X_i^{(n)} + \mu_2 \Delta X_i^{(n-1)}}{1 + \mu_1 + \mu_2} \tag{2.54}$$

where $X_i = \ln K_i$ and $\Delta X_i = \ln[f_{Li}(\underline{x})/f_{Vi}(\underline{y})]$, and μ_1 and μ_2 are determined from

$$\mu_1 = \frac{(b_{02}b_{12} - b_{01}b_{22})}{(b_{11}b_{12} - b_{12}b_{12})} \tag{2.55}$$

and

$$\mu_2 = \frac{(b_{01}b_{12} - b_{02}b_{11})}{(b_{11}b_{12} - b_{12}b_{12})} \tag{2.56}$$

Occasionally, in the critical region this version of GDEM may not converge as rapid as wanted because of round-off errors introduced when subtracting almost equal terms in Eqs. 2.55 and 2.56. Zick (1985) suggests reformulating the expressions for μ_1 and μ_2 using perturbation techniques. Defining ϵ_{ij} as

$$\epsilon_{ij} = (b_{ij} - b_{12})/b_{12} \tag{2.57}$$

it can be shown that μ_1 and μ_2 become

$$\mu_1 = \frac{\epsilon_{02} - \epsilon_{01} - \epsilon_{22} - \epsilon_{01}\epsilon_{22}}{\epsilon_{11} + \epsilon_{22} + \epsilon_{11}\epsilon_{22}} \tag{2.58}$$

and

$$\mu_2 = \frac{\epsilon_{01} - \epsilon_{02} - \epsilon_{11} - \epsilon_{02}\epsilon_{11}}{\epsilon_{11} + \epsilon_{22} + \epsilon_{11}\epsilon_{22}} \tag{2.59}$$

and the term $1+\mu_1+\mu_2$ is expressed

$$1 + \mu_1 + \mu_2 = \frac{\epsilon_{11}\epsilon_{22} - \epsilon_{01}\epsilon_{22} - \epsilon_{02}\epsilon_{11}}{\epsilon_{11} + \epsilon_{22} + \epsilon_{11}\epsilon_{22}} \tag{2.60}$$

Zick (1985) suggests for secure and fast convergence that μ_i eventually be reduced or eliminated to ensure such that $0 \leq 1+\mu_1+\mu_2 \leq 10^6$.

Likewise, GDEM is applied to accelerate SS for the stability analysis and the saturation pressure calculation. For these problems one eigenvalue of the

convergence matrix is non-zero, and for a promotion step ΔX_i in Eq. 2.16 is simply calculated from

$$\Delta X_i^{(n)} = \ln\left[\frac{1}{\sum_{j=1}^{N} Y_j}\,\frac{f_i(\underline{z})}{f_i(\underline{y})}\right]^{(n)} \frac{1}{|1+\mu_1|} \tag{2.61}$$

where

$$\mu_1 = -\,(b_{01}/b_{11}) \tag{2.62}$$

Crowe and Nishio (1975) suggest that a promotion step after a minimum number of SS iterations, should be taken when change in the norm of the apparent solution, $X^{(n)}$, at iteration n is sufficiently low, that is,

$$\frac{||\Delta X^{(n)}||}{||X^{(n)}||} < \epsilon \tag{2.63}$$

with $\epsilon \approx 0.05\text{-}0.1$. However, it has been experienced that this criterion may postpone the first promotion step several iterations and do not result in the optimal convergence rate.

Examples

Yarborough Mixture No. 8

Performance of the flash algorithm was tested on the Yarborough Mixture No. 8, (Yarborough, 1972) at various pressures along the T=75°F [22.9°C] isotherm. Initial K-values were provided from stability analysis. The results are shown in Table 2.1 for the SS method, and for SS+GDEM with 2, 3, 4, or 5 SS iterations prior to a promotion. Reduction in the norm of the error vector e (Eq. 2.45) is shown Fig. 2.6 versus number of iterations. The results are obtained with the PR EOS, using the same fluid characterization as Risnes et al. (1981). At p=3075 [212 bar], the SS method had not converged after 300 iterations.

The iteration scheme used in this work compares favorably with the acceleration method tested by Risnes et al. Partly, this may be explained with better K-value estimates obtained from stability analysis. Also, it is seen that two SS iterations prior to a GDEM promotion gives optimal performance for this six-component mixture. This is in conflict with the

recommendations given by Michelsen (1982b) and Zick (1985) who suggest five SS iterations be performed prior to a GDEM promotion for the flash problem. However, it is believed that the optimum iteration scheme to some degree depends on the specific mixture. Thus, for a reservoir fluid mixture characterized with non-zero BIPs which will result in a more coupled system of equations, the optimum iteration scheme may require more SS iterations prior to a promotion. Michelsen (1982b) studied systems for which all BIPs were zero, and found that the largest eigenvalue of **S** (Eq. 2.47) is independent of the number of components in a mixture.

TABLE 2.1 -- Performance of SS+GDEM Iteration Scheme for the Yarborough Mixture No. 8 (Yarborough, 1972), T=75°F [23.9°C].

Pressure (psia)	Liquid Mole Fraction	SS	One Iteration Cycle: n = n-1 SS + 1 GDEM			
			3	4	5	6
2000	0.2622	17	7	9	11	10
2500	0.3189	29	11	10	11	13
2750	0.3538	47	10	13	16	14
2875	0.3741	68	13	13	16	19
3000	0.3954	138	11	14	21	25
3050	0.3988	253	10	13	16	19
3075	0.3873	NC[1)]	10	13	16	19

Note:
1. After 300 SS iterations convergence was not obtained.
2. K-value estimates are calculated from stability analysis.

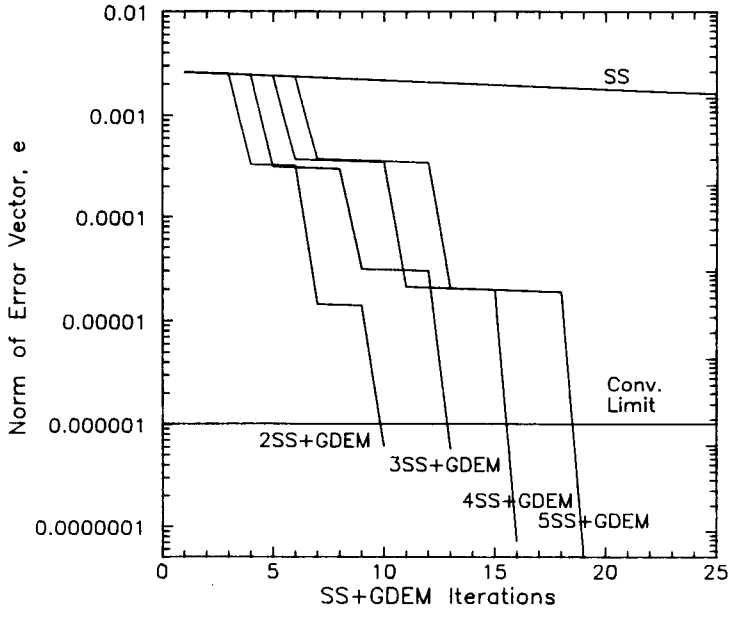

Fig. 2.6 Performance of various SS+GDEM iteration schemes.

Jacoby Synthetic Mixture

The flash algorithm was also tested on the Jacoby synthetic mixtures (Jacoby et al., 1959). A fluid characterization for these near-critical gas condensates is presented in Section 5.5. 125 flash calculations were performed for nine different CCE experiment with the various SS+GDEM iteration schemes used in the previous example. The results listed in Table 2.2, show that three SS iterations prior to a GDEM promotion seems to be an optimal iteration scheme for this system.

TABLE 2.2 -- Performance of SS+GDEM Iteration Scheme for the Jacoby Synthetic Mixtures.

	Iteration Cycle n = n-1 SS + 1 GDEM			
	3	4	5	6
TOTAL :	1832	1779	1992	2437
AVERAGE :	14.5	14.1	15.8	19.3
MAXIMUM :	69	65	52	188

Note:
1. TOTAL refers to total number of iterations for 125 flash calculations.
2. AVERAGE refers to average number of iterations per flash calculation.
3. MAXIMUM refers to maximum number of iterations for any of the flash calculations.

CHAPTER 3
HEPTANES-PLUS CHARACTERIZATION

3.1 Introduction

Naturally occurring petroleum fluids are complex mixtures including components such as methane, ethane, nitrogen, carbon dioxide, intermediate components C_3-C_6, and a large number of heptanes and heavier components (C_{7+}). Simulating phase and volumetric behavior with an equation of state requires mixture composition in addition to molecular weight, acentric factor, critical pressure and critical temperature for all components.

Laboratory analyses of reservoir fluids usually give a limited description of the heavy components. Hydrocarbons heavier than hexane which is the heaviest "pure" component reported, are normally lumped into a C_{7+} fraction with measured molecular weight and specific gravity. The objective of C_{7+} characterization is thus to obtain a description of the heavy, undefined components using pseudocomponents such that experimental PVT data are matched with the predicted EOS characterization.

Occasionally, the plus-fraction of a petroleum mixture may be analyzed by performing a true boiling point (TBP) distillation with predetermined temperature intervals slightly above the normal boiling points of adjoining n-paraffins (Katz and Firoozabadi, 1978). This analysis yields composition and the inspection properties: molecular weight, specific gravity, and normal boiling point for each distillation cut. Then, critical properties and acentric factor for each cut may be estimated based on measured properties. The TBP analysis is normally terminated at the boiling point of nC_{20} to avoid cracking, or even before that for gas condensates. For the residue, e.g. C_{21+}, molecular weight, mass and volume are measured while normal boiling point must be estimated. Fractional distillation procedures are described by Bergman (1976), Maddox and Erbar (1982) and Austad et al. (1981).

An alternative method for characterizing the C_{7+} fraction is by simulated distillation using gas chromatography. This results in pure component weight fractions. Components with normal boiling point between those of two adjoining n-paraffins, are lumped together, and molecular weight, specific gravity, and average boiling point for this single-carbon-number (SCN) group must be estimated. A description of simulated distillation using gas chromatography is given by Austad et al. (1981) and Chorn (1984).

When only limited C_{7+} experimental data are reported, characterization is performed by splitting the C_{7+} fraction into pseudocomponents for which molecular weight and mole fraction are calculated. Based on the molar distribution and overall C_{7+} properties, specific gravity and normal boiling point are estimated. These properties are usually needed for calculating critical properties and acentric factor from general correlations.

Methods for characterizing petroleum fractions for EOS applications have been reported by several authors, among these are Katz and Firoozabadi (1978), Robinson and Peng (1978), Yarborough (1979), Whitson (1983a, 1983b), Pedersen et al. (1984a,b, 1985a, 1988) and Whitson et al. (1988). A comprehensive review of some of the early characterization methods is given by Whitson (1984) and recently by Whitson and Brule (1989).

The methods for example given by Robinson and Peng (1978), Pedersen et al. (1984a) and Cotterman and coworkers (1985) include a split of each fraction into three hydrocarbon groups: paraffins (P), naphthenes (N) and aromatics (A). These methods are empirical and may result in negative PNA compositions. Bergman (1976) propose upper and lower bounds on the P, N, and A weight fractions to avoid this. Whitson (1984) does not recommend PNA splitting of petroleum fractions since the split methods may not be reliable.

This chapter is mainly divided into two separate sections. First methods for splitting the C_{7+} fraction are described and following in the next sections physical properties estimation which also is an important part of the characterization, is discussed. The methods presented are easily generalized for any plus-fraction (C_{6+}, C_{8+}, C_{9+} or C_{10+}).

3.2 Splitting the C_{7+} Fraction

3.2.1 Introduction

It is commonly assumed that a unique relationship exists between cumulative mole fraction and molecular weight or carbon number. Such a relationship is called the molar distribution, and can be modelled with a simple exponential function to divide the C_{7+} fraction into pseudocomponents. An assumption inherent in these methods is that C_{7+} mole fractions decrease exponentially. A more general approach for generating the molar distribution is to use a probability distribution function such as the continuous three-parameter gamma function as proposed by Whitson (1983a). This requires a procedure for discretizing the continuous distribution into a fixed number of pseudocomponents. Special attention is given to a discretization procedure which combines the gamma function with Gaussian quadrature theory.

3.2.2 Criteria for Splitting Procedures

A procedure for splitting the C_{7+} fraction may be summarized as follows:

1) Select a molar distribution model which uniquely defines a relationship between mole fraction and molecular weight.

2) Specify the number of pseudocomponents to split the C_{7+} fraction into.

3) Apply the molar distribution model to determine mole fraction and molecular weight of each pseudocomponent.

Certain constraints are active in the splitting procedure. For example, the combined properties of the pseudocomponents should result in the known properties of the overall C_{7+} fraction.

For C_{7+} data these constraints can be expressed as:

$$z_{7+} = \sum_{i=1}^{N} z_i \tag{3.1}$$

and

$$M_{7+} = \left(\sum_{i=1}^{N} z_i M_i \right) / z_{7+} \tag{3.2}$$

where M_i and z_i represent pseudocomponent molecular weight and mole fraction, respectively, and N denotes the number of pseudocomponents.

3.2.3 The Exponential Molar Distribution

Whitson (1987) gives a set of equations for an exponential distribution which can be solved explicitly,

$$z_i = z_7 \exp[b(i-7)] \tag{3.3}$$

$$M_i = 14i + c \tag{3.4}$$

$$b = \ln(1-z_7) \tag{3.5}$$

$$z_7 = \frac{14}{M_{7+}-84-c} \tag{3.6}$$

where z_i is mole fraction of SCN component i and z_7 is the heptane mole fraction. c is a parameter indicating the average molecular type, i.e. c=2 for paraffins, c=0 for napthenes, and c=-6 for aromatics. Note that z_i is a C_{7+} normalized mole fraction, i.e. $\Sigma_i z_i=1$ for i=7,...,N.

An alternative representation of the molar distribution model is to combine Eqs. 3.4 and 3.6 with Eq. 3.3 to express z_i as a discrete function of M_i

$$z_i = z_7 \exp\left[\frac{b(M_i-c)}{14} - 7\right] \tag{3.7}$$

For a specific carbon number i, mole fraction and molecular weight follow immediately from Eqs. 3.7 and 3.4.

Eqs. 3.1 and 3.2 will be satisfied if N is chosen large enough (e.g. N=1000). When the split is carried out to N-1 SCNs, mole fraction and molecular weight of the remaining material, N+, are determined from

$$z_{N+} = 1 - \sum_{i=7}^{N-1} z_i \tag{3.8}$$

and

$$M_{N+} = \frac{M_{7+} - \sum_{i=7}^{N-1} z_i M_i}{1 - \sum_{i=7}^{N-1} z_i} \tag{3.9}$$

The easiest though least reliable way of determining mole fractions and molecular weights of e.g. 5 pseudocomponents is to define pseudocomponents 1 through 4 as SCN groups C_7, C_8, C_9, and C_{10}, and let the fifth represent C_{11+}. Pseudocomponents with approximate equal weight or equal mole fractions can also be used (Pedersen et al. 1985b) where N can be specified as high as 80 or until $z_i<\epsilon$, where typically $\epsilon=(10^{-6})$.

Other simple exponential models for generating the molar distribution are e.g. described by Lohrenz et al. (1964), Yarborough (1979), Katz (1983), Pedersen et al. (1984a) and Ahmed et al. (1984, 1985).

3.2.4 Whitson Gamma Distribution

The molar distribution may alternatively be modelled as a continuous function of molecular weight. Pseudocomponents are defined within an upper and a lower molecular weight bound. This section describes how pseudocomponent molecular weights and mole fractions can be determined provided that the molecular weight bounds are defined.

The distribution model proposed by Whitson (1983a) is based on the three-parameter gamma distribution where the probability density function, p(M),

relates frequency of occurrence (normalized mole fraction) to molecular weight

$$p(M) = \frac{(M-\eta)^{\alpha-1}\exp[-(M-\eta)/\beta]}{\beta^{\alpha}\,\Gamma(\alpha)} \tag{3.10}$$

Γ is the gamma function, η may be interpreted as the minimum molecular weight of any component occurring in the C_{7+} fraction, and α is a measure of the form of the distribution. For α=1, p(M) represents an exponential distribution, and for α>1 the distribution is a right-skewed distribution. The third parameter, β, is a composite parameter expressed in terms of M_{7+}, α, and η

$$\beta = (M_{7+}-\eta)/\alpha \tag{3.11}$$

For specified values of M_{7+}, α, and η, Eq. 3.10 represents a unique relationship between mole fraction and molecular weight of the C_{7+} fraction.

The continuous probability density function p(M) should be defined in the interval $[\eta,\infty]$, and such that Eqs. 3.1 and 3.2 are fulfilled. The integral of p(M) over an interval $[\eta,M_{bi}]$ can be regarded as a cumulative probability function, $P(M_{bi})$, and is equivalent to cumulative, normalized mole fraction

$$P(M_{bi}) = \int_{\eta}^{M_{bi}} p(M)dM \tag{3.12}$$

Eq. 3.12 represents the area under the p(M) curve from η to M_{bi} as illustrated in Fig. 3.1(b). Eq. 3.1 is fulfilled if the integral of p(M) over the interval $[\eta,M_{bi}]$ sums to unity as M_{bi} approaches infinity.

A material balance for C_{7+} corresponding to Eq. 3.2, requires the following relationship to be fulfilled:

$$\int_{\eta}^{\infty} Mp(M)dM = M_{7+} \tag{3.13}$$

The expectation value given by Eq. 3.13 is an expression for the total mass of the C_{7+} fraction.

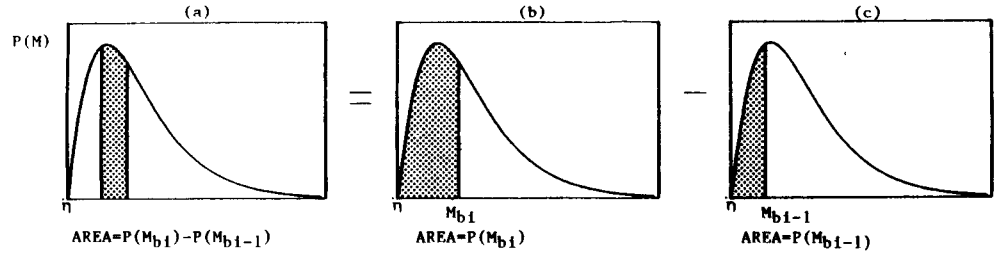

Fig. 3.1 Graphical illustration of the relation between cumulative probability function, P(M), and C_{7+} cumulative mole fraction (From Whitson and Brule).

Mole fraction z_i of pseudocomponent i, bound by the molecular weight interval M_{bi-1} to M_{bi}, is expressed by integrating p(M) between these limits, as illustrated in Fig. 3.1,

$$z_i = \int_{M_{bi-1}}^{M_{bi}} p(M)dM \tag{3.14}$$

Average molecular weight M_i of this pseudocomponent is given by

$$M_i = \frac{\int_{M_{bi-1}}^{M_{bi}} Mp(M)dM}{z_i} \tag{3.15}$$

$P(M_{bi})$, defined by Eq. 3.12, may be expressed as an infinite series

$$P(M_{bi}) = \frac{e^{-X} X^{\alpha}}{\Gamma(\alpha)} \sum_{j=0}^{\infty} \frac{X^j}{\prod_{k=0}^{j} (\alpha+j)} \tag{3.16}$$

as function of α and $x_i=(M_{bi}-\eta)/\beta$. For a pseudocomponent with molecular weight bounds M_{bi-1} and M_{bi}, normalized mole fraction z_i becomes

$$z_i = [P(M_{bi}) - P(M_{bi-1})] \tag{3.17}$$

with $P(M_{bi-1})$ and $P(M_{bi})$ calculated from Eq. 3.16. Average molecular weight M_i is determined from

$$M_i = \eta + \alpha\beta[1 - \frac{T_i - T_{i-1}}{z_i \Gamma(\alpha+1)}] \tag{3.18}$$

where

$$T_i = e^{-x_i} x_i^{\alpha} \tag{3.19}$$

FORTRAN programs for calculating z_i, M_i, $P(M_{bi})$ and $\Gamma(\alpha)$ are given in Appendix B. These may be used to discretize the molar distribution if it is assumed that the M_b-values are chosen arbitrarily e.g. by defining $\Delta M_i = M_{bi} - M_{bi-1} = 14$. In general, the location of these bounds depend on the discretization method used. Usually they must be determined by an iterative method to fulfill specified constraints.

For a particular hydrocarbon system the distribution parameters must be specified prior to splitting the C_{7+} fraction. Parameters α and η can be determined from TBP analysis as proposed by Whitson et al. (1986). They found that η was related to α through the empirical relation

$$\eta = 110[1-(1+4.043/\alpha^{0.723})^{-1}] \tag{3.20}$$

If no TBP analysis data are available for the actual sample, distribution parameters have to be estimated. In that case, Fig. 3.2 can be used as a guide for choosing distribution parameters. The figure shows best fit α parameters resulting from regression performed with η fixed at 90, and is based on about 65 C_{7+} samples for which TBP data exist. It is observed that α generally varies between 0.5 and 1.0, and that it has a tendency to increase with increasing M_{7+}.

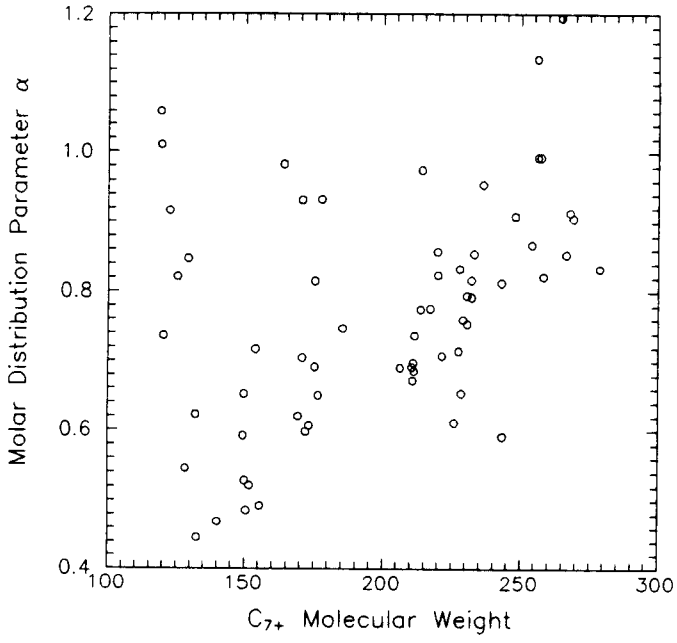

Fig. 3.2 Molar distribution α parameters obtained by regression for about 65 samples with η=90.

3.2.5 Fixed Discretization of Molar Distributions

Methods for generating a continuous C_{7+} molar distribution have been presented. The next step consists of discretizing a continuous molar distribution into a fixed number of pseudocomponents.

The two main questions related to such a procedure are: how many pseudocomponents should be used and how to determine the upper and lower bounds that define each pseudocomponent. From 3 to 10 pseudocomponents may be used to describe the C_{7+} fraction. This depends on the type of reservoir fluid to be described, and the recovery processes anticipated. For example, relative few pseudocomponents may be used to model depletion of an oil. A more detailed splitting may be needed to model condensation and revaporization processes for volatile oils and rich gas condensates. Pedersen et al. (1988) always use three C_{7+} pseudocomponents. Coats and Smart (1986) used one to four pseudocomponents to characterize twelve reservoir fluids, and concluded that there is no need for a more extensive C_{7+} splitting. Fixed discretization procedures are presented by several authors

including Whitson (1983a), Pedersen et al. (1984a), Li et al. (1984), and Wu and Batycky (1986).

The simplest grouping method consists of defining molecular weight bounds with a constant interval between each. For example, define the bounds M_{bi} and M_{bi-1} such that $\Delta M=M_{bi}-M_{bi-1}$ is constant for i=1,..,N-1. These bounds may be located such that each pseudocomponent, except the heaviest, corresponds to a SCN-component. Another discretization method requires that each pseudocomponent is assigned an equal weight fraction, as suggested by Pedersen et al. (1985b). Alternatively, it can be required that all pseudocomponents are assigned an equal mole fraction. Procedures for these two alternatives are outlined below.

Equal weight fraction discretization procedure:

1. Specify the number of pseudocomponents, N, and calculate the constant weight fraction value, Δw

$$\Delta w = 1/N \tag{3.21}$$

2. Determine or estimate α and η. Calculate β from Eq. 3.11 as a function of the experimental M_{7+}.

3. For i=1, $P(M_{bi-1})=P(\eta)$ and for i>1, $P(M_{bi-1})$ is evaluated for the previous pseudocomponent.

4. Estimate an upper molecular weight bound, M_{bi}.

5. Determine $P(M_{bi})$, and calculate z_i and M_i from Eqs. 3.17 and 3.18, respectively.

6. Check if normalized weight fraction, w_i,

$$w_i = \frac{z_i M_i}{\sum_{j=1}^{N} z_j M_j} \tag{3.22}$$

equals the required weight fraction, Δw, within a preset tolerance, e.g. (10^{-6}). If not, adjust the upper molecular weight bound M_{bi} and go back to step 5. Use a Newton or interval halving method to determine the correct M_{bi} value.

7. Repeat steps 3 to 6 for all pseudocomponents. Since $M_{bN}=\infty$, z_N and M_N can be back calculated.

Equal mole fraction discretization procedure:

1. Specify the number of pseudocomponents, N, and calculate the required mole fraction value, Δz

$$\Delta z = 1/N \tag{3.23}$$

2. Determine or estimate α and η. Calculate β from Eq. 3.11 as a function of the experimental M_{7+}.

3. For i=1, $P(M_{bi-1})=P(\eta)$, and for i>1, $P(M_{bi-1})$ is evaluated for the previous pseudocomponent.

4. Estimate a upper molecular weight bound, M_{bi}.

5. Determine $P(M_{bi})$, and z_i from Eq. 3.17.

6. Check if estimated z_i equals Δz within a preset tolerance, e.g. (10^{-6}). If not, adjust the upper molecular weight bound M_{bi} and go back to step 5. Apply a Newton or interval halving method to determine the correct M_{bi}.

7. Calculate average molecular weight M_i from Eq. 3.18.

8. Repeat steps 3 to 7 for all pseudocomponents. Since $M_{bN}=\infty$, z_N and M_N can be back calculated.

The equal weight fraction discretization procedure is generally considered to be superior to the equal mole fraction procedure.

Whitson et al. (1988) describe a different discretization procedure which is based on Gaussian quadrature. This procedure is presented below.

3.2.6 Discretization by Gaussian Quadrature

Behrens and Sandler (1986) used Gaussian quadrature to define an "optimal" discretization method for a continuous molar distribution. They first define the C_{7+} molar distribution with a three-parameter exponential function, usually truncated at an upper bound near C_{50}. Gaussian quadrature is then applied to determine carbon number and mole fraction of <u>two</u> pseudocomponents. Molecular weights are determined as a function of carbon number.

Cotterman and coworkers (1985) also use Gaussian quadrature to discretize a continuous molar distribution, and discuss the problem that pseudocomponent

mole fractions and molecular weights do not result in the known properties of the overall C_{7+} fraction. This mass conservation deficiency occurs because Gaussian quadrature is only a discrete approximation to the continuous distribution, and this approximation may not always be accurate enough.

Whitson et al. (1988) generalized the method for discretizing a molar distribution using Gaussian quadrature. The C_{7+} fraction, originally described by a continuous gamma distribution function, can be split into an arbitrary number of pseudocomponents. Also, the new approach overcomes the mass conservation problem, and preserves overall C_{7+} fraction properties.

The Gaussian quadrature method is used to provide a discrete representation of the continuous gamma distribution using N quadrature points,

$$\int_0^\infty e^{-x} f(x)dx = \sum_{i=1}^{N} w_i f(x_i) \tag{3.24}$$

where x_i are quadrature points and w_i are weighting factors. By combining Eq. 3.10 with 3.24 and defining $x=(M-\eta)/\beta$ in the interval $[0,\infty]$, it can be shown that f(x) becomes

$$f(x) = \frac{x^{(\alpha-1)}}{\Gamma(\alpha)} \tag{3.25}$$

Sets of x_i and w_i are tabulated for various numbers of quadrature points N (e.g., see Abramowitz and Stegun, 1972, pp. 923). Table 3.1 lists values of x_i and w_i for N=5.

TABLE 3.1 -- Gaussian Quadrature Points and Weights For Five Points, (From Abramowitz and Stegun, 1972).

i	Point x_i	Weight w_i
1	0.263 560 319 718	$5.217\ 556\ 105\ 83(10^{-1})$
2	1.413 403 059 107	$3.986\ 668\ 110\ 83(10^{-1})$
3	3.596 425 771 041	$7.594\ 244\ 968\ 17(10^{-2})$
4	7.085 810 005 859	$3.611\ 758\ 679\ 92(10^{-3})$
5	12.640 800 844 276	$2.336\ 997\ 238\ 58(10^{-5})$

Pseudocomponent molecular weight is determined from quadrature point x_i and distribution parameters β and η: $M_i=\eta+\beta x_i$, and mole fraction is given by $z_i=w_i f(x_i)$. The location of the quadrature points and weighting factor values are not randomly chosen, but determined from a class of orthogonal Laguerre polynomials. It can be shown that Gaussian quadrature using N points integrates a polynomial of degree 2N-1, exactly. Cotterman et al. claim this implies that N pseudocomponents defined using Gaussian quadrature results in an approximation to the continuous molar distribution with the same accuracy as 2N-1 pseudocomponents chosen randomly.

Many North Sea reservoirs exhibit a continuous compositional variation with depth or area. Fluids sampled from different well locations in such reservoirs may have different composition and overall C_{7+} properties, e.g. different M_{7+} and α. The Gaussian quadrature method presented above will result in one set of pseudocomponent molecular weights for each reservoir fluid with a specific set of M_{7+} and distribution parameters. A different set of molecular weights will be determined for a fluid sample collected elsewhere in the reservoir with different overall C_{7+} properties. This is due to a variation in parameter β as a result of different values of M_{7+} and α, (and β is included in the expression for M_i).

Whitson et al. (1988) propose a method resulting in a single set of pseudocomponent molecular weights for C_{7+} fractions with different M_{7+} and α values. Using this method any fluid sample from a reservoir with compositional variation can be characterized with an identical set of C_{7+} pseudocomponent properties, where only fluid composition varies. This is achieved by introducing a modification to the β parameter,

$$\beta = \beta_o/[1+\ln(\delta)] \tag{3.26}$$

where β_o and δ are parameters of a modified distribution function, $p_o(M)$, rewritten from the original gamma distribution function

$$p_o(M)= \frac{(M-\eta)^{(\alpha-1)}\ \exp[-(M-\eta)/\beta_o]}{\beta_o^{\alpha}\ \Gamma(\alpha)} \frac{(1+\ln\delta)^{\alpha}}{\delta^{[(M-\eta)/\beta_o]}} \equiv p(M) \tag{3.27}$$

$p_o(M)$ is numerically identical to the original function p(M) for a given value of M.

To obtain a variable which can be integrated by Gaussian quadrature, a new variable x_o is defined as

$$x_o = \frac{M-\eta}{\beta_o} \tag{3.28}$$

Noting that $dM=\beta_o dx_o$, the cumulative density function integrated from 0 to ∞, becomes

$$\int_0^\infty \frac{x_o^{(\alpha-1)} \exp(-x_o)}{\Gamma(\alpha)\ \delta^{x_o}\ (1+\ln\delta)^{-\alpha}}\, dx_o \equiv 1 \tag{3.29}$$

$f(x_o)$ corresponding to $f(x)$ in Eq. 3.24, is defined as

$$f(x_o) = \frac{x_o^{(\alpha-1)}}{\Gamma(\alpha)} \frac{(1+\ln\delta)^{\alpha}}{\delta^{x_o}} \tag{3.30}$$

Thus, mole fraction for pseudocomponent i is given by

$$z_i = w_i f(x_{o\,i}) \tag{3.31}$$

and its molecular weight is given by

$$M_i = \eta+\beta_o x_{o\,i} \tag{3.32}$$

Gaussian quadrature combined with the original gamma distribution (Eq. 3.10) may result in molecular weight for the last pseudocomponent, M_N, as high as 1500 with N=7. Physical properties assigned to such heavy pseudocomponents involve large uncertainties. Behrens and Sandler use a gamma function truncated at the upper bound near C_{50}, to avoid such heavy pseudocomponents. With fewer points M_N is reduced, but this results in larger material balance error. By introducing β_o and δ it becomes possible to specify M_N, e.g. M_N=500, and the N points will be distributed in the interval $[\eta,M_N]$.

Calculation Procedure

Pseudocomponent mole fractions and molecular weights of a C_{7+} fraction can be obtained from the following procedure:

1. Specify the number of pseudocomponents N, and obtain the Gaussian quadrature values x_{oi} and w_i.

2. Specify η, e.g. for a C_{7+} fraction; $86<\eta<95$.

3. Specify M_N, e.g. $M_N=500$, and calculate β_o from Eq. 3.28 as

$$\beta_o = \frac{M_N-\eta}{x_{oN}} \tag{3.33}$$

where x_{oN} is the last quadrature point.

4. Determine or estimate α (see Fig. 3.2 or Whitson et al., 1986).

5. Calculate parameter δ by combining Eqs. 3.11 and 3.26, to fulfill the requirements given by Eqs. 3.1 and 3.2

$$\delta = \exp\left[\frac{\alpha\beta_o}{M_{7+}-\eta} - 1\right] \tag{3.34}$$

6. Calculate z_i and M_i from Eqs. 3.31 and 3.32, respectively, for all pseudocomponents.

7. Check if calculated M_{7+}

$$M_{7+} = \frac{\sum_{i=1}^{N} z_i M_i}{\sum_{i=1}^{N} z_i} \tag{3.35}$$

equals the experimental M_{7+}. If not, adjust δ until a match is obtained. For each δ update, recalculate mole fractions from Eq. 3.31.

For simultaneous C_{7+} characterization of several fluid samples with a single set of pseudocomponent molecular weights, apply identical M_N, η, and β_o values to all samples. Specific values for M_{7+} and α may be specified for each individual sample. When the above procedure is repeated for all samples with identical M_N, η, and β_o values this will result in a specific δ value for each sample.

Identical sets of other pseudocomponent physical properties, required by the EOS, (γ, T_b, T_c, p_c and ω) must also be specified for the actual fluid samples. Estimation of such properties are described in the next section.

A FORTRAN program which calculates mole fraction and molecular weight for five pseudocomponents (N=5) using the above procedure is shown in Appendix B. This program was applied to generate the molar distribution of an oil and a gas condensate (Hoffmann et al., 1952) resulting in an identical set of pseudocomponent molecular weights. These results are shown in Table 3.2. Observe that δ=0.5863 and δ=1.2252 for the oil and the gas condensate sample, respectively, when calculated from Eq. 3.34. To match overall z_{7+} and M_{7+}, the δ parameters had to be slightly adjusted to 0.5846 for the oil and 1.2218 for the gas condensate. Also, note that α for the Hoffmann gas condensate is larger than other α values shown in Fig. 3.2.

TABLE 3.2 -- Definition of Molar Distribution for the Hoffmann Reservoir Fluids (Hoffmann et al., 1952).

Pseudo-Component	Composition (Mole %) Oil	Gas Condensate	Molecular Weight
C_{7+} (1)	3.4999	0.3365	98.55
C_{7+} (2)	12.7400	0.9273	135.84
C_{7+} (3)	13.2405	0.2646	206.65
C_{7+} (4)	5.9994	0.0115	319.83
C_{7+} (5)	1.0600	0.0001	500.00
z_{7+}	36.54	1.54	
M_{7+}	198.7	141.0	
C_{7+} Distribution Parameters:			
α	1.562	1.901	
η	90.0	90.0	
β	69.590	26.959	
β_o	32.435	32.435	
δ (Eq. 3.34)	0.5863	1.2252	
δ (to match M_{7+})	0.5846	1.2218	

3.2.7 Comparison of Molar Distribution Models

In this section some of the procedures presented for establishing a C_{7+} molar distribution are compared. Pseudocomponent mole fractions and molecular weights are calculated based on average C_{7+} properties, z_{7+} and M_{7+}. Distribution parameters, if required, are defined as follows: α=1.0 and η=90.

Table 3.3 presents generated C_{7+} molar distributions for a light gas condensate sample from the Tyra field (Söreide et al., 1988). This fluid was chosen to illustrate what is seemingly a paradox: the C_{7+} characterization is important for VLE calculations of gas condensates, even though z_{7+} is less than one percent. Predicted dew point pressure for the Tyra gas condensate varied from 3254 to 3494 psia [224.4, 240.9 bar] for the various distribution models. All other characterization parameters are kept constant.

Whitson et al. (1988) also studied the various C_{7+} grouping methods described above, and indicate that the gamma distribution model combined with Gaussian quadrature discretization yields the most consistent EOS results.

TABLE 3.3 -- Estimated Molar Distribution for Reservoir Fluid Tyra 1A Based on Various Split Methods (From Söreide et al., 1988).

Pseudo Component	Normalized Mole Fraction	Molecular Weight	Normalized Weight Fraction
Gaussian Quadrature. ps=3431 psia			
C_{7+} (1)	0.55216	99	0.4535
C_{7+} (2)	0.38431	136	0.4350
C_{7+} (3)	0.06132	207	0.1056
C_{7+} (4)	0.00220	320	0.0059
C_{7+} (5)	0.00001	500	0.0000
Equal Weight Fractions, ps=3300 psia.			
C_{7+} (1)	0.25479	94	0.20
C_{7+} (2)	0.23069	104	0.20
C_{7+} (3)	0.20526	117	0.20
C_{7+} (4)	0.17633	136	0.20
C_{7+} (5)	0.13294	180	0.20
Equal Mole Fractions, ps = 3264 psia.			
C_{7+} (1)	0.20	93	0.1554
C_{7+} (2)	0.20	101	0.1680
C_{7+} (3)	0.20	111	0.1850
C_{7+} (4)	0.20	127	0.2112
C_{7+} (5)	0.20	168	0.2805
SCN + Residue Split, ps=3494 psia			
C_{7+} (1)	0.38889	96	0.3111
C_{7+} (2)	0.23765	107	0.2119
C_{7+} (3)	0.14523	121	0.1464
C_{7+} (4)	0.08875	134	0.0991
C_{7+} (5)	0.13947	199	0.2314

Note:
1. M_{7+}=120 and z_{7+}=2.28 percent, M_N=M_{7+}(5)=500, α=1 and η=90.
2. p_s refers to predicted dew point pressure at 156°F [68.9°C], measured dew point at this temperature is 3565 psia [245.8 bar].

3.3 Inspection Properties Estimation

The first step in characterizing a reservoir fluid is to define the C_{7+} molar distribution. Secondly, the EOS requires critical pressure, critical temperature and acentric factor for each pseudocomponent. These parameters are usually estimated from empirical correlations expressed as functions of specific gravity and normal boiling point.

With a TBP analysis available for the actual reservoir fluid, critical properties and acentric factor can be calculated directly from general correlations as function of measured TBP data. If a TBP analysis is not available, the molar distribution must be generated using one of the methods described in Sec. 3.2, and pseudocomponent specific gravities and normal boiling points must be estimated. Generalized procedures and correlations for determining specific gravity and normal boiling point are described below and correlations for estimating critical properties and acentric factor are presented in the following sections.

The second best alternative to estimating physical properties from general correlations is to use tabulated properties for SCN groups such as first given by Katz and Firoozabadi (1978), and later modified by Whitson (1983a). The data represent average SCN properties of compounds boiling between two adjoining n-paraffins, except for the heaviest SCN groups ($>C_{25}$) for which the parameters are estimated from generalized correlations. These SCN physical properties may not be used for petroleum fractions if the estimated Watson characterization factor K_w deviates significantly from the tabulated K_ws as given by Whitson (1983a). Also, it may be difficult to match overall C_{7+} properties if generalized SCN physical properties are used.

3.3.1 Specific Gravity

Whitson Correlation

Procedures for estimating specific gravity are usually based on measured or estimated molar distribution and a characterization factor, for example the

Watson factor K_w which is assumed to reflect the average molecular type of the sample (Watson and Nelson, 1933; Watson et al., 1935).

Such a procedure was presented by Whitson (1983a,b). He combined the Riazi-Daubert (1980) molecular weight correlation given as a function of specific gravity, γ, and normal boiling point, T_b:

$$M = 4.5673(10^{-5})\ T_b^{2.19620}\ \gamma^{-1.01640} \tag{3.36}$$

with the definition of the Watson K_w factor

$$K_w = \frac{T_b^{1/3}}{\gamma} \tag{3.37}$$

This resulted in a correlation for K_w as a function of M and γ

$$K_w = 4.5579\ M^{0.15178}\ \gamma^{-0.84573} \tag{3.38}$$

which is easily expressed in terms of specific gravity as

$$\gamma_i = 6.0108\ M_i^{0.17947}\ K_w^{-1.18241} \tag{3.39}$$

Whitson suggested that a common characterization factor could apply to all pseudocomponents. Requiring that average specific gravity, γ_{7+}, calculated from

$$\gamma_{7+} = z_{7+}M_{7+}/\left(\sum_{i=1}^{N} z_i M_i/\gamma_i\right) \tag{3.40}$$

equals the measured value, and combining Eq. 3.38 with Eq. 3.40, results in an expression for K_w which fulfills this requirement

$$K_w = [0.16637\ \gamma_{7+}S_o/(z_{7+}M_{7+})]^{-0.84573} \tag{3.41}$$

where

$$S_o = \sum_{i=1}^{N} z_i M_i^{0.82053} \tag{3.42}$$

Specific gravities estimated from this method were compared to experimental data of 68 petroleum samples with complete TBP analysis available. This TBP-database is described in more detail in Appendix A. For each sample the

absolute average deviation, AAD, ranged from 0.5 to 4 percent. An overall AAD, AAD_T, was equal to 2.2 percent when including 68 samples.

Instead of applying a universal K_w factor for all fractions of a C_{7+} sample, Haaland (1981) assumed that K_w is varying, and generalized this variation in K_w for SCN groups up to C_{40}.

The Riazi-Daubert correlation, upon which Whitson based his specific gravity procedure, was developed from properties of pure hydrocarbons, and is valid in the molecular weight range 70-300. Thus, better estimates for specific gravity may eventually be determined if this correlation is modified to match available TBP data from samples in the actual reservoir or area. A correlation on the same form as Eq. 3.36 was developed by matching molecular weight data in the TBP database. This correlation is expressed as

$$M = 8.7517(10^{-5})\ T_b^{2.1329}\ \gamma^{-0.08546} \tag{3.43}$$

Applying the Whitson procedure combined with Eq. 3.43, improved the specific gravity estimates slightly, resulting in AAD_T=1.8 percent.

Proposed Modification to Whitson Correlation

Specific gravity measured from TBP analyses, and plotted versus molecular weight on a log-log scale usually produces an almost straight line as shown in Fig. 3.3. This relationship between specific gravity and molecular weight can be expressed on the form

$$\log\gamma = a + b\log M \tag{3.44}$$

Improvements over the Whitson procedure were achieved by adjusting the molecular weight exponent of Eq. 3.38. This is equivalent to adjusting constant b of Eq. 3.44. The new correlation was determined using non-linear regression minimizing the objective function

$$E_\gamma = \sum_{j=1}^{L} \sum_{i=1}^{N-1} (\gamma_{ji}^m - \gamma_{ji}^e)^2 \tag{3.45}$$

where L represents number of petroleum samples and N is the number of pseudocomponents in sample j. γ^m and γ^e refer to model and experimental specific gravity, respectively. This proposed modification introduces a new

characterization factor, denoted F_c, which is no longer equal to or related to boiling point or to the Watson K_w; i.e. $F_c \neq T_b^{1/3}/\gamma$:

$$F_c = 4.5579\ M^{0.11452}\ \gamma^{-0.84573} \tag{3.46}$$

Comparing calculated specific gravities for 68 samples with experimental data, resulted in AAD_T=1.2 percent, and AAD for any sample was lower than 3 percent.

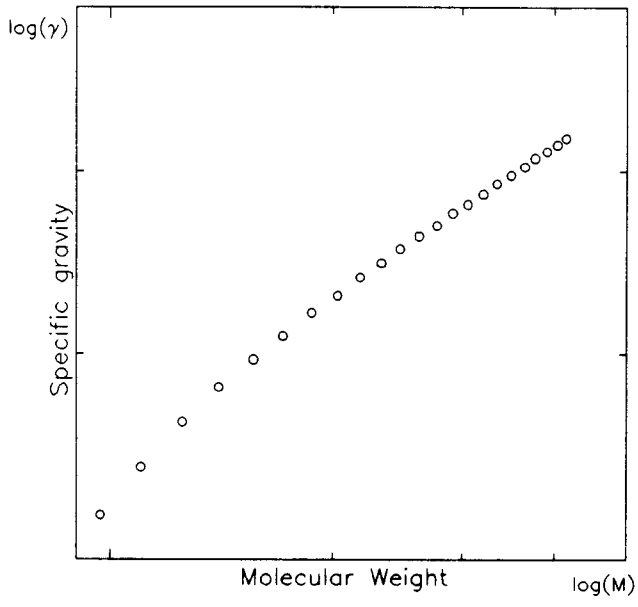

Fig. 3.3 Specific gravity versus molecular weight on a log-log scale for the C_{7+} sample of a reservoir fluid.

Procedure for Calculating Specific Gravity Using F_c:

A procedure for estimating specific gravities based on a constant characterization factor, F_c, is given below:

1. Determine mole fraction z_i and molecular weight M_i for all pseudocomponents.

2. Calculate the overall characterization factor F_c from

$$F_c = [0.16637\ \gamma_{7+}S_o/(z_{7+}M_{7+})]^{-0.84573} \tag{3.47}$$

where

$$S_o = \sum_{i=1}^{N} z_i M_i^{0.86459} \tag{3.48}$$

3. Calculate pseudocomponent specific gravities, γ_i, from

$$\gamma_i = 6.0108\ M_i^{0.13541}\ F_c^{-1.18241} \tag{3.49}$$

where F_c has been determined from Eqs. 3.47 and 3.48.

An average F_c value, calculated from the individual F_cs, is used in Eq. 3.49 in case several samples are characterized with an identical set of pseudo-component properties.

The characterization factors K_w and F_c may be used to check the consistency of C_{7+} properties. Whitson (1983a) shows that the variation in C_{7+} Watson K_w is usually within 0.02 units for the same field. So, if K_w (or F_c) for a new sample differs from the value that has been established based on analysis of already available samples, it is reason to believe that either M_{7+} or γ_{7+} is incorrect. The accuracy of M_{7+} and γ_{7+} measurements are usually within ±5 and ±1 percent, respectively. Thus, we can try to adjust the M_{7+} value maximum ±5 percent to see if this will yield a value for K_w (or F_c) which is in agreement with the earlier established field value.

Jacoby Correlation

Alternatively, specific gravity can be estimated from molar distribution data and the Jacoby aromaticity factor, J_a (Jacoby, 1964). Whitson (1983a) correlated J_a to M and γ based on charts presented by Jacoby

$$J_a = (\gamma - 0.8468 + 15.8/M)/(0.2456 - 1.77/M) \tag{3.50}$$

In terms of specific gravity this relation becomes

$$\gamma_i = 0.8468 - 15.8/M_i + J_a(0.2456 - 1.77/M_i) \tag{3.51}$$

The Watson K_w varies between 10 and 13 for highly aromatic and paraffinic compounds, respectively, while J_a=1.0 for aromatic compounds and J_a=0.0 for paraffinic compounds. Thus, J_a indicates increasing aromaticity as K_w indicates decreasing paraffinicity. Note that for paraffins (J_a=0.0), Eq. 3.51 relates specific gravity to the inverse of molecular weight as a linear function.

Yarborough (1979) modified the Jacoby aromaticity factor, and introduced the Yarborough aromaticity factor, Y_a which is expressed in terms of specific

gravity and carbon number. Compared to other methods for estimating specific gravities, the Yarborough approach is more complex, and performance is not significantly improved compared with the J_a-correlation.

Procedure for Calculating Specific Gravity From J_a:

A procedure for estimating specific gravities from the Jacoby aromaticity factor and molecular weight data can be presented as:

1. Estimate J_a from Eq. 3.50 using M_{7+} and γ_{7+}.

2. Calculate γ_i for i=1,...,N from Eq. 3.51.

3. Calculate total volume of C_{7+} as

$$v_{7+}^m = \sum_{i=1}^{N} w_i/\gamma_i \tag{3.52}$$

where w_i is weight fraction.

4. Define a function, f(v), expressing the difference between experimental and calculated C_{7+} volumes

$$f(v) = v_{7+}^m - v_{7+}^e \tag{3.53}$$

5. If f(v) is larger than a preset tolerance, e.g. $|f(v)|<10^{-7}$, update J_a using an iterative method

$$J_a^{k+1} = J_a - \frac{f(v)}{f'(v)} \tag{3.54}$$

where k indicates iteration level, and f'(v) is the derivative of f(v) with respect to J_a.

6. Repeat the procedure from step 2 until the convergence criteria in (5.) is achieved.

Specific gravities calculated using this procedure combined with Eq. 3.50, resulted in AAD_γ=1.8 percent when compared with experimental data from 68 samples. For one specific sample AAD varied from 0.2 to maximum 6 percent. It was observed that Eq. 3.50 yields better fit to specific gravity data of gas condensate samples than oil samples.

Proposed Modifications to Jacoby Correlation

Also, Eq. 3.50 was modified using non-linear regression to fit experimental specific gravities in the TBP-database. The modified correlation can be expressed as

$$J_{am} = (\gamma - 0.8468 + 14.8822/M)/(0.2456 - 14.1892/M) \quad (3.55)$$

where J_{am} is a "modified Jacoby aromaticity factor" slightly higher than J_a. Specific gravities calculated using the above procedure combined with Eq. 3.55, resulted in AAD_T=1.4 percent when compared to experimental data from 68 samples.

It was observed that specific gravity errors for the heaviest TBP-cut correlated with M_{7+} of the actual samples. This observation led to a slight modification of Eq. 3.50 by also including M_{7+}

$$J_{am}(M_{7+}) = [\gamma + 1.643(10^{-3})M_{7+} - 1.07179 + 14.9739/M]/[0.2456 - 6.8573/M] \quad (3.56)$$

Comparing specific gravities calculated using the above procedure and Eq. 3.56 to experimental data from 68 samples, resulted in AAD_T=1.2 percent.

Developed Correlation

A better equation for expressing the relation between specific gravity and molecular weight, suggested by Whitson (1989), can be written as

$$\gamma_i = a + C_f(M_i - M_o)^c \quad (3.57)$$

where C_f is a constant adjusted to ensure equality between calculated and experimental γ_{7+}. Typically, C_f varies between 0.27 and 0.31. The correlation constants were determined using non-linear regression to fit experimental data from the TBP-database, yielding: a=0.28554, M_o=65.94185, and c=0.129969. Based on a comparison of experimental and calculated specific gravities for the 68 samples, AAD_T was found to be equal to 0.94 percent. The highest AAD for any of the 68 sample was equal to 2.55 percent.

Comparing Specific Gravity Correlations

The characterization factors K_w, F_c, J_a, J_{am} and C_f are estimated for some pure aromatic and paraffinic compounds and for the C_{7+} fraction of several oil and gas condensates. These results are shown in Table 3.4.

TABLE 3.4 -- Comparison of Characterization Factors Estimated From Various Correlations

	Experimental		Characterization Factors				
Sample	M_{7+}	SG_{7+}	K_w	F_c	J_a	J_{am}	C_f
Standing-Katz	228.5	0.8682	11.71	9.57	0.381	0.487	0.3006
Hoffmann Oil	198.7	0.8409	11.78	9.67	0.311	0.413	0.2942
Albuskjell No. 3	153.7	0.7871	11.98	9.93	0.184	0.260	0.2804
Albuskjell No. 4	176.5	0.8043	12.02	9.91	0.200	0.268	0.2814
Albuskjell No. 5	175.2	0.8033	12.02	9.91	0.198	0.267	0.2813
RRI: Austad et al.	177.5	0.8067	12.00	9.89	0.208	0.279	0.2824
Eldfisk No. 1	219.7	0.8517	11.83	9.68	0.323	0.416	0.2943
Eldfisk No. 3	232.1	0.8601	11.84	9.66	0.342	0.434	0.2956
Ekofisk No. 1	232.9	0.8534	11.92	9.73	0.313	0.395	0.2920
Benzene	78.114	0.885	9.79	8.33	1.079	4.515	0.4332
n-Hexane	86.178	0.6644	12.67	10.73	0.004	-0.114	0.2563
Ethylbenzene	106.168	0.8721	10.39	8.73	0.761	1.629	0.3629
n-Octane	114.232	0.7073	12.54	10.51	-0.005	-0.070	0.2548

Overall C_{7+} properties for each C_{7+} sample included in modifying/developing the specific gravity correlations, are presented in Table A-1, Appendix A. Results from comparing calculated and measured properties are also given in terms of absolute average deviations for each sample. Table A-2 lists the various characterization factors for all samples.

Specific gravities calculated from the correlations are plotted versus measured data in Fig. 3.4 for the Hoffmann et al. oil and in Fig. 3.5 for the Albuskjell No. 3 gas condensate. The calculated specific gravities are based on measured molar distribution data from TBP analyses.

It is observed from these figures that Eq. 3.39 [$\gamma(K_w)$] overestimates and Eq. 3.51 [$\gamma(J_a)$] underestimates specific gravity of the heaviest fractions. The effect of using various specific gravity correlations on predicted saturation pressures is presented in Table 3.5. The results are based on using PR EOS (Robinson and Peng, 1978) and a standard procedure for characterizing the C_{7+} fraction. It is observed that calculated saturation pressure for the Hoffmann oil varies between 3786 psia [261.1 bar] and 3819 psia [263.4 bar] for J_a and K_w, respectively. As expected the scatter is much larger for the gas condensate where the lowest estimated pressure is 6309 psia [435.1 bar] for J_a and the highest is 6682 psia [460.8 bar] for K_w.

TABLE 3.5 -- Effect of Using Various Specific Gravity Correlations on Predicted Saturation Pressures for the Hoffmann Oil and Albuskjell No.3 Gas Condensate.

Specific Gravity Correlation	Saturation Pressure, psia	
	Hoffmann Oil	Albuskjell GC
K_w, Eq. 3.39	3819	6682
F_c, Eq. 3.49	3802	6448
C_f, Eq. 3.57	3803	6436
J_a, Eq. 3.51	3786	6309
J_{am}, Eq. 3.55	3802	6371
$J_{am}(M_{7+})$, Eq. 3.56	3801	6337

Note:
1. Saturation pressure for the Hoffmann Oil is calculated at 201°F and for the Albuskjell gas condensate at 280°F.
2. The PR EOS and a standard characterization procedure, except for C_{7+} γs, have been used.

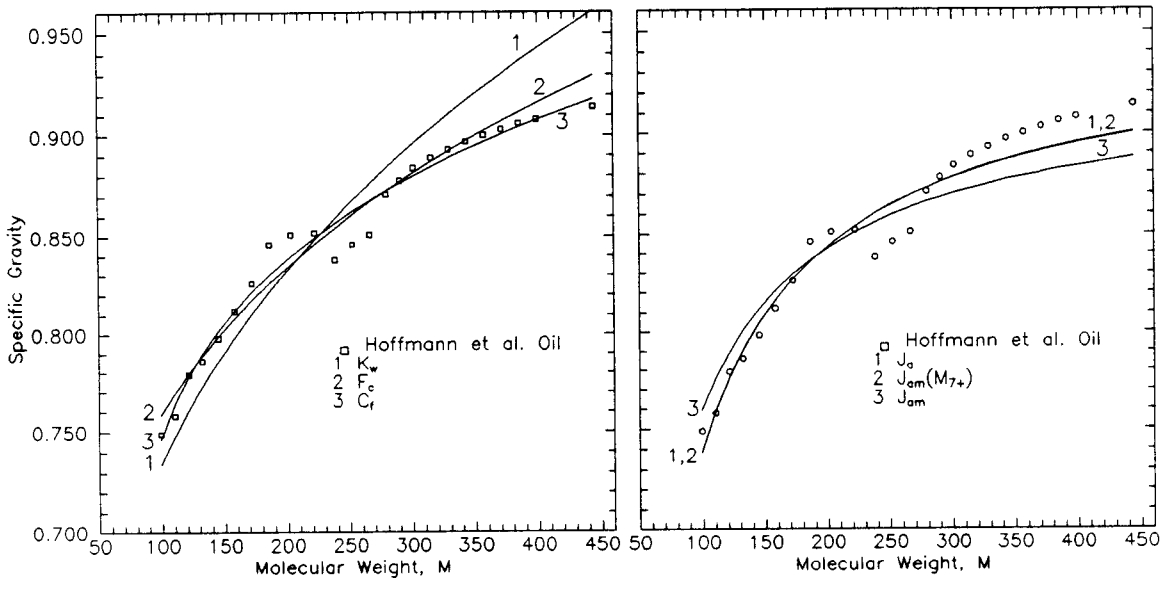

Fig. 3.4 Comparison of measured and estimated C_{7+} specific gravities for the Hoffmann oil.

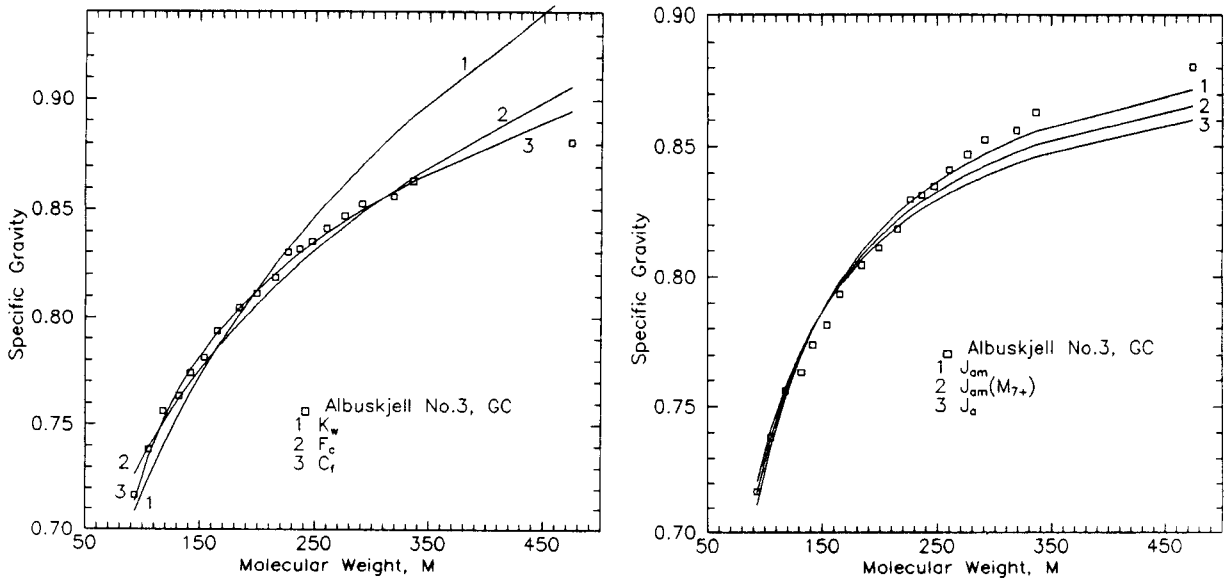

Fig. 3.5 Comparison of measured and estimated C_{7+} specific gravities for the Albuskjell No. 3 gas condensate.

3.3.2 Normal Boiling Point

Normal boiling point, T_b, is used as an input parameter to generalized correlations for critical properties and acentric factor of petroleum fractions. Several choices exist for estimating T_b from inspection properties, and some of these are presented here.

Generalized correlations for boiling point as functions of molecular weight and specific gravity have been proposed by Riazi and Daubert in 1980 and 1987. The latter, a five-parameter correlation denoted RD87, is presented here because the original publication includes some errors

$$T_b = \exp[3.7741(10^{-3})M + 2.9840\gamma - 4.2529(10^{-3})M\gamma]$$
$$6.7786M^{0.40167}\,\gamma^{-1.58262} \qquad (3.58)$$

The RD80 and RD87 T_b correlations were compared to T_b data of 843 petroleum fractions included in the TBP database. This resulted in absolute average deviations of 2.166 and 1.054 percent, respectively. These results are listed in Table 3.6 together with maximum absolute deviations of 16.89 and 4.30 percent, respectively. Riazi and Daubert claimed that their two correlations,

developed from data for pure hydrocarbons up to C_{20}, are applicable in the boiling point range from 540 to 1100°R [300-610 K].

TABLE 3.6 -- Results From Comparing Experimental and Estimated Boiling Points From Various Generalized Correlations.

	RD80	RD87	Twu	Eq. 3.59
AAD	2.166	1.054	2.104	0.939
BIAS	1.358	-0.368	1.616	-0.024
MAXD	16.892	4.300	8.446	5.039

Notes:
1. RD80 and RD87 refer to Riazi and Daubert (1980) and (1987), respectively.

Probably, the most widely used T_b-correlation for petroleum fractions has been proposed by Twu (1984). This rather complex correlation generally seems to perform quite well, but occasionally fails to estimate T_b when molecular weight becomes higher than about 600. Table 3.6 shows that a comparison of estimated T_bs from the Twu correlation with measured data from the TBP database, results in AAD=2.10 percent and MAXD=8.45 percent.

Proposed Correlation

A new boiling point relation has been developed using non-linear regression to fit T_b data in the TBP database. The correlation is given on the following form

$$T_b^{\infty} = T_b - a \exp[bM + c\gamma + dM\gamma] \, M^e \, \gamma^f \qquad (3.59)$$

and correlation constants, yielding T_b in °R, are presented in Table 3.7. A comparison of T_b estimated from Eq. 3.59 with measured data, resulted in AAD=0.95 percent and MAXD=4.05 percent. These results compare favorably with corresponding results from the other T_b correlations referred. The temperature interval for which Eq. 3.59 is valid ranges from 650 to 1500 °R [361, 830 K]. However, because of good extrapolating capabilities, it may predict reasonable boiling point estimates also for much heavier fractions.

In Fig. 3.6 boiling points estimated from the various correlations are plotted versus molecular weight and compared to measured data for the Hoffmann oil.

The calculated C_{7+} T_bs are based on inspection properties determined as follows:

(1) a best-fit to the reported molar distribution was determined with α and η equal to 1.564 and 90, respectively.

(2) the molar distribution was discretized into 10 pseudocomponents using Gaussian quadrature. M_N was set as high as 800 to observe the performance of the various T_b correlations for very heavy fractions.

(3) pseudocomponent specific gravities were estimated using the C_f correlation given by Eq. 3.57.

TABLE 3.7 -- Correlation Constants for Proposed Boiling Point Correlation Which Yields T_b in °R.

T_b^{∞}	:	1928.3
a	:	$1.695(10^{+5})$
b	:	$-4.922(10^{-3})$
c	:	-4.7685
d	:	$3.462(10^{-3})$
e	:	$-3.522(10^{-2})$
f	:	3.266

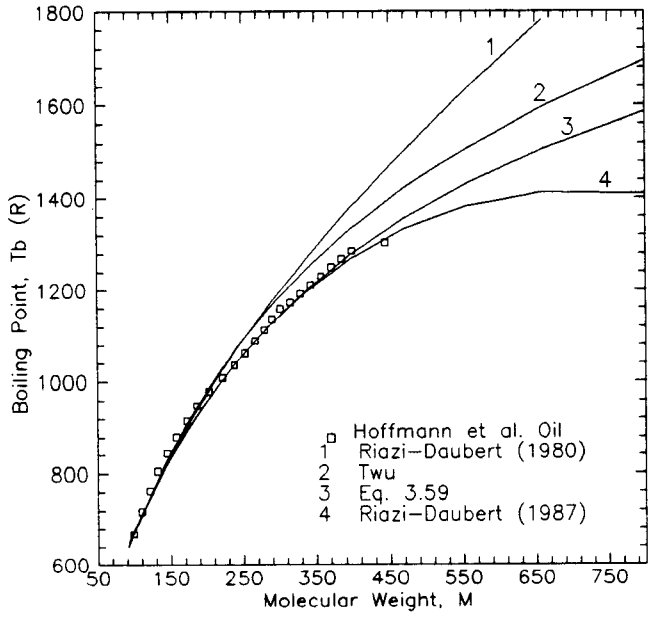

Fig. 3.6 Comparison of measured and estimated boiling points for the Hoffmann oil.

It is observed that the RD80 and Twu correlations overestimates T_b for M larger than 250. The RD87 correlation and Eq. 3.59 result in almost identical matches to the measured data up to M=450. Also, it is noticed that the RD87 correlation goes through a maximum at M=650, and thus may not be used for fractions with molecular weight heavier than 500. The behavior of Eq. 3.59 for very heavy fractions seems to be more realistic. The effect of estimating T_b from various correlations on predicted bubble point, is shown in Table 3.8.

TABLE 3.8 -- Effect of Using Various Boiling Point Correlations on Predicted Bubble Point Pressures for the Hoffmann oil at 201°F [93.9°C].

	Boiling Point Correlation			
	Eq. 3.59	RD80	RD87	Twu
p_s, (psia)	3803	11597	3797	3829

Notes:
1. RD87 and RD80 refer to Riazi and Daubert (1987) and (1980), respectively.
2. p_s refers to predicted bubble point pressure at temperature 201°F, based on use of the PR EOS and a standard characterization procedure, except for the C_{7+} T_bs. C_{7+} γs are estimated from Eq. 3.57.

3.4 Critical Properties Estimation

In this section some of the many critical properties correlations are discussed. For a more complete review see Whitson (1984).

Probably the most well-known correlations for estimating critical pressure and temperature for petroleum fractions are those presented by Cavett (1962), Kesler and Lee (1976) and Riazi and Daubert (1980). The Kesler-Lee relations are based on experimental data of petroleum fractions with boiling point up to 1650°R [916 K]; modifications were introduced to extend the correlations beyond this limit. The Kesler-Lee critical pressure correlations have been developed so that p_c will equal atmospheric pressure when T_c coincides with T_b. The very simple three-parameter correlations presented by Riazi and Daubert are claimed to be valid in the boiling point range 550-1100°R [300-611 K]. Whitson (1984) proposed an extension to the Riazi-Daubert (1980) critical pressure correlation for heavier boiling points. No limitations or ranges of validity are given for the Cavett correlations.

In 1984 Twu presented correlations for estimating critical properties that were based on perturbation theory. These are rather complex and interrelated, which according to Riazi and Daubert (1987) may be a drawback: an error in predicting one property may propagate into a larger error when predicting another property. The relations are based on systems with boiling points up to 1800°R [1000 K] and specific gravities up to 1.436.

Lately, Riazi and Daubert (1987) presented a set of critical property correlations which are claimed to be superior to other correlations. These are given by the simple form

$$\theta = a \exp[bT_b + c\gamma + dT_b\gamma]\, T_b^e\, \gamma^f \qquad (3.60)$$

where θ refers to properties T_c or p_c, and the five constants of the respective correlations are presented in Table 3.9 since the correlation constants in the original publication are not correct. Also, these correlations are developed based on data in the boiling point range 550-1100°R [300-611 K].

TABLE 3.9 -- Correlation Constants for the Riazi-Daubert (1987) Critical Property Correlations.

θ	T_c	p_c
a	10.6443	$6.162(10^{+6})$
b	$-5.1747(10^{-4})$	$-4.725(10^{-3})$
c	-0.54444	-4.8014
d	$3.5995(10^{-4})$	$3.194(10^{-3})$
e	0.81067	-0.4844
f	0.53691	4.0846

Note:
1. T_c will result in °R and p_c in psia with T_b reported in °R and γ as relative density at (60°F/60°F).

Critical volume, V_c, may be calculated using the RD80 correlation. In addition the V_c correlation proposed by Twu (1984) can be used. Critical volume is not input directly to any EOS, but may be used for calculating viscosities e.g. from the Lohrenz-Bray-Clark (1964) procedure or for calculating binary interaction parameters from the Chueh-Prausnitz (1967b) correlation.

Pseudocomponent critical properties (p_c,T_c) for the Hoffmann oil are estimated from the various correlations referred. C_{7+} T_bs and γs are estimated as described in Section 3.3.2. In the boiling point range 650-1000°R [361-555 K], it is observed from Fig. 3.7 that highest critical pressures result from the Cavett correlation. In the same range the Riazi-Daubert correlations result in lowest critical pressures. The Cavett correlation seems to go through a minimum at 1400°R [780 K], which may not be physically realistic. Kesler-Lee critical pressures are lowest for T_b>1300°R [>722 K].

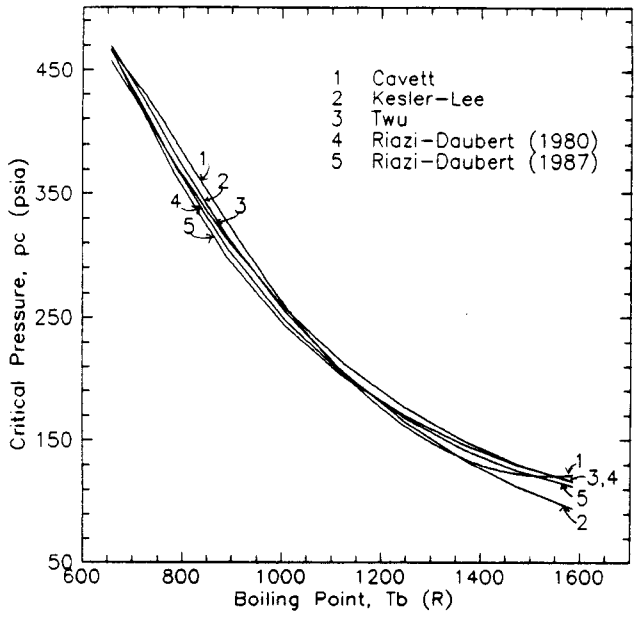

Fig. 3.7 Estimated C_{7+} critical pressures plotted versus boiling point for the Hoffmann oil.

Critical temperatures for Hoffmann oil pseudocomponents are estimated using the various correlations and plotted versus boiling point in Fig. 3.8. At high boiling points, the Kesler-Lee and Riazi-Daubert (1987) result in lowest and highest critical temperatures, respectively. The Cavett and Riazi-Daubert (1980) correlations predict nearly identical critical temperatures, while T_cs from the Twu correlation are slightly higher. Table 3.10 shows the effect of using various critical temperature and critical pressure correlations on predicted bubble point pressure of the Hoffmann oil at temperature 201°F [93.9°C].

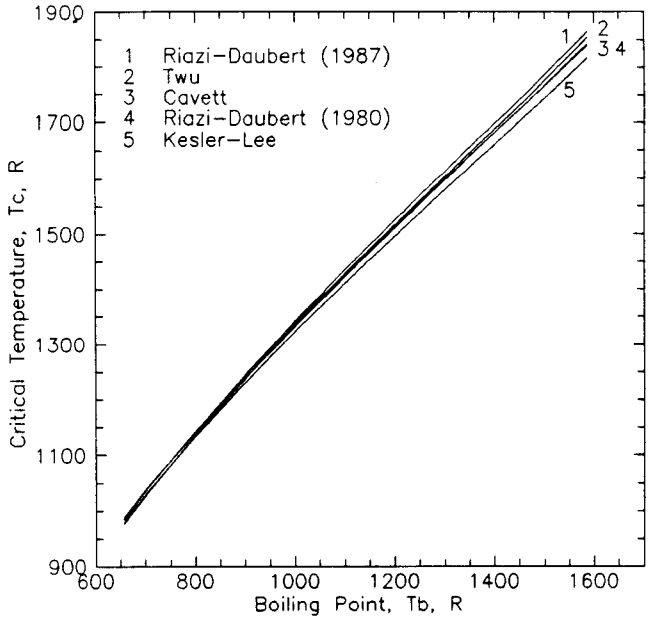

Fig. 3.8 Estimated C_{7+} critical temperatures plotted versus boiling point for the Hoffmann oil.

TABLE 3.10 -- Effect of Using Various Critical Temperature and Critical Pressure Correlations on Predicted Bubble Point Pressure of the Hoffmann oil at 201°F [93.9°C].

	Critical Properties Correlations				
	RD87	RD80	K-L	Twu	Cavett
p_s (psia)	3803	3904	4287	4134	4126

Notes:
1. RD87 and RD80 refer to Riazi and Daubert (1987) and (1980), respectively. K-L refers to Kesler and Lee, (1976).
2. p_s refers to predicted bubble point pressure at temperature 201°F, based on using the PR EOS and a standard characterization procedure, except for critical properties. C_{7+} T_bs are calculated From Eq. 3.59 and C_{7+} γs are estimated from Eq. 3.57.

3.5 Acentric Factor

Two correlations for estimating acentric factor are commonly used for petroleum fractions. One is suggested by Lee and Kesler (Lee and Kesler, 1975, Kesler and Lee, 1976). The first relation was developed for pure components with a T_b/T_c-ratio lower than 0.8, and the latest was based on data for petroleum fractions with $T_b/T_c>0.8$. The second acentric factor correlation is proposed by Edmister (1958). For petroleum fractions, Whitson (1984) strongly suggests that the Lee-Kesler relations be used.

Proposed Procedure

In this section a procedure for estimating C_{7+} acentric factors resulting in boiling points correctly predicted by the EOS, is proposed.

A basic requirement of EOS fluid characterization should be that pure component phase and volumetric behavior are correctly predicted. For example, Zudkevitch and coworkers (1970) proposed adjusting EOS constants Ω_a and Ω_b for each pure component to match measured saturated vapor pressure and liquid density data at various subcritical temperatures. For petroleum fractions two experimental data points are given in terms of the inspection properties: the normal boiling point and specific gravity representing liquid density at standard conditions. The EOS characterization should ensure that the EOS predicts these two data points.

Yarborough (1979) suggested that EOS constants Ω_a and Ω_b, also for heavy, undefined fractions be adjusted to attain a consistent EOS characterization for each fraction. Another approach is to adjust C_{7+} critical properties, p_c and T_c (Whitson, 1984). In this work it is proposed that each C_{7+} acentric factor be adjusted to obtain an EOS consistent boiling point.

The procedure for estimating acentric factor resulting in a correctly EOS-predicted boiling point, is presented as follows:

1. Estimate inspection and critical properties for the actual pseudocomponent, i.e. M, γ, T_b, T_c and p_c. Also, obtain an initial estimate for ω, e.g. from the Lee-Kesler ω-relations.

2. At atmospheric pressure, p_{sc}, and temperature T_b, calculate vapor and liquid phase compressibility factors, Z_V and Z_L, respectively, with the actual EOS.

3. If $Z_V=Z_L$, p_{sc} and T_b represent conditions in the single phase region, and a higher ω value will move the coexistence curve upwards until the actual conditions (p_{sc},T_b) are inside the two phase region.

4. Calculate vapor and liquid phase fugacities, f_V and f_L, respectively.

5. Check if $|f_L-f_V| \leq (10^{-6})$. If not, iterate on ω until this criterion is fulfilled.

In Fig. 3.9 a pressure-volume diagram illustrates how the EOS predicted vapor pressure at the normal boiling point varies as a result of acentric factor adjustments.

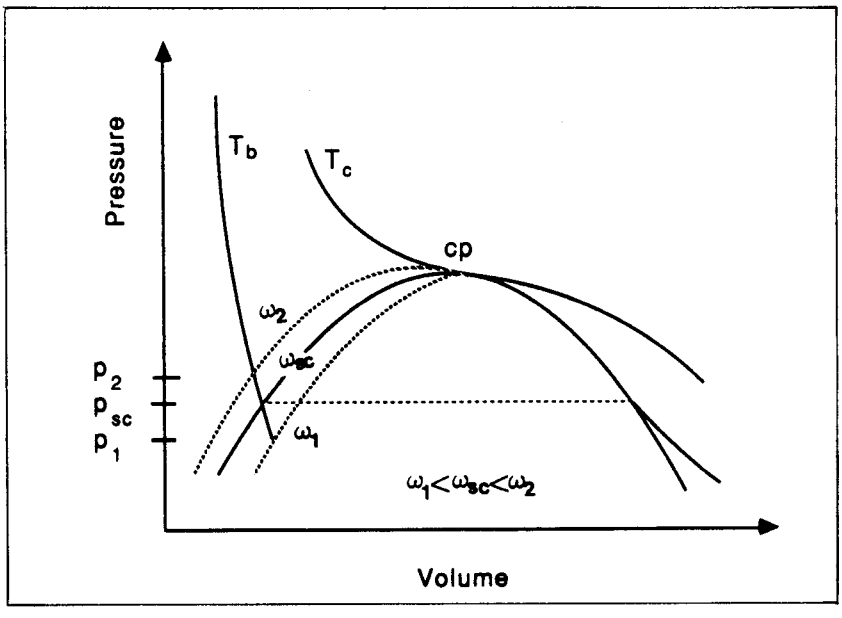

Fig. 3.9 Pressure-volume diagram for a C_{7+} pseudocomponent illustrating the effect of acentric factor estimates on vapor pressure.

In Fig. 3.10 pseudocomponent acentric factor estimated from the Lee-Kesler and Edmister correlations and the proposed procedure are plotted versus boiling point for the Hoffmann oil. C_{7+} inspection properties are estimated as described in Section 3.3.2. Critical properties are estimated using the RD87 correlations. The modified Peng-Robinson EOS was used for the EOS-based procedure (Robinson and Peng, 1978). The Edmister correlation results in the

lowest acentric factors. It is interesting to note that acentric factors estimated from the EOS-based procedure and the Lee-Kesler relations are almost identical up to T_b=1250 °R [695 K]. At higher boiling points the Lee-Kesler relations show peculiar behavior. The effect of estimating acentric factor from different correlations or procedures on predicted bubble point pressure is shown in Table 3.11. Note that the difference in predicted saturation pressure using either Lee-Kesler or the EOS-based method is only a few psia.

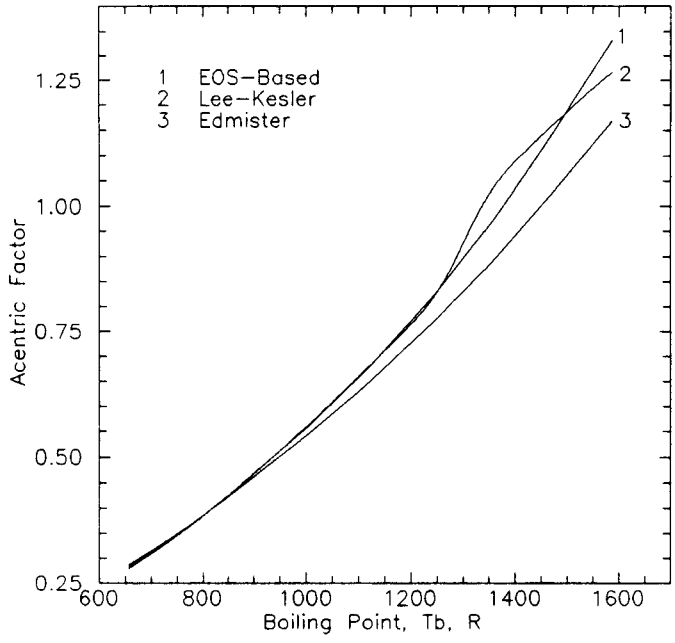

Fig. 3.10 Estimated C_{7+} acentric factors plotted versus boiling point for the Hoffmann oil.

TABLE 3.11 -- Effect of Estimating C_{7+} Acentric Factor From Different Correlations and Procedures on Predicted Bubble Point Pressure for the Hoffmann oil at 201°F [93.9°C].

	Acentric Factor		
	EOS-Based	L-K	Edmister
p_s, (psia)	3803	3819	3717

Notes:
1. "EOS-Based" refers the EOS based acentric factor estimation procedure resulting consistent C_{7+} T_bs.
2. L-K refers to the acentric factor relations proposed by Lee and Kesler, (1975, 1976).
3. p_s refers to predicted bubble point pressure at temperature 201°F, based on using a standard characterization procedure except for acentric factor.

3.6 Volume Translation

Proposed Procedure

In this section a method is proposed for determining shift parameters of C_{7+} petroleum fractions. The procedure is analogous to the EOS-based method for determining pseudocomponent acentric factors.

The EOS-based volume translation approach resulting in consistent pseudocomponent specific gravities is presented below:

1. Estimate pseudocomponent inspection and critical properties: M, T_b, γ, T_c, p_c, and ω.
2. At standard conditions calculate EOS liquid molar volume, v_{EOS}.
3. Convert the pseudocomponent measured (or estimated) specific gravity, γ, to molar volume, $v_e=0.0160185M/\gamma$ (ft^3/lb-mol), and calculate volume correction c, $c=(v_e-v_{EOS})$, or shift parameter s, $s=c/b$.

The various methods for estimating pseudocomponent shift parameters are compared in Table 3.12 for a reservoir oil from the Gorm field (Söreide et al., 1988). Saturated oil densities predicted with the modified PR EOS including volume translation are also shown.

In Fig. 3.11, PR EOS shift parameters determined from various correlations and procedures are plotted versus molecular weight. The data refer to the C_{7+} fraction of the Hoffmann oil. It should be noted that the Jhaveri and Youngren shift parameter correlation for heavy fractions results in monotonously increasing shift parameters for increasing molecular weights. This behavior is not consistent with the declining functional form of s versus M which results from the EOS-based procedure.

A more detailed comparison of EOS predicted volumetric behavior with and without volume translation is given in Section 5.

TABLE 3.12 -- Pseudocomponent PR EOS Shift Parameters For a Gorm Oil Calculated From Various Correlations or Procedures (From Söreide et al., 1988).

Pseudo Component	Volume Translation Shift Parameters, s			
	EOS-Based	J-Y[1]	J-Y[2]	C-M
C_{7+} (1)	0.0212	-0.0758	0.0018	-0.0221
C_{7+} (2)	0.0686	-0.0154	0.0639	0.0302
C_{7+} (3)	0.1374	0.0585	0.1392	0.1045
C_{7+} (4)	0.1499	0.1296	0.2112	0.1210
C_{7+} (5)	0.0392	0.1969	0.2787	0.0068
$\rho_{l,sat}$ (lb/ft^3)	43.265	42.697	45.177	42.296

Notes:
1. "EOS-Based" refers to the EOS-based proposed procedure.
2. J-Y_1 refers to the s-correlation presented by Jhaveri and Youngren (1984) (Eq. 1.71). For J-Y^1; d=2.458 and e=0.18, and for J-Y^2; d=2.5, e=0.2.
3. C-M refers to the s-correlation proposed by Chien and Monroy (1986).
4. $\rho_{l,sat}$ represents saturated liquid densities predicted with the modified PR EOS (Robinson and Peng 1978), and a standard C_{7+} characterization. Pure component shift parameters used are tabulated in Table 1.3.
5. Experimental saturated liquid density is 43.93 lb/ft^3 [γ_o=0.7037].

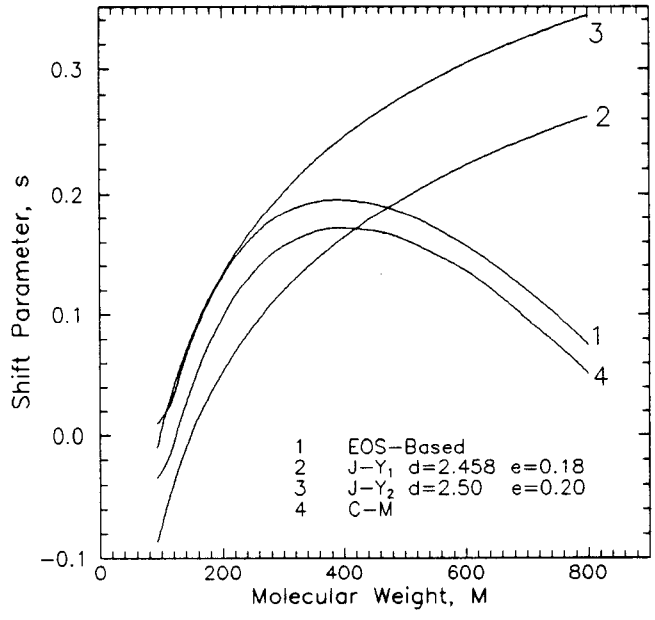

Fig. 3.11 Estimated C_{7+} shift parameters plotted versus boiling point for the Hoffmann oil.

3.7 Binary Interaction Parameters

Binary interaction parameters (BIPs) are used to enhance the predictive capabilities of an EOS used for VLE calculation of reservoir fluids. Several approaches exist for estimating BIPs for binaries including heavy, undefined fractions. Hydrocarbon-hydrocarbon (HC) BIPs, k_{ij}, may be calculated from a modified Chueh-Prausnitz (1967b) relation

$$k_{ij} = A\{1-[\frac{2(V_{cj}V_{ci})^{1/6}}{V_{cj}^{1/3}+V_{ci}^{1/3}}]^B\} \tag{3.61}$$

where V_c is the critical molar volume (ft^3/lb-mole). B is set equal to 6.0, and A is adjusted to match saturation pressure and other available VLE data. Usually, a good prediction of the saturation pressure of reservoir fluids is obtained with A=0.2-0.25. Another relation for estimating HC-HC binaries is given by Pedersen et al. (1985b)

$$k_{ij} = A(M_i/M_j)^B \ , \quad i>j \tag{3.62}$$

$$k_{ij} = A(M_j/M_i)^B \ , \quad j>i \tag{3.63}$$

with A≈0.001 and B≈1.0

Katz and Firoozabadi (1978) correlated PR EOS interaction parameters for methane-C_{7+} binaries as function of specific gravity of the C_{7+} fraction. Based on data presented by these authors, Whitson (1983a) developed the following relation

$$k_{1j} = 0.14\gamma_j - 0.0668 \tag{3.64}$$

where subscript 1 and j refer to methane and the $C_{7+}(j)$ fraction, respectively.

Slot-Pedersen (1987) propose a method for calculating BIPs for the PR EOS as function of component molecular weights. He claims that the procedure is physically consistent and simple to use.

Varotsis et al. (1986) suggest relations for calculating interaction parameters for the binaries N_2-HC, C_1-HC and CO_2-HC as function of acentric factor and reduced temperature. Binaries of N_2-HC and CO_2-HC are also corrected for pressure, which is thermodynamically inconsistent.

Interaction parameters for CO_2-, N_2-, H_2S- HC binaries are proposed by Nagy and Shirkovskiy (1982) as presented in Table 3.13.

TABLE 3.13 -- Interaction Parameters for Non-hydrocarbon -- Hydrocarbon Binaries (after Nagy and Shirkovskiy, 1982).

	N_2	CO_2	H_2S
N_2	0.000	0.000	0.130
CO_2	0.000	0.000	0.135
C_1	0.025	0.105	0.070
C_2	0.010	0.130	0.085
C_3	0.090	0.125	0.080
iC_4	0.095	0.120	0.075
nC_4	0.095	0.115	0.075
iC_5	0.100	0.115	0.070
nC_5	0.100	0.115	0.070
C_6	0.110	0.115	0.070
C_{7+}	0.115	0.115	0.055

CHAPTER 4
NON-LINEAR REGRESSION

This chapter describes regression used as a tool for matching PVT data with a cubic equation of state. Following an introduction to the topic, a definition of the least-squares minimization problem is given. Various regression models are presented, such as Gauss-Newton, steepest descent and rotational discrimination. Some practical aspects related to using regression to match PVT data are also discussed. Finally, performance of the various models are compared for specific example calculations.

4.1 Introduction

Because of limitations associated with the EOS itself, and uncertainties with respect to C_{7+} characterization, EOS prediction may be inadequate. Manual EOS tuning by adjusting pseudocomponent critical properties may result in a reasonable match to the experimental PVT data set, however manual matching is cumbersome and time consuming. A more efficient approach is to use non-linear regression to simultaneously adjust the selected EOS parameters such that EOS predicted PVT data "match" the measured data set.

Use of regression for tuning of an EOS characterization is not a straightforward procedure. Different views exist on which regression methods are best suited, and which EOS parameters should be adjusted. Basically, any parameter which affects the objective function may be defined as a regression parameter. Practically, however, the regression is limited to EOS parameters with highest uncertainty and greatest influence on the calculated properties.

Estimation methods based on least-squares minimization assume that parameter and data errors are distributed approximately according to the Gaussian distribution. Methods where the objective function is given in terms of absolute deviations of residuals assumes that parameter and data errors are distributed according to an exponential probability distribution (Press et

al., 1988). A method applying successive solution of the linear programming (LP) problem, has also been tested during this thesis work. However, the LP approach was found to require a large amount of computer storage and CPU time, especially for large problems with many data points, and is thus not described here.

Coats and Smart (1986) present a general procedure for matching PVT data of reservoir fluids with an EOS. They use a modified linear programming method to minimize the objective function in a least-squares sense. Coats and Smart suggest that EOS constants Ω_a and Ω_b for C_1 and the heaviest C_{7+} pseudo-component should be selected as regression parameters in addition to BIPs for C_1-C_{7+}.

Agarwal et al. (1987) proposed a "dynamic" parameter selection of EOS characterization parameters for PVT matching. They divide the regression parameter candidates into two groups: active and non-active parameters based on the magnitude of objective function derivatives with respect to the parameters. The former group consists of parameters with the largest potential for reducing the objective function. The group of non-active regression parameters may have little impact on the objective function. Definition of active and non-active parameters is reconsidered after each iteration. The authors claim that this approach will keep the number of simultaneously adjusted parameters relatively low, and still maintain a high convergence rate.

Agarwal et al. suggest that pseudocomponent critical properties and acentric factor be used as regression parameters, in addition to interaction parameters for non-hydrocarbon--hydrocarbon binaries, and for C_1-C_{7+} binaries. Agarwal et al. use an adaptive regression method which can be switched between two models: a Gauss-Newton model which is used for the first iterations, and later a Secant model (Dennis et al., 1981). Gani and Fredenslund (1987) also suggest that effective regression parameter candidates be determined from sensitivity analysis.

4.2 Least-Squares Models

Formulation

The least-squares minimization problem can be formulated as follows:

An objective function, $F(\underline{x})$, is defined as:

$$F(\underline{x}) = \underline{r}^T\underline{r} \tag{4.1}$$

where vector $\underline{x}=[x_1,x_2,\ldots,x_N]$ represents N independent variables, or here, regression parameters. The elements of $\underline{r}$ are the dependent variables, $r_i(\underline{x})$, or residuals. $r_i(\underline{x})$ expresses relative difference between an experimental data point, y_i, and the corresponding EOS predicted point, $g_i(\underline{x})$,

$$r_i = w_i[g_i(\underline{x})-y_i]/y_i, \quad i = 1,\ldots,M \tag{4.2}$$

where w_i is a weighting factor. The objective function $F(\underline{x})$ can also be described as a sum of squares of the residuals $r_i(\underline{x})$

$$F(\underline{x}) = \sum_{i=1}^{M} r_i^2 \tag{4.3}$$

Usually $g_i(\underline{x})$, and thus $F(\underline{x})$, is non-linear in $\underline{x}$, and an iterative process is required. At iteration k, the location of the base point in the parameter space is defined by $\underline{x}_k$. The iteration procedure continues until convergence is achieved, that is $\{[F(\underline{x}_{k+1})-F(\underline{x}_k)]/F(\underline{x}_k)\}<\epsilon$, where e.g. $\epsilon=10^{-6}$. The procedure may also be terminated for other reasons, e.g. the elements of $\Delta\underline{x}_k=\underline{x}_{k+1}-\underline{x}_k$ are very small.

If it is assumed that $F(\underline{x}_k)$ is continuous, and that its first and second derivatives exist, a minimum of $F(\underline{x}_k)$ can only be found at a stationary point. That is a point where

$$\frac{\partial F(\underline{x}_k)}{\partial x_i} = 0, \quad i=1,\ldots,N \tag{4.4}$$

$F(\underline{x}_k)$ is expanded in a Taylor series around the k'th iterate $\underline{x}_k$, ignoring third and higher order terms:

$$F(\underline{x}_k+\Delta\underline{x}_k) = F(\underline{x}_k) + \nabla F(\underline{x}_k)\Delta\underline{x}_k + \\ + 1/2\ \Delta\underline{x}_k\nabla^2 F(\underline{x}_k)\Delta\underline{x}_k + (0)^3 \tag{4.5}$$

The first and second derivatives of F are described as follows:

$$\nabla F(\underline{x}_k) = 2\mathbf{J}(\underline{x}_k)^T\underline{r}(\underline{x}_k) \tag{4.6}$$

$$\nabla^2 F(\underline{x}_k) = 2[\mathbf{J}(\underline{x}_k)^T\mathbf{J}(\underline{x}_k) + \mathbf{Q}(\underline{x}_k)] \tag{4.7}$$

where elements of the Jacobian matrix, **J**, are

$$J(\underline{x}_k)_{ij} = \frac{\partial \underline{r}(\underline{x}_k)_i}{\partial x_j} \tag{4.8}$$

and where $\nabla^2 F$ is the Hessian matrix, **H**, of second derivatives of F with respect to the parameters $\underline{x}$. Matrix **Q** is defined from:

$$\mathbf{Q}(\underline{x}_k) = \sum_{i=1}^{M} r_i(\underline{x}_k)\ \nabla^2 r_i(\underline{x}_k) \tag{4.9}$$

The elements of **Q** are difficult (or expensive) to obtain, and since these are assumed to be small, **Q** is neglected. At first sight, this seems to be a good approximation only close to the solution. However, since the residuals usually are rather evenly distributed between positive and negative values, it is in general a fair approximation unless the data set includes systematic errors.

Gauss-Newton Model

The Gauss-Newton method always assumes **Q** can be neglected. The least-squares problem can then be expressed on the form:

$$(\mathbf{J}^T\mathbf{J})\Delta\underline{x}_k = \mathbf{J}^T\underline{r} \tag{4.10}$$

Since the Hessian matrix is approximated by first derivatives of the residuals $\underline{r}$ and simplifies to $\mathbf{H}\approx\mathbf{J}^T\mathbf{J}$, the solution to Eq. 4.10 can be written as:

$$\Delta\underline{x}_k = -\mathbf{H}^{-1}\mathbf{J}^T\underline{r} \tag{4.11}$$

A necessary condition for a minimum to exist is that **H** is positive definite, i.e. all eigenvalues of **H** are positive. When some or all eigenvalues of **H** are

less than zero, the parameter space is a saddle point or a maximum. When **H** is singular or nearly so, its inverse does not exist, and Eq. 4.11 has no solution. In this case, **H** may have one or more eigenvalues equal to zero. Even when the eigenvalues are close to zero, matrix **H** approaches singularity. This leads to round-off errors in the inversion of **H**, and results in unrealistically large values for $\Delta\underline{x}_k$. Typically, this occurs when a regression parameter with a negligible effect on the sum of squares is defined; i.e., a "null-effect" parameter.

When **H** is positive definite, the Gauss-Newton method results in a solution vector $\Delta\underline{x}_k$ with a direction which always leads to a lower sum of squares in the neighborhood of $\underline{x}_k$. This is known as the property of truncation convergence. The solution obtained by the Gauss-Newton method does not necessarily yield the global minimum. Also, a local minimum may fulfill the requirements of Eq. 4.4.

An algorithm called the modified Gram-Schmidt algorithm (MGS) (Dahlquist et al., 1974) may bed used for determining the solution vector from Eq. 4.11 without forming the **H** matrix and thus $(\mathbf{J}^T\mathbf{J})$. Compared to other methods this algorithm requires a larger number of operations, but the numerical stability of the solution method is very good. An disadvantage with the modified Gram-Schmidt algorithm is that no information about the eigenstructure of **H** and uncertainty associated with the parameters are obtained.

Steepest Descent Model

A steepest descent model (SD) with solution vector given by

$$\Delta\underline{x}_k = -\mathbf{J}^T\underline{r} \tag{4.12}$$

always guarantees the property of truncation convergence, i.e. reduction of the sum of squares. But, this method may not converge as fast as the Gauss-Newton method when the parameters are close to their optimal values.

The Gauss-Newton method may fail to converge when the base point is far from the solution and $F(\underline{x})$ is large. In this situation the steepest descent method may be optimal. Actually, the Marquardt-Levenberg method combines the Gauss-

Newton and steepest descent methods such that the advantageous characteristics of both methods are fully utilized.

Law (1967) proposed a weighted steepest descent method (WSD). The expression weighted is used because the elements of the search vector are weighted to coincide with a search vector calculated by the Gauss-Newton method when **H** is strongly positive definite. This combines the fast convergence of Gauss-Newton with the guaranteed truncation convergence of the steepest descent method. The weighted steepest descent requires that the original system is transformed into an orthogonal coordinate system to remove all interaction between the variables. Then each element of the search vector can be adjusted individually without affecting the other elements.

Rotational Discrimination

The method of rotational discrimination (RD) arises from the weighted steepest descent method and was proposed by Law and Fariss (1972).

Transformation of $\Delta\underline{x}_k$ into a new coordinate system may be performed by transforming the **H**-matrix into a diagonal form such that

$$\mathbf{S}^T\mathbf{H}\mathbf{S} = \mathbf{D} \tag{4.13}$$

where **D** is a diagonal matrix, $\mathbf{D}=[d_{11},\ldots,d_{ii},\ldots,d_{NN}]$. Matrix **S** contains column vectors $\underline{V}_i$, i=1,...,N, which are orthogonal to the remaining vectors, V_j, $i\neq j$. These are the eigenvectors of **H**, and diagonal elements of **D**, d_{ii}, are the eigenvalues of **H**.

Since $\mathbf{S}^T\mathbf{S}=\mathbf{I}$, where **I** is an identity matrix, Eq. 4.11 becomes

$$\mathbf{S}^T\mathbf{H}\mathbf{S}\ \mathbf{S}^T\Delta\underline{x}_k = -\mathbf{S}^T[\mathbf{J}^T\underline{r}] \tag{4.14}$$

when $\mathbf{S}^T$ has been pre-multiplied on both sides. Written on a more compact form this results in

$$\mathbf{D}\underline{Y} = \underline{P} \tag{4.15}$$

where

$$\underline{Y} = \mathbf{S}^T\Delta\underline{x}_k \tag{4.16}$$

and

$$\underline{P} = -\mathbf{S}^T[J^T\underline{r}] \tag{4.17}$$

The solution to Eq. 4.14 or 4.15 is simply

$$y_i = -1/d_{ii}\ P_i \tag{4.18}$$

and y_i may be transformed back into a $\Delta\underline{x}$-vector as:

$$\Delta\underline{x}_k = \mathbf{S}\underline{Y} \tag{4.19}$$

The rotational discrimination method which requires properly scaled or normalized parameters, leaves the y_i's calculated from Eq. 4.18, unaltered unless one of the two following situations occur:

1. y_i is larger than a constant y_h, e.g. y_h=0.2. A large y_i is indicative of matrix **H** being ill-conditioned, and thus y_i is altered so that $|y_i| \leq y_h$;

2. an eigenvalue of **H**, d_{ii}, corresponding to y_i is many orders of magnitude smaller than the largest eigenvalue, or it is negative, $d_{ii}<0$. The former situation indicates that y_i is a locally null-effect variable. In these cases, y_i is set to zero, and the corresponding columns of **S** and **D**, $\underline{V}_i$ and d_{ii}, are removed. Thus, the system is reduced to an N-1 dimensional system.

Note that if any of the above situations are avoided, the rotational discrimination method is equivalent to the Gauss-Newton method, including the good convergence characteristics of this method. An algorithm for the rotational discrimination method is presented below:

Rotational Discrimination Algorithm:

1. At iteration k, a base point $\underline{x}_k$ is defined. Also, a maximum allowable distance factor is set, e.g. y_h=0.2.

2. Calculate $F(\underline{x}_k)$, and the forward differences. Set up matrix **J** and **H**.

3. Determine matrix **D** and **S** so that d_{ii} are given in descending order.

4. Calculate y_i, i=1,...,N, from Eq. 4.18 until one of the following occurs:

a. $i=N$

b. $d_{ii}/d_{max}=d_{ii}/d_{11}<10^{-8}$, or $d_{ii}<0.0$

c. $|y_i|>y_h$

5. If step 4 is terminated at $i=j$ for reason b, set $y_i=0$, $i=j,\ldots,N$, and continue from step 7. If step 4 is terminated for reason c at $i=\ell$ then

$$y_\ell = -y_h \text{ sign}(P_\ell) \tag{4.20}$$

where P_ℓ is defined by Eq. 4.17.

6. Parameters following the ℓ'th; $\ell<i<j$, are determined according to the method of weighted steepest descent:

$$y_i = y_\ell s_i P_i / P_\ell \tag{4.21}$$

s_i is a scale factor defined by

$$s_i = A^r$$

where

$$r = 1-\exp\left(\frac{-0.5}{\ln A} \ln\frac{d_{\ell\ell}}{d_{ii}}\right) \tag{4.22}$$

and A is a constant, e.g. A=100. If $|y_i|>y_h$, when calculated from Eq. 4.21, it should be truncated so that $|y_i|=y_h$.

7. Convert $\underline{Y}$ back into the original x-coordinate system with Eq. 4.19, and update the regression parameters:

$$\underline{X}_{k+1} = \underline{X}_k + \Delta\underline{X}_k \tag{4.23}$$

4.3 Special Considerations

This section discusses several computational aspects of non-linear regression such as parameter scaling, evaluation of numerical derivatives, definition of parameter bounds, solution step length and parameter identifiability.

Scaling

An efficient regression algorithm requires that the regression parameters are properly scaled. Agarwal et al. (1987) suggest that parameter x_i be scaled according to

$$x_i = \frac{(\theta_i - \theta_{imax})}{(\theta_{imax} - \theta_{imin})} \tag{4.24}$$

where θ_i is an EOS characterization parameter. Subscripts max and min refer to the upper and lower parameter bounds, respectively. In this work the regression parameters are defined as multiplication factors to one or several EOS parameters

$$x_{ik} = \theta_{ik}/\theta_{io} \tag{4.25}$$

where θ_{io} and θ_{ik} represent the initial EOS parameter value (predicted) and the adjusted value after k iterations, respectively. It is believed that this gives sufficient scaling.

Numerical Differentiation

Derivatives of the objective function with respect to the parameters are normally determined by numerical differentiation (forward differences). This is because it may be difficult or even impossible to obtain exact analytical derivatives. Selecting a proper perturbation size may be troublesome, and can have an effect on the results. If it is too small, round-off errors will overshadow the effect of the perturbation, and if the perturbation is too large one may not obtain the correct gradients at the base point. Agarwal et al. propose that a perturbation of 1 percent in the parameters is adequate to compute derivatives by numerical differentiation. In this work we use a somewhat smaller perturbation: 0.05-0.01 percent.

Parameter Bounds

Another important aspect connected to regression methods is definition of upper and lower regression parameter bounds. These are recommended to be quite close to the initial estimates to honor the à priori estimates which usually should be quite good. However, if the bounds are too narrow, the global minimum of the objective function may not be found, and if they are too loose, the resulting EOS characterization may not be realistic. Also, at the solution the regressed parameters should be physical in the sense that pseudocomponent critical pressures decrease with carbon number and critical temperatures increase with carbon number.

Parameter Identifiability

A qualitative analysis of parameter identifiability rely heavily on the Hessian-matrix and its eigenstructure, i.e. eigenvectors and eigenvalues (Foss, 1987). Some guidelines for interpretation of the eigenstructure information is given below:

The **condition number**, $\kappa(H)$, is defined as the ratio of the maximum to the minimum eigenvalue of the Hessian matrix at the solution. A high condition number illustrates that the objective function is elongated in the direction of the smaller eigenvalues. A low condition number implies a more "circular" and smoother parameter space, and the regression run will be more effective and converge faster.

Low eigenvalues indicate parameters with high uncertainties since the square root of the eigenvalue is inversely proportional to the standard deviation of the parameter estimates. Foss (1987) shows how this relation can be used to obtain quantitative information on the confidence intervals of the parameters by treating them as stochastic variables.

The maximum element of the eigenvector corresponding to the minimum eigenvalue gives the direction of the most uncertain parameter. The eigenvector can also be used to detect linearly dependent parameters. For example, if parameters i and j are linearly dependent, then $\underline{V}_i$ will be parallel to $\underline{V}_j$, or $\underline{V}_i = \text{const}.\underline{V}_j$.

Also, the Hessian matrix itself includes information about the parameter space and uncertainty associated with the obtained parameters. The diagonal elements of **H**, H_{ii}, give an indication of the confidence of the solution. Large and almost equal H_{ii}-values imply significant curvature, and a well defined solution.

A regression run with 20 parameters was performed to illustrate how the eigenvalues of **H** later can be used to select effective regression parameters. The problem is based on experimental data for a North Sea volatile oil. Table 4.1 lists the regression parameter candidates, and their corresponding Hessian matrix eigenvalues at the start and end of a run. Table 4.1 indicates that parameter 1 adjusting all C_{7+} critical temperatures, is more appropriate than parameter 13 adjusting all C_{7+} critical pressures, since $\lambda_1 \approx 10^6$ and $\lambda_{13}=0.007$. Note that parameter 9 which adjusts C_1-C_{7+} BIPs (A of Eq. 3.61), has a relatively limited effect on the objective function with $\lambda_9=0.061$.

The eigenvalues shown in Table 4.1 will be dependent on the type of data included in the data set and the type of fluid to which the data set belongs. For example, it is observed that parameter 14, the molar distribution α parameter, has a greater impact on the objective function for a gas condensate.

The C_{7+} fraction of this reservoir fluid is characterized by forcing the EOS to yield consistent inspection properties (T_b, γ) from adjusting C_{7+} acentric factors and shift parameters. Because of this characterization method, parameters 16, 17 and 20, adjusting Ω_a, Ω_b and ω of $C_{7+}(5)$, become practically null-effect parameters. It is observed that eigenvalues of parameter 7, which adjusts C_{7+} Ω_bs, and parameter 15 which adjusts C_{7+} Ω_as, are slightly higher, but these are still not recommended as regression candidates.

Parameter identifiability will be further discussed in connection with example calculations.

TABLE 4.1 -- Regression Parameter Candidates and Corresponding Eigenvalues of Hessian Matrix After One Iteration and at Solution.

i	Parameter Description	Eigenvalue of Hessian Matrix	
		First Iter.	At Solution
1	C_{7+} Crit. temperatures	$0.125(10^{6})$	$0.748(10^{6})$
2	C_{7+} Molecular weight	281.25	2016.9
3	Ω_a for C_1	$0.440(10^{-3})$	151.70
4	C_{7+} Boiling Points	89.184	44.780
5	Crit. temp. of $C_{7+}(5)$	2.3768	15.880
6	Crit. pressure of C_1	$0.305(10^{-4})$	8.8303
7	C_{7+} Ω_b	0.3642	2.3588
8	Ω_b for C_1	10.241	0.2515
9	C_1-C_{7+} BIPs	$0.650(10^{-2})$	$0.612(10^{-1})$
10	Crit. temp. of C_1	25.773	$0.362(10^{-1})$
11	Boiling point of $C_{7+}(5)$	$0.123(10^{-5})$	$0.209(10^{-1})$
12	C_{7+} Shift parameters	0.5860	$0.152(10^{-1})$
13	C_{7+} Crit. pressures	$0.118(10^{-1})$	$0.710(10^{-2})$
14	C_{7+} Alpha parameter, α	$0.859(10^{-3})$	$0.218(10^{-2})$
15	C_{7+} Ω_a	$0.129(10^{-2})$	$0.458(10^{-3})$
16	Ω_a of $C_{7+}(5)$	$0.631(10^{-12})$	$0.530(10^{-4})$
17	Ω_b of $C_{7+}(5)$	$0.162(10^{-7})$	$0.111(10^{-4})$
18	Acentric factor of C_1	$0.212(10^{-5})$	$0.395(10^{-5})$
19	Crit. pressure of $C_{7+}(5)$	$0.776(10^{-5})$	$0.849(10^{-5})$
20	Acentric factor of $C_{7+}(5)$	$0.774(10^{-8})$	$0.698(10^{-7})$

Step Length

The parameters are updated after each iteration according to

$$\underline{x}_{k+1} = \underline{x}_k + \alpha\Delta\underline{x}_k \tag{4.26}$$

where α is a "step length" parameter usually varying between 0 and 1, which is used to guarantee that

$$F(\underline{x}_{k+1}) < F(\underline{x}_k) \tag{4.27}$$

A one-dimensional search method is commonly used to obtain the optimum step length. In that case additional evaluations of $F(\underline{x}_k)$ are required for α, e.g. for α=0.5. The optimum α corresponding to the lowest sum of squares value is then determined as the minimum point of a polynomial going through the three known points at α=0.0, 0.5 and 1.0.

In this work a different approach is used. If Eq. 4.26 is not satisfied for α=1.0, i.e. $F(\underline{x}_{k+1})>F(\underline{x}_k)$, α is reduced by a constant factor (e.g. 0.6) until Eq. 4.27 is satisfied. This α is then saved for the next iteration and used in Eq. 4.26 if Eq. 4.27 is not fulfilled with α=1.0. When α becomes less than e.g. 10^{-4}, the estimation run will be terminated.

4.4 Examples

The regression methods described are tested on two examples. In the first example coefficients of an exponential function are adjusted to fit a specific data set. In the second example an EOS is used to match measured PVT data for a North Sea volatile oil.

Exponential Function

Performance of the Gauss-Newton and the rotational discrimination method are compared for the following ideal problem:

$$y(\underline{x}) = x_1 e^{-x_2} + x_3 e^{-x_4} \tag{4.28}$$

Initial and final set of parameters are shown in Table 4.2 for the Gauss-Newton and rotational discrimination methods. Only minor differences in performance is observed for the various methods. The initial parameters listed in Table 4.2, are fairly close to their optimal values for these runs. In Fig. 4.1 sum of squares for the two regression methods (denoted GN_2 and RD_2) are plotted versus number of function calls. After about 20 function calls (3 iterations) the rotational discrimination method yields a significantly lower sum of squares compared to the Gauss-Newton method. Sum of squares values at the end of these runs are almost identical.

In order to pose a more challenging problem, the set of initial parameters were changed, corresponding to a much higher initial sum of squares. The Gauss-Newton method converged at a local minimum, SSQ=3.32, after 107 function calls, and the final parameters were far off from the correct values. The rotational discrimination method performed satisfactorily, and used only one more function call to reach the same sum of squares level as with the first run. These results are also tabulated in Table 4.2 and the sum of squares are

plotted in Fig. 4.1 with the Gauss-Newton and rotational discrimination methods denoted GN_1 and RD_1, respectively.

TABLE 4.2 -- Performance of Various Regression Methods With Good and Poor Initial Estimates of the Parameters of Eq. 4.28.

Method[1]	Function Calls	SSQ[2]	Parameter Values x_1	x_2	x_3	x_4
		Good Initial Estimates				
Initial	-	50.131	7.0	0.1	2.5	0.3
GN_2	36	0.00787	5.6745	0.2072	2.7316	0.05939
RD_2	36	0.00787	5.6745	0.2072	2.7317	0.05939
		Poor Initial Estimates				
Initial	-	82.333	2.0	0.3	4.0	0.3
GN_1	102	3.3254	5.7924	0.1591	3.3710	0.14012
RD_1	37	0.00787	5.6741	0.2072	2.7321	0.05939

Notes:
1. GN: Gauss-Newton Method
   RD: Rotational Discrimination Method
2. SSQ: Sum of Squares of objective function.

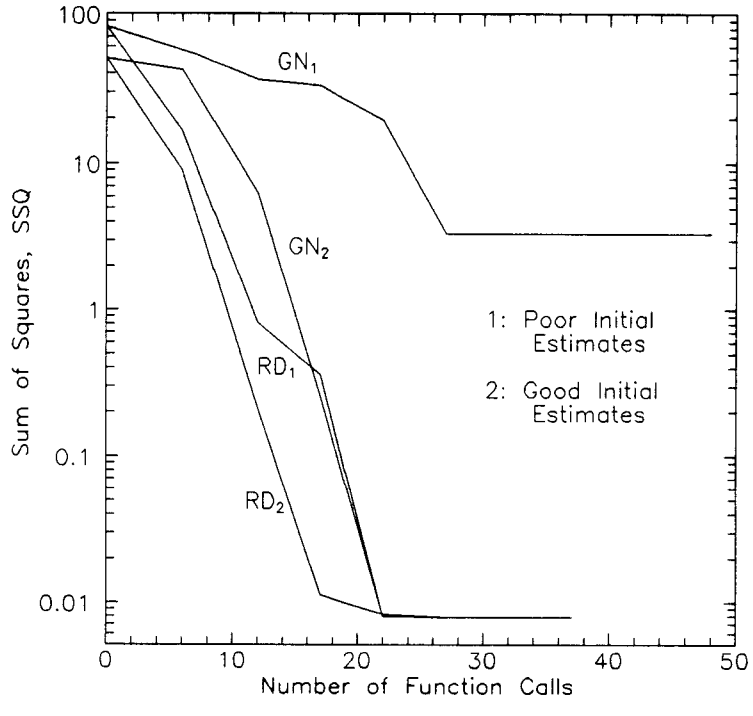

Fig. 4.1 Performance of various regression methods applied to fit Eq. 4.28 to a given data set.

Reservoir Fluid

Performance of the regression methods have been compared on a more realistic problem. Regression is used to obtain an EOS characterization that fits available PVT data for a North Sea volatile oil. Composition of the oil is given in Table 4.3, and the PVT data used in the regression include a differential liberation experiment (DLE) and a multi-contact vaporization (MCV) experiment with 0%, 5% and 10% N_2 injected into the original oil fluid. These data are presented in Tables 4.4 and 4.5. A standard procedure was used to obtain the PR EOS fluid characterization.

TABLE 4.3 -- Composition of North Sea Volatile Oil.

Component	Composition (Mole Frac.)
Carbon Dioxide	0.0300
Nitrogen	0.0012
Methane	0.5753
Ethane	0.0738
Propane	0.0441
i-Butane	0.0074
n-Butane	0.0242
i-Pentane	0.0073
n-Pentane	0.0157
n-Hexane	0.0207
Heptanes Plus	0.2003
Total	1.0000
M_{7+}	225.0
γ_{7+}	0.8585

TABLE 4.4 -- Reported DLE Experiment for a North Sea Volatile Oil.

Pressure psia	Oil FVF bbl/STB	Solution GOR scf/STB	Oil Density lb/ft^3	Gas Gravity	Vapor Z-Factor
5520.7	2.394	2350	35.615		
5317.7	2.227	2065	36.470	1.053	1.016
4915.7	2.020	1705	37.719	0.996	0.985
4414.7	1.854	1400	39.124	0.912	0.934
3914.7	1.736	1168	40.254	0.843	0.897
3414.7	1.640	978	41.304	0.833	0.872
2914.7	1.561	817	42.251	0.817	0.874
2413.7	1.493	675	43.181	0.774	0.874
1914.7	1.432	546	44.074	0.776	0.875
1412.7	1.374	424	43.825	0.799	0.883
813.7	1.309	287	45.978	0.840	0.928
216.7	1.236	129	46.834	1.075	0.942
14.7	1.092		49.587	2.138	

TABLE 4.5 -- Reported MCV Experiment for a North Sea Volatile Oil.

Original Fluid			+ 5% N_2		+ 10% N_2	
$p^{1)}$	$S_L{}^{2)}$	$V/V_s{}^{3)}$	p	V/V_s	p	V/V_s
7518.7	1.0000	1.0000	7366.7	0.9659	7234.7	0.9722
6520.7	1.0000	0.9601	6528.7	0.9853	6426.7	0.9895
5732.7	1.0000	0.9772	5762.7*	1.0000	6002.7*	1.0000
5513.7*	1.0000	0.9944	5485.7	1.0146	5746.7	1.0124
5462.7	0.9697	1.0023	4959.7	1.0468	4661.7	1.0849
4890.7	0.7979	1.0353	4218.7	1.1134	3849.7	1.1791
4118.7	0.6814	1.1043	2506.7	1.5089	3969.7	1.3711
3423.7	0.5881	1.2052			2269.7	1.6633
2968.7	0.5245	1.3078				

Note:
1. p = pressure, (psia)
2. S_L = liquid volume fraction
3. V/V_s = total volume relative to volume at saturation pressure

Six EOS parameters, described in Table 4.6, were selected as candidates for regression. In order to compare the performance of the various methods on a more challenging problem, initial values of parameter 5 and 6 were set to 0.95 and 1.05, respectively.

Table 4.6 also lists the final parameters for each estimation method, and eigenvalues of **H** at solution are listed in Table 4.7. The run referred to as Gauss-Newton is actually performed with the rotational discrimination solution method, but in practice it is a Gauss-Newton run since $y_h=\infty$ and $\lambda_h/\lambda_{max}=10^{-32}$. The runs referred to as RD_A and RD_B are based on the rotational discrimination method with $y_h=0.2$ and $\lambda_h/\lambda_{max}=10^{-8}$ for RD_A and with $y_h=0.05$ and $\lambda_h/\lambda_{max}=10^{-4}$ for RD_B. Fig. 4.2 shows results from monitoring the sum of squares versus number of function calls for the various estimation methods. One function call represents one call to the phase behavior model to calculate all PVT data. It is clear from Fig. 4.2 that the performance of the rotational discrimination method is superior to the Gauss-Newton method. The difference between the RD_A and RD_B runs with ratio $\lambda_{min}/\lambda_{max}$ larger than 10^{-8} and 10^{-4}, respectively, is also significant. This is because a high $\lambda_{min}/\lambda_{max}$ ratio will exclude null-effect parameters and result in a smoother parameter space to search. Note that the final parameters of RD_A and RD_B are quite different.

TABLE 4.6 -- Final Value of Parameters and Sum of Squares From Comparing Performance of Various Regression Methods.

Parameter Description	Initial Parameter	Final Parameters		
		RD_A [1]	RD_B [2]	GN [3]
C_1-C_{7+} BIPs	1.0	1.1905	1.0000	1.3004
T_b of C_{7+}(5)	1.0	.9000	1.0056	1.0705
T_c of C_{7+}(5)	1.0	.9298	1.0000	0.9701
P_c of C_{7+}(5)	1.0	1.1000	1.0000	1.0372
C_{7+} T_bs	0.95	1.0092	0.9845	0.9623
C_{7+} T_cs	1.05	1.0047	0.9717	1.0105
SSQ [4]	196.46	0.1571	0.2133	2.9031
AAD, %	-	1.596	1.9657	3.7198

Note:
1. RD_A: Rotational Discrimination, $y_h=0.2$, $\lambda_h/\lambda_{max}=10^{-8}$
2. RD_B: Rotational Discrimination, $y_h=0.05$, $\lambda_h/\lambda_{max}=10^{-4}$
3. GN: Gauss-Newton Method, (RD with $y_h=\infty$, $\lambda_h/\lambda_{max}=10^{-32}$)
4. SSQ: Weighted Sum of Squares of objective function.
   AAD: Absolute Average Deviation of data set, %.

TABLE 4.7 -- Eigenvalues of Hessian Matrix at Solution for the Two Rotational Discrimination Runs (RD_A, RD_B) and the Gauss-Newton Run.

Parameter Description	Eigenvalues		
	RD_A	RD_B	GN
C_1-C_{7+} BIP	0.023	0.032	0.019
T_b of C_{7+}(5)	1.170	1.297	2.250
T_c of C_{7+}(5)	420.600	21.378	105.680
P_c of C_{7+}(5)	0.440	0.012	0.003
C_{7+} T_bs	1095.4	1230.0	1519.9
C_{7+} T_cs	346000.0	309320.0	351110.0

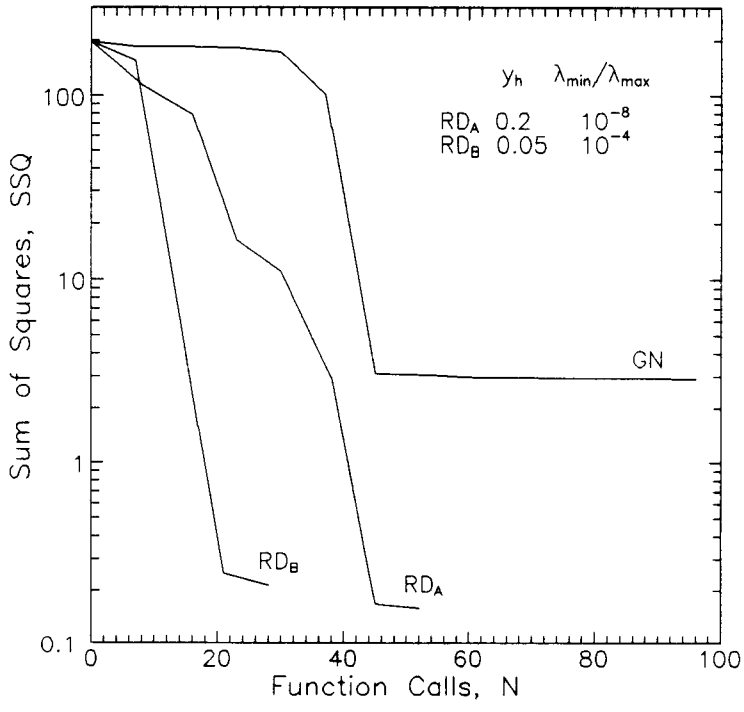

Fig.4.2 Performance of various regression methods applied to adjust an EOS characterization to fit PVT data for a North Sea volatile oil.

CHAPTER 5
APPLICATIONS OF PROPOSED CHARACTERIZATION METHODS

So far, we have described EOS theory, characterization procedures and regression methods. This section presents results generated from a phase behavior model developed during this thesis work based on the previously described theory. The model is coded in standard FORTRAN '77 and has been executed on computers ranging from personal computers to a CRAY X-MP.

A procedure for predicting phase and volumetric behavior of reservoir fluids using either the modified PR EOS or the SRK EOS is presented in Section 5.1. The method for improving EOS predicted volumetric behavior, called volume translation (VT) is demonstrated. Predicted liquid densities and vapor Z-factors are compared to measured data for a separator oil and a separator gas, respectively.

The predictive capabilities of the proposed characterization procedure are shown for the reservoir fluids described by Coats and Smart (1986), including both oils and gas condensates. Predicted data are here compared with measured saturation pressures, saturated densities, compressibility factors, and black-oil PVT parameters. The predicted EOS characterization has been adjusted using non-linear regression to fit available PVT data for several fluids, and the resulting matches to such measured data are presented. The adjusted characterizations and key regression results are also given.

Absolute average deviation (AAD), bias (BIAS) and absolute maximum deviation (MAXD) are used throughout the chapter to quantify comparisons of measured and calculated data. Expressions for these statistical parameters are given in the nomenclature.

5.1 Summary of Proposed Characterization Methods

The proposed C_{7+} characterization procedure for the PR EOS (Robinson and Peng, 1978) and the SRK EOS (Soave, 1972) can be described as follows:

Molar Distribution

C_{7+} molar distribution is determined from the Gaussian quadrature method described. Molecular weight of the heaviest of the five pseudo-components, M_N, is set to 500. Distribution parameters α and η are also specified as α=1.0 and η=90, unless TBP data are available for the actual sample. β_o is calculated from Eq. 3.33.

Specific Gravity

Pseudocomponent specific gravities are determined from Eq. 3.57. The characterization factor C_f is adjusted to ensure that experimental and calculated γ_{7+} are equal.

Boiling Point

Pseudocomponent normal boiling points are estimated from the proposed correlation presented in Eq. 3.59, with correlation constants given in Table 3.7.

Critical Properties

The critical property correlations proposed by Riazi and Daubert (1987), are chosen for estimating critical temperature and critical pressure. Eq. 3.60 presents the form of the correlations, and correlation constants are given in Table 3.9. The Twu correlation (Twu, 1984) is used to estimate pseudocomponent critical volumes.

Acentric Factor

Acentric factor is determined from the EOS-based procedure resulting in normal boiling points correctly predicted by the EOS.

Volume Translation

PR EOS shift parameters for the lightest components (N_2, CO_2, H_2S, C_1, C_2 and C_3) are calculated from Eq. 1.82 as function of reduced temperature. The constants to be used in Eq. 1.82 are given in Table 1.4. SRK shift parameters for the same components are calculated from Eq. 1.83 with the constants given in Table 1.5. Shift parameters for the intermediate components (C_4-C_6) are calculated from Eq. 1.78 as function of reduced temperature and acentric factor. Constants of Eq. 1.78 are given in Table 1.2 for both PR and SRK EOSs.

Pseudocomponent shift parameters are determined using the EOS-based procedure which results in correctly EOS predicted liquid densities at standard conditions.

Binary Interaction Parameters

Non-HC--HC binary interaction parameters are taken from Table 3.13 after Nagy and Shirkovskiy (1982). The modified Chueh-Prausnitz correlation, Eq. 3.61, is applied to calculate interaction parameters for C_1-C_{7+} HC binaries, with B=6.0. For the PR EOS, parameter A of Eq. 3.61 is set equal to 0.2, and for the SRK EOS it is slightly higher, A=0.215.

TABLE 5.1 -- Summary of Proposed C_{7+} Characterization Procedure.

C_{7+} Prop.	Eq.	Table	Description
z	3.31		Gaussian quadrature
M	3.32		Gaussian quadrature
γ	3.57		Developed γ-correlation
T_b	3.59	3.7	Developed T_b-correlation
p_c	3.60	3.9	Riazi-Daubert (1987)
T_c	3.60	3.9	Riazi-Daubert (1987)
ω	-	-	EOS-based proc., matches T_b
k_{ij}	-	3.13	Non-HC--HC BIPs
k_{ij}	3.61	-	HC-HC BIPs
s	-	-	EOS-based proc., matches γ

5.2 Rio Bravo Reservoir Fluids

Sage and Reamer (1941) studied volumetric behavior of the reservoir fluids from a field called Rio Bravo. This fluid was produced from reservoir conditions at pressure 4750 psia [327.6 bar] and at a temperature of 250°F [121.1°C] into a test separator (trap) at 495 psia [34.1 bar] with GOR=1040 ft^3/bbl [185.2 m^3/m^3]. Composition of the separator oil and gas, hereafter referred to as trapped liquid and trapped gas samples, are given in Table 5.2. The 39.9°API (γ_o=0.825) trapped liquid was analyzed by fractional distillation (TBP analysis). These results are presented in Table 5.3, and provide the basis for the C_{6+} characterization shown in Table 5.4 where critical properties, acentric factor and shift parameters were calculated according to the proposed procedure given in Sec. 5.1. C_1-C_{6+} BIPs were calculated from the Chueh-Prausnitz BIP correlation (Eq. 3.61), and to obtain a reasonable match of the bubble point pressures, parameter A was adjusted to 0.271206 and 0.265586 for PR and SRK EOS, respectively. The trapped gas sample was characterized using nC_6 data for C_{6+}, and all BIPs equal to zero.

TABLE 5.2 -- Composition of Rio Bravo Trapped Liquid and Gas Samples (Sage and Reamer, 1941).

	Composition Mole%	
Component	Liquid	Gas
Methane	10.577	86.020
Ethane	5.452	7.700
Propane	8.716	4.260
i-Butane	2.242	0.570
n-Butane	9.465	0.870
i-Pentane	2.092	0.110
n-Pentane	2.587	0.140
Hexanes+	58.870	0.330
Total	100.00	100.00

TABLE 5.3 -- Reported TBP Analysis for the C_{6+} Fraction of the Rio Bravo Trapped Liquid Sample (Sage and Reamer, 1941).

Pseudo-Component	z (mole %)	M (lb/mol)	γ (60/60)	T_b (°R)
$C_{6+}(1)$	11.9549	97.0	0.7271	647.7
$C_{6+}(2)$	11.7109	107.0	0.7620	697.7
$C_{6+}(3)$	9.5765	137.0	0.7985	791.7
$C_{6+}(4)$	7.6422	179.0	0.8319	899.7
$C_{6+}(5)$	6.0986	230.0	0.8529	1002.7
$C_{6+}(6)$	11.8867	402.0	0.9371	1331.6[1)]
C_{6+}(total)	58.87	191.5	0.8495	

Note:
1. $C_{6+}(6)$ T_b was estimated from Eq. 3.59, and adjusted upwards by 4 percent to improve prediction of the measured bubble points.

TABLE 5.4 -- PR and the SRK EOS C_{6+} Characterization of the Rio Bravo Trapped Liquid Sample.

Pseudo Component	T_c (°R)	p_c (psia)	Acentric Factor		C_1-C_{6+} BIPs		Shift Parameter	
			PR EOS	SRK EOS	PR EOS	SRK EOS	PR EOS	SRK EOS
$C_{6+}(1)$	972.8	468.4	0.2792	0.2763	0.0440	0.0434	-0.0663	0.0728
$C_{6+}(2)$	1035.5	443.5	0.3061	0.3036	0.0501	0.0495	-0.0105	0.1188
$C_{6+}(3)$	1139.0	374.8	0.3733	0.3724	0.0642	0.0634	0.0299	0.1496
$C_{6+}(4)$	1250.5	308.7	0.4581	0.4596	0.0805	0.0795	0.0697	0.1808
$C_{6+}(5)$	1347.9	253.5	0.5537	0.5584	0.0967	0.0956	0.0990	0.2039
$C_{6+}(6)$	1655.9	160.5	0.8904	0.9116	0.1341	0.1325	0.2418	0.3261

Note:
1. All properties are calculated according to the proposed characterization method.
2. C_1-C_{6+} BIPS are calculated from Eq. 3.61 with A=0.271206 for the PR EOS and with A=0.265586 for the SRK EOS. B=6.0 for both cases.

Sage and Reamer measured liquid densities, ρ_L, for the trapped liquid sample at four different temperatures between 100° and 250°F [37°-121°C] at pressures from ≈500 to 3250 psia [34-221 bar]. Several runs were made for both the PR and SRK EOSs using the following pure component volume translation approaches: (1.) s=0: volume translation turned off, (2.) s determined at T_r=0.7 (Table 1.3), and (3.) s determined as function of T_r and ω (Eqs. 1.82, 1.83, and 1.78, Tables 1.4, 1.5 and 1.2). The EOS-based procedure was used to calculate C_{6+} shift parameters. Liquid densities from the Standing-Katz (1942) and

Alani-Kennedy (1960) correlations were also calculated.

AAD, BIAS and MAXD resulting from a comparison of these calculated densities with measured data are presented in Table 5.5. The use of volume translation reduces AAD for PR EOS liquid densities from 7.48 percent to 0.963 with $s(T_r=0.7)$ or to 1.74 percent with $s(T_r)$. For the SRK EOS, AAD is reduced even more; from 17.43 percent to 0.69 percent with $s(T_r=0.7)$ or to 2.08 percent with $s(T_r)$. BIAS values show that liquid densities are underpredicted when not using volume translation, and generally overpredicted with volume translation. Notice that better results are obtained with pure component shift parameters calculated from $s(T_r=0.7)$ than from $s(T_r)$. If the liquid densities are overestimated with pure component shift parameters defined from $s(T_r=0.7)$, the overestimation will be even more pronounced using $s=s(T_r)$ because this method yields higher shift parameter values for the light and intermediate components. This can be shown in Table 5.6 which reports SRK shift parameters s and the cumulative liquid volume correction, $c=\Sigma_i s_i b_i$, for the two cases: $s(T_r=0.7)$ and $s(T_r)$ at 3250 psia [221 bar] and 190°F [87.7°C]. It should <u>not</u> be concluded from these results that volume translation with $s(T_r=0.7)$ in general yields better results than volume translation with $s(T_r)$, even though this is true for these data. The liquid density overestimation may be due to too high C_{6+} shift parameters.

TABLE 5.5 -- Results of Comparing Measured and Predicted Properties of the Rio Bravo Trapped Oil and Gas Sample.

Liquid Densities for Trapped Oil

	1) Standing -Katz	2) Alani-Kennedy	PR EOS 3) s=0.0	PR EOS s(0.7) EOS	PR EOS s(Tr) EOS	PR EOS 4) J-Y	SRK EOS s=0.0	SRK EOS s(0.7) EOS	SRK EOS s(Tr) EOS
AAD, % :	0.940	0.930	7.476	0.963	1.739	3.135	17.429	0.692	2.076
BIAS, % :	0.930	0.915	-7.476	0.959	1.739	-3.135	-17.429	0.565	2.076
MAXD, % :	2.271	1.650	-8.777	2.316	3.368	4.307	-18.485	1.967	3.974
STD, % :	0.554	0.465	0.833	0.734	1.116	0.782	0.762	0.695	1.005

Vapor Z-Factors for Trapped Gas

	1) Standing -Katz	PR EOS s=0 3)	PR EOS s(0.7)	PR EOS $s(T_r)$	PR EOS J-Y 4)	SRK EOS s=0.0	SRK EOS s(0.7)	SRK EOS $s(T_r)$	SRK EOS PRF 5)
AAD, % :	0.659	2.329	1.128	1.011	1.037	2.781	1.930	0.616	1.918
BIAS, % :	-0.611	-2.329	0.701	0.547	0.581	2.781	1.930	0.167	1.918
MAXD, % :	-1.308	-5.395	3.026	2.838	2.865	5.610	4.525	2.462	4.512
STD, % :	0.452	0.850	1.082	1.020	1.029	1.413	1.074	0.810	1.070

Note:

1. Standing-Katz refers to the Standing-Katz liquid density correlation or the Standing-Katz Z-factor charts for which a correlation has been given by Hall and Yarborough.
2. Alani-Kennedy refers to the liquid density correlation proposed by Alani and Kennedy (1960).
3. s=0.0 means volume translation is not used. s(0.7) and $s(T_r)$ refer to using pure component shift parameters determined at T_r=0.7 or at the actual T_r value, respectively. EOS refers to using the EOS-based method for determining pseudocomponent shift parameters.
4. J-Y refers to shift parameters given by Jhaveri and Youngren (1984). C_{6+} fraction shift parameters are eventually estimated from their proposed relation: $s=1-dM^{e}$ with d=2.458 and e=0.18.
5. PRF refers to the volume correction correlation given by Peneloux et al. (1982).

TABLE 5.6 -- SRK EOS Shift Parameters and Cumulative Volume Correction, c, For Rio Bravo Trapped Liquid Sample at 3250 psia [221 bar] and 190°F [87.7°C].

Comp.	$s(T_r=0.7)$ s_i	$s(T_r=0.7)$ $c=\Sigma_i s_i b_i$	$s(T_r)$ s_i	$s(T_r)$ $c=\Sigma_i s_i b_i$
C_1	0.0234	0.0012	0.0839	0.0042
C_2	0.0605	0.0036	0.1608	0.0106
C_3	0.0825	0.0108	0.3328	0.0397
iC_4	0.0830	0.0132	0.2151	0.0459
nC_4	0.0975	0.0251	0.1903	0.0692
iC_5	0.1022	0.0285	0.1731	0.0749
nC_5	0.1209	0.0335	0.1799	0.0824
$C_{6+}(1)$	0.0728	0.0503	0.0728	0.0992
$C_{6+}(2)$	0.1188	0.0805	0.1188	0.1294
$C_{6+}(3)$	0.1496	0.1210	0.1496	0.1698
$C_{6+}(4)$	0.1808	0.1730	0.1808	0.2219
$C_{6+}(5)$	0.2039	0.2345	0.2039	0.2834
$C_{6+}(6)$	0.3261	0.6063	0.3261	0.6552
Predicted ρ_L :		47.40		48.26
|Dev.| % :		1.67		3.52

Figs. 5.1 and 5.2 illustrates liquid density deviations at various pressures and temperatures for the PR EOS without and with volume translation [$s(T_r=0.7)$], respectively. Note that the base plane in Fig. 5.1 is located at -10.0 and at -1.0 in Fig. 5.2. Figs. 5.3 and 5.4 show similar plots for the SRK EOS with the base plane located at -20.0 and at -1.0, respectively. The BPs on these figures refer to bubble points of the trapped oil. The observed temperature dependence on the deviations, especially at high pressures, seems to be the same whether volume translation is used or not for both PR and SRK. Deviations resulting from comparing Alani-Kennedy liquid densities to measured data, shown in Fig. 5.5, also seem to be temperature dependent, but not as much as for PR and SRK EOSs.

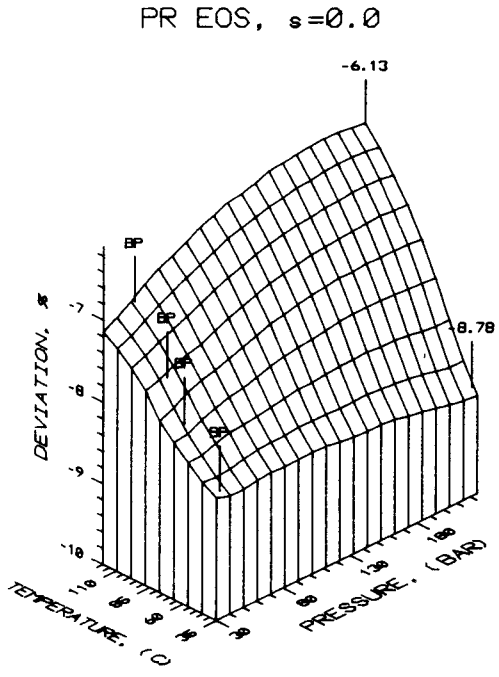

Fig. 5.1 PR EOS liquid density deviations as function of pressure and temperature for the Rio Bravo Trapped Liquid. Volume translation is not used.

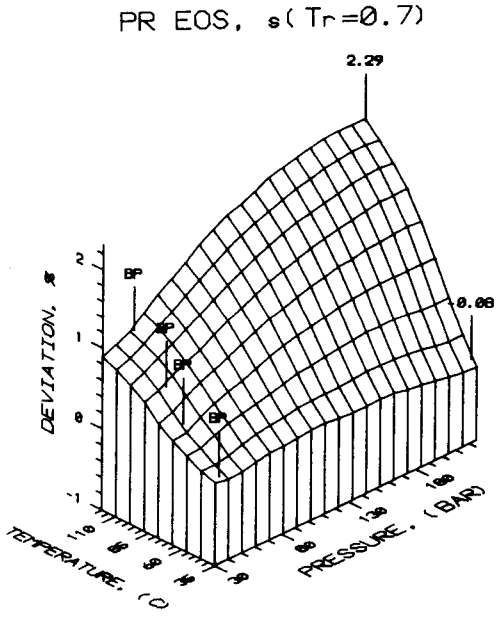

Fig. 5.2 PR EOS liquid density deviations as function of pressure and temperature for the Rio Bravo Trapped Liquid. Volume translation is used and pure component shift parameters are determined at T_r=0.7.

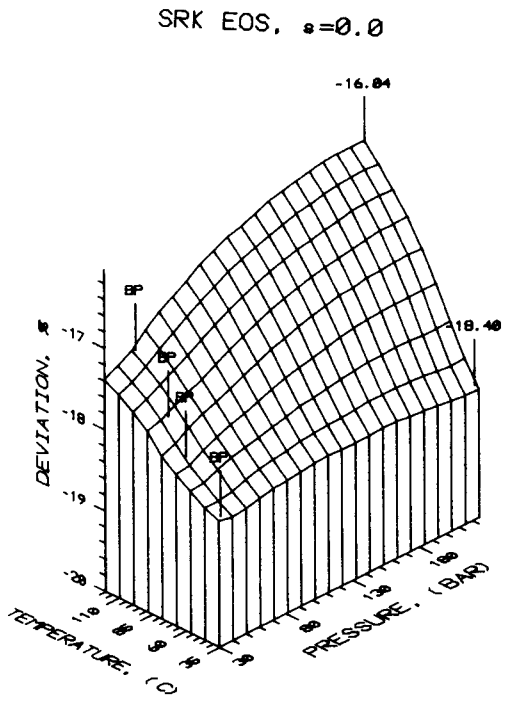

Fig. 5.3 SRK EOS liquid density deviations as function of pressure and temperature for the Rio Bravo Trapped Liquid. Volume translation is not used.

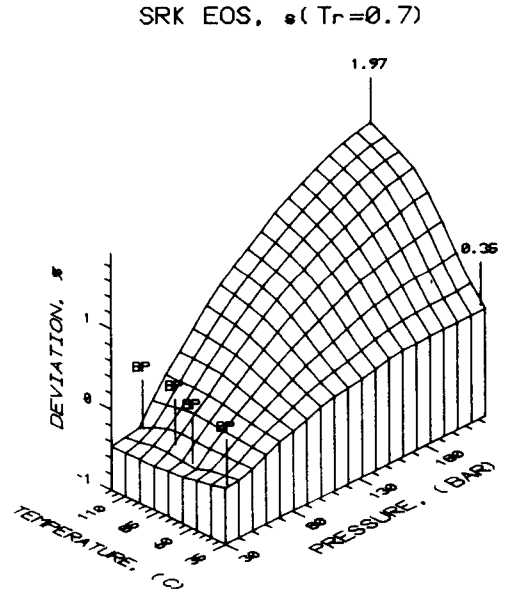

Fig. 5.4 SRK EOS liquid density deviations as function of pressure and temperature for the Rio Bravo Trapped Liquid. Volume translation is used and pure component shift parameters are determined at T_r=0.7.

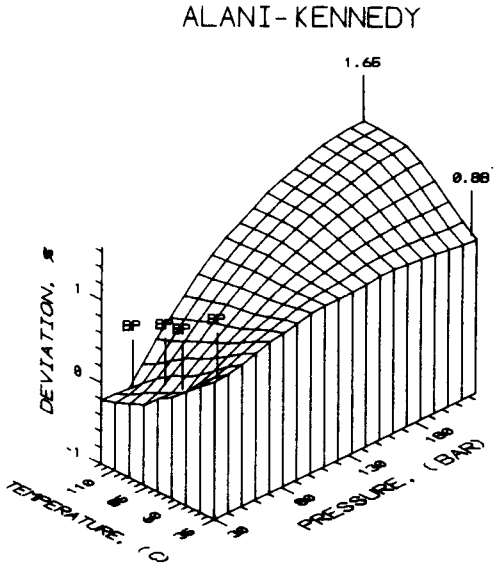

Fig. 5.5 Alani-Kennedy liquid density deviations as function of pressure and temperature for the Rio Bravo Trapped Liquid.

Sage and Reamer present measured compressibility factors, Z, for the trapped gas sample at seven different temperatures between 100° and 280°F [37°, 137.8°C] at pressures from 15 to 5000 psia [1, 340 bar]. An attempt was made to reproduce these measured data with the PR and the SRK EOS. Several runs were made for both EOSs with the various volume translation approaches.

AAD, BIAS, and MAXD resulting from comparing measured and calculated Z-factors are also shown in Table 5.5. These data show that the Standing-Katz Z-factor correlation with AAD=0.66 percent, is superior to the PR and SRK EOSs. Without volume translation, the PR EOS underpredicts Z-factors (BIAS=-2.33%), and SRK overpredicts Z-factors (BIAS=2.78%). The PR EOS yields AAD=1.13 percent with $s(T_r=0.7)$, and AAD=1.01 percent with $s(T_r)$. Thus, PR EOS Z-factor prediction with temperature dependent shift parameters is slightly better than with $s(T_r=0.7)$. Similar results are obtained for PR EOS using the shift parameters presented by Jhaveri and Youngren, yielding AAD=1.04 percent.

The SRK EOS yields an AAD of 1.93 and 0.616 percent for $s(T_r=0.7)$ and $s(T_r)$, respectively. These results favor the use of temperature dependent shift parameters. Z-factor prediction with the SRK seems to be the same whether

the Peneloux et al. (1982) volume correction or the proposed method with $s(T_r=0.7)$ is used.

Figs. 5.6 and 5.7 show Z-factor deviations at various pressures and temperatures for the PR EOS with s=0.0 and $s(T_r)$, respectively. Note that the base plane in both cases is defined at -6.0 percent. These two plots illustrate very clearly the effect of using volume translation. The PR EOS with s=0.0, underpredicts the Z-factor, and the deviation increases with increasing pressure. At 5000 psia [340 bar], it is observed that Z-factor deviation also varies with temperature. Fig. 5.7 shows that PR EOS with $s(T_r)$, slightly underpredicts the Z-factor at low pressure (-1.0%) and slightly overpredicts Z at high pressures (+1.0%). Figs. 5.8 and 5.9 show Z-factor deviations at various pressures and temperatures for the SRK EOS with s=0.0 and $s(T_r)$, respectively. Note that the base plane for both figures is defined at -3.0 percent.

Z-factors for the Rio Bravo trapped gas sample were also calculated with the Standing-Katz (SK) Z-factor charts for which a correlation has been given by Hall and Yarborough. Fig. 5.10 shows deviations between measured and SK Z-factors.

On all figures illustrating Z-factor deviations, a "bump" is observed at 2000 psia [140 bar] and 86°F [30°C], even for the Standing-Katz Z-factor correlation. This may indicate a systematic error in the measured Z-factors at these conditions.

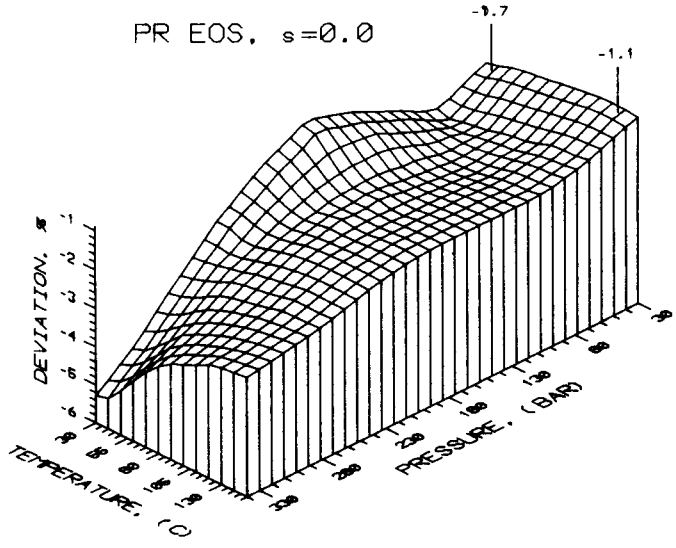

Fig. 5.6 PR EOS dense phase Z-factor deviations as function of pressure and temperature for the Rio Bravo Trapped Gas. Volume translation is not used.

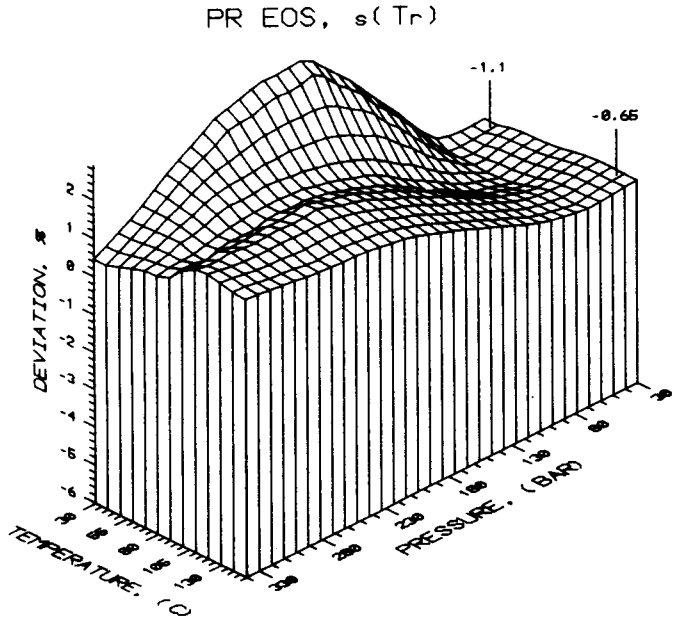

Fig. 5.7 PR EOS dense phase Z-factor deviations as function of pressure and temperature for the Rio Bravo Trapped Gas. Volume translation shift parameters determined as function of reduced temperature.

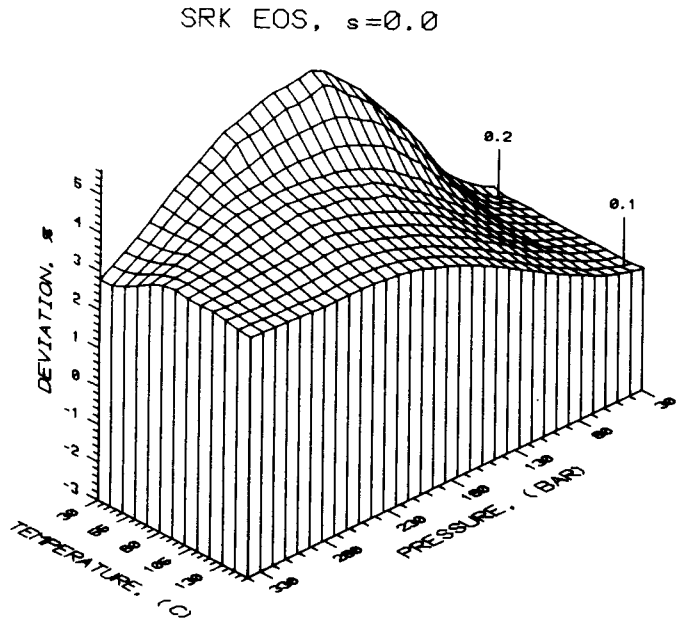

Fig. 5.8 SRK EOS dense phase Z-factor deviations as function of pressure and temperature for the Rio Bravo Trapped Gas. Volume translation is not used.

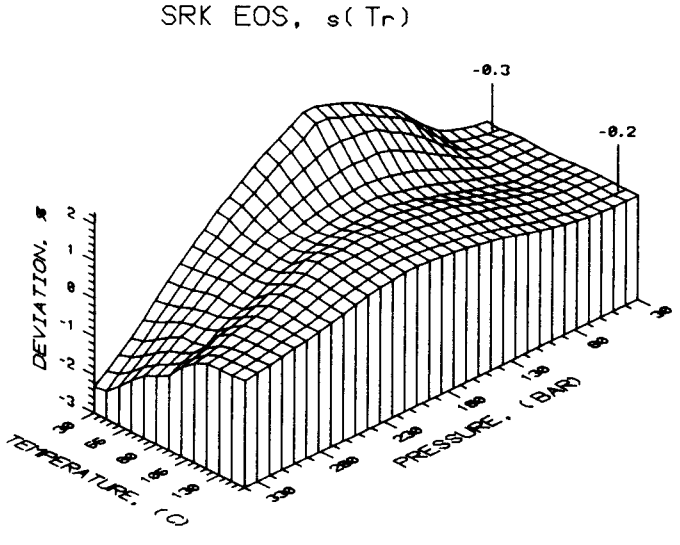

Fig. 5.9 SRK EOS dense phase Z-factor deviations as function of pressure and temperature for the Rio Bravo Trapped Gas. Volume translation shift parameters determined as function of reduced temperature.

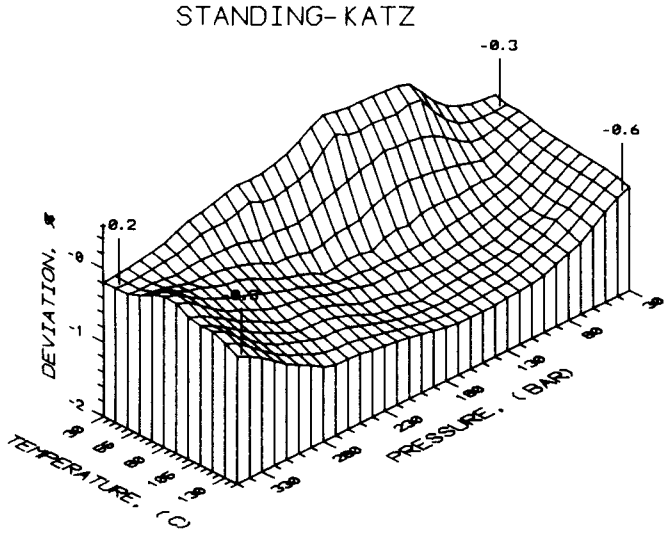

Fig. 5.10 Standing-Katz dense phase Z-factor deviations as function of pressure and temperature for the Rio Bravo Trapped Gas.

5.3 Coats and Smart Reservoir Fluids

EOS Prediction

Coats and Smart (1986) give a detailed description of twelve reservoir fluids. Table 5.7 reports composition and M_{7+} and γ_{7+} for seven oils and five gas condensates. These are denoted Oil 1 to 7 and Gas 1 to 5. The proposed PR and SRK EOS fluid characterization procedures given above were applied to these reservoir fluids, except Gas 4 which contains 18 mole percent H_2S.

Oil 5 is the reservoir oil presented by Hoffmann et al. (1952). A complete set of fractional distillation data are given for this oil. Molar distribution parameters were thus determined using regression to fit the reported molar distribution, resulting in α=1.562 and η=90. The same procedure was used to estimate the molar distribution of the accompanying gas-cap fluid (here denoted: Oil 5,gas), yielding α=1.901 and η=90.

The reported composition of Oil 3 which contains 60 mole percent CO_2, is extended to C_{10+}. Thus, an estimate for the C_{7+} molar distribution was obtained as described for Oil 5, resulting in α=1.03 and η=90. SCN molecular weights and specific gravities for C_7, C_8, and C_9 (Katz and Firoozabadi, 1978) were used to calculate overall C_{7+} properties, yielding M_{7+}= 186.33 and γ_{7+}=0.8325. It was experienced during this study that better predictions are obtained with CO_2-C_{7+} BIPs equal to 0.125 for PR EOS and 0.135 for the SRK EOS instead of 0.115 as shown in Table 3.13.

Saturation pressure prediction is crucial for obtaining a reasonable match to measured data from PVT experiments. Table 5.8a shows that saturation pressures for these fluids using PR and SRK EOSs, are predicted reasonably well, except for Oil 2 and Gas 3. Overall AAD is equal to 3.41 and 5.02 percent for the PR and SRK EOSs, respectively. The characterization procedure used by Coats and Smart underpredicts the saturation pressure significantly since BIAS equal -14.06 and -12.41 percent for the PR and ZJRK EOSs, respectively. The corresponding AADs are 14.28 percent for PR EOS and 16.85 percent for ZJRK EOS.

Tables 5.8b through 5.8h compare other PR and SRK predicted PVT parameters with experimental data. Comparisons of measured data with PR and ZJRK predictions given by Coats and Smart are also presented. Table 5.8b shows saturated densities, ρ_s. Saturation pressure prediction will to a certain extent effect ρ_s prediction. Underpredicted saturation pressures result in too low saturated densities. AAD=0.99 and BIAS=0.05 percent for the PR EOS, compared to AAD=1.60 and BIAS=2.07 percent for the SRK EOS. It is noticed that Coats and Smart with the ZJRK EOS obtained AAD=2.47 and BIAS=-1.63, which is remarkable good considering that the saturation pressures were highly underpredicted. However, from these results one may claim that predicted saturation densities possibly will be too high if the saturation pressures get closer to the measured. These thoughts are confirmed by Whitson (1983b) who concluded that ZJRK overpredicts liquid densities.

TABLE 5.7 -- Description of Coats and Smart Fluids (From Coats and Smart, 1986)

FLUID COMPOSITIONS AND PROPERTIES AT RESERVOIR CONDITIONS										
	Gas 2*	Gas 2**	Gas 4	Gas 5	Oil 1	Oil 2	Oil 3	Oil 4	Oil 6	Oil 7
CO_2	0.0069	0.0061	0.0350	0.0217	0.0044	0.0090	0.6031	0.0235	0.0103	0.0008
N_2		0.0042	0.0114	0.0034	0.0045	0.0030	0.0093	0.0011	0.0055	0.0164
H_2S	0.0004	0.0004	0.1819							
C_1	0.5832	0.5749	0.5762	0.7064	0.3505	0.5347	0.0705	0.3521	0.3647	0.2840
C_2	0.1355	0.1345	0.0739	0.1076	0.0464	0.1146	0.0157	0.0672	0.0933	0.0716
C_3	0.0761	0.0752	0.0302	0.0494	0.0246	0.0879	0.0306	0.0624	0.0885	0.1048
C_4	0.0403	0.0415	0.0231	0.0302	0.0166	0.0456	0.0331	0.0507	0.0600	0.0840
C_5	0.0241	0.0233	0.0129	0.0135	0.0160	0.0209	0.0268	0.0523	0.0378	0.0382
C_6	0.0190	0.0179	0.0554†	0.0090	0.0546	0.0151	0.0258	0.0410	0.0356	0.0405
C_7	0.1145†	0.1220†		0.0588†	0.4824†	0.1692†	0.0216	0.3497†	0.3043†	0.3597†
C_8							0.0226			
C_9							0.0210			
C_{10}							0.1199†			
$M+$	193	193	117	153	225	173	229	213	200	252
$\gamma+$	0.8135	0.8115	0.7748	0.8100	0.9000	0.8364	0.8570	0.8405	0.8366	0.8429
p_s	4,450	4,415	3,360	4,842	2,520	4,460	2,597	2,547	2,746	1,694
ρ_s	28.85	29.54		19.15	47.96	33.01	44.17	40.34	38.01	44.48
T	190	190	240	267	180	176	179	250	234	131

*Dewpoint sample.
**Bubblepoint sample.
†Plus fraction.

TABLE 5.8a -- Comparison of Measured and Predicted Saturation Pressure of Some Reservoir Fluids Presented by Coats and Smart.

		Saturation Pressure (psia)								
							Coats and Smart, 1986			
Sample	Temp. °F	Experimental	PR	Dev. %	SRK	Dev. %	PR	Dev. %	ZJRK	Dev. %
Gas 1	181	4076	4136	1.48	4412	8.25	3334	-18.20	3461	-15.08
Gas 2-1	190	4480	4462	-0.39	4556	1.71	3680	-17.86	3593	-19.80
Gas 2-2	190	4445	4432	-0.30	4520	1.70	3664	-17.57	3571	-19.66
Gas 3	226	4468	4957	10.93	5152	15.30	4547	1.77	4857	8.71
Gas 5	267	4857	4771	-1.77	5058	4.14	4494	-7.47	4165	-14.25
Oil 1	180	2535	2457	-3.07	2495	-1.58				
Oil 2	176	4475	3949	-11.75	4030	-9.94	3344	-25.27	3477	-22.30
Oil 3,1	140	2130	2115	-0.68	2067	-2.96	1761	-17.32	1818	-14.65
Oil 3,2	160	2377	2350	-1.14	2297	-3.37	1985	-16.49	2014	-15.27
Oil 3,3	180	2612	2563	-1.87	2509	-3.96	2195	-15.96	2200	-15.77
Oil 3,4	200	2807	2756	-1.82	2701	-3.79	2388	-14.93	2375	-15.39
Oil 4,1	110	2562	2450	-4.35	2441	-4.69	2259	-11.82	2300	-10.22
Oil 4,2	180	2298	2212	-3.74	2217	-3.52	2018	-12.17	2100	-8.60
Oil 4,3	250	1973	1882	-4.59	1906	-3.40	1679	-14.89	1805	-8.50
Oil 5	201	3825	3742	-2.18	3778	-1.24	3284	-14.14	3342	-12.63
Oil 5,gas	201	3825	3915	2.35	4298	12.37				
Oil 6	234	2761	2589	-6.20	2591	-6.15	2383	-13.68	2432	-11.91
Oil 7	131	1709	1662	-2.77	1670	-2.29	1531	-10.42	1631	-4.56
			BIAS :	-1.77		-0.21		-14.06		-12.41
			AAD :	3.41		5.02		14.28		16.85
			MAXD :	11.75		15.30		25.27		15.08

TABLE 5.8b -- Comparison of Measured and Predicted Saturated Densities.

		Saturated Densities (lb/ft^3)								
							Coats and Smart, 1986			
Sample	Temp. °F	Experimental	PR	Dev. %	SRK	Dev. %	PR	Dev. %	ZJRK	Dev. %
Gas 1	181	15.8	15.9	0.42	16.8	6.29	14.3	-9.67	14.4	-9.03
Gas 2-1	190	28.8	29.6	2.73	30.4	5.43	27.8	-3.63	28.2	-2.24
Gas 2-2	190	29.5	30.1	2.05	30.9	4.62	28.3	-4.07	28.7	-2.71
Gas 5	267	19.2	19.0	-0.69	20.1	4.77	19.2	0.26	18.1	-5.48
Oil 1	180	48.0	47.9		48.2					
Oil 2	176	33.0	33.1	0.22	33.8	2.27	31.1	-5.79	32.2	-2.45
Oil 3,1	140	45.9	46.2	0.66	46.2	0.64	43.1	-6.13	46.5	1.28
Oil 3,2	160	45.1	45.3	0.49	45.4	0.68	42.3	-6.21	45.6	1.11
Oil 3,3	180	44.2	44.5	0.66	44.6	0.99	41.5	-6.04	44.8	1.43
Oil 3,4	200	43.3	43.5	0.52	43.7	1.02	40.6	-6.24	44.0	1.62
Oil 4,3	110	40.3	39.9	-1.17	40.1	-0.69	36.8	-8.78	39.5	-2.08
Oil 4,2	180	42.4	42.0	-1.04	42.1	-0.64	38.4	-9.43	41.7	-1.65
Oil 4,1	250	44.4	43.6	-1.77	43.9	-0.97	40.0	-9.85	43.8	-1.28
Oil 5	201	41.6	40.8	-1.88	41.1	-1.21	37.4	-10.10	40.2	-3.37
Oil 6	234	38.0	38.1	0.14	38.4	1.04	35.6	-6.34	37.7	-0.82
Oil 7	131	44.5	44.2	-0.60	44.5	0.04	40.7	-8.50	44.9	0.94
			BIAS :	0.05		1.60		-6.63		-1.63
			AAD :	0.99		2.07		6.66		2.47
			MAXD :	2.73		6.29		10.10		9.03

Table 5.8c and 5.8d list oil formation volume factor, B_{od}, and solution gas oil ratio, R_{sd}, at bubble point obtained from differential liberation expansion (DLE) experiments. The latter parameter is quite difficult to predict accurately, thus the obtained AAD≈6.8 percent for both EOSs with the proposed characterization method, is considered satisfactorily. Comparison of measured and predicted B_{od}, results in AAD=3.06 percent for the PR EOS and AAD=2.88 percent for the SRK EOS. The corresponding PVT parameters obtained from surface separation, B_{of} and R_{sf}, are presented in Table 5.8e and 5.8f. Also, these data are predicted reasonably well with AAD(PR)=1.98 percent and AAD(SRK)=1.55 percent for B_{of}, and AAD(PR,SRK)≈4.9 for R_{sd}.

TABLE 5.8c -- Comparison of Measured and Predicted Bubble Point Oil Formation Volume Factor From DLE Experiment.

		Bubble Point FVF From DLE (bbl/STB)								
							Coats and Smart, 1986			
Sample	Temp. °F	Experimental	PR	Dev. %	SRK	Dev. %	PR	Dev. %	ZJRK	Dev. %
Oil 2	176	2.9210	2.8477	-2.51	2.7699	-5.17	2.419	-17.19	2.641	-9.59
Oil 4,1	110	1.3410	1.3661	1.87	1.3543	0.99	1.294	-3.50	1.353	0.89
Oil 4,3	250	1.6710	1.7381	4.02	1.7260	3.29	1.517	-9.22	1.638	-1.97
Oil 6	234	1.8660	1.9309	3.48	1.9086	2.28	1.659	-11.09	1.802	-3.43
Oil 7	131	1.3240	1.3692	3.41	1.3589	2.64	1.296	-2.11	1.365	3.10
			BIAS :	2.05		0.81		-8.62		-2.20
			AAD :	3.06		2.88		8.62		3.80
			MAXD :	4.02		5.17		17.19		9.59

TABLE 5.8d -- Comparison of Measured and Predicted Bubble Point Solution GOR From DLE Experiment.

		Bubble Point Solution GOR (scf/STB)								
							Coats and Smart, 1986			
Sample	Temp. °F	Experimental	PR	Dev. %	SRK	Dev. %	PR	Dev. %	ZJRK	Dev. %
Oil 2	176	3377	3284	-2.76	3243	-3.97	2550	-24.49	2880	-14.72
Oil 4,1	110	701	708	1.05	707	0.84	611	-12.84	611	-12.84
Oil 4,3	250	932	1010	8.41	1007	8.02	756	-18.88	878	-5.79
Oil 6	234	1230	1341	8.99	1335	8.55	1002	-18.54	1155	-6.10
Oil 7	131	557	634	13.90	632	13.53	542	-2.69	633	13.64
			BIAS :	5.62		5.09		-15.49		-5.16
			AAD :	6.84		6.78		15.49		10.62
			MAXD :	13.82		13.20		24.49		14.72

TABLE 5.8e -- Comparison of Measured and Predicted Bubble Point Oil Formation Volume Factor From Surface Separation.

		Bubble Point FVF (bbl/STB)								
							Coats and Smart, 1986			
Sample	Temp. °F	Experimental	PR	Dev. %	SRK	Dev. %	PR	Dev. %	ZJRK	Dev. %
Oil 2	176	2.172	2.3631	8.80	2.3151	6.59	2.052	-5.52	2.303	6.03
Oil 4,1	110	1.467	1.4838	1.15	1.4758	0.60	1.276	-13.02	1.461	-0.41
Oil 4,2	150	1.520	1.5347	0.97	1.5242	0.28	1.306	-14.08	1.503	-1.12
Oil 4,3	180	1.563	1.5773	0.91	1.5681	0.33	1.329	-14.97	1.533	-1.92
Oil 5	201	1.475	1.4752	0.01	1.4637	-0.77	1.247	-15.46	1.436	-2.64
Oil 6	234	1.722	1.7211	-0.05	1.7025	-1.13	1.487	-13.65	1.704	-1.05
Oil 7	131	1.340	1.3665	1.98	1.3556	1.16	1.188	-11.34	1.380	2.99
			BIAS :	1.97		1.01		-12.58		0.27
			AAD :	1.98		1.55		12.58		2.31
			MAXD :	8.80		6.59		15.46		6.03

TABLE 5.8f -- Comparison of Measured and Predicted Bubble Point Solution Gas Oil Ratio From Surface Separation.

		Bubble Point Solution GOR (scf/STB)								
							Coats and Smart, 1986			
Sample	Temp. °F	Experimental	PR	Dev. %	SRK	Dev. %	PR	Dev. %	ZJRK	Dev. %
Gas 2	190	3410	3276	-3.93	3265	-4.24	3092	-9.33	3497	2.55
Gas 5	210	8933	8601	-3.72	8569	-4.07	8407	-5.89	8502	-4.82
Oil 2	176	2061	2522	22.35	2520	22.24	2189	6.21	2460	19.36
Oil 4,1	110	685	696	1.61	695	1.42	604	-11.82	693	1.17
Oil 4,2	150	753	764	1.47	762	1.14	649	-13.81	750	-0.40
Oil 4,3	180	810	820	1.24	819	1.03	683	-15.68	791	-2.35
Oil 5	201	910	890	-2.24	888	-2.42	760	-16.48	876	-3.74
Oil 6	234	1059	1065	0.53	1061	0.14	910	-14.07	1046	-1.23
Oil 7	131	580	624	7.61	622	7.27	545	-6.03	635	9.48
			BIAS :	2.77		2.50		-9.66		2.23
			AAD :	4.97		4.89		11.04		5.01
			MAXD :	22.35		22.24		16.48		19.36

Lastly, relative stock tank oil density from DLE experiments, γ_{od} and surface separation, γ_{of}, are compared to experimental data in Tables 5.8g and 5.8h, respectively. For both EOSs, the γ_{od} AAD is about 0.41-0.42 percent and for γ_{of} AAD is around 0.65-0.66 percent.

TABLE 5.8g -- Comparison of Measured and Predicted Relative Density of Stock Tank Oil From DLE Experiment

		Relative Density of Stock Tank Oil (60°/60°F)								
							Coats and Smart, 1986			
Sample	Temp. °F	Experimental	PR	Dev. %	SRK	Dev. %	PR	Dev. %	ZJRK	Dev. %
Oil 2	176	0.827	0.8284	0.17	0.8282	0.15	0.709	-14.27	0.8030	-2.90
Oil 4,1	110	0.820	0.8143	-0.70	0.8145	-0.67	0.711	-13.29	0.8150	-0.61
Oil 4,3	250	0.841	0.8362	-0.57	0.8358	-0.61	0.717	-14.74	0.8300	-1.31
Oil 6	234	0.835	0.8323	-0.33	0.8319	-0.37	0.715	-14.37	0.8230	-1.44
Oil 7	131	0.826	0.8238	-0.27	0.8237	-0.28	0.722	-12.59	0.8380	1.45
			BIAS :	-0.34		-0.36		-13.85		-0.96
			AAD :	0.41		0.42		13.85		1.54
			MAXD :	0.70		0.67		14.74		2.90

TABLE 5.8h -- Comparison of Measured and Predicted Relative Density of Stock Tank Oil From Surface Separation.

		Relative Density of Stock Tank Oil (60°/60°F)								
							Coats and Smart, 1986			
Sample	Temp. °F	Experimental	PR	Dev. %	SRK	Dev. %	PR	Dev. %	ZJRK	Dev. %
Gas 2	190	0.780	0.777	-0.37	0.777	-0.34	0.789	1.15	0.829	6.28
Gas 5	210	0.781	0.777	-0.48	0.777	-0.51	0.765	-2.05	0.744	-4.74
Oil 2	176	0.819	0.804	-1.84	0.805	-1.75	0.703	-14.16	0.787	-3.91
Oil 4,1	110	0.819	0.813	-0.69	0.813	-0.67	0.711	-13.19	0.814	-0.61
Oil 4,2	150	0.827	0.819	-0.92	0.820	-0.91	0.713	-13.78	0.819	-0.97
Oil 4,3	180	0.831	0.824	-0.83	0.824	-0.85	0.714	-14.08	0.823	-0.96
Oil 5	201		0.827	0	0.826	0.00	0.717		0.827	
Oil 6	234	0.821	0.818	-0.35	0.818	-0.38	0.712	-13.28	0.816	-0.61
Oil 7	131	0.827	0.824	-0.41	0.823	-0.44	0.722	-12.70	0.838	1.33
			BIAS :	-0.66		-0.65		-9.12		-0.46
			AAD :	0.66		0.65		9.38		2.16
			MAXD :	1.84		1.75		14.16		6.28

It can be concluded from these comparisons that the PR EOS with the proposed characterization method predicts PVT data slightly better than SRK. This is further shown in Table 5.9 where overall AADs are reported based on all available PVT data for samples Gas 2 and 5 and Oil 2-5. The PVT data are calculated twice for each EOS, using the two different pure component shift parameter approaches; $s=s(T_r)$ and $s=s(0.7)$. For all fluids except Gas 2, it is observed that a lower AAD is obtained with $s(T_r)$ than with $s(0.7)$. The total AAD is higher than five percent only for two fluids, namely Gas 2 and Oil 2. The large deviations for Gas 2 are mainly due to prediction of an

incorrect saturation pressure type; a bubble point was predicted instead of a dew point. This results in large deviations between measured and calculated CCE data. The proposed characterization methods seems to have a common deficiency: mixture critical temperature is too high for near critical fluids. Saturation pressures of near critical fluids though, are usually predicted within a few percent, while predicted saturation pressures of light gas condensates and non-volatile oils may deviate more.

TABLE 5.9 -- Total Absolute Average Deviations Between Measured and Predicted Properties for the Coats and Smart Fluids.

	Absolute Average Deviations, %			
	PR EOS		SRK EOS	
Sample	$s(T_r)$ [1]	$s(0.7)$ [2]	$s(T_r)$	$s(0.7)$
Gas 2	8.53	8.38	9.15	8.55
Gas 5	1.64	1.72	2.82	2.66
Oil 2	8.95	9.16	8.65	9.22
Oil 3	3.28	3.34	4.62	4.73
Oil 4	4.03	4.08	3.96	4.48
Oil 5	1.58	1.71	2.47	2.76
Oil 6	4.74	4.79	4.75	5.19
Oil 7	4.38	4.42	4.18	4.30

Note:
1. $s(T_r)$ refers to using pure component shift parameters determined as function of reduced temperature.
2. $s(0.7)$ refers using to pure component shift parameters determined at reduced temperature of 0.7 (Table 1.3).

EOS Adjustment of Oil 4

An attempt was made to match measured PVT data of some of the reservoir fluids described by Coats and Smart (1986). A good basis for the PVT matching is provided with the proposed characterization procedure. Normally, relative few regression parameters (4-6) need to be adjusted within tight preset bounds, to obtain a good match to the measured data.

Oil 4 is a volatile oil which is matched without problems using six parameters (see Table 5.10). Regression parameters and eigenvalues of the Hessian matrix

at solution are also given in Table 5.10, with the corresponding eigenvectors given in Table 5.11. From these results it is obvious that parameter 6 which adjusts all C_{7+} critical temperatures, is associated with the least uncertainty, since $\lambda_6 \approx 5.46(10^5)$. Also, parameter 5 which adjusts C_{7+} boiling points is well determined with $\lambda_5=13063$. Parameter 1, which adjusts the C_1-C_{7+} BIPs, is associated with the minimum eigenvalue, $\lambda_1=0.15$. The condition number of the Hessian matrix for this problem thus becomes $3.6(10^6)$, which is somewhat high. The final C_{7+} characterization for Oil 4 is presented in Table 5.12. When using EOS-based procedures to estimate acentric factors (C_{7+} ω) and shift parameters (C_{7+} s), and C_{7+} T_bs and T_cs are adjusted during regression, the final C_{7+} ω and s values can be altered significantly. In this case, the shift parameters are slightly high, and ω of $C_{7+}(5)$ is lower than ω of $C_{7+}(4)$. ω of $C_{7+}(1\text{-}5)$ would probably become a smooth, monotonic increasing function if also T_b for $C_{7+}(4)$ and $C_{7+}(3)$ were adjusted.

TABLE 5.10 -- Final Regression Parameters and Eigenvalues of Hessian Matrix at Solution for Oil 4.

i	Regression Parameters	Final Value	Eigen-Value
1	C_1-C_{7+}(1-5) BIPs	1.3597	0.15
2	Boiling point of $C_{7+}(5)$	1.0600	6.38
3	Crit. temperature of $C_{7+}(5)$	1.0600	80.08
4	C_{7+} molecular weight	0.9950	4.89
5	C_{7+} boiling points	1.0558	13063.0
6	C_{7+} critical temperatures	0.9623	546040.0

TABLE 5.11 -- Eigenvectors of Hessian Matrix at Solution for Oil 4.

$$S = \begin{bmatrix} 0.951 & -0.216 & -0.193 & -0.043 & 0.041 & 0.087 \\ 0.253 & 0.769 & 0.191 & 0.496 & -0.238 & -0.071 \\ 0.175 & 0.044 & 0.819 & -0.480 & 0.060 & -0.251 \\ -0.003 & -0.550 & 0.416 & 0.715 & 0.072 & -0.092 \\ 0.010 & 0.238 & -0.016 & 0.100 & 0.965 & 0.036 \\ -0.023 & 0.027 & 0.287 & -0.020 & -0.035 & 0.956 \end{bmatrix}$$

TABLE 5.12 -- PR EOS C_{7+} Characterization for Oil 4.

Pseudo Component	z (mole %)	M (lb/mol)	T_c (°R)	p_c (psia)	ω	γ (60/60)	T_b (°R)	Shift Parameter s	BIPs C_1-C_{7+}
$C_{7+}(1)$	5.665	98.5	999.3	395.3	0.5252	0.7376	712.3	0.1133	0.03039
$C_{7+}(2)$	10.239	135.8	1128.9	316.0	0.6648	0.7847	838.2	0.1598	0.04116
$C_{7+}(3)$	10.002	206.6	1303.2	222.8	0.9426	0.8322	1026.9	0.2422	0.05728
$C_{7+}(4)$	6.488	319.8	1484.5	154.9	1.4052	0.8758	1241.6	0.3042	0.07317
$C_{7+}(5)$	2.689	500.0	1818.4	93.2	1.1376	0.9184	1553.1	0.4949	0.09164
C_{7+}(total)	35.083	211.93				0.8405			

Note:
1. The molar distribution is defined by α=1.0, η=90.
2. BIPs for C_1-C_{7+} are calculated from Eq.3.61 with A=0.1358 and B=6.0. BIPs between pairs of non-HC and HC are taken from Table 3.13.

An almost perfect match to the saturation pressures at 110°, 180° and 250°F [43.3°, 82.2°, 121.1°C] was obtained, with a maximum error of 10 psia. The sum of squares was 0.65 and AAD=2.29 percent.

Comparison of measured and calculated DLE data at 110° and 250°F are given in Figs. 5.11 and 5.12. Oil formation volume factor, B_{od}, and solution gas oil ratio, R_{sd}, are plotted versus pressure in Fig. 5.11. At 250°F and at low pressures, R_{sd} is slightly high and B_{od} is somewhat underestimated. At 110°F, both B_{od} and R_{sd} almost duplicate the measured data. Overall, the match is satisfactory. Liquid density, ρ_{Ld}, and vapor Z-factor, Z_{Vd}, are plotted versus pressure in Fig. 5.12. Liquid density is underpredicted 0.9 percent at the saturation pressure at 110°F [43.3°C], but this deviation is reduced to zero at lower pressures. The opposite pattern is observed for ρ_L at 250°F: a perfect fit is obtained at pressures above 1200 psia [82.76 bar], and below it is overpredicted, with maximum 1.1 percent at 400 psia [27.59 bar]. The vapor Z-factor match is acceptable at 110°F, and not very good at 250: Z_{Vd} is two percent high at the saturation pressure and almost four percent low at 100 psia [6.90 bar]. In view of the good Z-factor match at 110°F, these results are somewhat unexpected. It may be due to poor weighting of the measured data, i.e. R_{sd} or ρ_L data points are emphasized on behalf of the Z_{Vd} data.

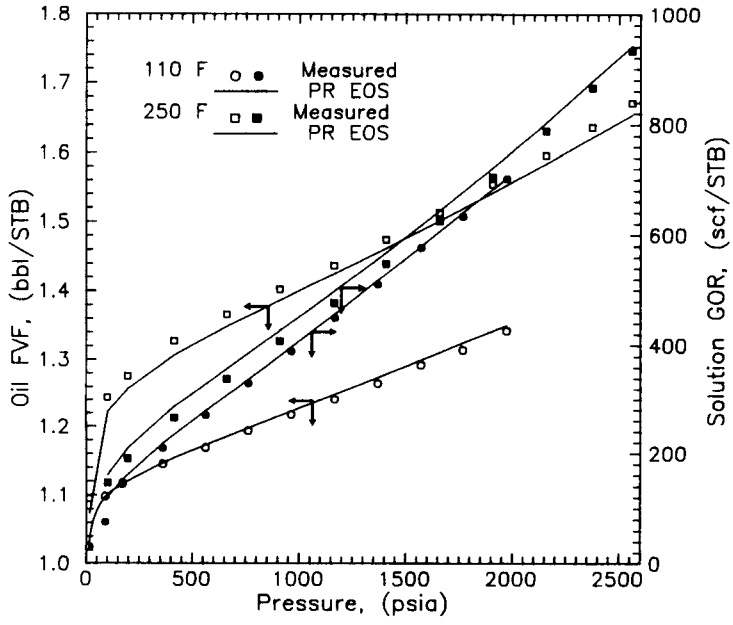

Fig. 5.11 Oil FVFs and solution GORs from DLE experiment for Oil 4 of Coats and Smart.

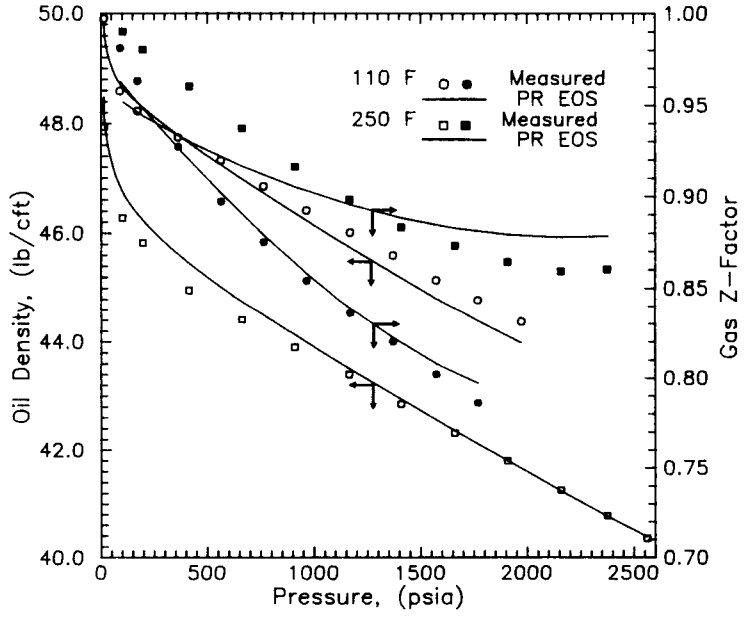

Fig. 5.12 Liquid densities and vapor Z-factors from DLE experiment for Oil 4 of Coats and Smart.

Table 5.13 presents oil FVF, B_{of}, solution GOR, R_{sf}, and liquid density, ρ_{Lf}, resulting from simulating various surface separation alternatives i.e. several multistage separator trains with different pressure and temperature conditions. These results are also quite encouraging. AAD for B_{of} and ρ_{Lf} are 0.81 and 0.46 percent, respectively. At first glance, the R_{sf} results do not look very promising with AAD=7.58 and BIAS=5.78 percent, but a closer look reveals that a very good match to the measured data is obtained at all separator stages, except for the last stage where R_{sf} is off by 20-30 percent.

TABLE 5.13 -- Comparison of Calculated and Measured Surface Separation Data for Oil 4.

Temp. (°F)	Pressure (psia)	Oil FVF, bbl/STB			Solution GOR, scf/STB			Oil Density, lb/ft^3		
		Exp.	Calc.	Dev. %	Exp.	Calc.	Dev. %	Exp.	Calc.	Dev. %
250	2562	1.563	1.541	-1.43	810	800	-1.19	40.34	40.38	0.10
180	265	1.145	1.149	0.35	677	651	-3.88	47.76	47.58	-0.37
180	60	1.111	1.101	-0.93	81	81	0.29	47.88	48.38	1.04
180	15	1.059	1.047	-1.11	52	68	31.50	48.94	49.07	0.25
60	15							51.90	51.38	-1.00
250	2562	1.520	1.505	-1.01	753	753	-0.07	40.34	40.38	0.10
150	265	1.120	1.122	0.85	620	606	-2.26	47.94	47.88	-0.13
150	60	1.089	1.084	-0.47	80	81	1.64	48.44	48.69	0.51
150	15	1.044	1.036	-0.75	53	65	23.10	49.38	49.35	-0.06
60	15							51.60	51.14	-0.89
250	2562	1.467	1.461	-0.43	685	692	0.96	40.34	40.38	0.10
110	265	1.086	1.103	1.52	551	549	-0.35	49.07	48.37	-1.43
110	60	1.056	1.060	0.41	85	82	-3.06	49.26	49.16	-0.19
110	15	1.025	1.021	-0.40	49	60	22.70	49.82	49.76	-0.12
60	15							51.12	50.80	-0.64
		AAD :		0.81			7.58			0.46
		BIAS :		-0.28			5.78			-0.18
		MAXD :		1.52			31.5			1.43

EOS Adjustment of Oil 3

Oil 3, also described by Coats and Smart, is special because it consists of 60 (mole)percent CO_2. Six parameters, defined in Table 5.14, were adjusted during a regression run for Oil 3. Because of the high CO_2 content, CO_2-C_{7+} BIPs were adjusted instead of C_1-C_{7+} BIPs.

Eigenvalues at the solution are also presented in Table 5.14 with the corresponding eigenvectors listed in Table 5.15. Again the parameter adjusting C_{7+} T_cs shows the largest eigenvalue, λ_4=97790, and now T_b of C_{7+}(5)

is associated with the minimum eigenvalue, λ_2=0.05. This may be due the low mole fraction of $C_{7+}(5)$. Also, $C_{7+}(5)$ critical pressure is a weak parameter, as usual. The condition number for the Hessian matrix $\kappa(H)$ at the solution is $1.9(10^6)$. The final C_{7+} characterization is presented in Table 5.16. Note that large negative shift parameters are obtained, which is due to the final combination of C_{7+} T_c, p_c and ω, and partly to the adjustment of C_{7+} shift parameters during regression (parameter 6).

TABLE 5.14 -- Final Regression Parameters and Eigenvalues of Hessian Matrix at Solution for Oil 3.

i	Regression Parameters	Final Value	Eigen-Value
1	CO_2-C_{7+}(1-5) BIPs	0.9962	22.59
2	Boiling point of $C_{7+}(5)$	0.94	0.05
3	C_{7+} boiling points	0.90	41.11
4	C_{7+} critical temperatures	1.0035	97790.0
5	C_{7+} critical pressures	1.10	0.21
6	C_{7+} shift parameters	1.1050	3.16

TABLE 5.15 -- Eigenvectors of Hessian Matrix at Solution for Oil 3.

$$S = \begin{bmatrix} 0.3907 & -0.0151 & 0.7377 & 0.1602 & -0.5224 & 0.0660 \\ 0.1228 & 0.9415 & -0.7431 & 0.0376 & -0.0660 & -0.2952 \\ -0.7428 & 0.1375 & 0.5951 & -0.0382 & 0.2586 & -0.0828 \\ -0.3062 & -0.0297 & -0.2094 & 0.8940 & -0.2496 & 0.0004 \\ 0.4037 & -0.1443 & 0.2115 & 0.3677 & 0.6609 & -0.4466 \\ 0.1543 & 0.2696 & 0.0874 & 0.1924 & 0.3959 & 0.8380 \end{bmatrix}$$

TABLE 5.16 -- PR EOS C_{7+} Characterization for Oil 3.

Pseudo Component	z[1] (mole %)	M (lb/mol)	T_c (°R)	p_c (psia)	ω	γ (60/60)	T_b (°R)	Shift Parameter s	BIPs[2] C_1-C_{7+}
$C_{7+}(1)$	3.71600	98.5	942.4	612.2	0.2516	0.7436	607.3	-0.5201	0.0276
$C_{7+}(2)$	6.36572	135.8	1068.5	501.4	0.3265	0.7913	715.5	-0.4567	0.0402
$C_{7+}(3)$	5.24842	206.6	1238.5	369.0	0.4533	0.8395	876.3	-0.3500	0.0601
$C_{7+}(4)$	2.53357	319.8	1416.1	268.9	0.6172	0.8836	1058.1	-0.2833	0.0813
$C_{7+}(5)$	0.64628	500.0	1534.9	239.2	0.7069	0.9268	1172.1	-0.6215	0.0897
C_{7+}(total)	18.510	186.33				0.8325			

Note:
1. The molar distribution is defined by fitting the reported C_{7+} molar distribution data, yielding α=1.03, η=90, and M_{7+}=186.33.
2. BIPs for CO_2-C_{7+} are adjusted to 0.1238 during regression.

With regression a perfect match was obtained of the saturation pressures at temperatures from 140° to 200°F [60°, 93.3°C] was obtained. The match to saturated liquid densities was also good with AAD=0.58 percent. The final sum of squares from the regression was 0.0299, and overall AAD was 0.9634 percent.

Measured data from four CCE experiments at 140°, 160°, 180°, and 200°F [60°,71.1°, 82.2°, 93.3°C] were reported by Coats and Smart. These experiments yield liquid volume fraction, S_L, and total volume relative to volume at saturation pressure, V/V_s. Measured and calculated S_L and V/V_s at temperatures 140° and 180°F are compared in Fig. 5.13, and at temperatures 160° and 200°F in Fig. 5.14. Excellent matches are obtained for both S_L (AAD=1.22 %) and V/V_s (AAD=0.88 %) over the actual pressure and temperature ranges. These results show that a CO_2-rich reservoir fluid can be matched without using temperature dependent EOS constants Ω_a and Ω_b for CO_2, as proposed by Turek et al. (1980) and Chaback and Turek (1986).

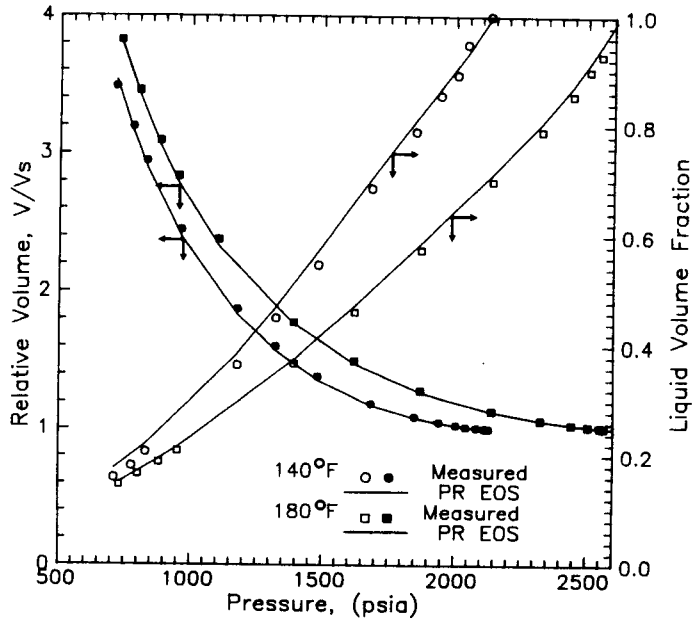

Fig. 5.13 Liquid volume fractions and relative volumes from CCE experiments at the 140° and 180°F [60°, 82.2°C] isotherms for Oil 3 of Coats and Smart.

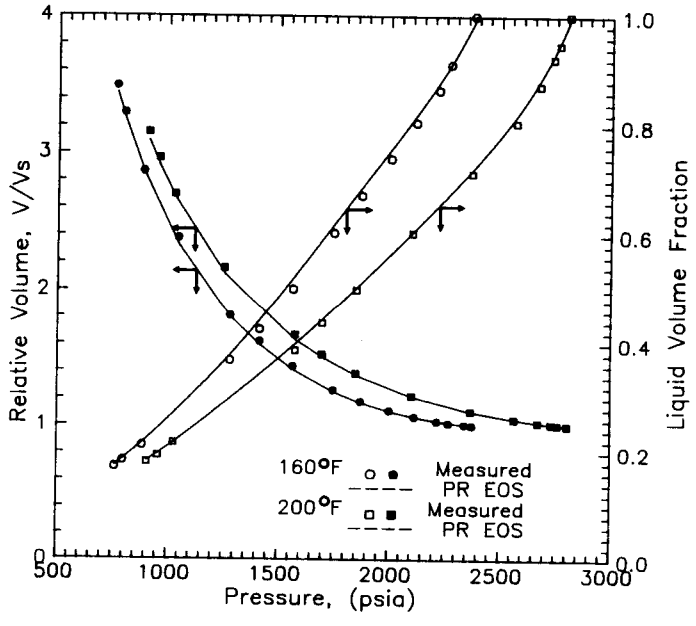

Fig. 5.14 Liquid volume fractions and relative volumes from CCE experiments at the 160° and 200°F [71.1°, 93.3°C] isotherms for Oil 3 of Coats and Smart.

5.4 NS-1 (Whitson-Torp) Gas Condensate

The NS-1 fluid presented by Whitson and Torp (1983) is a rich gas-condensate fluid from a North-Sea reservoir which had a test GOR of 5500 scf/STB [980 Sm^3/Sm^3] and a 44°API [γ=0.8063] stock-tank condensate gravity. Initial reservoir pressure is 7300 psia [503.4 bar] at 280°F [137°C]. Whitson and Torp also presented TBP data for a fluid sampled from a well in the same field. Molar distribution parameters determined for this fluid are used for NS-1, with α=0.65 and η=90.

PR and SRK EOS predicted saturation pressures for the NS-1 fluid at 280°F are, respectively, 6978 psia [481 bar] and 7221 psia [498 bar] using the proposed C_{7+} characterization procedures. This is 3.14 and 6.74 percent higher than the measured saturation pressure of 6765 psia [466.5 bar].

A constant volume depletion (CVD) experiment was performed on the NS-1 fluid. Fig. 5.15 compares PR predicted (dashed line) liquid volume fraction, S_L, and vapor Z-factor, Z_V, with measured data at the various pressure stages. S_L is predicted too high at all pressures. Vapor Z-factor prediction is good at high pressures, and is slightly underestimated at lower pressures. The S_L curve shows clearly that an accurate saturation pressure estimate does not necessarily result in accurate VLE behavior in the two-phase region. The sharp increase in predicted S_L with too high S_{Lmax} is a deficiency common for many EOS characterization methods. Minor adjustments in C_{7+} properties will in most cases result in a good match to the S_L curve. For example, adjustment of T_b or T_c for the heaviest pseudocomponent will usually improve the S_L match close to the dew point, and adjustment of all C_{7+} T_cs with a single parameter usually fits the region of maximum liquid dropout.

The NS-1 C_{7+} characterization for PR EOS was adjusted using regression. Table 5.17 presents the parameters adjusted and their final values. The eigenstructure of the Hessian matrix at the solution is given with reported eigenvalues and eigenvectors in Table 5.17 and 5.18, respectively. PR EOS C_{7+} characterization for NS-1 is shown in Table 5.19.

TABLE 5.17 -- PR EOS Final Regression Parameters and Eigenvalues of Hessian Matrix at Solution for the NS-1 Gas Condensate.

i	Regression Parameters	Final Value	Eigen-Value
1	Boiling point of C_{7+}(3)	1.0100	0.14
2	Boiling point of C_{7+}(4)	0.9500	1.33
3	Boiling point of C_{7+}(5)	0.9400	4.10
4	Crit. temperature of C_{7+}(5)	0.9515	141.90
5	C_{7+} molecular weight	1.0323	16.59
6	C_{7+} boiling points	0.9679	912.09
7	C_{7+} crit. temperatures	1.0204	271300.

TABLE 5.18 -- Eigenvectors of Hessian Matrix at Solution for NS-1 Gas Condensate.

$$S = \begin{bmatrix} 0.646 & -0.672 & 0.337 & 0.108 & 0.008 & -0.074 & -0.017 \\ 0.711 & 0.554 & -0.251 & -0.206 & 0.063 & -0.276 & 0.034 \\ -0.074 & 0.413 & 0.842 & 0.202 & 0.028 & -0.271 & 0.015 \\ 0.050 & 0.077 & -0.223 & 0.706 & 0.174 & -0.082 & -0.638 \\ -0.083 & -0.081 & -0.007 & -0.075 & 0.972 & -0.070 & 0.178 \\ 0.250 & 0.240 & 0.143 & 0.182 & 0.100 & 0.896 & 0.113 \\ 0.009 & -0.001 & -0.210 & 0.607 & -0.102 & -0.173 & 0.740 \end{bmatrix}$$

TABLE 5.19 -- PR EOS C_{7+} Characterization for NS-1 Gas Condensate.

Pseudo Component	z[1] (mole %)	M (lb/mol)	T_c (°R)	p_c (psia)	ω	γ (60/60)	T_b (°R)	Shift Parameter s	BIPs[2] C_1-C_{7+}
C_{7+}(1)	2.20112	98.5	998.2	459.7	0.2110	0.7269	653.4	0.0195	0.03822
C_{7+}(2)	2.33761	135.8	1127.1	373.3	0.2800	0.7729	767.0	0.0589	0.05290
C_{7+}(3)	1.83153	206.6	1311.3	260.6	0.4099	0.8193	949.6	0.1438	0.07589
C_{7+}(4)	1.11066	319.8	1445.0	214.8	0.5023	0.8619	1082.2	0.1248	0.09475
C_{7+}(5)	0.49273	500.0	1536.1	162.6	1.2254	0.9035	1266.5	0.0053	0.11104
C_{7+}(total)	7.9737	192.2				0.8160			

Note:
1. The molar distribution is defined by fitting measured TBP data of a fluid sampled from a well in the same field as NS-1, yielding α=0.65, η=90.
2. C_1-C_{7+} BIPs are calculated from Eq. 3.61 with A=0.201 and B=6.0. BIPs between pairs of non-HC and HC are taken from Table 3.13.

Maximum and minimum eigenvalues are associated with parameters 7 and 1: λ_{max}=271300 and λ_{min}=0.14. This yields a condition number ,κ(H), of 1.93(10^6). One possibility to reduce κ(H) is to remove parameter 1, T_b of C_{7+}(3), but that only reduces κ(H) to about 2(10^5). Another possibility is to redefine parameter 6 which adjusts C_{7+} T_cs, but this does not give such a good match to the measured data.

Fig. 5.15 shows that the regressed S_L curve (continuous line) results in an almost perfect match to the measured data, except at very low pressures. However, the important part of the S_L curve to match is for pressures above 2000 psia [138 bar], since the reservoir pressure will probably not drop below this level. From Fig. 5.15 it is observed that vapor Z-factors have not been changed significantly during the regression; predicted and regressed Z-factors are almost equal except at the dew point.

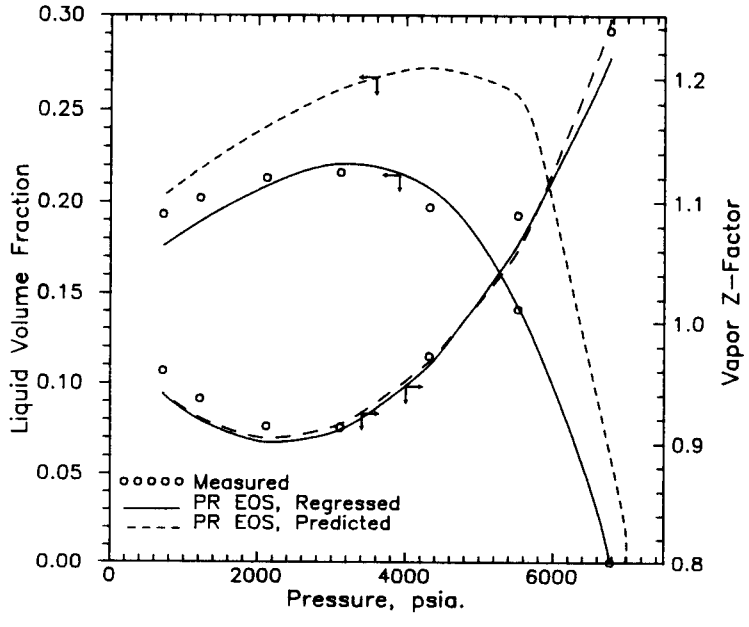

Fig. 5.15 PR EOS calculated liquid volume fractions and vapor Z-factors from CVD experiment at 280°F [137.8°C] for the NS-1 Gas Condensate.

The NS-1 saturation pressure was predicted 6 percent high with the SRK EOS. This partly explains the poor match of S_L shown in Fig. 5.16. To improve this match, a regression run adjusting the SRK EOS characterization was performed. Table 5.20 describes the nine parameters that were adjusted simultaneously to obtain an acceptable match to the measured data. The eigenstructure of the Hessian matrix at the solution is illustrated with eigenvalues and eigenvectors in Table 5.20 and 5.21, respectively. SRK EOS C_{7+} characterization for NS-1 is shown in Table 5.22.

TABLE 5.20 -- SRK EOS Final Regression Parameters and Eigenvalues of Hessian Matrix at Solution for the NS-1 Gas Condensate.

i	Regression Parameters	Final Value	Eigen-Value
1	Boiling point of $C_{7+}(3)$	1.020	0.038
2	Boiling point of $C_{7+}(4)$	0.950	3.654
3	Boiling point of $C_{7+}(5)$	0.920	0.301
4	Crit. temperature of $C_{7+}(4)$	0.978	1.127
5	Crit. temperature of $C_{7+}(5)$	0.940	91.108
6	C_{7+} molecular weight	1.056	16.884
7	C_{7+} boiling points	0.916	579.490
8	C_{7+} crit. temperatures	1.021	1950600.0
9	C_{7+} shift parameters	0.500	0.007

TABLE 5.21 -- Eigenvectors of Hessian Matrix at Solution for the NS-1 Gas Condensate.

$$S=\begin{bmatrix} 0.547 & -0.573 & 0.348 & -0.460 & -0.038 & 0.002 & -0.071 & 0.183 & 0.005 \\ -0.096 & 0.534 & 0.771 & -0.114 & 0.117 & 0.046 & -0.257 & 0.126 & 0.025 \\ -0.035 & -0.416 & 0.363 & 0.556 & 0.491 & -0.005 & 0.037 & -0.374 & 0.040 \\ 0.789 & 0.354 & -0.150 & 0.365 & -0.044 & 0.059 & -0.258 & -0.156 & -0.005 \\ 0.007 & 0.127 & -0.261 & -0.545 & 0.586 & 0.132 & -0.216 & -0.461 & -0.009 \\ -0.074 & -0.098 & -0.024 & 0.086 & -0.052 & 0.976 & -0.072 & 0.130 & -0.010 \\ 0.249 & 0.250 & 0.069 & -0.076 & 0.285 & 0.117 & 0.871 & 0.111 & 0.007 \\ 0.009 & -0.027 & -0.234 & 0.149 & 0.561 & -0.106 & -0.227 & 0.738 & -(10^{-4}) \\ 0.003 & 0.007 & -0.039 & -0.019 & -0.020 & 0.009 & -0.004 & 0.007 & 0.999 \end{bmatrix}$$

TABLE 5.22 -- SRK EOS C_{7+} Characterization of the NS-1 Gas Condensate.

Pseudo Component	z[1] (mole %)	M (lb/mol)	T_c (°R)	p_c (psia)	ω	γ (60/60)	T_b (°R)	Shift Parameter s	BIPs[2] C_1-C_{7+}
$C_{7+}(1)$	2.08309	98.5	963.3	510.0	0.1777	0.7247	618.7	-0.0205	0.03933
$C_{7+}(2)$	2.24269	135.8	1088.2	417.9	0.2421	0.7705	725.8	-0.0088	0.05466
$C_{7+}(3)$	1.80333	206.6	1275.4	288.7	0.3702	0.8166	907.6	0.0566	0.08188
$C_{7+}(4)$	1.13984	319.8	1367.4	244.8	0.5879	0.8590	1024.6	-0.0374	0.09470
$C_{7+}(5)$	0.54018	500.0	1451.8	197.7	1.1824	0.9004	1174.2	-0.1293	0.11164
C_{7+}(total)	7.80913	196.62				0.8601			

Note:
1. The molar distribution is defined by fitting measured TBP data of a fluid sampled from a well in the same field as NS-1, yielding α=0.65, η=90.
2. C_1-C_{7+} BIPs are calculated from Eq. 3.61 with A=0.215 and B=6.0. BIPs between pairs of non-HC and HC are taken from Table 3.13.

The final match to measured S_L and Z_V data are shown in Fig. 5.16 (continuous lines). The quality of this S_L match is comparable with the match obtained with the PR EOS, while the SRK Z_V match is somewhat poorer than the PR EOS match.

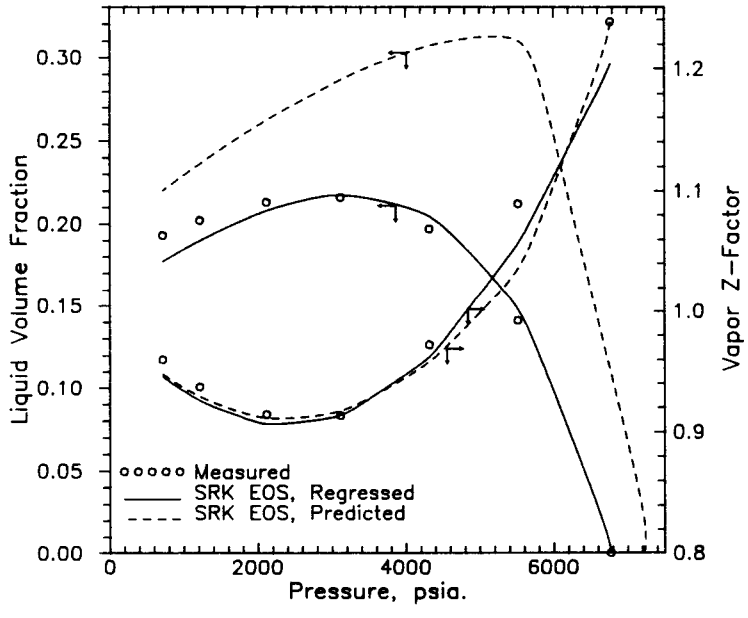

Fig. 5.16 SRK EOS calculated liquid volume fractions and vapor Z-factors from CVD experiment at 280°F [137.8°C] for the NS-1 Gas Condensate.

Table 5.23 compares CVD liquid densities reported by Whitson and Torp (1983) with calculated densities using PR and SRK and the respective fluid characterizations.

TABLE 5.23 -- Calculated Liquid Densities for the NS-1 Gas Condensate.

	Calculated Liquid Densities (lb/ft^3)					
	[1]		PR EOS		SRK EOS	
Pressure (psia)	Material Balance	Alani-Kennedy	VT[2]	no VT	VT	no VT
5514.7	41.827	37.96	36.874	36.440	36.835	35.027
4314.7	42.451	40.52	38.117	37.126	37.881	35.414
3114.7	42.950	41.83	40.486	38.954	40.270	37.186
2114.7	43.700	42.58	43.008	40.963	42.868	39.252
1214.7	44.386	43.70	45.723	43.029	45.637	41.484
714.7	45.079	44.39	47.509	44.295	47.409	42.920

Note:
1. Material Balance and Alani-Kennedy densities, reported by Whitson and Torp (1983), are calculated based on measured CVD data.
2. VT: volume translation.

It is observed from Table 5.20 that $\lambda_{max}=\lambda_8=1.95(10^6)$and that $\lambda_{min}=\lambda_9=0.007$, which results in $\kappa(H)=2.78(10^8)$. Since $\kappa(H)$ is high, an additional regression run was performed without parameter 9 which adjusts C_{7+} shift parameters. Table 5.24 compares some key parameters concerning the quality of the match for these two runs, with and without parameter 9. The parameter space is more complex and thus more difficult to search when parameter 9 is included. However, a better match is obtained with parameter 9 included.

TABLE 5.24 -- Comparison of Results With and Without the C_{7+} Shift Parameters Selected as Regression Parameter.

	Parameter Adjusting C_{7+} s	
Parameter	Included	Not Included
No. of Iterations	9	5
SSQ (weighted)	0.236	0.328
AAD for S_L	0.824	1.330
AAD for ρ_L	4.800	5.990
AAD for Z_V	1.470	2.230

5.5 Jacoby Synthetic Mixtures

Phase and volumetric behavior of seven synthetic systems are reported by Jacoby et al. (1959). These mixtures, denoted S-1 through S-7, were recombined in various portions of companion separator oil and gas samples produced from a gas-condensate reservoir. The result is a family of seven related mixtures composed of the same components. Therefore, the seven fluids must be characterized with an identical set of C_{7+} pseudocomponents properties. This can be achieved with the split method which combines Gaussian quadrature and the gamma distribution model.

A fractional distillation analysis is reported for the separator oil C_{6+} fraction. Measured inspection properties and the recombined compositions are used to calculate overall C_{7+} mole fraction, molecular weight and specific gravity. These data are reported in Table 5.25. The reported $C_{6+}(1)$ cut is treated as if it consists of various C_6 components (Standing, 1979) as noted in Table 5.25. The gamma distribution parameters α and η are determined by matching the reported C_{7+} molar distributions for S-1 through S-7, yielding α=1.518 and η=90. The proposed characterization procedure is used to describe the C_{7+} fraction, except that molecular weight of the heaviest pseudocomponent is changed from 500 to 350. Also, to obtain pseudocomponent specific gravities that are the same for all mixtures, an average "characterization factor" F_c calculated from the individual sample F_c values, is used in Eq. 3.49. However, this procedure hardly alters the individual C_{7+} γs, since measured γ_{7+} are practically identical for all samples.

TABLE 5.25 -- Fluid Descriptions of the Jacoby et al. Synthetic Mixtures.

	Composition of Synthetic Mixtures (Mole %)						
Comp.	S-1	S-2	S-3	S-4	S-5	S-6	S-7
N_2	1.28040	1.52581	1.57722	1.65511	1.76662	1.90572	1.94422
CO_2	1.39160	1.55891	1.59402	1.64711	1.72312	1.81792	1.84422
C_1	56.34800	65.26000	67.12700	69.95800	74.01000	79.06100	80.46100
C_2	7.08721	7.01036	6.99427	6.96986	6.93497	6.89146	6.87936
C_3	5.09171	4.27384	4.10244	3.84273	3.47103	3.00763	2.87913
iC_4	1.64370	1.22611	1.13861	1.00601	0.81621	0.57960	0.51401
nC_4	3.75680	2.85343	2.66413	2.37732	1.96672	1.45481	1.31291
iC_5	2.08000	1.49261	1.36951	1.18301	0.91611	0.58321	0.49100
nC_5	2.48870	1.77122	1.62082	1.39301	1.06691	0.66031	0.54771
C_6s [1]	3.65100	2.55312	2.32232	1.97252	1.47181	0.84761	0.67461
C_{7+}	15.1803	10.4746	9.4890	7.9949	5.8563	3.1899	2.4511
Total	100.00	100.00	100.00	100.00	100.00	100.00	100.00
C_{7+} Properties:							
M_{7+}	142.72	142.67	142.66	142.62	142.55	142.31	142.15
γ_{7+}	0.7717	0.7716	0.7715	0.7714	0.7713	0.7712	0.7711
K_{w7+}	12.05	12.05	12.05	12.05	12.05	12.05	12.05

Note:
1. C_6s is composed of 50 % n-hexane, 25 % 2-metylpentane and 25 % 3-metylpentane (Standing, 1979).
2. C_{7+} molar distribution parameters are determined by regression to match measured TBP data yielding α=1.518 and η=90.

Gas-oil ratios for the Jacoby Mixtures varies from 2000 scf/bbl [356 m^3/m^3] for S-1 to 20000 scf/bbl [3560 m^3/m^3] for S-7. Saturation point measurements show that S-1 and S-2 exhibit bubble points at 163°F [72.8°C], and that S-4 through S-7 exhibit dew points at this temperature. System S-3 shows bubble points at 96.5° and 131.8°F [35.8°, 55.4°C], and dew points at 163.5° and 207.3°F [73.1°, 97.4°C]. Critical temperature for the S-3 mixture is probably in the range from 140°F to 150°F. CCE experiments were performed in the laboratory for all systems at 163°F [73.1°C], and for S-3 at 96.5°, 131.8°, and 207.3°F [35.8°, 55.4°, 97.4°C]. A comparison of PR predicted saturation pressures with measured data is shown in Table 5.26. The mixture critical temperature is estimated too high, as bubble points are predicted instead of dew points for S-3 at 163.5° and 207.3°F.

TABLE 5.26 -- Comparison of Measured and Calculated Saturation Pressures for the Jacoby Synthetic Mixtures.

		Saturation Pressure (psia)				
			Predicted		Regressed	
Sample	Temp. °F	Experimental	Calc.	Dev. %	Calc.	Dev. %
S-1	163.5	3194	3324.5	4.08	3213.7	0.61
S-2	164.0	3809	3399.4	4.87	3811.3	0.06
S-3	96.5	3750	3883.9	3.57	3745.3	-0.12
S-3	131.8	3840	4039.3	5.19	3896.5	1.47
S-3	163.5	3941	4122.4*	4.60	3973.5	0.82
S-3	207.3	4000	4150.0*	3.76	3990.0	-0.24
S-4	163.5	4183	4294.0	2.66	4142.7	-0.96
S-5	163.5	4520	4461.8	-1.29	4530.5	0.23
S-6	163.5	4964	4380.9	-11.70	4965.5	0.03
			AAD:	4.63		0.51

Note:
*) A bubble point was obtained instead of a dew point.

Defining the data set to be minimized is an important aspect of regression performance. With only saturation pressure and liquid volume fraction data available, regression will only slightly affect the mixture critical temperature of S-3. It has proven more efficient to include the feed composition in the data set. The feed composition $\underline{z}$ is identical to the liquid phase composition $\underline{x}$ of an oil and the vapor phase composition $\underline{y}$ of a gas condensate. Thus, for mixture S-3 the following data are included in the regression data set: $\underline{x}=\underline{z}$ at 96.5° and 131.8°F, and $\underline{y}=\underline{z}$ at 163.5° and 207.3°F. In addition the data set consisted of liquid volume fractions and saturation pressures for all systems, except S-7.

Some additional regression parameters, A and B, were defined to adjust e.g. C_{7+} properties. These are defined according to

$$\theta_i = \theta_{io}[A + 0.1(B-1)\log_{10}(M_i-\eta)] \qquad (5.1)$$

where θ_i and θ_{io} represent the regressed and predicted property of $C_{7+}(i)$, respectively, e.g. T_bs, T_cs or p_cs. A seven parameter regression run was performed, and the parameters are listed in Table 5.27, together with their final values. The eigenstructure of the Hessian matrix at solution is characterized with the eigenvalues reported in Table 5.27 and the eigenvectors reported in Table 5.28.

The rotational discrimination method, as used here, disregard all parameters i for which $\lambda_i/\lambda_{max} \leq (10^{-8})$. With $\lambda_{max}=\lambda_2=2.28(10^9)$ parameter number 1 and 7 have not been adjusted during the last regression iteration.

Some parameters were adjusted manually, these are defined in Table 5.29. The C_{7+} properties based on the final regressed and modified parameters are listed in Table 5.30, and the final C_{7+} compositions are listed in Table 5.31.

TABLE 5.27 -- Final Regression Parameters and Eigenvalues of Hessian Matrix at Solution for the Jacoby Synthetic Mixtures.

i	Regression Parameters	Final Value	Eigen-Value
1	C_1-C_{7+} BIPs	1.65334	0.89
2	Crit. temperature of $C_{7+}(5)$	0.96450	$2.28(10^{+9})$
3	A of Eq. 5.1 for C_{7+} T_b	0.93000	$3.76(10^{+5})$
4	B of Eq. 5.1 for C_{7+} T_b	0.95532	569.56
5	A of Eq. 5.1 for C_{7+} T_c	1.01162	79010.00
6	B of Eq. 5.1 for C_{7+} T_c	0.86023	13693.00
7	C_{7+} shift parameters	1.00430	0.18

TABLE 5.28 -- Eigenvectors of Hessian Matrix for Jacoby Synthetic Mixtures.

$$S = \begin{bmatrix} 0.982 & -0.017 & 5(10^{-5}) & 0.055 & 0.037 & -0.004 & 0.178 \\ -4(10^{-6}) & 0.817 & -8(10^{-5}) & -2(10^{-5}) & 0.408 & 0.408 & 1(10^{-7}) \\ 0.016 & 0.162 & 0.848 & 0.096 & -0.472 & 0.149 & 9(10^{-5}) \\ -0.062 & -0.039 & -0.016 & 0.986 & 0.138 & -0.059 & 0.002 \\ -0.026 & -0.200 & 0.526 & -0.126 & 0.742 & -0.342 & -3(10^{-5}) \\ -0.013 & -0.515 & 0.063 & 0.002 & 0.199 & 0.831 & -0.001 \\ -0.178 & 0.003 & 1(10^{-5}) & -0.012 & -0.007 & 0.001 & 0.984 \end{bmatrix}$$

TABLE 5.29 -- Modified PR EOS Parameters for the Jacoby Synthetic Mixtures.

i	Modified Parameter	Value
1	Boiling point of C_{7+}(5)	1.064
2	A of Eq. 5.1 for C_{7+} p_cs	1.050
3	B of Eq. 5.1 for C_{7+} p_cs	0.875
4	C_{7+} α for S-3	0.950
5	C_{7+} α for S-5	1.010
6	C_{7+} α for S-6	1.050

TABLE 5.30 -- PR EOS C_{7+} Characterization of the Jacoby Synthetic Mixtures.

Pseudo Component	M (lb/mol)	T_c (°R)	p_c (psia)	ω	γ (60/60)	T_b (°R)	Shift Parameter s	BIPs[1] C_1-C_{7+}
C_{7+}(1)	95.4	938.6	497.7	0.2537	0.7135	617.1	-0.1789	0.026653
C_{7+}(2)	119.1	1006.1	433.1	0.3402	0.7424	685.0	-0.1781	0.033949
C_{7+}(3)	164.0	1125.0	348.2	0.4602	0.7863	801.1	-0.1314	0.046276
C_{7+}(4)	235.7	1272.7	273.1	0.6187	0.8393	949.9	-0.0810	0.060644
C_{7+}(5)	350.0	1438.6	187.3	1.4403	0.9010	1190.8	0.0660	0.081902

Note:
1. C_1-C_{7+} BIPs are calculated from Eq. 3.61 with A=0.16534 and B=6.0. BIPs between pairs of non-HC and HC are taken from Table 3.13.

TABLE 5.31 -- C_{7+} Composition of the Jacoby Synthetic Mixtures.

	C_{7+} Composition (Mole %)						
Component	S-1	S-2	S-3	S-4	S-5	S-6	S-7
C_{7+}(1)	2.22647	1.54438	1.50906	1.18379	0.86007	0.45150	0.37903
C_{7+}(2)	6.51009	4.49074	3.99399	3.42740	2.51872	1.38996	1.04896
C_{7+}(3)	4.92918	3.39510	3.00203	2.58750	1.89959	1.04507	0.78124
C_{7+}(4)	1.39537	0.96192	0.89698	0.73322	0.53305	0.28167	0.22236
C_{7+}(5)	0.11919	0.08244	0.08694	0.06295	0.04483	0.02174	0.01954
C_{7+}	15.1803	10.4746	9.4890	7.9949	5.8563	3.1899	2.4511

Note:
1. To match experimental phase and volumetric data, the α-parameters for S-3, S-5 and S-6 was adjusted by a factor of 0.95, 1.01 and 1.05, respectively.

The resulting liquid volume fractions are compared with measured data in Fig. 5.17 for mixtures S-1 through S-6 at 163.5°F [73.1°C]. The obtained match is very good for the systems S-1 through S-4, with a slight underestimation of S_L for systems S-5 and S-6. Similar results are shown in Fig. 5.18 for system S-3 at various temperatures. From this plot it is observed that the critical temperature still may be somewhat high, with S_L slightly overestimated at 131°F (and at 96.5°F), but the match is in general reasonable considering the wide range in composition, pressure and temperature covered.

Slot-Petersen (1987) also obtained a good match to the Jacoby systems with the PR EOS. However, he used one specific set of BIPs for each system at each temperature. Slot-Petersen claims that non-zero interaction parameters for C_2-, C_3-, and C_4-C_{N+} binaries are necessary to obtain a good fluid characterization of near-critical mixtures. From this work it is found that such binaries have only minor influence on the phase behavior compared to other characterization parameters, such as C_{7+} critical temperatures. For many fluids, predicted phase behavior may not be greatly influenced by interaction parameters for C_1-C_{7+} binaries. The eigenvalues reported in Table 5.27 emphasize this.

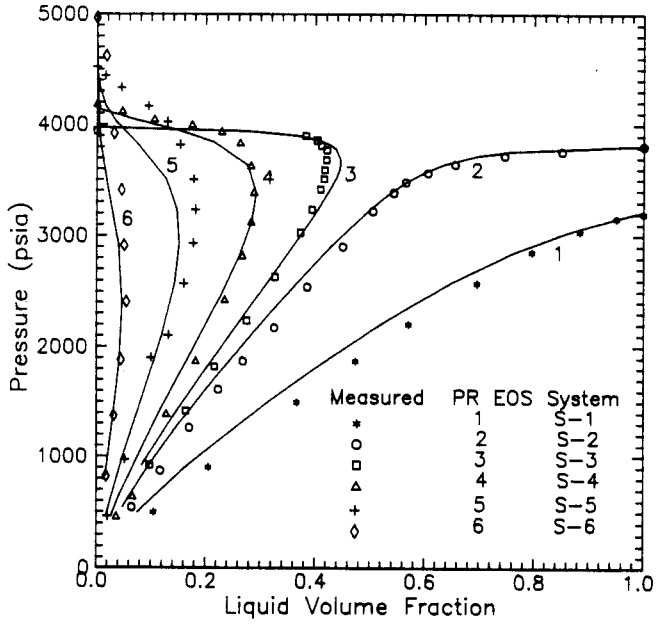

Fig. 5.17 CCE liquid volume fractions for the Jacoby synthetic mixtures S-1 through S-6 at 163.5°F [73.1°C].

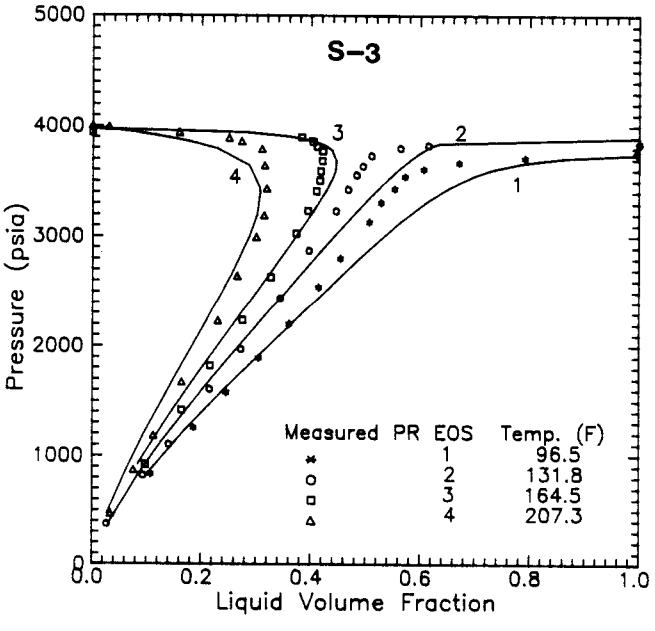

Fig. 5.18 CCE liquid volume fractions for the Jacoby synthetic mixture S-3 at various temperatures.

5.6 GPA Paraffinic Gas Condensate

The Gas Processors Association (GPA) has recently performed several depletion studies on a natural gas condensate system with GOR in the range 8400-9000 scf/STB [1496-1600 Sm^3/Sm^3] (Ng et al., 1985, 1986). Liquid volume fractions, S_L, were measured at selected pressures below dew point at temperatures 100°, 150°, 200°, and 250°F [37.8°, 65.6°, 93.3°, and 121.1°C]. At the same temperatures Z-factor measurements were also performed in the dense phase region. Phase compositions and properties were measured along the 200°F [93.3°F] isotherm. These data represent an unusually large database, and provide a good basis for obtaining an accurate EOS fluid characterization.

Ng et al. (1986) report the gas condensate composition based on a chromatographic analysis. Fluid composition, given in terms of mole fractions, is extended up to C_{27}. Table 5.32 reports the gas condensate composition with all components heavier than nC_6 lumped into a C_{7+} fraction. Since C_{7+} properties are not reported for the sample, tabulated SCN properties (Katz and Firoozabadi, 1978) were used to estimate overall C_{7+} properties: M_{7+}=113.58 and γ_{7+}=0.7598, and to determine molar distribution parameters: α=0.6784 and η=90.0.

Thirteen parameters of the PR characterization were adjusted to match the reported PVT data for this gas condensate. The parameters and their final values are listed in Table 5.33. The matching has been performed in several runs. Finally, when an approximate match was obtained, a regression run was performed with all 13 parameters to fine tune the EOS. Eigenvalues are reported in Table 5.33 and the resulting PR EOS C_{7+} characterization is given in Table 5.34. Highest uncertainties are associated with the parameters adjusting on C_1-C_{7+} BIPs, T_b of C_{7+}(3), α, and C_{7+} p_cs since the eigenvalues are quite low for these parameters.

TABLE 5.32 -- Composition and Estimated C_{7+} Properties of Recombined GPA Gas Condensate (Ng et al. 1985, 1986).

Component	Composition (Mole %)
C_1	73.8427
C_2	7.2998
C_3	4.6031
iC_4	0.9098
nC_4	1.8082
iC_5	0.8626
nC_5	0.9655
nC_6	1.4289
C_{7+}	8.2797
Total	100.000
M_{7+}	113.58
γ_{7+}	0.7598
K_{w7+}	11.79
α	0.6784
η	90.0

TABLE 5.33 -- Adjusted Parameters of GPA Gas Condensate and Eigenvalues of Hessian Matrix at Solution.

No.	Parameter Description	Final Value	Eigenvalue
1	C_1-C_{7+} BIPs	0.9500	0.008
2	Boiling point of C_{7+}(3)	0.9858	0.039
3	Boiling point of C_{7+}(4)	1.0661	2.013
4	Boiling point of C_{7+}(5)	1.1011	54.101
5	Crit. temperature of C_{7+}(3)	1.0414	0.549
6	Crit. temperature of C_{7+}(4)	0.9805	15.096
7	Crit. temperature of C_{7+}(5)	0.9400	$5.429(10^6)$
8	Critical pressure C_{7+}(5)	0.9649	0.090
9	C_{7+} α-parameter	0.5000	0.074
10	C_{7+} Molecular weight	1.0100	37928.0
11	C_{7+} Boiling points	0.9440	410.60
12	C_{7+} Crit. temperatures	1.0000	10174.0
13	C_{7+} Crit. pressures	0.9571	0.373

TABLE 5.34 -- PR EOS C_{7+} Characterization for the GPA Gas Condensate.

Pseudo Component	z[1] (mole %)	M (lb/mol)	T_c (°R)	p_c (psia)	ω	γ (60/60)	T_b (°R)	Shift Parameter s	BIPs[2] C_1-C_{7+}
$C_{7+}(1)$	4.24956	94.4	949.7	486.1	0.2404	0.7287	623.4	-0.0950	0.01058
$C_{7+}(2)$	2.37901	113.5	1021.2	439.0	0.2786	0.7593	683.9	-0.0854	0.01295
$C_{7+}(3)$	1.11385	149.7	1169.3	372.2	0.1826	0.7955	775.5	-0.0931	0.01667
$C_{7+}(4)$	0.38206	207.7	1292.0	239.2	0.6631	0.8316	981.0	0.2296	0.02629
$C_{7+}(5)$	0.07995	300.0	1410.9	156.7	1.5911	0.8683	1190.7	0.3311	0.03477
C_{7+}(total)	8.20443	114.72				0.7598			

Note:
1. Molar distribution α parameter is adjusted to 0.3392 with η=90. M_N=300.
2. C_1-C_{7+} BIPs are calculated from Eq. 3.61 with A=0.095 and B=6.0. BIPS between pairs of non-HC and HC are taken from Table 3.13.

Calculated condensation curves are compared with measured data at temperatures 100° and 200°F [37.8° and 93.3°C] in Fig. 5.19 and at temperatures 150° and 250°F [65.6° and 121.1°C] in Fig. 5.20. Notice in Fig. 5.19 that calculated liquid volume fraction, S_L, at the 100°F isotherm increases from 0.0 to 0.35 corresponding to a pressure drop of 300 psia [20 bar]. This may be surprising since the measured critical temperature is -6.5°F [-21.4°C]. Except for the maximum S_L region, the match to measured data at 100°F is good. However, few measurements are reported in the region of maximum liquid dropout as shown in Fig. 5.21 which presents the original p-T diagram with isovolume lines (Fig. 4 of Ng et al. 1985). A 30% isovolume line may exist as indicated in Fig. 5.21 (dashed line). The calculated liquid dropout curve matches measured data almost exactly at the 150°F isotherm, and is slightly underestimated at the 200° and 250°F isotherms.

Firoozabadi (1988) also reports condensation curves for the GPA gas condensate. Because of a poor S_L match to measured data in the retrograde region, he concludes that "cubic equations, such as the PR and SW equations, cannot handle these sharp changes". However, the comparison shown in Fig. 5.19, verify that cubic EOSs can handle sharp changes in liquid dropout. The important element though may not be the EOS itself, but the C_{7+} characterization.

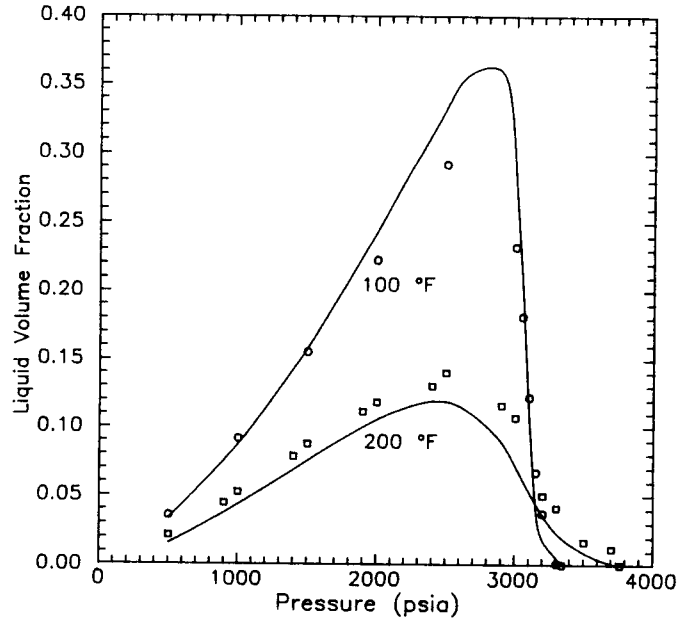

Fig. 5.19 Measured and PR EOS calculated liquid volume fractions from CCE experiments at the 100° and 200°F [37.8°, 93.3°C] isotherms for the GPA gas condensate.

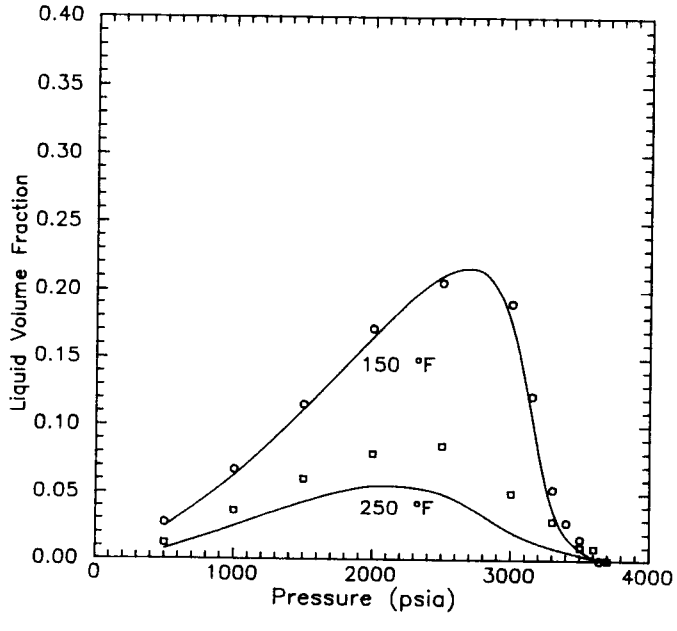

Fig. 5.20 Measured and PR EOS calculated liquid volume fractions from CCE experiments at the 150° and 250°F [65.6°, 121.1°C] isotherms for the GPA gas condensate.

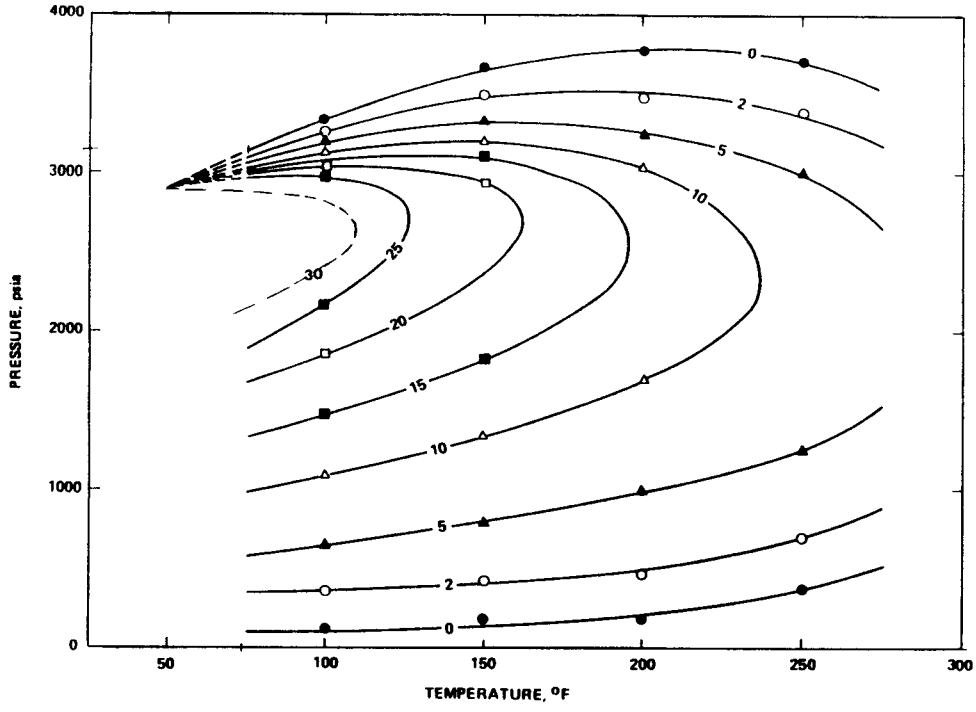

Fig. 5.21 Measured pressure-temperature diagram with isovolume lines for the GPA gas condensate (from Ng et al. 1985).

Dense phase Z-factors are compared with measured data in Table 5.35. For comparison, corresponding SW EOS calculated Z-factors recently reported by Firoozabadi (1988), are also given. It is observed that Z-factors resulting from this work compares favorable with the SW EOS Z-factors, except at 250°F [121.1°C]. Based on all data given in Table 5.35, AAD is 1.06 percent for PR EOS and 1.21 percent for SW EOS.

Fig. 5.22 compares measured and calculated equilibrium K-values for the GPA gas condensate at temperature 200°F [93.3°C]. The match is relatively good, except for C_{7+} K-values above 2400 psia [165.5 bar] which are somewhat high.

TABLE 5.35 -- Comparison of Measured and Calculated Z-Factors for the GPA Gas Condensate.

Pressure (psia)	100°F			150°F		
	Measured	PR EOS	SW EOS[1)]	Measured	PR EOS	SW EOS
6000	1.133	1.114	1.104	1.101	1.098	1.089
5500	1.050	1.043	1.033	1.037	1.033	1.025
5000	0.978	0.971	0.962	0.970	0.969	0.961
4500	0.906	0.898	0.890	0.903	0.904	0.897
4000	0.828	0.825	0.817	0.834	0.840	0.833
3500	0.756	0.751	0.754			
	AAD :	0.85	1.53		0.32	1.09
	BIAS:	-0.85	-1.53		-0.02	-1.09

Pressure (psia)	200°F			250°F		
	Measured	PR EOS	SW EOS	Measured	PR EOS	SW EOS
6000	1.107	1.088	1.085	1.082	1.098	1.087
5500	1.042	1.031	1.027	1.035	1.046	1.036
5000	0.979	0.974	0.970	0.972	0.995	0.985
4500	0.913	0.917	0.914	0.918	0.945	0.936
4000	0.859	0.863	0.858	0.868	0.898	0.889
	AAD :	0.84	0.91		2.27	1.26
	BIAS:	-0.48	-0.87		2.27	1.26

Note:
1. Schmidt-Wenzel EOS calculated Z-factors are reported by Firoozabadi (1988).

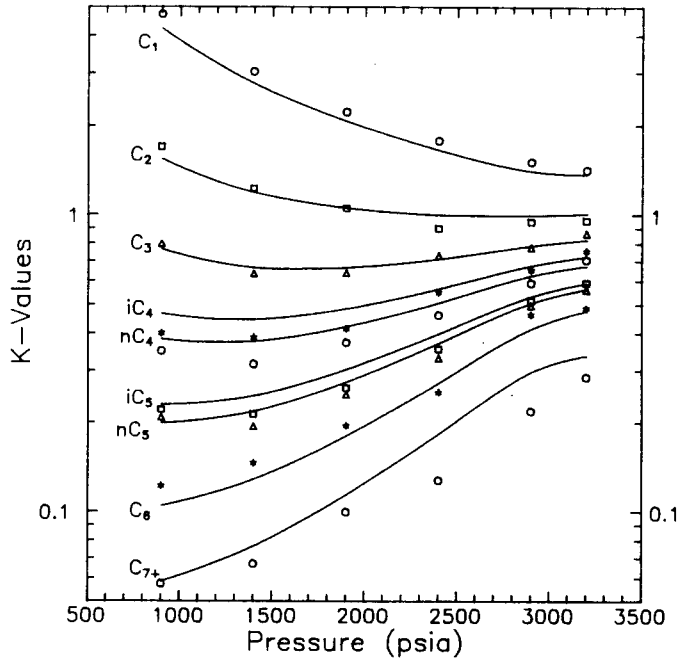

Fig. 5.22 Measured and PR EOS calculated equilibrium K-values from a CCE experiment at 250°F [121.1°C] for the GPA gas condensate.

CONCLUSIONS

The main objective of this study has been to develop an EOS characterization method for improving prediction of phase and volumetric behavior of reservoir fluids. To a certain degree this objective has been met. But, predicted phase behavior does not always result in the desired accuracy. Volumetric prediction is slightly better. However, it is believed that a limited compositional analysis where the reported composition is extended up to C_{7+} only, does not give enough information to predict the phase behavior accurately. This is particularly true for gas condensates. When composition are further extended, phase behavior prediction is much better. Also, a fully predictive characterization method relies heavily on the quality of reported fluid composition and PVT data.

Based on results and discussions given in this thesis, the following conclusions can be made:

Volume Translation

An approach for improving liquid density prediction of two-parameter EOSs, called volume translation, has been extended. It is proposed that the volume correction shift parameter for pure components be determined as function of reduced temperature. This shift parameter may be obtained from graphs and/or correlations presented for the PR and SRK EOSs. Also, PR and SRK EOS shift parameters for pure hydrocarbons (C_1-C_{10}) and non-hydrocarbons (N_2, CO_2, H_2S) at reduced temperature of 0.7 are presented.

VLE Calculations

Effective routines for performing stability analysis, two-phase flash and saturation pressure calculations have been implemented. An iteration scheme consisting of successive substitution promoted with GDEM generally results in satisfactory convergence rates when solving the set of non-linear equations introduced in VLE calculations. For

flash calculations the optimum iteration cycle consists of three SS iterations followed by a GDEM promotion. Also, a flash algorithm that conveniently permits vapor fraction to go outside the interval [0,1], avoids problems normally encountered in regions close to a phase boundary.

C_{7+} Characterization

An EOS characterization procedure has been proposed. The procedure, described in Sec. 5.1, relies partly on earlier published methods and partly on methods and procedures developed during this study, including:

(1) a C_{7+} split method which combines the gamma distribution function with Gaussian quadrature to yield mole fractions and molecular weights for an arbitrarily number of pseudocomponents.

(2) a developed C_{7+} specific gravity correlation given by Eq. 3.57.

(3) a developed C_{7+} boiling point correlation given by Eq. 3.59.

(4) the Riazi-Daubert (1987) critical properties correlations given by Eq. 3.60.

(5) an EOS-based procedure for adjusting the C_{7+} acentric factors resulting in boiling points correctly predicted by the EOS.

(6) an EOS-based procedure for adjusting the C_{7+} volume translation shift parameters resulting in correctly EOS predicted liquid densities at standard condition.

Regression

An efficient regression method called rotational discrimination has been implemented. The method deals effectively with null-effect and linearly dependent parameters. It also yields qualitative information concerning parameter identifiability and confidence. The method has been shown superior to other methods, such as the Gauss-Newton.

Volumetric Prediction of Rio Bravo Fluids

With the proposed volume translation method, accuracy of PR and SRK predicted liquid densities are comparable with the Standing-Katz and Alani-Kennedy correlations. The accuracy of SRK Z-factor prediction is comparable with the Standing-Katz correlation. For the PR EOS, deviations are slightly higher.

PVT Prediction of Coats and Smart Fluids

It has been shown that the PR EOS predictive capabilities, with the proposed C_{7+} characterization methods, is slightly better than with the SRK EOS. With the proposed characterization procedure PR and SRK results compare favorably with PR and ZJRK predictions reported by Coats and Smart. Prediction of VLE for reservoir fluids, and especially gas condensates, are improved if fluid composition is extended by experimental C_{7+} distillation.

PVT Matching of Coats and Smart Fluids

Volatile oils are predicted with acceptable accuracy, and only minor adjustments in EOS characterization are needed to obtain a good match to reported PVT data. For one CO_2-rich reservoir fluid, PVT data were matched without significant adjustments in the predicted characterization, and without using temperature dependent EOS constants Ω_a and Ω_b.

NS-1 Gas Condensate

PR EOS predictions of PVT data for the NS-1 gas condensate are better than given by SRK. After adjusting the EOS characterization the match to measured PVT data is comparable for the two EOSs.

Jacoby Synthetic Mixtures

It has been shown that related fluid systems such as the Jacoby family of synthetic mixtures covering a wide range in pressure, temperature and composition can accurately be characterized with a single set of C_{7+} pseudocomponent properties.

GPA Paraffinic Gas Condensate

With a proper adjustment of the C_{7+} characterization, it is shown that a modified two-parameter EOS can model sharp changes in liquid dropout and composition. PR EOS volumetric performance with the proposed characterization method has been shown to compare favorably with the more complex three-parameter SW EOS.

Future Work

Improvements of the proposed EOS characterization method for predicting phase and volumetric behavior of reservoir fluids are possible:

- Liquid densities may be improved by introducing a temperature-dependent shift parameter for pseudocomponents, which also correctly predicts liquid density at standard conditions with the EOS.

- Generalized correlations for pseudocomponent acentric factors and shift parameters could be developed from the EOS-based procedures currently used. Such correlations would have to be expressed in terms of inspection and critical properties and would require less calculations.

- Generalized critical properties correlations seem to go through a maximum or minimum for heavy petroleum fractions. Correlations should be developed which result in monotonic behavior, i.e. increasing critical temperatures and decreasing critical pressures.

- The mixture critical temperature is typically overpredicted. A correction to pseudocomponent critical temperatures could be developed to remove this failure without deteriorating saturation pressure prediction of volatile oils and gas condensates.

NOMENCLATURE

Latin letters

A = parameter in modified BIP correlation, Eq. 3.61

AAD = absolute average deviation (%)

$$AAD = \frac{100}{N} \sum_{i=1}^{N} \left[\frac{|\theta_{ic} - \theta_{ie}|}{\theta_{ie}} \right]$$

AAD_T = overall absolute average deviation (%)

A,B,C,D = dimensionless parameters of Martin EOS, Eqs. 1.48

a,b,c,d,e,f = constants in inspection and critical properties correlations

a,b,c,d = EOS parameters, Eqs. 1.49

B = parameter in modified BIP correlation, Eq. 3.61

$BIAS$ = bias (%)

$$BIAS = \frac{100}{N} \sum_{i=1}^{N} \left[\frac{(\theta_{ic} - \theta_{ie})}{\theta_{ie}} \right]$$

b = parameter in discrete exponential distribution, Eq. 3.5

$\underline{b}$ = pseudo EOS constant b, $\underline{b}=b_{EOS}-c$

b_{kj} = GDEM variable, Eq. 2.53

C_f = characterization factor, Eq. 3.57

c = molecular type constant in exponential distribution, Eq. 3.4

c = volume translation correction parameter, Eq. 1.68-69

c_L = mixture liquid phase volume correction, Eq. 1.72

c_V = mixture vapor phase volume correction, Eq. 1.74

$\mathbf{D}$ = diagonal matrix containing eigenvalues of Hessian matrix, Eq. 4.13

d_{ii} = eigenvalues of Hessian matrix

d,e = constants in shift parameter correlation, Eq. 1.71

$E\gamma$ = specific gravity objective function, Eq. 3.45

e = norm of error vector for VLE calculations, Eq. 2.45

F = least-squares objective function, Eq. 4.1

F_c = characterization factor, Eq. 3.46

F_s = objective function in saturation pressure calculation, Eq. 2.42

$F(V)$ = Rachford-Rice flash function, Eq. 2.27

f = fugacity

$f(x)$ = continuous function in gamma distribution, Eq. 3.25

$f(x_i)$ = discrete function used in Gaussian quadrature, Eq. 3.30

G = Gibbs free energy, Eq. 2.1

GOR = solution gas-oil ratio (scf/STB)

g = reduced molar Gibbs free energy, g=G/RT, Eq. 2.34

$g(\underline{y})$ = stability analysis objective function, Eq. 2.11

H,h = stability analysis constant, Eqs. 2.10, 2.11, 2.13

$\mathbf{H}$ = Hessian matrix, Eqs. 4.7, 4.11

$\mathbf{I}$ = identity matrix

Latin letters (cont'd)

J_a = Jacoby aromaticity factor, Eq. 3.50
J_{am} = modified Jacoby aromaticity factor, Eq. 3.55
$J_{am}(M_{7+})$ = modified Jacoby aromaticity factor, Eq. 3.56
$\mathbf{J}$ = Jacobian matrix, Eq. 4.8
K_i = equilibrium K-value, Eq. 2.24
K_w = Watson characterization factor ($=T_b^{1/3}/\gamma$)
k_{ij} = a_m interaction parameter for binary i,j, Eq. 3.61-64
ℓ_{ij} = b_m interaction parameter for binary i,j, Eq. 1.17
M = number of data point in objective function
M = molecular weight
MAXD = maximum absolute deviation (%)

$$MAXD = \max_i \left[\frac{|\theta_{ic} - \theta_{ie}|}{\theta_{ie}} \right] 100$$

M_{bi} = upper bound on molecular weight for subfraction i
M_{bi-1} = lower bound on molecular weight for subfraction i
M_i = average molecular weight of subfraction i
M_{7+} = heptanes-plus molecular weight
m = slope of EOS α function, Eqs. 1.20, 1.24, 1.26-27, 1.31
N = number of regression parameters
N = number of pseudocomponents
n = VLE iteration counter
P = Parachor
P = rotational discrimination variable, Eq. 4.17
$P(M)$ = cumulative probability density function, Eqs. 3.12, 3.16
p = pressure (psia)
p_c = critical pressure (psia)
p_k = convergence pressure (psia)
p_r = reduced pressure, $p_r=p/p_c$
p_s = saturation or saturated vapor pressure (psia)
p_{sc} = atmospheric pressure (psia)
$p(M)$ = probability density function, Eq. 3.10
$p_o(M)$ = modified probability density function, Eq. 3.27
$\mathbf{Q}$ = matrix included in second derivative of F(x), Eq. 4.9
r = objective function residuals, Eq. 4.2
$\mathbf{S}$ = VLE calculation convergence matrix, Eq. 2.47
$\mathbf{S}$ = matrix containing eigenvectors V of Hessian matrix, Eq. 4.13
S_o = summation variable, Eqs. 3.42, 3.48
STD = standard deviation

$$STD = \left[\frac{1}{N} \sum_{i=1}^{N} (\theta_{ie} - \theta_{ic})^2 \right]^{0.5}$$

s = volume translation shift parameter, dimensionless, Eq. 1.70
s = rotational discrimination scaling factor, Eq. 4.22a
T_b = normal boiling point temperature (°R)
T_{br} = relative normal boiling point temperature, $T_{br}=T_b/T_c$
T_c = critical temperature (°R)
T_i = composite gamma function variable, Eq. 3.18

Latin letters (cont'd)

$T(\underline{y})$ = tangent plane at composition y, Eq. 2.5
T_r = reduced temperature, $T_r=T/T_c$
TPD = tangent plane distance, Eq. 2.6
V = vapor phase mole fraction
$\underline{V}_i$ = eigenvector of Hessian matrix
v_c = critical volume (ft^3/lb-mol)
v_i = molar volume
v_{LK} = Lee-Kesler saturated liquid molar volume, Eq. 1.79
v_{sL} = saturated liquid molar volume, Eq. 1.77
w_i = quadrature weighting factor, Eq. 3.24
w_i = normalized weight fraction
w_j = objective function weighting factor, Eq. 4.2
X = iteration variable for VLE calculations, Eq. 2.26
x = probability function variable, $x=(M-\eta)/\beta$
x_o = modified probability function variable, $x_o=(M-\eta)/\beta_o$
x_i = quadrature point, Eq. 3.24
x_i = liquid phase normalized mole fraction
$\underline{x}$ = liquid phase composition
$\underline{x}$ = least-squares independent variable
Y_{Lf} = mole number for liquid like feed
Y_{Vf} = mole number for vapor like feed
$\underline{Y}$ = rotational discrimination transformed solution vector, Eq. 4.16
y_i = vapor phase normalized mole fraction
$\underline{y}$ = vapor phase composition
Z = compressibility factor
Z_{LK} = Lee-Kesler compressibility factor,
Z_{RA} = Rackett compressibility factor, Eq. 1.79
z_i = normalized mole fraction of feed
$\underline{z}$ = feed composition

Subscripts

b = boundary
c = calculated
d = property from DLE experiment
EOS = property predicted by EOS model
e = experimental
f = property from flash or surface separation experiment
g = gas phase
i = component or pseudocomponent index
k = regression iteration counter
L = liquid
m = measured
m = mixture
max = maximum
min = minimum
N+ = plus fraction N
o = oil phase
o = modified
O = original
r = relative
r = reduced
sp = separator
V = vapor
7+ = heptanes-plus

Superscripts

e = measured property
m = model property
n = iteration counter
T = transposed vector
∞ = infinite property

Greek letters

α = least-squares solution step length, Eq. 4.26
α = EOS a parameter correction, $a=a_c\alpha(T)$, Eq. 1.9
α,β,η = parameters in gamma distribution function
β = EOS b parameter correction, $b=b_c\beta(T)$
β_o,δ = parameters in modified distribution function
Δw = required pseudocomponent weight fraction, Eq. 3.21
$\Delta \underline{x}$ = least-squares solution vector, Eqs. 4.11, 4.12, 4.19
Δz = required pseudocomponent mole fraction, Eq. 3.23
δ = EOS d parameter correction, $d=d_c\delta(T)$
ϵ = convergence tolerance
ϵ_{kj} = modified GDEM variable, Eq. 2.57
Φ = fugacity coefficient, Eqs. 1.58, 1.60
Γ = gamma function
γ = specific gravity
γ_{API} = API gravity, $\gamma_{API} = 141.5/\gamma - 131.5$
θ = property
κ = condition number of Hessian matrix
λ = Martin EOS variable, Eq. 1.57
λ_j = j'th eigenvalue of convergence matrix **S**, Eq. 2.51
μ = chemical potential
μ_l = l'th eigencoefficient of the characteristic polonium, Eq. 2.51
ν = number of dominant eigenvalues of **S**
Ω = EOS critical constants
ω = acentric factor
π = multiplication
ρ = density (lb/ft^3)
Σ = summation
σ = sum-chart value, Eq. 1.53
ξ = EOS c parameter correction, $c=c_c\xi(T)$
∂ = partial derivative
∇ = gradient operator

Abbreviations

BIP = binary interaction parameter
CCE = constant composition expansion
CVD = constant volume depletion
DLE = differential liberation expansion
EOS = equation of state
FVF = formation volume factor
GOR = gas oil ratio
MCV = multi-contact vaporization
VT = volume translation

REFERENCES

Abbott, M.M.: "Cubic Equation of State," AIChE J. (May 1973) 596-601.

Abbott, M.M.: "Cubic Equations of State: An Interpretive Review," Equations of State in Engineering, Advances in Chemistry Series, K.C.Chao and R.L Robinson (eds.), American Chemical Soc., Washington, DC (1979) **182**, 47-97.

Abramowitz, M. and Stegun, I.A.: Handbook of Mathematical Functions., New York (1972).

Adachi, Y., Lu, B.C.-Y., and Sugie, H.: "Three-Parameter Equations of State," Fluid Phase Equilibria (1983) **13**, 133-142.

Adachi, Y., Lu, B.C.-Y., and Sugie, H.: "A Four-Parameter Equation of State," Fluid Phase Equilibria (1983) **11**, 29-48.

Adachi, Y. and Lu, B.C.-Y.: " Simplest Equation of State for Vapor-Liquid Equilibrium Calculation: A Modification of the van der Waals Equation," AIChE J. (1984) **30**, No. 6.

Agarwal, R. Li, Y-K. Nghiem, L.X.: "A Regression Technique With Dynamic-Parameter Selection for Phase Behavior Matching," paper SPE 16343 presented at the SPE California Regional Meeting, Ventura (April 8-10, 1987)

Ahmed, T.H.: "Comparative Study of Eight Equations of State for Predicting Hydrocarbon Volumetric Phase Behavior," paper SPE 15673 presented at the 61st Annual SPE Meeting, New Orleans, (Oct. 5-8, 1986).

Ahmed, T.H., et al.: "An Accurate Method for Extending the Analysis of C_{7+}," paper SPE 12916 presented at the Rocky Mountain Meeting, Casper (May 21-23, 1984).

Ahmed, H.T., Cady, G.V., and Story, A.L.: "A Generalized Correlations for Characterizing the Hydrocarbon Heavy Fractions," paper SPE 14266 presented at the 60th Annual Technical Conference and Exhibition, Las Vegas (Sept. 22-25, 1985).

Alani, G.H. and Kennedy, H.T.: "Volumes of Liquid Hydrocarbons at High Temperatures and Pressures," Trans., AIME, **219** (1960).

Asselineau, L., Bogdanic, G., and Vidal, J.: "A Versatile Algorithm for Calculating Vapor-Liquid Equilibria," Fluid Phase Equilibria (1979) **3**, 273-90.

Austad, T., Hvidsten, J., Norvik, H., and Whitson, C.H.: "Practical Aspects of Characterizing Petroleum Fluids," presented at the conference on North Sea Condensate Reservoirs and Their Development, London (May 24-25, 1983).

Aziz, K. and Settari, A.: Petroleum Reservoir Simulation, Applied Science Publishers LTD, London (1979).

Baker, L.E., Pierce, A.C., and Luks, K.D.: "Gibbs Energy Analysis of Phase Equilibria," SPEJ (Oct. 1982); Trans., AIME, **273**.

Behrens, R.A. and Sandler, S.I.: "The Use of Semicontinuous Description to Model the C_{7+} Fraction in Equation of State Calculations," paper SPE/DOE 14925, presented at the Fifth Symposium on Enhanced Oil Recovery, Tulsa (April 20-23. 1986).

Benedict, M., Webb, G.B., and Rubin, L.C., J. Chem. Phys., (1940) **8**, 334.

Beret, S. and Prausnitz, J.M., AIChE J. (1975) **21**, 1123.

Bergman, D.F.: "Predicting the Phase Behavior of Natural Gas in Pipelines, " PhD Dissertation, U. Michigan, Ann Arbor (1976).

Briano, J.G. and Glandt, E.D.: "Statistical Thermodynamics of Polydisperse Fluids," J. Chem. Phys. (1984) **80**, No.7, 3336.

Brule, M.R., Kumar, M.R., and Watanasiri, S.: "Characterization Methods Improve Phase-Behavior Predictions," Oil&Gas J. (Feb. 11, 1985)

Cavett, R.H.: "Physical Data for Distillation Calculations - Vapor-Liquid Equilibria," Proc., 27th API Meeting, San Francisco (1962) 351-366.

Chaback, J.J. and Turek, E.A.: "Phase Behavior of Mixtures of San Andres Formation Oils with Acid Gases. Application of a Modified Redlich-Kwong Equation of State," American Chemical Soc., Washington, DC (1986) 389-405.

Chien, M.C.H. and Monroy, M.R.: "Two New Density Correlations," paper SPE 15676 presented at the 61st Annual SPE Meeting, New Orleans (Oct. 5-8, 1986).

Chorn, L.G.: "Simulated Distillation of Petroleum Crude Oil by Gas Chromatography. Characterizing the Heptanes-Plus Fraction," J. of Chrom. Sci. (Jan. 1984) 17-21.

Chou, G.F. and Prausnitz, J.M.: " A Phenomenological Correction to an Equation of State for the Critical Region," paper presented at the AIChE Spring Meeting, New Orleans, (March 6-10, 1988).

Chueh, P.L. and Prausnitz, J.M.: "Vapor-Liquid Equilibria at High Pressures: Vapor-Phase Fugacity Coefficients in Nonpolar and Quantum-Gas Mixtures," Ind. Eng. Chem. Fundam. (1967a) **6**, No.4.

Chueh, P.L. and Prausnitz, J.M.: "Vapor-Liquid Equilibria at High Pressures: Calculation of Partial Molar-Volume in Non-Polar Liquid Mixtures," AIChE J. (1967b) **13**, No. 6, 1099-1113.

Chueh, P.L. and Prausnitz, J.M.: " Calculation of High-Pressure Vapor-Liquid Equilibria." Ind. Eng. Chem. (1968) **60**, No. 13.

Coats, K.H.: "An Equation of State Compositional Model," SPEJ, (Oct. 1980); Trans., AIME, **269**.

Coats, K.H.: "Simulation of Gas Condensate Reservoir Performance," paper SPE 10512 presented at the Fourth SPE Symposium on Reservoir Simulation, Dallas, New Orleans (Jan. 31-Feb. 3, 1982).

Coats, K.H.: "Implicit Compositional Simulation of Single-Porosity and Dual-Porosity Reservoirs," paper SPE 18427 presented at the Symposium on Reservoir Simulation, Houston (Feb. 6-8, 1989).

Coats, K.H. and Smart, G.T.: "Application of a Regression-Based EOS PVT Program to Laboratory Data," SPERE (May 1986) 277-299.

Collins, D.A., Nghiem, L.X., and Li, Y-K.: "An Efficient Approach to Adaptive-Implicit Compositional Simulation With an Equation of State," paper SPE 15133 presented at the 56th California Meeting of SPE, Oakland (April 2-4, 1986).

Cotterman, R.L., Dimitrelis, D., and Prausnitz, J.M.: "Supercritical-Fluid Extraction Calculations for High-Boiling Petroleum Fractions Using Propane, Application of Continuous Thermodynamics," Ber. Bunsen. Physik. Chem. (1984) **87**, No. 9.

Cotterman, R.L., Bender, R., and Prausnitz, J.M.: "Phase Equilibria for Mixtures Including Very Many Components. Development and Application of Continuous Thermodynamics for Chemical Process Design," Ind. Eng. Chem. Proc. Des. Dev. (1985) **24**,194.

Cotterman, R.L., and Prausnitz, J.M.: "Flash Calculations for Continuous or Semicontinuous Mixtures Using an Equation Of State," Ind. Eng. Chem. Proc. Des. Dev. (1985) **24**, 434.

Dahlquist, G. and Bjorck, A.: Numerical Methods, Prentice-Hall Inc., Englewood Cliffs, NJ (1974).

Dennis, J.E. Jr., Gay, D.M., and Welsch, R.E.: "An Adaptive Nonlinear Least-Squares Algorithm," ACM Trans. Math. Software (1981) **7**, No. 3, 348-68.

Crowe, A.M. and Nishio, M.: "Convergence Promotion in the Simulation of Chemical Processes-the General Dominant Eigenvalue Method," AIChE (1975) **21**, 528-523.

Donahue, M.D. and Prausnitz, J.M., AIChE J. (1978) **24**, 849.

Drohm, J.K., Goldthorpe, W.H., and Trengove, R.: "Enhancing the Evaluation of PVT DATA," paper OSEA 88174 presented at the Seventh Offshore South East Asia Conference, Singapore (Feb. 2-5, 1988).

Drohm, J.K., Trengove, R., and Goldthorpe, W.H.: "On the Quality of Data from Standard Gas-Condensate PVT Experiments," paper SPE 17768 presented at the Gas Technology Symposium, Dallas (June 13-15, 1988).

Edmister, W.C.: "Applied Hydrocarbon Thermodynamics, Part 4: Compressibility Factors and Equations of State," Pet. Refiner (April 1958) 173- 179.

Edmister, W.C. and Lee, B.I.: Applied Hydrocarbon Thermodynamics, Vol. 1, second edition, Gulf Publishing Co., New York (1983).

Eilerts, C.K., et al.: Phase Relations of Gas-Condensate Fluids, Vol. I and II, Monograph 10, American Gas Association, New York (1957).

Eilerts, C.K.: "Gas Condensate Reservoir Engineering, 1. The Reserve Fluid, Its Composition and Phase Behavior," Oil&Gas J. (Feb. 1, 1947).

Enick, R.M., Holder, G.D., and Mohamed, R.: "Four-Phase Flash Equilibrium Calculations Using The Peng-Robinson Equation of State and A Mixing Rule for Asymmetric Systems," SPERE (Nov. 1987).

Firoozabadi, A.: "Reservoir Fluid Phase Behavior and Volumetric Prediction Using Equations of State," JPT (April 1988) 397.

Foss, B. A.: On Parameter Identification in Reservoirs, Dr.Ing. thesis (1987) Norwegian Institute of Technology,

Fuller, G.G.: "A Modified Redlich-Kwong-Soave Equation of State Capable of Representing the Liquid State," Ind. Eng. Chem. Fundam. (1976) **15**, No. 4.

Fussell, D.D. and Yarborough, L.: "The Effect of Phase Data on Liquids During Cycling of a Gas Condensate Reservoir," SPEJ (April 1972); Trans., AIME, **253**.

Fussel, D.D. and Yanosik, J.L.: "An Iterative Sequence for Phase-Equilibria Calculation Incorporating the Redlich-Kwong Equation of State," SPEJ (June 1978) 173-82.

Gani, R. and Fredenslund, Aa.: "Thermodynamics of Petroleum Mixtures Containing Heavy Hydrocarbons: An Expert Tuning System," Ind. Eng. Chem. Res. (1987) **26**, 1304-1312.

Graboski, M.S. and Daubert, T.E. Ind. Eng. Chem. Proc. Des.Dev. (1978) **17**, 443.

Gray, R.D.Jr.: "Industrial Experience in Applying the Redlich- Kwong Equation to Vapor-Liquid Equilibria," Advances in Chemistry Series, K.C.Chao and R.L Robinson (eds.), American Chemical Soc., Washington, DC (1979).

Greenberg, M.D.: Foundation of Applied Mathematics, Prentice Hall Inc., Englewood Cliffs, New Jersey (1978) 15-16.

Gundersen, T.: "Numerical Aspects of the Implementation of Cubic Equations of State in Flash Calculation Routines," Computer and Chem. Eng. (1982) **3**, 245.

Haaland, S.: Characterization of North Sea Crude Oils and Petroleum Fractions, MSc Thesis, Norwegian Institute of Technology (NTH), Department of Petroleum Engineering (1981).

Hall, K.R. and Yarborough, L: "New, Simplified Correlation for Predicting Critical Volume," Chem. Eng. (Nov. 1971) 76-77.

Hamam, S.E.M., Chung, W.K., Elshayal, I.M., and Lu, B.C.-Y.: "Generalized Temperature-Dependent Parameters of the Redlich-Kwong Equation of State for Vapor-Liquid Equilibrium Calculations," Ind. Eng. Chem. Proc. Des. Dev. (1977) **16**, No. 1.

Hariu, O.H., and Sage, R.C.: "Crude Split Figured by Computer," Hydro.Proc. (1969) 143-148

Harmens, A., Cryogenics (1975) **15**, 217.

Harmens, A. and Knapp, H.:"Three-Parameter Equation of State for Normal Substances," Ind. Eng. Chem. Fundam. (1980) **19**, 291-294.

Heyen, G.: "A Cubic Equation of State With Extended Range of Applications," 2nd World Congress Chem. Eng., Montreal (Oct. 4-9, 1983)

Hoffmann, A.E., Crump, J.S., Hocott, C.R.: "Equilibrium Constants for a Gas-Condensate System," Trans., AIME, **198** (1953).

Huang, W.W.: "Some Experiences With a Critical Reservoir Fluid," paper 14415 presented at the 60th Annual Technical Conference and Exhibition, Las Vegas (Sept. 22-25, 1985).

Hurst, W. and McCarty, G.M.: "The Application of Electrical Models to the Study of Recycling Operations in Gas Distillate Fields," Drilling and Production Practice, American Petroleum Inst. (1941).

Hustad, O.S.: An Explicit Phase Behaviour Model for Pseudocompositional Reservoir Simulation, Dr.Ing. thesis, IPT Report 1989:3, Norwegian Institute of Technology, Department of Petroleum Technology (1983).

Jacoby, R.H.: "NGPA Phase Equilibrium Project," Proc., API (1964) 1-10.

Jacoby, R.H., Koeller, R.C., and Berry Jr., V.J.: "Effect of Composition and Temperature on Phase Behavior and Depletion Performance of Rich Gas-Condensate Systems," Trans., AIME, **216** (1959).

Jhaveri, B.S. and Youngren, G.K: "Three-Parameter Modification of the Peng-Robinson Equation of State to Improve Volumetric Predictions," SPE Paper 13118 presented at the 59th Annual SPE Meeting, Houston (Sept. 16-19, 1984).

Joffe, J., Scroeder, G.M., and Zudkevitch, D.: "Vapor-Liquid Equilibria with the Redlich-Kwong Equation of State," AIChE J. (May 1970) 496-98.

Katz, D.L.: "Overview of Phase Behavior in Oil and Gas Production," JPT (June 1983) 1205-1214.

Katz, D.L. and Hachmuth, K.H.:"Vaporization Equilibrium Constants in a Crude-Oil Natural Gas System," Ind. Eng. Chem. (1937) **29**, 1072.

Katz, D.L. and Firoozabadi, A.: "Predicting Phase Behavior of Condensate/Crude-Oil Systems Using Methane Interaction Coefficients," JPT (Nov. 1978) 1649-55, Trans., AIME, **265**.

Kehlen, R., Raetzsch, M.T., and Bergman, J.: "Continuous Thermodynamics of Multicomponent Systems," AIChE J. (1985) **31**, No. 7, 1136-1148.

Kenyon, D.E. and Behle, A.: "Third SPE Comparative Solution Project: Gas Cycling of Retrograde Condensate Reservoirs," JPT (Aug. 1987); Trans., AIME, **238**.

Kesler, M.G. and Lee, B.I.: "Improve Predictions of Enthalpy of Fractions," Hydro.Proc. (March 1977) 153-158.

Klara, S.M. and Hemanth-Kumar, K.: " Comparisons of Computational Efficiencies of Different Equations of State and Transport Property Correlations in a Compositional Simulator," paper SPE 16942 presented at the 62nd Annual Technical Conference and Exhibition, Dallas (Sept. 27-30, 1987).

Klara, S.M. and Hemanth-Kumar, K.: "Comparisons of Different Equations of State and Transport Property Correlations in a Compositional Simulator," paper SPE 16492 presented at the 62nd Annual Technical Conference and Exhibition, Dallas (Sept. 27-30, 1987).

Lapidus, L. and Pinder, G.F.: Numerical Solution of Differential Equations in Science and Engineering, John Wiley & Sons, New York (1982).

Law, V.J.: Prepared Lecture Notes, Chemical Engineering Department, Tulane University, New Orleans (1967).

Law, V.J. and Fariss, R.H.: "Transformational Discrimination for Unconstrained Optimization," Ind.Eng.Chem. Fundam. (1972) **11**, No. 2.

Lee, B.I. and Kesler, M.G.: "A Generalized Thermodynamic Correlation Based on Three-Parameter Corresponding States," AIChE J. (1975) **21**, 510-527.

Li, Y-K. and Nghiem, L.X.: "The Development of a General Phase Envelope Construction Algorithm for Reservoir Fluid Studies," paper SPE 11198 presented at the 57th Annual SPE Meeting, New Orleans (Sept. 26-29 1982).

Li, Y-K., Nghiem, L.X., and Siu, A.: "Phase Behavior Computation for Reservoir Fluid: Effects of Pseudo Component on Phase Diagrams and Simulations Results," paper 84-35-19 presented at the CIM Annual Meeting, Calgary (June 10-13, 1984).

Lohrenz, J., Bray, B.G., and Clark, G.C.: "Calculating Viscosities of Reservoir Fluids Form Their Compositions," JPT (Oct. 1964) 1171-1176.

Lyckman, E.W., Eckert, C.A., and Prausnitz, J.M., Chem. Eng. Sci. (1965) **20**, 685-91.

Maddox, R.N. and Erbar, J.H.: "Predicting Properties of Hexanes Plus (C_{6+}) Fractions," Gas Conditioning and Processing, Campbell Petroleum Series (1982).

Martin, J.J.: "Equations of State," Ind. Eng. Chem. (1967) **59**, No. 12.

Martin, J.J.: "Cubic Equation of State - Which?" Ind. & Eng.Chem. (1979) **18**, No 2, 81-70.

Martin, J.J. and Hou, Y.C., AIChE J. (1955) 1,142.

Mehra, R.K., Heidemann, R.A., and Aziz, K.: "Computation of Multiphase Equilibrium for Compositional Simulation," SPEJ (Feb. 1982) 61-68.

Mehra, R.K., Heidemann, R.A., and Aziz, K.: " An Accelerated Successive Substitution Algorithm," J. Cdn. Chem. Eng. (Aug. 1983) 590-96.

Metcalfe, R.S. Vogel, J.L., and Morris, R.W.: "Compositional Gradient in the Anshutz Ranch East Field," SPE 14412 presented at the 60th Annual Technical Conference and Exhibition, Las Vegas (Sept. 22-25, 1985).

Michelsen, M.L.: "The Isothermal Flash Problem. Part 1. Stability," Fluid Phase Equilibria (1982a) **9**.

Michelsen, M.L.: "The Isothermal Flash Problem. Part 2. Phase Split Calculation," Fluid Phase Equilibria (1982b) **9**.

Michelsen, M.L.: "Saturation Point Calculation," Fluid Phase Equilibria (1985) **23**.

Morris, R.W. and Turek, E.A.: "Optimal Temperature-Dependent Parameters of the Redlich-Kwong Equation of State," American Chemical Soc., Washington, DC, 407-433 (1986).

Nagy, Z. and Shirkovskiy, A.I.: "Mathematical Simulation of Natural Gas Condensation Processes Using the Peng-Robinson Equation of State", SPE Paper 10982 presented at the 57th Annual SPE Meeting, New Orleans (Sept. 26-29 1982).

Ng, H.J. and Robinson, D.B.: "Vapor Liquid Equilibrium and Condensing Curves for a Typical Gas Condensate," Research Report PR-89, Gas Processes Assn., Tulsa (1985).

Ng, H.J., Chen, C.J., and Robinson, D.B.: "Vapor Liquid Equilibrium and Condensing Curves in the Vicinity of the Critical Point for a Typical Gas Condensate," Research Report PR-96, Gas Processes Assn, Tulsa (1986).

Nghiem, L.X. and Aziz, K.: "An Robust Iterative Method for Flash Calculations Using the Soave-Redlich-Kwong or the Peng-Robinson Equation of State," paper SPE 8285 presented at the 54th Annual Fall Technical Conference and Exhibition, Las Vegas (Sept. 23-26, 1979).

Nghiem, L.X. and Li, Y-K.: "Phase-Equilibrium Calculations for Reservoir Engineering and Compositional Simulation," presented at the First International Forum on Reservoir Simulation, Alpach, Austria (Sept. 12-16, 1988).

Nghiem, L.X., Fong, D.K., and Aziz, K.: "Compositional Modeling With an Equation of State Model," SPEJ (Dec. 1981); Trans., AIME, **271**.

Nokay, R.: "Estimate Petrochemical Properties," Chem. Eng. (Feb. 23, 1959) 147-148.

Nutakki, R., Wong, T., Firoozabadi, A., and Aziz, K.: "Development of General Purpose Simulators - Part 1: Vapor-Liquid Equilibrium Calculations Using Three Equations of State and Accelerated Successive Substitution," Dept. of Petroleum Engineering, Stanford University (1985).

Patel, V.C. and Teja, A.S.: "A New Cubic Equation of State for Fluids and Fluid Mixtures," Chem. Eng. Sci. (1982) **37**, No. 3, 463-473.

Pearson, K.: "Contributions to the Mathematical Theory of Evolution. II. Skew Variations in Homogeneous Material," Philosophical Trans., Royal Society of London, Series A, **186**, 343-414, (1895).

Pedersen, K.S., Thomassen, P., and Fredenslund, Aa.: "Thermodynamics of Petroleum Mixtures Containing Heavy Hydrocarbons. 1. Phase Envelope Calculations by Use of the Soave-Redlich-Kwong Equation of State," Ind. Eng. Chem. Proc. Des. Dev. (1984a) **23**, 163-170.

Pedersen, K.S., Thomassen, P., and Fredenslund, Aa.: "Thermodynamics of Petroleum Mixtures Containing Heavy Hydrocarbons. 2. Flash and PVT Calculations with the SRK Equation of State," Ind. Eng. Chem. Proc. Des. Dev. (1984b) **23**, 566-573.

Pedersen, K.S., Thomassen, P., and Fredenslund, Aa.: "Thermodynamics of Petroleum Mixtures Containing Heavy Hydrocarbons. 3. Efficient Flash Calculation Procedures Using the SRK Equation of State," Ind. Eng. Chem. Proc. Des. Dev. (1985a) **24**, 948-954.

Pedersen, K.S., Thomassen, P., and Fredenslund, Aa.: "On the Dangers of "Tuning" Equation of State Parameters, " paper SEP 8501, Phase Equilibria and Separation Processes (1985b).

Peneloux , A., Rauzy, E., and Freze, R.: "A Consistent Correction for Redlich-Kwong-Soave Volumes," Fluid Phase Equilibria (1982) **8**.

Peng, D.-Y. and Robinson, D.B.: "A New Two-Constant Equation of State," Ind. Eng. Chem. Fund. (1976) **15**, No. 1, 59-64.

Pitzer, K.S., et al.: "The Volumetric and Thermodynamic Properties of Fluids. II. Compressibility Factor, Vapor Pressure, and Entropy of Vaporization," J. Amer. Chem. Soc. (1955) **77**, 3433-3440.

Press. W.H., et al.: Numerical Recipes, The Art of Scientific Computing, Cambridge University Press, Cambridge (1988).

Rachford, H.H. and Rice, J.D.: "Procedure for Use of Electronic Digital Computers in Calculating Falsh Vaporization Hydrocarbon Equilibrium," Trans., AIME **195** (1952).

Reid, R.C., and Prausnitz, J.M., and Poling, B.E.: The Properties of Gases and Liquids, 4th edition, McGraw-Hill, New York (1987).

Riazi, M.R. and Daubert, T.E.: "Simplify Property Predictions," Hydro. Proc. (March 1980) 115-116.

Riazi, M.R. and Daubert, T.E.: "Characterization Parameters for Petroleum Fractions," Ind. Eng. Chem. Res. (1987) **26**, 755-759.

Riemens, W.G., Shulte, A.M., and de Jong, L.N.J.: "Birba Field PVT Variations Along the Hydrocarbon Column and Confirmatory Field Tests," JPT (Jan. 1988) 83-88.

Risnes, R. and Dalen, V.: "Equilibrium Calculations for Coexisting Liquid Phases," SPEJ (Feb. 1984) 87-96.

Risnes, R., Dalen, V., and Jensen, J.I.: "Phase Equilibrium Calculations in the Near-Critical Region," European Symposium on EOS, Bournemouth, 329-50 (1981) .

Robinson, D.B. and Peng, D.-Y.: "The Characterization of the Heptanes and Heavier Fractions," Research Report 28, GPA, Tulsa (1978).

Roess, L.C.: "Determination of Critical Temperature and Pressure of Petroleum Fractions," **JPT** (Oct. 1936) **22**, 1270-1279.

Sage, B.H. and Reamer, H.H.: "Volumetric Behavior of Oil and Gas From the Rio Bravo Field," Trans., AIME, **142** (1941).

Sage, B.H. and Olds, R.H.: "Volumetric Behavior of Oil and Gas From Several San Joaquin Valley Fields," Trans., AIME, **170** (1947).

Schmidt, G. and Wenzel, H.: "A Modified van der Waals Type Equation of State," Chem. Eng. Sci (1980) **35**, 1503-12.

Slot-Petersen, C.: "A Systematic and Consistent Approach To Determine Binary Interaction Coefficients for The Peng-Robinson Equation of State," paper SPE 16941 presented at the 62nd Annual Technical Conference and Exhibition, Dallas (Sept. 27-30, 1987).

Soave, G.: "Equilibrium Constants from a Modified Redlich-Kwong Equation of State," Chem. Eng. Sci. (1972) **27**, 1197-1203.

Soave, G.: " Application of a Cubic Equation of State to Vapor-Liquid Equilibria of Systems Containing Polar Compounds," I. Chem. Symposium Series (1979) No. 56.

Standing, M.B.: Volumetric and Phase Behavior of Oil Field Hydrocarbon Systems, 8th Printing, Society of Petroleum Engineers of AIME, Dallas (1977).

Standing, M.B.: "A Set of Equations for Computing Equilibrium Ratios of a Crude Oil /Natural Gas System at Pressures Below 1,000 psia," JPT (Sept. 1979) 1193-95.

Standing, M.B. and Katz, D.L.: "Density of Crude Oils Saturated with Natural Gas," Trans., AIME, **146**, 159-165 (1942).

Standing, M.B. and Katz, D.L.: " Vapor-Liquid Equilibria of Natural Gas-Crude Oil Systems," Trans., AIME, **155**, 233 (1944).

Starling, K.E., Hydro. Proc. (1971) **50**, No. 3, 101.

Starling, K.E., and Han, M.S., Hydro. Proc. (1972) **51**, No. 5, 129.

Søreide, I., Reffstrup, J., and Whitson, C.H.: Procedures for Reservoir Fluid Characterization Using an Equation of State Model. Application to Fluids in the Danish North Sea, Technical University of Denmark, The Laboratory of Energetics (1988).

Technical Data Book - Petroleum Refining, American Petroleum Institute, Washington, D.C. (1976) Vol. 1, 3rd ed.: Procedures 5A1.10 (Lee-Kesler) and 6A2.13 (modified Rackett).

Trangenstein, J.A.: "Minimization of Gibbs Energy in Compositional Reservoir Simulation," Chem. Eng. Sci. (1985) **12**, 2847-2863.

Trebble, M.A. and Bishnoi, P.R.: "Accuracy and Consistency Comparisons of Ten Cubic Equations of State for Polar and Non-Polar Compounds," Fluid Phase Equilibria (1986) **29**, 465-474.

Trebble, M.A. and Bishnoi, P.R.: "Development of a New Four-Parameter Cubic Equation of State." Fluid Phase Equilibria (1987) **35**, 1-18.

Tsonopoulos, C. and Heidman, J.L.: "From Redlich-Kwong to the Present," Fluid Phase Equilibria (1985) **24**, 1-23

Turek, E.A., Metcalfe, R.S., Yarborough, L., and Robinson, R.L.Jr.: "Phase Equilibria in CO_2-Multicomponent Hydrocarbon Systems: Experimental Data and an Improved Prediction Technique," SPEJ (June 1984) 308-24.

Twu, C.H.: "An Internally Consistent Correlation for Predicting the Critical Properties and Molecular Weights of Petroleum and Coal-Tar Liquids," Fluid Phase Equilibria (1984) **16**, 137-150.

Usdin, E. and McAuliffe, J.C.: "A One Parameter Family of Equations of State," Chem. Eng. Sci. (1976) **31**, 1077-1084.

van der Waals, J.D. : Doctoral Dissertation, Leiden, Holland, 1873.

Varotsis, N., Stewart, G., Todd, A.C., and Clancy, M.: "Phase Behavior of Systems Comprising North Sea Reservoir Fluids and Injection Gases," JPT (Nov. 1986) 1221-33.

Watson, K.M. and Nelson, E.F.: "Improved Methods for Approximating Critical and Thermal Properties of Petroleum Fractions," Ind. Eng. Chem. (1933) **25**, No. 8, 880-887.

Whitson, C.H.: "Characterizing Hydrocarbon Plus Fractions," SPEJ (Aug. 1983a) 683-694; Trans., AIME, **275**.

Whitson, C.H.: Topics on Phase Behavior and Flow of Petroleum Reservoir Fluids. Dr.Techn. thesis, Norwegian Institute of Technology, Department of Petroleum Engineering (1983b).

Whitson, C.H.: "Effect of C_{7+} Properties on Equation-of-State Predictions," SPEJ (Dec. 1984) 685-696; Trans., AIME, **277**.

Whitson, C.H.: Prepared Lecture Notes, Norwegian Institute of Technology, Department of Petroleum Engineering (1987).

Whitson, C.H., Personal communication, (1989).

Whitson, C.H. and Torp, S.B.: "Evaluating Constant Volume Depletion Data," paper SPE 10067 presented at the 56th Annual Fall Technical Conference and Exhibition, San Antonio (Oct. 5-7, 1981)

Whitson, C.H. and Torp, S.B.: "Evaluating Constant-Volume-Depletion Data," JPT (March 1983); Trans., AIME, **275**.

Whitson, C.H. and Michelsen, M.L.: "The Negative Flash" paper presented at the Fifth International Conference on Fluid Properties & Phase Equilibria for Chemical Process Design, Banff, Alberta (April 31-May 5, 1989).

Whitson, C.H. and Brule, M.R.: Phase Behavior Monograph, Society of Petroleum Engineers of AIME, Dallas (to appear).

Whitson, C.H., Anderson, T.F., and Søreide, I.: "Application of the Gamma Distribution Model to Molecular Weight and Boiling Point Data for Petroleum Fractions," paper presented at the AIChE Annual Meeting, Miami (Nov. 2-7, 1986).

Whitson, C.H., Anderson, T.F., and Søreide, I.: "C_{7+} Characterization of Related Equilibrium Fluids Using the Gamma Distribution," paper presented at the AIChE Spring Meeting, New Orleans (March 6-10, 1988).

Whitson, C.H., da Silva, F., and Søreide, I.: "Simplified Compositional Formulation for Modified Black Oil Simulators," paper SPE 18315 presented at the 63rd Annual Technical Conference and Exhibition, Houston (Oct. 2-5, 1988).

Wilson, G.M.: "Calculation of Enthalpy Data From a Modified Redlich-Kwong Equation of State," Adv. Cryog. Eng. (1966) **11**, 392.

Wilson, G.M.: "A Modified Redlich-Kwong Equation of State, Application to General Physical Data Calculations," paper No. 15c presented at the AIChE 65th National Meeting, Cleveland (May 4-7, 1969).

Wu, R.S. and Batycky. J.P.: "Pseudocomponent Characterization for Hydrocarbon Miscible Displacement," paper SPE 15404 presented at the 61st Annual Fall Technical Conference and Exhibition, New Orleans (Oct. 5-6, 1986).

Yarborough, L.: "Vapor-Liquid Equilibrium Data for Multicomponent Mixtures Containing Hydrocarbon and Non-Hydrocarbon Components," J. Chem. Eng. Data, **17** (1972) 129-133.

Yarborough, L.: "Application of a Generalized Equation of State to Petroleum Reservoir Fluids," Equations of State in Engineering, Advances in Chemistry Series, K.C.Chao and R.L.Robinson (eds.), American Chemical Soc., Washington, DC (1979) **182**, 385-435.

Young, L. and Stephenson, R.E.: "A Generalized Compositional Approach for Reservoir Simulation," SPEJ (Oct. 1983); Trans., AIME, **275**.

Young, L.: "Equation of State Compositional Modeling on Vector Processors" paper SPE 16023 presented at the Ninth SPE Symposium on Reservoir Simulation, San Antonio (Feb. 1-4, 1987).

Zick, A., Personal communication (1985).

Zick, A.A.: "A Combined Condensing/Vaporizing Mechanism in the Displacement of Oil by Enriched Gases," paper 15493 presented at the 61st Annual Fall Technical Conference and Exhibition, New Orleans (Oct. 5-6, 1986).

Zudkevitch, D. and Joffe, J.: "Correlation and Prediction of Vapor-Liquid Equilibrium with the Redlich-Kwong Equation of State," AIChE J. (Jan. 1970) 112-19.

APPENDIX A
SUMMARY OF TBP DATABASE

TABLE A-1 Overall C_{7+} Properties and Results of Comparing Measured Pseudocomponent Specific Gravities With Calculated From Various Correlations Given in Sec. 3.3.

No	Sample	N	BO/GC	M_{7+}	γ_{7+}	Absolute Average Deviations, %					
						K_w	F_c	J_a	J_{am}	$J_{am}(M_{7+})$	C_f
1	Standing-Katz	7	BO	229	0.8682	2.070	1.870	4.390	2.940	2.760	2.020
2	Hoffman et al. Oil	24	GC	199	0.8409	2.240	0.830	1.660	1.000	1.010	0.650
3	Jacoby, et al. (1)	7	BO	143	0.7717	0.820	0.540	0.230	0.330	0.220	0.280
4	Jacoby, et al. (2)	7	BO	193	0.7995	2.540	1.540	0.910	0.840	0.960	1.090
5	Lee, et al. 1 (A)	6	BO	289	0.9032	2.430	2.200	6.460	4.320	3.270	2.550
6	Lee, et al. 2 (B)	6	BO	206	0.8498	2.460	1.130	2.190	1.210	1.220	0.350
7	Lee, et al. 3 (C)	6	BO	348	0.9386	4.430	1.990	4.680	1.910	0.640	1.140
8	Hariu	15	BO	228	0.8518	1.930	1.160	3.760	2.540	2.140	1.420
9	RRI (Austad, et al.)	15	BO	178	0.8067	2.020	0.970	0.870	0.770	0.760	0.570
10	Haaland Sample A	16	BO	257	0.8725	1.740	1.030	3.450	2.510	2.040	1.120
11	Haaland Sample B	15	BO	206	0.8406	1.750	1.050	1.730	1.210	1.200	0.430
12	Haaland Sample C	15	BO	258	0.8948	1.730	1.280	3.330	1.870	1.730	1.140
13	Berge 1	16	BO	256	0.8759	3.520	2.010	2.090	1.010	0.680	1.140
14	Pedersen BO-1	14	BO	211	0.8451	1.850	0.770	2.100	1.420	1.330	0.530
15	Pedersen BO-2	14	BO	226	0.8528	1.970	0.760	2.870	1.980	1.850	0.920
16	Pedersen BO-3	17	BO	254	0.8834	4.030	2.430	1.660	0.600	0.470	1.400
17	Pedersen BO-4	17	BO	217	0.8449	2.440	1.210	1.380	0.910	0.940	0.390
18	Pedersen BO-5	17	BO	236	0.8525	2.860	1.640	1.590	0.860	0.670	0.830
19	Pedersen BO-6	17	BO	265	0.8687	2.600	1.400	2.190	1.400	0.980	0.910
20	Pedersen BO-7	14	BO	232	0.8658	1.830	0.660	2.920	1.840	1.630	0.820
21	Pedersen BO-8	14	BO	230	0.8650	1.820	0.660	2.890	1.840	1.640	0.820
22	Pedersen BO-9	13	BO	231	0.8564	3.150	1.370	2.010	1.120	1.010	0.630
23	Pedersen BO-10	14	BO	211	0.8448	1.850	0.770	2.100	1.410	1.330	0.530
24	Pedersen BO-11	24	BO	214	0.8458	2.070	0.850	1.410	1.080	1.100	0.490
25	Pedersen BO-12	15	BO	228	0.8542	2.320	0.820	2.080	1.400	1.490	0.630
26	Pedersen GC-1	11	GC	149	0.8177	1.720	1.580	0.710	0.820	0.640	0.950
27	Pedersen GC-2	5	GC	120	0.7955	0.570	1.220	0.520	0.890	0.480	0.380
28	Pedersen GC-3	12	GC	119	0.7597	0.620	1.380	1.040	0.300	1.300	0.540
29	Pedersen GC-4	12	GC	150	0.8165	2.420	2.100	1.110	1.240	1.040	1.410
30	Pedersen GC-5	12	GC	151	0.8162	2.540	2.200	1.140	1.240	1.060	1.470
31	Pedersen GC-6	26	GC	150	0.8201	4.180	2.230	0.720	1.960	0.930	1.980
32	Pedersen GC-7	14	GC	155	0.8086	1.690	0.810	0.670	1.000	0.710	0.630
33	Midg. No.2	12	GC	129	0.7865	0.850	0.810	0.820	0.820	0.770	0.460
34	Midg. No.3	14	BO	214	0.8598	3.430	1.900	0.950	1.720	1.740	1.680

TABLE A-1 (continued)

No	Sample	N	BO/ GC	M_{7+}	γ_{7+}	Absolute Average Deviations, %					
						K_w	F_c	J_a	J_{am}	$J_{am}(M_{7+})$	C_f
35	Albuskjell No.1	19	GC	171	0.8005	1.580	0.700	1.010	0.690	0.680	0.330
36	Albuskjell No.3	19	GC	169	0.8008	1.670	0.750	0.920	0.720	0.690	0.340
37	Albuskjell No.4	19	GC	154	0.7871	1.690	0.750	0.900	0.590	0.680	0.360
38	Albuskjell No.5	19	GC	177	0.8043	1.610	0.950	1.010	0.680	0.680	0.430
39	Albuskjell No.6	19	GC	175	0.8033	1.620	0.770	1.000	0.610	0.610	0.260
40	Eldfisk No.1	13	BO	220	0.8517	1.940	1.020	2.290	1.420	1.350	0.590
41	Eldfisk No.2	14	BO	220	0.8554	1.290	0.890	2.750	1.870	1.730	1.020
42	Eldfisk No.3	11	BO	232	0.8601	2.120	0.910	3.080	1.650	1.220	0.820
43	Eldfisk No.4	5	BO	256	0.8626	2.000	1.180	3.230	1.070	0.820	1.040
44	Ekofisk No.1	24	BO	233	0.8534	2.160	1.800	2.320	1.480	1.150	1.220
45	North Sea BO-1	24	BO	243	0.8833	2.850	1.740	1.400	0.730	0.730	1.000
46	North Sea BO-2	24	BO	211	0.8458	2.170	0.900	1.320	1.020	1.040	0.490
47	North Sea BO-3	14	BO	243	0.8602	3.420	1.280	2.180	1.680	1.800	0.850
48	North Sea BO-4	14	BO	211	0.8459	1.920	0.710	2.110	1.400	1.350	0.470
49	North Sea BO-5	13	BO	229	0.8569	3.070	1.160	1.980	1.230	1.280	0.560
50	North Sea BO-6	5	BO	173	0.8372	1.230	1.340	1.440	1.670	1.010	0.930
51	North Sea BO-7	14	BO	267	0.8606	5.220	2.920	0.870	1.670	2.720	2.300
52	North Sea BO-8	14	BO	269	0.8797	3.070	0.790	2.610	1.570	1.710	0.600
53	North Sea BO-9	24	BO	248	0.8830	2.630	1.680	1.550	0.600	0.600	0.960
54	North Sea BO-10	14	BO	222	0.8338	2.210	0.540	2.340	1.770	1.800	0.620
55	North Sea GC-1	5	GC	125	0.7737	0.560	0.980	0.520	0.400	0.540	0.400
56	North Sea GC-2	14	GC	132	0.8012	2.810	1.550	1.230	2.920	1.410	2.010
57	North Sea GC-3	14	GC	128	0.7909	2.750	1.590	1.070	2.460	1.110	1.770
58	North Sea GC-4	14	GC	133	0.8048	2.250	1.630	1.120	2.510	1.180	1.580
59	North Sea GC-5	14	GC	172	0.8127	2.310	1.370	0.680	1.160	0.970	1.250
60	North Sea GC-6	14	GC	152	0.7917	1.820	0.770	0.870	1.340	0.980	0.970
61	North Sea GC-7	11	GC	123	0.7633	1.550	0.690	0.580	1.130	0.570	0.830
62	North Sea GC-8	14	GC	140	0.8068	2.060	1.270	0.740	2.020	0.880	1.250
63	North Sea GC-9	14	GC	171	0.8113	1.720	0.670	0.680	1.050	0.930	0.740
64	North Sea GC-10	14	GC	175	0.8055	1.870	0.790	0.900	1.160	1.110	0.870
65	North Sea GC-11	12	GC	119	0.7838	0.950	1.570	1.490	1.060	1.510	0.820
66	Alaska No.1	9	BO	279	0.9039	2.220	1.220	4.640	1.680	1.660	1.400
67	Alaska No.2	14	BO	268	0.9033	2.090	1.360	4.580	2.590	2.040	1.480
68	Alaska No.3	9	GC	164	0.8137	2.480	1.350	0.360	1.010	0.720	1.200
69	Hoffmann et al.gas	16	GC	141	0.7867	1.170	0.780	1.400	0.980	1.300	0.790
					AAD:	2.182	1.240	1.823	1.390	1.193	0.940

TABLE A-2 Overall C_{7+} Properties and Characterization Factors Used to Calculate Pseudocomponent Specific Gravities From Various Correlations Given in Sec. 3.3.

						"Characterization Factors"					
No	Sample	N	BO/GC	M_{7+}	γ_{7+}	K_w	F_c	J_a	J_{am}	$J_{am}(M_{7+})$	C_f
1	Standing-Katz	7	BO	229	0.8682	12.06	9.79	0.393	0.499	1.126	0.294
2	Hoffman et al. Oil	24	GC	199	0.8409	11.89	9.75	0.316	0.408	0.820	0.293
3	Jacoby, et al. (1)	7	BO	143	0.7717	12.10	10.05	0.157	0.209	0.205	0.276
4	Jacoby, et al. (2)	7	BO	193	0.7995	12.40	10.16	0.154	0.186	0.597	0.272
5	Lee, et al. 1 (A)	6	BO	289	0.9032	12.16	9.77	0.474	0.573	1.644	0.297
6	Lee, et al. 2 (B)	6	BO	206	0.8498	12.02	9.81	0.347	0.451	0.913	0.292
7	Lee, et al. 3 (C)	6	BO	348	0.9386	11.97	9.58	0.576	0.670	2.151	0.307
8	Hariu	15	BO	178	0.8067	12.20	10.03	0.217	0.282	0.550	0.279
9	RRI (Austad, et al.)	15	BO	228	0.8518	12.16	9.89	0.322	0.403	1.037	0.288
10	Haaland Sample A	16	BO	257	0.8725	12.15	9.83	0.373	0.456	1.306	0.291
11	Haaland Sample B	15	BO	206	0.8406	12.12	9.89	0.309	0.400	0.868	0.288
12	Haaland Sample C	15	BO	258	0.8948	11.86	9.60	0.466	0.574	1.411	0.303
13	Berge 1	16	BO	256	0.8759	12.12	9.81	0.388	0.476	1.314	0.293
14	Pedersen BO-1	14	BO	211	0.8451	12.09	9.86	0.319	0.408	0.915	0.289
15	Pedersen BO-2	14	BO	226	0.8528	12.13	9.87	0.330	0.415	1.037	0.289
16	Pedersen BO-3	17	BO	254	0.8834	12.04	9.74	0.423	0.523	1.338	0.297
17	Pedersen BO-4	17	BO	217	0.8449	12.17	9.91	0.309	0.392	0.950	0.287
18	Pedersen BO-5	17	BO	236	0.8525	12.23	9.93	0.314	0.388	1.091	0.286
19	Pedersen BO-6	17	BO	265	0.8687	12.23	9.89	0.349	0.422	1.330	0.288
20	Pedersen BO-7	14	BO	232	0.8658	12.02	9.77	0.375	0.472	1.129	0.294
21	Pedersen BO-8	14	BO	230	0.8650	12.02	9.77	0.374	0.471	1.117	0.294
22	Pedersen BO-9	13	BO	231	0.8564	12.15	9.87	0.338	0.424	1.078	0.289
23	Pedersen BO-10	14	BO	211	0.8448	12.09	9.86	0.318	0.408	0.911	0.289
24	Pedersen BO-11	24	BO	214	0.8458	12.12	9.88	0.318	0.406	0.934	0.288
25	Pedersen BO-12	15	BO	228	0.8542	12.11	9.85	0.332	0.416	1.050	0.289
26	Pedersen GC-1	11	GC	149	0.8177	11.68	9.67	0.337	0.494	0.473	0.298
27	Pedersen GC-2	5	GC	120	0.7955	11.48	9.60	0.353	0.588	0.249	0.304
28	Pedersen GC-3	12	GC	119	0.7597	11.91	9.96	0.202	0.312	0.053	0.283
29	Pedersen GC-4	12	GC	150	0.8165	11.73	9.70	0.332	0.486	0.470	0.297
30	Pedersen GC-5	12	GC	151	0.8162	11.75	9.72	0.329	0.482	0.472	0.296
31	Pedersen GC-6	26	GC	150	0.8201	11.66	9.65	0.347	0.509	0.486	0.299
32	Pedersen GC-7	14	GC	155	0.8086	11.90	9.84	0.283	0.401	0.456	0.290
33	Midg. No.2	12	GC	129	0.7865	11.74	9.78	0.273	0.421	0.230	0.292
34	Midg. No.3	14	BO	214	0.8598	11.87	9.69	0.374	0.480	0.998	0.297

TABLE A-2 (continued)

No	Sample	N	BO/ GC	M_{7+}	γ_{7+}	"Characterization Factors" K_w	F_c	J_a	J_{am}	$J_{am}(M_{7+})$	C_f
35	Albuskjell No.1	19	GC	171	0.8005	12.19	10.03	0.207	0.272	0.486	0.279
36	Albuskjell No.3	19	GC	169	0.8008	12.18	10.03	0.213	0.281	0.482	0.280
37	Albuskjell No.4	19	GC	154	0.7871	12.13	10.03	0.194	0.262	0.338	0.279
38	Albuskjell No.5	19	GC	177	0.8043	12.22	10.04	0.210	0.274	0.536	0.279
39	Albuskjell No.6	19	GC	175	0.8033	12.21	10.04	0.208	0.271	0.523	0.279
40	Eldfisk No.1	13	BO	220	0.8517	12.07	9.83	0.333	0.422	0.994	0.290
41	Eldfisk No.2	14	BO	220	0.8554	12.03	9.80	0.348	0.442	1.012	0.292
42	Eldfisk No.3	11	BO	232	0.8601	12.07	9.81	0.351	0.439	1.103	0.292
43	Eldfisk No.4	5	BO	256	0.8626	12.12	9.83	0.331	0.401	1.247	0.290
44	Ekofisk No.1	24	BO	233	0.8534	12.23	9.93	0.322	0.401	1.077	0.286
45	North Sea BO-1	24	BO	243	0.8833	11.94	9.68	0.435	0.545	1.274	0.299
46	North Sea BO-2	24	BO	211	0.8458	12.11	9.87	0.322	0.412	0.922	0.289
47	North Sea BO-3	14	BO	243	0.8602	12.23	9.91	0.339	0.421	1.173	0.288
48	North Sea BO-4	14	BO	211	0.8459	12.09	9.86	0.322	0.413	0.922	0.289
49	North Sea BO-5	13	BO	229	0.8569	12.13	9.86	0.343	0.432	1.073	0.290
50	North Sea BO-6	5	BO	173	0.8372	11.69	9.63	0.355	0.487	0.676	0.300
51	North Sea BO-7	14	BO	267	0.8606	12.29	9.94	0.313	0.376	1.303	0.285
52	North Sea BO-8	14	BO	269	0.8797	12.09	9.78	0.390	0.473	1.407	0.294
53	North Sea BO-9	24	BO	248	0.8830	11.98	9.70	0.428	0.532	1.300	0.298
54	North Sea BO-10	14	BO	222	0.8338	12.35	10.05	0.256	0.319	0.923	0.280
55	North Sea GC-1	5	GC	125	0.7737	11.84	9.88	0.235	0.361	0.150	0.288
56	North Sea GC-2	14	GC	132	0.8012	11.63	9.68	0.328	0.514	0.321	0.299
57	North Sea GC-3	14	GC	128	0.7909	11.69	9.74	0.297	0.466	0.252	0.295
58	North Sea GC-4	14	GC	133	0.8048	11.61	9.66	0.343	0.540	0.343	0.301
59	North Sea GC-5	14	GC	172	0.8127	12.06	9.92	0.257	0.346	0.554	0.285
60	North Sea GC-6	14	GC	152	0.7917	12.05	9.97	0.220	0.306	0.352	0.282
61	North Sea GC-7	11	GC	123	0.7633	11.92	9.96	0.201	0.304	0.084	0.283
62	North Sea GC-8	14	GC	140	0.8068	11.70	9.71	0.323	0.490	0.381	0.297
63	North Sea GC-9	14	GC	171	0.8113	12.00	9.89	0.252	0.338	0.537	0.286
64	North Sea GC-10	14	GC	175	0.8055	12.15	10.00	0.217	0.284	0.533	0.281
65	North Sea GC-11	12	GC	119	0.7838	11.62	9.72	0.307	0.507	0.185	0.298
66	Alaska No.1	9	BO	279	0.9039	11.85	9.58	0.482	0.584	1.573	0.305
67	Alaska No.2	14	BO	268	0.9033	11.87	9.59	0.491	0.602	1.509	0.305
68	Alaska No.3	9	GC	164	0.8137	11.90	9.82	0.279	0.384	0.516	0.290
69	Hoffmann et al.gas	16	GC	141	0.7867	11.90	9.88	0.228	0.325	0.276	0.286

APPENDIX B - FORTRAN LISTING

The FORTRAN program AVGPR calculates pseudocomponent mole fractions and molecular weights for a given discretization of the continuous molar distribution. This is expressed by the gamma distribution.
Program AVGPR calls the functions GMPRB and GAMA.

```
      SUBROUTINE AVGPR (ALF,BTA,ETA,PRO,PRN,ZFRAC,PROP)
C-------------------------------------------------------+
C     Calculates the average molecular weight within the +
C     specified interval (PRO,PRN) for the Gamma         +
C     distribution given by (ALF,BTA,ETA).               +
C-------------------------------------------------------+
      IMPLICIT DOUBLE PRECISION (A-H,O-Z)

C---  CALCULATE INTERVAL FRACTION, I.E. MOLE FRACTION
      FRACN = GMPRB(ALF,BTA,ETA,PRN)
      FRACO = GMPRB(ALF,BTA,ETA,PRO)
      ZFRAC = FRACN - FRACO
C---  CALC AVERAGE MOLECULAR WEIGHT
      IF (PRO.LE.ETA)THEN
       YO=0.0
      ELSE
       YO=(PRO-ETA)/BTA
      ENDIF
      YN=(PRN-ETA)/BTA
      TO= DEXP(-YO)*YO**ALF
      TN= DEXP(-YN)*YN**ALF
      GFA1=GAMA(ALF+1)
      FAC=1-(TN-TO)/(GFA1*ZFRAC)
      PROP = BTA*ALF*FAC + ETA
      RETURN
      END
```

```
      DOUBLE PRECISION FUNCTION GMPRB (ALF,BTA,ETA,PRP)
C-------------------------------------------------------------+
C     This program generates the partial integral of the Gamma  +
C     distribution for ALF, BTA, ETA, and PRP  (PRP>ETA)         +
C     The recurrence relation is used for values greater than    +
C     2 and between 0 and 1.                                     +
C-------------------------------------------------------------+
      IMPLICIT DOUBLE PRECISION (A-H,O-Z)
       X = (PRP-ETA)/BTA
         TERM=1.0/ALF
         SUM=TERM
         ICNT = 0
   20    IF (DABS(TERM).GT.1.0D-10) THEN
            ICNT = ICNT + 1
            TERM=TERM*X/(ALF+ICNT)
            SUM=SUM+TERM
            GOTO 20
         ENDIF
         GMPRB = SUM*DEXP(-X)*X**ALF/GAMA(ALF)
      RETURN
      END
```

```
      DOUBLE PRECISION FUNCTION GAMA
C-------------------------------------------------------------+
C     This program generates the gamma function of ALF using a  +
C     polynomial approximation for Gamma(ALPHA+1) taken from     +
C     Abromowitz mathematical functions and tables.  The         +
C     recurrence relation is used for values greater than 2 and  +
C     between 0 and 1.                                           +
C-------------------------------------------------------------+
      IMPLICIT DOUBLE PRECISION(A-H,O-Z)
      DIMENSION B(8)
      DATA B /-0.57719165200, 0.98820589100,-0.89705693700,
     .         0.91820685700,-0.75670407800, 0.48219939400,
     .        -0.19352781800, 0.03586834300 /
      CONST=1.0D0
      XX=X
      IF (X.LT.1.0D0) XX=X+1.0D0
  100 IF (XX.LE.2.0D0) GOTO 200
      XX=XX-1.0D0
      CONST=XX*CONST
      GOTO 100
  200 XX=XX-1.0D0
      Y=1.0D0
      DO 300 I=1,8
         Y=Y+B(I)*XX**I
  300 CONTINUE
      GAMA=CONST*Y
      IF (X.LT.1.0D0) GAMA=GAMA/X
      RETURN
      END
```

GAUSSIAN QUADRATURE SPLIT

QSPLIT is a FORTRAN program for calculating pseudocomponent mole fractions and molecular weights. The molar distrubution described with a modified gamma distribution, is split into five pseudocomponents using Gaussian quadrature. QSPLIT calls the function GAMF which is above.

```
      SUBROUTINE QSPLIT(ALFA,BETA,ETA,DLTA,MWN,MWC7P,MFC7P,MWI)
C-------------------------------------------------------------+
C                                                             +
C   PROGRAM DEVELOPED BY: CURTIS H.WHITSON, TOMAS F. ANDERSON +
C                         AND INGOLF SOREIDE                  +
C-------------------------------------------------------------+
      IMPLICIT DOUBLE PRECISION (A-H,O-Z)
      PARAMETER (MPS=5)
      DOUBLE PRECISION MWN, MFC7P(MPS),MWI(MPS),MWC7P,MWC7N
      DIMENSION X(5),W(5), X5(5),W5(5),
C
C---- 5 Quadrature points.
C
      DATA X5 /0.263560319718D0, 1.41340305910 7D0,
     *     3.596425771041D0, 7.085810005859D0, 12.640800844276D0/
      DATA W5 / 5.217556105 83D-1,  3.98666811083D-1,
     *     7.59424496817D-2, 3.61175867992D-3,  2.33699723858D-5/
      NQDR=5
      SQWT=0.0D0
      SQPD=0.0D0
C
C---- Set up appropriate weights and X's.
C
         DO 50 I=1,NQDR
            X(I)=X5(I)
            W(I)=W5(I)
            SQWT=SQWT+W(I)
            SQPD=SQPD+X(I)*W(I)
   50    CONTINUE
C----  Calc. Molecular Weight of last fraction as: 2.5* Mw7+
       IF (MWN.EQ.0.D0) MWN=2.5*MWC7P
C
C---- Calc. Beta based on the molecular weight of the last fraction
C
      BETA= (MWN-ETA)/X(NQDR)
      DLTA = DEXP( ALFA*BETA/(MWC7P-ETA) - 1.0 )
      IT=0
333   CONTINUE
       IT=IT+1
       IF (IT.GT.20) GO TO 999
C---- CALCULATE USEFUL FACTORS
      GM = GAMA(ALFA)
      ALM1 = ALFA-1.0
      CNORM = GM/(1.0+DLOG(DLTA))**ALFA
C---- CALCULATE MOLECULAR WEIGHTS AND MOLE FRACTIONS
      MWC7N=0.D0
      SMFRC=0.D0

      DO 400 I=1,NQDR
         MWI(I) = X(I)*BETA + ETA
         MFC7P(I) = W(I)*X(I)**ALM1/CNORM/DLTA**X(I)
         SMFRC=SMFRC + MFC7P(I)
         MWC7N=MWC7N + MWI(I)*MFC7P(I)
  400 CONTINUE
```

%

```
        MWC7N=MWC7N/SMFRC
      DO 500 I=1,NQDR
        MFC7P(I)=MFC7P(I)/SMFRC
 500  CONTINUE
       ERRMWN=(MWC7N-MWC7P)/MWC7P
       IF (DABS(ERRMWN).LT.1.D-6) GO TO 999
       ERRMWH=ERRMWN
       DLTAH=DLTA
       IF (IT.EQ.1) DLTA=DLTA*1.01
       IF (IT.GT.1) DLTA=DLTA
     *                  -ERRMWN*(DLTA-DLTAO)/(ERRMWN-ERRMWO)
       DLTAO=DLTAH
       ERRMWO=ERRMWH
       GO TO 333
999   CONTINUE
      RETURN
      END
```